

Universidade do Minho
Escola de Engenharia

Artur Jorge de Oliveira Feio

**Inspection and Diagnosis of Historical Timber
Structures: NDT Correlations and Structural Behaviour**

**Inspecção e Diagnóstico de Estruturas Históricas de
Madeira: Correlações com Métodos Não Destrutivos
e Comportamento Estrutural**

Dezembro de 2005

Acknowledgements

The research reported in this thesis was carried out at the Civil Engineering Department of University of Minho, Portugal, at the Timber Structures Division of National Laboratory for Civil Engineering, Portugal, and at the DISTAF of University of Florence, Italy. This research has been supported by the Portuguese Foundation for Science and Technology (FCT) under grant SFRH/BD/6411/2001, since March 2002.

I would like to express my deep gratitude to my supervisors, Paulo B. Lourenço and José S. Machado, for their invaluable guidance, teaching, patience and support during these years and for the creative and stimulating atmosphere in our frequent discussions. I would like also to thank for having responded swiftly to ideas and masses of writing material giving constructive feedback and suggestions that directed this work forward.

Prof. Luca Uzielli deserves many thanks for his inspiration and participation in this work and for the time I was able to spend in Italy. Special thanks are also due to Marco Togni for making my stay in Florence so pleasant.

There are many important contributors that have made possible to achieve this work. I am grateful to all the staff of the Civil Engineering Department of University of Minho and of the Structures Division of National Laboratory for Civil Engineering, especially António Matos, José Louro and Manuel Ferreira, for the stimulating and intense discussions, advices and laboratory assistance. Thanks also to António Silva, César Leite, Nuno Silvestre and Paulo Marques. I am also indebted with José Pina-Henriques and Miguel Ferreira for generously taking the time to read a draft of my thesis.

My special thanks also go to Lina Nunes and Helena Cruz. I learned a great deal and was honoured to work with them.

My grateful acknowledge to Foundation for Science and Technology (FCT), for PhD grant SFRH/BD/6411/2001. I am also grateful to the support of Augusto de Oliveira Ferreira Lda. (compression and tension specimens preparation and supply), and the support of Domingos da Silva Teixeira, S. A. (mortise and tenon joint specimens preparation and supply).

To my friends Alexandre Antunes, Ângela do Valle, Francisco Fernandes, Jorge Branco, José Pina-Henriques, Luís Neves, Miguel Fernandes, Pedro Lança, Ricardo Brites Tânia Nobre and Tiago Miranda, I am forever grateful.

Special thanks to Adriano Borges, Bertinho, Calinhos, Catarina, Charinha, Dú Paraíba, Guida, Helena, Ivan, Lambes, Lastrincha, Nelinha, Palmeirinha, Piri, Portela, Ramoa, Nóquio, Rosinha, Súsú, Tirinha, Tita and Turiz, for being unconditional friends.

I would like to thank all my wonderful family who have always encouraged and inspired me, despite having no real interest in my research subject.

Finally, I would like to dedicate this thesis to you Rute for your smile and for having supported me with care, time and energy while I completed this thesis. Thank you for being always there when I need you: I finish this thesis!

Abstract

The work presented in this thesis was carried out at the Civil Engineering Department of University of Minho, Portugal, at the Timber Structures Division of National Laboratory for Civil Engineering, Portugal, and at the D.I.S.T.A.F of University of Florence, Italy.

In order to assess the safety of old structures and preserve their original essence as much as possible, *in situ* inspection and evaluation of actual mechanical properties represent a first step towards diagnosis, structural analysis and the definition of possible remedial measures. The objective of this research is to contribute to the present state of knowledge in these fields, providing novel correlations between destructive and non-destructive testing (ultrasounds, Resistograph and Pilodyn) for chestnut wood (*Castanea sativa* Mill.) and for a typical traditional wood-wood connection. For this purpose, it was decided to consider specimens from recently sawn timber, which is now available on the market for structural purposes, and specimens from old wood, obtained from structural elements belonging to ancient buildings.

In a first phase, an experimental investigation has been conducted on a total of 342 specimens of clear wood, with no visible chemical, biological or physical damage, which included standard compression tests, parallel and perpendicular to the grain, and standard tension tests, parallel to the grain. These specimens have been tested in a destructive and non-destructive way. The possibility of predicting wood properties by application of non-destructive techniques is discussed based on simple linear regressions models. Application of the regression models obtained from recent cut wood to the results obtained from old timber beams is also analyzed.

In a second phase, the strength capacity of wood-wood mortise and tenon connection (typology often found in historical Portuguese timber structures) is characterized, investigating the static behaviour of real scale old timber connections and characterizing the ultimate strength capacity, the global deformation of the joint and the failure patterns. Taking into account the need for practical assessment of existing wood-wood mortise and tenon joints, the results of the destructive tests are combined with non-destructive tests of the connections, in order to produce novel linear regressions for the connection.

Finally, a finite element non-linear analysis of the mortise and tenon joint tested is presented. The multi-surface plasticity model adopted comprehends a Rankine type yield surface for tension and a Hill type yield surface for compression. Sophisticated non-linear anisotropic models are becoming standard in several finite element based programs, but the issue of their validation remains under discussion. In the present study, the validation of the non-linear model is performed by means of a comparison between the calculated numerical results and experimental results, showing an excellent agreement and stressing the relevance of the interface properties in the global response.

Resumo

O trabalho apresentado nesta tese foi desenvolvido no Departamento de Engenharia Civil da Universidade do Minho, Portugal, no Núcleo de Madeiras do Laboratório Nacional de Engenharia Civil, Portugal, e no Departamento de Ciência e Tecnologia Ambiental e Florestal da Universidade de Florença, Itália.

Tendo por objectivo a determinação da segurança estrutural dos edifícios históricos, e a preservação, tanto quanto possível, da sua traça original, a inspecção e a avaliação *in situ* das suas actuais propriedades mecânicas, representam um primeiro passo na abordagem ao diagnóstico, análise estrutural e definição de possíveis medidas preventivas e/ou de reforço.

O objectivo deste trabalho é contribuir para o actual estado de conhecimento neste domínio, determinando, através de ensaios destrutivos e não destrutivos (Ultrasons, Resistógrafo e Pilodyn), as propriedades de um lote de madeira recentemente serrada (que estaria disponível no mercado para fins estruturais) e aquilo que foi designado por “madeira antiga”, madeira de castanho (*Castanea sativa* Mill.), obtida de elementos estruturais pertencentes a edifícios antigos.

Numa primeira fase, foram realizados uma série de ensaios num conjunto de 342 provetes de madeira livres de defeitos, sem aparentes danos químicos, biológicos ou físicos, que incluíram ensaios de compressão *standard*, paralelamente e perpendicularmente às fibras, e ensaios de tracção *standard*, paralelos às fibras. Estes provetes foram ensaiados de forma destrutiva e não destrutiva. A possibilidade de prever as propriedades da madeira através da aplicação de técnicas e métodos não destrutivos é discutida com base em modelos simples de regressão linear. A extrapolação dos modelos de regressão linear obtidos entre os dois grupos de madeiras considerados, “madeira nova” – NCW – e “madeira antiga” – OCW, é analisado.

Numa segunda fase, a capacidade resistente de uma ligação tradicional madeira-madeira, traduzida numa ligação de respiga e mecha (tipologia frequentemente encontrada nas estruturas históricas de madeira portuguesas), é caracterizada investigando-se o comportamento de ligações à escala real e caracterizando-se a capacidade resistente última, a deformação global da ligação e os diferentes modos de rotura. Os resultados são apresentados e discutidos tendo em atenção a aplicação prática dos mesmos na avaliação de estruturas existentes: os resultados dos ensaios destrutivos são combinados com os dos não destrutivos, e novas regressões lineares são propostas.

Finalmente, uma análise não-linear, com recurso a elementos finitos, da ligação ensaiada é apresentada. O modelo de plasticidade em superfícies múltiplas adoptado apresenta uma superfície de cedência de Rankine para tracção e uma superfície de cedência de Hill para compressão. De facto, sofisticados modelos anisotrópicos têm vindo a ser incorporados com frequência em diversos programas de cálculo baseados em elementos finitos, sendo que a sua validação ainda está em discussão. No presente trabalho, a

validação do modelo não-linear é feito através da comparação entre os resultados numéricos e os resultados experimentais, realçando a excelente correlação entre ambos e demonstrando o papel preponderante das propriedades dos elementos de interface na resposta global.

Contents

1	INTRODUCTION	1
1.1	A brief introduction to chestnut wood	2
1.2	The Portuguese wooden tradition in construction	3
1.3	The role of research on timber structures	5
1.4	Objectives and scope of this study	5
1.5	Outline of the thesis	6
2	BRIEF REVIEW OF NON-DESTRUCTIVE EVALUATION OF TIMBER.....	9
2.1	Introduction	9
2.2	Global test methods (GTM).....	11
2.3	Local test methods (LTM).....	17
2.4	Case studies: <i>in-situ</i> assesement of wood structures.....	20
3	ADOPTED TESTING EQUIPMENT AND PROCEDURES	21
3.1	Density determination	21
3.2	Ultrasonic pulse velocity method	21
3.2.1	Compression perpendicular to the grain.....	24
3.2.2	Compression parallel to the grain.....	26
3.2.3	Tension parallel to the grain	27
3.3	Resistograph method	28
3.4	Pilodyn 6J method	29
4	CHESTNUT IN COMPRESSION PERPENDICULAR TO THE GRAIN. EVALUATION BY NON-DESTRUCTIVE METHODS	31
4.1	Background.....	33
4.1.1	Influence of wood characteristics	33
4.1.2	Influence of testing procedure	35
4.1.2.1	Full versus partial loading test standards.....	36
4.1.2.2	Stress-strain diagrams and ultimate strength	39
4.1.2.3	Specimen size	41
4.1.3	Conclusion	42
4.2	Experimental set-up.....	42
4.2.1	Material.....	42
4.2.2	Test set-up and equipment.....	44
4.3	Results	46

4.3.1	Density determination	46
4.3.2	Destructive tests	47
4.3.3	Ultrasonic pulse velocity method.....	55
4.3.4	Correlations based in the NDE methods	57
	4.3.4.1 Correlations with density	57
	4.3.4.2 Correlations with the elasticity modulus.....	61
	4.3.4.3 Correlations with the strength	64
4.4	Conclusions	67
5 CHESTNUT WOOD IN COMPRESSION PARALLEL TO THE GRAIN. EVALUATION BY NON-DESTRUCTIVE METHODS.....		69
5.1	Experimental set-up.....	70
	5.1.1 Material	70
	5.1.2 Test set-up and equipment.....	71
5.2	Results	74
	5.2.1 Density determination	74
	5.2.2 Destructive tests	75
	5.2.3 Ultrasonic pulse velocity method.....	81
	5.2.4 Correlations based in the NDE methods	82
	5.2.4.1 Correlations with density	82
	5.2.4.2 Correlations with the elasticity modulus.....	85
	5.2.4.3 Correlations with the strength	88
5.3	Conclusions	91
6 CHESTNUT WOOD IN TENSION PARALLEL TO THE GRAIN. EVALUATION BY NON-DESTRUCTIVE METHODS		93
6.1	Experimental set-up.....	95
	6.1.1 Material	95
	6.1.2 Test set-up and equipment.....	96
6.2	Results	99
	6.2.1 Density determination	99
	6.2.2 Destructive tests	100
	6.2.3 Ultrasonic pulse velocity method.....	106
	6.2.4 Correlations based in the NDE methods	106
	6.2.4.1 Correlations with density	106
	6.2.4.2 Correlations with the elasticity modulus.....	108
	6.2.4.3 Correlations with strength	109

6.3	Conclusions	110
7	EVALUATION OF LOAD CARRYING CAPACITY OF A TRADITIONAL TIMBER JOINT	113
7.1	The mortise and tenon joint	115
7.2	Description of test specimens	116
7.2.1	Density determination	118
7.3	Destructive tests.....	119
7.3.1	Test set-up	119
7.4	Non-destructive tests	121
7.4.1	Pilodyn and Resistograph tests.....	122
7.4.2	Ultrasonic tests	123
7.5	Experimental results and observations	125
7.5.1	Load-displacement diagrams.....	128
7.5.2	Correlations with ultimate load and stiffness	133
7.6	Conclusions.....	136
8	MODELLING OF A TRADITIONAL TIMBER MORTISE AND TENON JOINT UNDER COMPRESSION	137
8.1	Adopted finite elements and solution strategies.....	139
8.2	The adopted anisotropic failure criteria.....	141
8.2.1	Rankine type yield criterion	142
8.2.2	Hill type yield criterion	143
8.3	Adopted material parameters.....	145
8.4	Numerical vs. experimental results	146
8.5	Effects of the material parameters	151
8.5.1	Normal stiffness of the interface	151
8.5.2	Tangential stiffness of the interface.....	152
8.5.3	Elastic modulus	153
8.5.4	Compressive strength	153
8.6	Conclusions	154
9	CONCLUSIONS	157
9.1	Future work	159
	REFERENCES	161
	ANNEX 1: Research conducted on the use of non-destructive techniques for <i>in situ</i> evaluation of wood members.....	173

ANNEX 2: Compression tests perpendicular to the grain	179
ANNEX 3: Compression tests parallel to the grain	189
ANNEX 4: Tension tests parallel to the grain.....	193
A.4.1 Full bridge system	194
A.4.2 Relations between the ultrasonic pulse velocity methods.....	196
A.4.2.1 Correlations with the elasticity modulus	197
A.4.2.2 Correlations with the strength	199
ANNEX 5: Evaluation of load carrying capacity of a traditional timber joint	203
A.5.1 Load-displacement diagrams.....	204
A.5.2 Test set-up details.....	207

Introduction

Wood, together with masonry and stone, is the material most uninterruptedly used by Man, being since the oldest civilizations until nowadays developed where novel applications and uses for the material. Thus, the heritage of timber structures is immense and the oldest examples date back to millennia ago, some of them still in good shape and performing their duties. Several and wide-ranging structural typologies and functions are assigned to these structures. The geometry is defined by elements that occupy a limited and well defined part of the tri-dimensional space, with a clear evidence of the hierarchy of the components, see Figure 1.1. Timber elements are often visible, which allows easier conservation, identification of the wood species, characterization of details and evaluation of deterioration.



Figure 1.1 – The complexity and extraordinary space between roof (timber carpentry of the XIII c.) and false ceiling (timber carpentry of the XVIII c.) of the Saint Mark's church in Florence, Italy.

Complex timber structures, such as those belonging to the roofs of large monuments, are often not easy to understand in a expedite way. As the coverings of monuments as cathedrals, public buildings, mansions or villas show very complicate features, not easy to be understood during the first inspection. This is not only due to the fact that the system is very elaborate and to the large number of members but also due to continuous changes and repair past works, mostly with additional stiffening or propping. The typical result of the history of the construction is the increase in the number and the heterogeneity of the members, together with a multiplicity of connections and diversity of supports. This means that the original must be distinguished from the additions and the

replacements. This complexity makes the field of conservation of historical timber structures not only a challenge but a field much in need of modern research.

1.1 A BRIEF INTRODUCTION TO CHESTNUT WOOD

Chestnut wood will be used in the present study due to its wide use in Portuguese historical timber structures. Chestnut is the name used for any species of the genus *Castanea*, deciduous trees of the family *Fagaceae*. They are characterized by thin-shelled, sweet, edible nuts borne in a bristly bur. Chestnuts are classified in the division Magnoliophyta, class Magnoliopsida, order Fagales. The leaves are simple, ovate or lanceolate, 10-30 cm long and 4-10 cm wide, with sharply pointed and widely-spaced teeth, incorporating shallow rounded sinuses between. The flowers are catkins, produced in mid summer. The fruit is a spiny cupule 5-11 cm diameter, containing 2-7 nuts, see Figure 1.2.



Figure 1.2 – Chestnut tree: (a) tree, and (b) detail of the fruits.

Being largely propagated in the past for nut harvesting, chestnut tree (*Castanea sativa* Mill.), represents today one of the most diffuse species in the European Mediterranean area. In Portugal, about 32,000 ha are pure chestnut forests (Fioravanti and Galotta, 1998). During some historical periods, in various regions of Europe the cultivation of chestnut became so dominant and indispensable for the survival of mountain populations that some authors do not hesitate to identify these cultures as “chestnut civilizations” (Gabrielli, 1994). Therefore, several studies and monographs have been dedicated to the study of chestnut.

The wood of chestnut is considered as moderate shrinking and not easy to dry. It shows high natural durability and it is therefore well suited for different uses. In the North of Portugal, besides roof and floor structures, windows and doors have also been manufactured of chestnut wood for

centuries. The results of investigations (Fioravanti and Galotta, 1998) showed that chestnut sawn-timber is also very well suited for glue-laminated timber. Chestnut wood is porous, but it is very durable in contact with soil and it has been popular for fence and electrical posts, railway ties, and beams.

In the European standards EN 350-1 (CEN, 1994) and EN 350-2 (CEN, 1994) chestnut wood is classified as durable and suitable for all applications with and without contact with soil, except of some particular cases of very extreme conditions. Deppe and Schmidt (1998) assessed the mechanical properties for different species after nine years of weathering exposure: chestnut wood showed the smallest decrease of bending strength (about 20%) in comparison with Robinia, Oak, and Larch.

1.2 THE PORTUGUESE WOODEN TRADITION IN CONSTRUCTION

There are several relevant time periods to point out the importance of wood in Portuguese traditional construction. The end of the Middle Age was a period of creative energy, where a changing society tried to keep and to revive tradition based on paradoxes and controversy. In this context, religious manifestations and profane events occurred with great apparatus and spectacularity. Wood played also a role in the collective life of medieval societies, in relation with architecture of the buildings needed for the festive events, and also with military constructions associated to the effort that the maritime expansion required, during the XV century.

The relevance of carpenters was also stressed during the period of the reconstruction of downtown Lisbon, after the disastrous 1755 earthquake. The new constructions were based on a composite wooden structure of plummets, crosspieces and diagonal lines, filled by masonry, constituting a three-dimensional frame of very high ductility and with an excellent anti-seismic behaviour. This, so-called “Pombaline” system, represents a genuine Portuguese structural typology especially conceived to enhance the seismic performance and following the experience in timber construction. Here “Pombaline” is the term coined after the Marquis of Pombal, the prime minister at the time of the 1755 earthquake, who took most of the decisions regarding the reconstruction of Lisbon. Figure 1.3 shows an internal timber wall arrangement example for downtown Lisbon, see Córias e Silva *et al.* (2001) for detailed information.

The traditional usage of wood takes into consideration the local predominance of species but also its structural or ornamental function. Noble wood, as chestnut, oak and pitch-pine (coming from the commercial exchange between Portugal and North America in the century XVI), was used in palaces, in castles or in the interior of churches. This use of noble wood could be combined with pine or the cypress for wood laths. However, in the North of Portugal the use of oak and chestnut is predominant in most buildings. In the rest of the country the use of pine predominates.

Wood has been traditionally used in the construction as piles for ground consolidation and for indirect foundations in case of poor soil conditions, particularly in regions close to water lines and high ground water level.

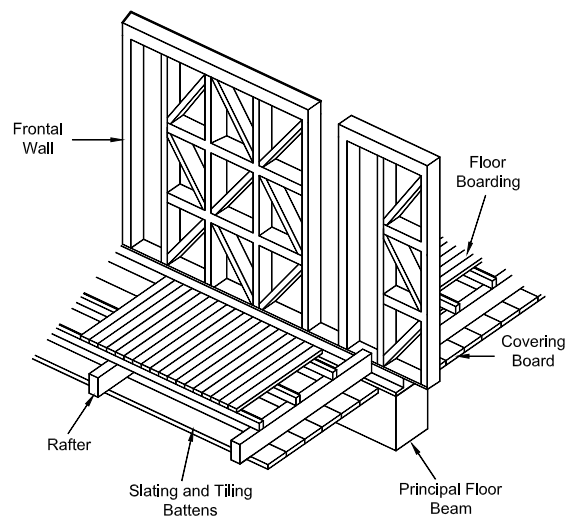


Figure 1.3 – Internal timber wall arrangement for downtown Lisbon: example of a composite timber-masonry wall.

Floors and stairs were frequently made by a system of beams up to 6-7 m of length, with a spacing around 400 mm up to 600 mm, see Figure 1.4. The dimensions and the transversal sections vary taking into account the wooden species. For spans larger than 7 m, after the XIXth century and following the development of the iron industry in the industrial revolution, it was common to use metallic beams and composite floors as an alternative to the traditional wooden solutions.

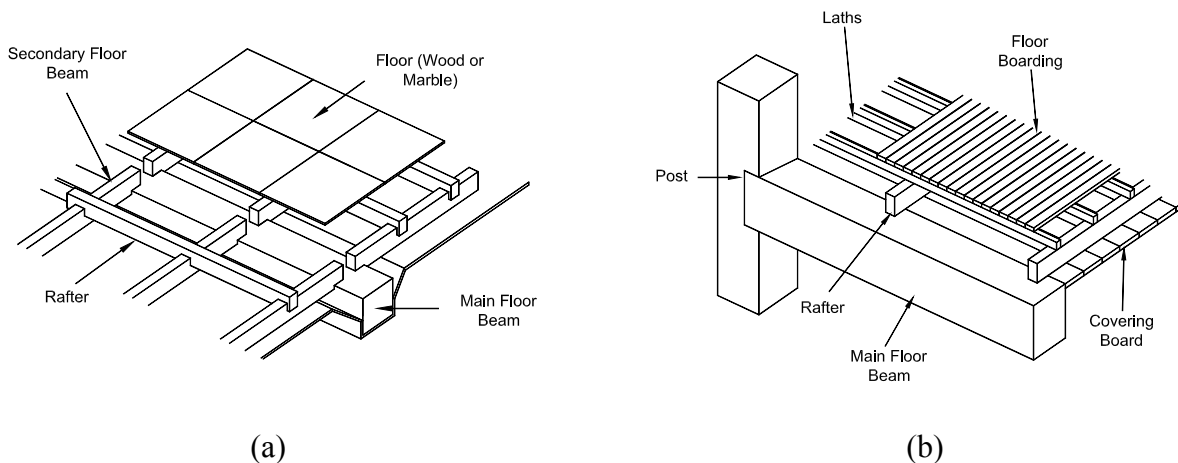


Figure 1.4 – Typical floor typologies.

The roofs of monumental and historical wooden buildings are probably the most emblematic structural systems and incorporate the larger structural complexity. The multiplicity of joints and constructive solutions varies taking into account the evolution of techniques and materials. The most typical timber roof structures in traditional constructions are the wooden trusses. The trusses

were mostly made of main roof beams, which received the purlins that supported the rafters, which, in turn, received the laths that supported the roofing tiles.

1.3 THE ROLE OF RESEARCH ON TIMBER STRUCTURES

In the past, timber structures were erected using traditional methods and rules-of-thumb passed from one generation to the other. Without mathematical or predictive methods, but with experience and great skill, an impressive empirical wisdom was obtained.

Presently, prejudices persist against timber structures in several countries, based on the claim that it is expensive, fragile, burnable, and dependent on unreliable workmanship and unknown quality. At the present state of knowledge, rational design rules, based on a thorough material description and a proper validation by comparison with a significant number of experimental results is available. However, safety assessment of existing structures and characterization of traditional wooden building techniques remain a true challenge. This means that experimental research in the behaviour of large-scale timber specimens and *in-situ* testing are needed. Inspection and evaluation of the *in-situ* structural properties represent an important part of the conservation of historical timber structures, and non-destructive evaluation methods are excellent to achieve a good level of knowledge in the structural analysis, diagnosis and inspection of ancient constructions

In addition, the introduction of sophisticated numerical tools, capable of predicting the behaviour of timber structures from the linear stage until complete loss of strength, based on nonlinear finite element analyses, will always be helpful to better understand the structural behaviour and to perform parametric studies. In particular, computations beyond the limit load down to a possibly lower residual load are needed to assess the safety of the structure.

1.4 OBJECTIVES AND SCOPE OF THIS STUDY

The general aims of the present work are: (a) to quantify the strength capacity of wood-wood mortise and tenon joint by physical testing of full-scale specimens; (b) to evaluate the reliability of different non-destructive techniques (NDT) for determining mechanical data and joint properties; (c) to propose adequate correlations between NDT and mechanical data or joint properties for chestnut wood.

For this purposes, old (OCW) and new (NCW) chestnut wood is used in the experimental campaign. It is further noted that the strategy adopted has a broad application in other timber joint typologies.

Other specific objectives of this study are:

- to characterize the elastic and inelastic properties of chestnut wood under compression and tension parallel and perpendicular to the grain, using destructive and non-destructive methods. Three non-destructive methods (ultrasonic testing, Resistograph and Pilodyn) are

proposed and the possibility of their application is discussed based on the application of simple linear regression models;

- to investigate the static behaviour of real scale old timber connections (wood-wood connections) and to characterize the ultimate strength capacity, the global deformation of the joint and the failure patterns;
- to validate the adopted nonlinear model by comparing the predicted behaviour with the experimental behaviour. The adopted model should be able to predict the failure mode and the ultimate load with reasonable accuracy. Moreover, a parametric analysis should indicate the most relevant parameters for the structural response.

1.5 OUTLINE OF THE THESIS

Chapter 2 addresses the criteria and methods mostly used to evaluate the residual cross section of timber elements, and the technological and mechanical characteristics of structural wooden elements.

Chapter 3 presents a brief introduction to non-destructive evaluation of timber structures and deals with the most relevant issues concerning the experimental use of the non-destructive techniques used later in this study to characterize mechanical properties, namely micro-drilling (Resistograph®), needle penetration (Pilodyn®) and ultrasounds (Pundit®).

Chapter 4 characterizes the compressive properties of chestnut wood under compression perpendicular to the grain, using destructive and non-destructive methods. The chapter includes also a proposal to define the ultimate strength value, aiming at an adequate design value. An overview of testing apparatus and results relevant for practical purposes is also presented. In addition, the performance of different NDT for assessing strength and stiffness is also evaluated. Extrapolation of regression models obtained from recently cut wooden material to that obtained from old timber beams is analysed.

Chapter 5 and Chapter 6 present the compressive and tensile properties of chestnut wood parallel to the grain, respectively. Again, the performance of different NDT for assessing strength and stiffness is evaluated, and a comparison between new and old wood is evaluated.

Chapter 7 characterizes the strength capacity of wood-wood mortise and tenon joint, investigating the static behaviour of real scale old timber connections (wood-wood connections) and characterizing the ultimate strength capacity, the global deformation of the joint and the failure patterns.

Chapter 8 presents a finite element nonlinear analysis of the mortise and tenon joint tested in Chapter 7. The multi-surface plasticity model adopted comprehends a Rankine type yield surface for tension and a Hill type yield surface for compression. Anisotropic elasticity is combined with anisotropic plasticity, in such a way that totally different behaviour can be predicted along the material axes, both in tension and compression. Validation of the model is performed by means of a comparison between the calculated numerical results and experimental results.

Chapter 9 presents the summary and final conclusions that can be obtained from the present study.

Brief review of non-destructive evaluation of timber

This chapter addresses the criteria and non-destructive methods frequently used to evaluate the residual cross section of timber elements, and the technological and mechanical characteristics of structural wooden elements.

2.1 INTRODUCTION

Structural evaluation of ancient or recent timber structures present particular problems (related to inherent wood material properties) and difficulties. *In-situ* evaluation (without damaging) of timber structural elements represents an initial and crucial step for the success of the rehabilitation process. Support for non-destructive inspection works includes nowadays a variety of tools (without damaging the structures) offering valuable information about the quality and biodeterioration status of timber elements.

Appraisal and repair of ancient timber structures has become a major topic of interest in the last decades. In the recent years this renewed interest considerably increased the number of technical interventions and design developments in Portugal. Conservation or rehabilitation of existing timber structures imply extensive knowledge about the properties of materials from which the structure is made. This knowledge constitutes the support for short-term structural behaviour assessment as well as to foresee the continuous adaptation and capacity of response of the material under long-term actions.

Due to the high variations intra and inter species, a large volume of wooden material is needed to be tested to characterize its mechanical properties with a minimum level of confidence. Quality control and preservation of artistic value were considered important issues leading to the development of some non-destructive test methods for wood which were used in the evaluation of the mechanical and physical properties of other materials (composite, metals, etc...). The non-destructive evaluation methods are an excellent alternative to achieve a good level of reliability in the structural analysis, diagnosis and inspection of ancient constructions.

Ross et al. (1998) defined non-destructive materials evaluation as “...*the science of identifying the physical and mechanical properties of a piece of material without altering its end-use capabilities and using this information to make decisions regarding appropriate applications...*”. A

wide variety of tests can be performed with selection dictated by the test performance or property of interest, depending on the nature and geometry of the object under study.

The efficiency and reliability of NDE (non-destructive evaluation) can be increased if laboratorial tests are used to study the variability of the mechanical characteristics of the wooden elements (Uzielli, 1992a; Cruz *et al.*, 1994; Bonamini *et al.*, 2001). For this it will be necessary that result well coordinate and conduct all the plural-disciplinary activity, which is composed by the execution, design, safety verification and the retrofitting design of structures. This work should be coordinated with laboratorial tests providing important information for the evaluation process. Therefore, laboratorial tests represent a vital role in NDE because they are a mean to explain properties and characteristics of wood and to validate NDE results.

In particular, the last decades witnessed developments in the testing techniques and equipments diminishing the subjectivity and increasing the accuracy of structural analysis, diagnosis and inspection of historical constructions. NDE, which is a term that encompasses a much broader range of activities than NDT (non-destructive testing) has an own special interest due to the fact that its use does not affect the present structural integrity and safety of the structure (Bodig, 2000).

In-situ diagnosis of ancient timber structures has been described by several authors (Ceccotti and Uzielli, 1989; Uzielli, 1992b; Tampone, 1996a; Tampone, 1996b; Ross *et al.*, 1998; Tampone *et al.*, 2002). All the authors state that an initial visual inspection of the entire structure and of the singular elements is required in order to determine the original timber characteristics and the changes suffered due to service conditions. This survey follow several steps, beginning with the purpose of a general prediction of mechanical properties and ending in a thorough examination using NDE. But an important characteristic of several ancient timber structures is that they can effectively bear higher loads than expected (Togni, 1995), which stresses the need of adequate procedures for diagnostic and assessment of the real bearing capacity, which can not be obtained with a simple visual inspection. Otherwise, the increasing interest in cultural heritage and restoration projects can also cause the loss of part of a common European cultural memory.

NDE can be classified in two distinct groups: Global Test Methods (GTM) and Local Test Methods (LTM) (Bertolini *et al.*, 1998; Ceraldi *et al.*, 2001). The former includes e.g. the application of the ultrasonic and vibration methods. The latter, being the Resistograph (Rinn, 1994) and the Pilodyn (Görlacher, 1987) the most common techniques, plays usually a major role in the support of visual inspection of wooden elements and structures.

Usual applications of LTM are related with the prediction of the element residual section by analyzing abnormal density variations in the element generally associated with mass loss, which could be due to biological degradation (Machado and Cruz, 1997).

Other NDE methods can be applied to wood and wood composites namely: thermography (Bonamini, 1995; Tanaka, 2000; Berglind and Dillenz, 2003), sonic stress waves (Ross *et al.*, 1999; U. S. Forest Products Laboratory, 1999; Divós, 2000), X-Ray (Lindgren *et al.*, 1992; Bucur *et al.*, 1997, Bergsten *et al.*, 2001), sniffer dogs (used to identify dry rot fungus in wood), isotope method (Madsen, 1994; Feinberg, 2005) and endoscopic methods. The development of these and other

NDE methods is in fast progress, however, owing to safety concerns, high costs involved, technical issues, etc., their use has been quite limited in structural timber evaluation.

A semi-destructive method based on testing of small non-standard samples taken from historic timber structures was developed by Kasal *et al.* (2003). Two kinds of samples were proposed: i) thin tension test specimens and ii) the core drilling specimens. Kasal (2005) concluded that a more reliable estimation of mechanical properties and density was possible since the strength and elasticity parameters were obtained directly from destructive tests of the material.

Core drilling has been also used in the dendrochronological chronology, analysis of wood structures and objects and determination of density (Lexa and Tokosova, 1983; Romagnoli *et al.*, 2004; Bernabei, 2005; Romagnoli *et al.*, 2005). Cores of approximately 12 mm diameter have been used to determine shear strength of glue lines in the laminate timbers in service (Selbo, 1962). Other use of the core drilling includes determination of strength characteristics of standard and core specimens. Theoretically, the mapping between the core strength and standard prismatic specimen should yield a correlation coefficient close to unity (Kasal, 2003) because sampling corresponds to conservation requirements concerning limited intervention and it does not influence the load carrying capacity of a tested element.

2.2 GLOBAL TEST METHODS (GTM)

Visual Inspection and Species Identification – this is the most simple and oldest NDE method. The visual evaluation consists in examining directly, and preferably at close distance, checking and registering wood features, signs of damage or deterioration, sometimes with the help of simple instruments (knife, chisel, hammer, etc.), providing a rapid means of identifying areas that may need further investigation. This is an essential part of diagnosis but the results depend severely on the experience of the person carrying out the task. The following aspects should be addressed:

- evaluation of the wood original quality (species and main characteristics of the element, natural defects such as spiral grain, knots, ring shakes, discoloration). Small samples of wood can be removed from the timber members for identifying wood species. This identification is accomplished by examining the anatomical features of the wood under a light microscope. Wood species identification restrains the variability of properties (density and mechanical) and allows the application of models (often regression) obtained in laboratory for specific wood species. Also it is essential for deciding on the historical importance of a particular wood element;
- identification and evaluation of biodeterioration through the presence of biological agents (fungi, insects, etc.) or recognition of damage (bore-holes, wood surface changes, bore dust near the damaged element);

- global location and relative position, structural function, dimensions, accessibility, cleanness of the surfaces of the element, light conditions, existence of survey drawings and their agreement with the actual structural conditions;
- location of the relative position of the attacked zones and problems related with the loading conditions;
- evaluation of the residual section.

However, the estimation of the serviceability properties of new and/or reconstructed timber constructions by means of the visual grading method is not entirely reliable due to the many factors influencing the mechanical properties of timber and, further, the biased influence of the human factor. Moreover, the information is mostly qualitative.

Ultrasonic Stress Wave – coupled with a thorough visual examination, this technique can add significantly to the quality of an inspector's evaluation by providing information on the internal condition of members and their residual load-carrying capacity (Sandoz, 1989; Machado *et al.*, 1992; Lemaster *et al.*, 1997; Ross *et al.*, 1997; Ross *et al.*, 1998; Zombori, 2000). Most of these studies do not show an effective relation between ultrasonic method and the residual load-carrying capacity of the elements. This can be explained by the wavelength that is generally larger than the dimensions of the localized defects (knots, slope of grain or other local defect). However, this method could also be used, with an extraordinary accuracy, to determine some local effect that could be explored and could allow a good interpretation of the local properties of the elements *in situ*.

It is well known that stress waves velocity can be directly related to the elastic properties of timber since impedance contrasts in the material cause scattering of elastic waves. The propagation velocity of the longitudinal stress waves in an elastic media depends essentially on the stiffness and the density of the media itself. On the other hand, it is normally possible to measure the propagation time of a set of elastic waves in the axial direction of the wooden elements or in the perpendicular directions to this (it is stressed again that the propagation time is an average time obtained from the measurement of the faster elastic waves). Presently, different standards emerged to measure the ultrasonic properties of materials with a particular reference to ASTM E494-89 (1989).

Evaluation of the complex wave-sequence transmission and propagation is a very difficult task to analyze and interpret: the early portion of the arriving signal is a *p-wave*; slower components (mostly composed by shear and surface waves) and reflected waves are not present at this stage, being the interpretation of the slower components of the wave (Yasutoshi, 2000) one of the most complex problems. One of the most important advantages of the ultrasonic method is that the wave is affected solely by the material in-between the two receivers (permitting a relatively straightforward evaluation).

The last few decades have witnessed extensive research aimed at finding a hypothetical connection between the propagation of elastic waves in a material and its ultimate strength (Berndt *et al.*, 1999). Several approaches have been assumed:

- the global belief and assumption that material failure results from pre-existing inhomogeneities in the material (Patton-Mallory and Cramer, 1987; Bodig and Jayne, 1993). These local inhomogeneities change the local elastic properties of the material and create impedance contrasts which cause scattering of elastic waves, and are usually interpreted and analyzed by mechanics of composite materials (Kachanov, 1993). The scattering behaviour is used for mapping unusual reflections in metals, one of the oldest non-destructive evaluation methods;
- the assumption that the control of the energy dissipation properties and mechanisms are the same that determine the static behaviour of wood materials (Jayne, 1959; Ross and Pellerin, 1994), which allows the statistical evaluation of correlations between wave propagation characteristics (velocity and waveform parameters such as damping, maximum amplitude, contained energy and spectral parameters of the signal) and wood strength parameters, such as modulus of elasticity and ultimate strength;
- the acoustic-ultrasonic (combination of conventional ultrasonic test and acoustic emission) evaluation which was originally developed as a means to assess flaw distribution and the mechanical properties of wood and wood composites (Vary, 1991; Biernacki and Beall, 1993), but today is used in other applications such as material anisotropy of composites, high-resolution imaging of wood (Berndt *et al.*, 1999) and detection of decayed wood (Patton-Mallory and De Groot, 1989).

For prismatic, homogeneous and isotropic elements and for those with a section width smaller than the stress wavelength, the relation:

$$E_{din} = V^2 \cdot \rho \quad (2.1)$$

holds, where E_{din} represents the (elasto)dynamic modulus of elasticity (N/mm²); V is the propagation velocity of the longitudinal stress waves (m/s) and ρ is the density of the specimens (kg/m³).

For practical purposes, the relation between the dynamic modulus of elasticity and the static value is particularly relevant ($E_{din} \geq 0.90 \cdot E_{sta}$). This relation is explained by the viscous-elastic behaviour of wood (Bonamini *et al.*, 2001). Generally a linear relation is adequate (U.S. Forest Products Laboratory, 1999; Bonamini *et al.*, 2001):

$$E_{sta} = a \times E_{din} + b \quad (2.2)$$

where a , b are constants depending on the material.

The propagation of elastic waves is affected by local elastic properties of the material. Depending on the wavelength and element dimensions, the measured properties are averaged over differently sized regions. Thus, the propagation velocity of elastic waves in a particular mode, together with the material density, show immediately information on the stiffness coefficients of the material. Finite element modelling showed how a wave propagates in an orthotropic material in various directions with respect to the fiber orientation (Lord *et al.*, 1988).

These and other fundamental efforts, coupled with advances being made in the evaluation of connections (Pollock *et al.*, 1996) and structural systems, suggest this method as one of the most used in timber evaluation (see Figure 2.1).

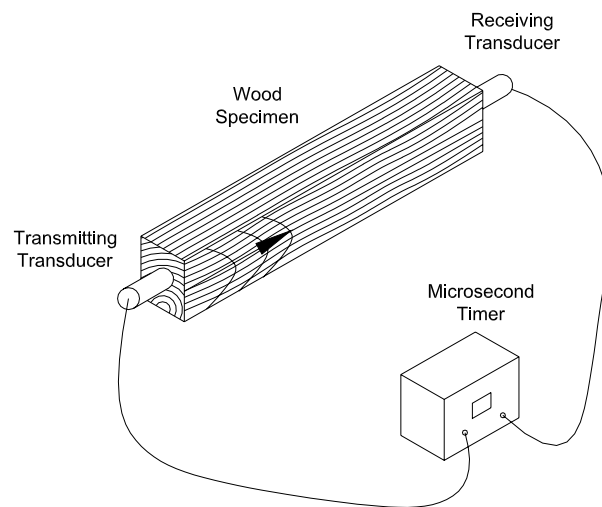


Figure 2.1 – Ultrasonic stress wave method (parallel to grain emission).

The ultrasonic method, which is very similar to the sonic stress wave method but uses higher frequencies (20 kHz-100 MHz), is often used in homogeneous, non-porous materials. In wood and wood composites materials it is less effective due to the porous and inhomogeneous nature of the material (Beall, 1987). Low frequencies (20 kHz-500 kHz) are often used in wood because of high wave attenuation (Zombori, 2000).

The velocity of ultrasonic stress wave travelling through a solid is dependent on its elastic properties. In high dispersive materials as wood, while travelling inside the material the wave suffers a series of reflection events originating new waves with different polarizations and each having a characteristic velocity. Most of ultrasonic equipments available considers only the fastest wave (showing a minimum of energy – generally defined by a volt threshold limit) to arrive at the receiver probe. It is expected that this wave travels through the highest quality zones of a wood element bypassing weaker zones (showing, knots, decay, slope grain) and therefore not allowing the local characterisation of that wood element, see Figure 2.2.

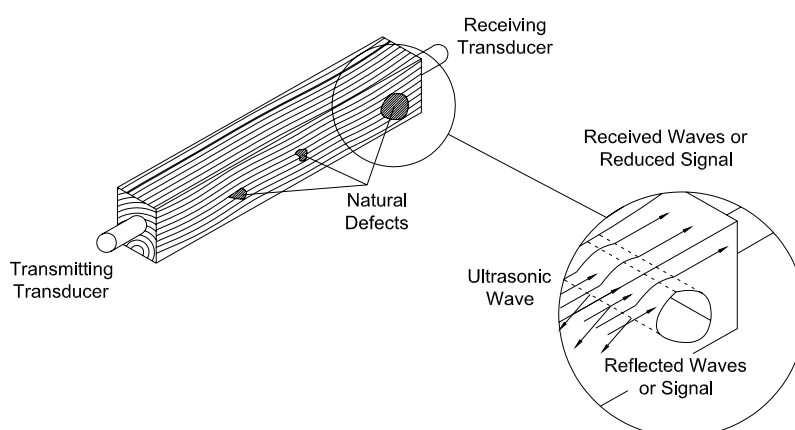


Figure 2.2 – Ultrasonic stress wave propagation and influence of defects.

If the signal is deviated, the transit time increases. Despite of their inhomogeneity, anisotropy and natural patterns of variability (inter and intra specie), it is possible to correlate the efficiency of wave propagation with the physical and mechanical properties of wood: high propagation velocities are associated with greater fracture resistance and absence of material defects.

Excellent results have been obtained using the velocity of propagation (both in longitudinal or transversal direction) for the estimation of the (elasto)dynamic modulus of elasticity and to quantify and locate decayed wood (Togni, 1995; Ross *et al.*, 1997; Machado, 2000).

Coupling of the transducers to the specimen surface is a major problem of the ultrasonic method. The presence of air is an inhibitor of the transmission velocity (different acoustic impedance), so it is necessary that the transducers are adequately coupled to the specimen surfaces during testing. Good coupling between the transducers and surfaces is guaranteed by a proper grease and pressure.

Another relevant issues regarding ultrasonic inspection of timber elements comprises the dimensions of the elements which often limits the choice of wave frequency (due to the high attenuation of the wave) and therefore the size of the defects able to be detected and the impossibility of getting free access to opposite faces of the elements which limits the method (transmission or shadow). Since high frequency stress waves attenuate significantly over relatively short distances in wood (particularly for wave propagation across the grain), the ultrasonic method is primarily effective in relatively small regions of wood members (Szymani and McDonald, 1981; Ross *et al.*, 1996; Emerson *et al.*, 1998; Ross *et al.*, 1998; Bonamini *et al.*, 2001; Tampone *et al.*, 2002). The requirements for access to opposite faces of timber members has been partially overcome with the development of techniques for introducing critically refracted longitudinal wave energy into wood (Dickens *et al.*, 1996).

Other open questions are the influence of environmental factors and wood characteristics in the ultrasonic method. For instance, ultrasound velocity increases as the moisture content of wood decreases. Due to the high hygroscopicity of wood the moisture content represents an important role when one is analysing the mechanical and physical properties of the material. For Red-Fir, Sandoz

(1989) proposed a reduction of 0.8% in the velocity of propagation for each 1% increase of moisture content, in a range between 5-30% of moisture content. This author reported also that the velocity of propagation is sensitive to grain direction. For Maritime Pine (*Pinus Pinaster* Ait.), Machado (2000) concluded that increasing the moisture content decreases the longitudinal and transversal velocity of propagation.

The ultrasonic wave velocity is around three times faster in longitudinal direction than in transversal direction, which enables sometimes this method to efficiently detect defects that evolves changes in grain direction, such as knots and spiral grain (Zombori, 2000). Discontinuities in the cells anatomy or the presence of surface decay caused by insects reduce the ultrasonic wave velocity. The velocity of propagation in decayed wood is slower because of its anatomic properties, which can include sometimes holes provoked by biological agents.

Finally, another factor that can be of relevance is the loading condition of the elements. Bucur (1995) observed, in the three directions of propagation of small specimens of Red-Fir, a small increase of the velocity of propagation for low stresses (up to one-fifth of the ultimate strength). For higher stresses this author observed a fast decrease with load increase.

In most of the recent studies involving this method the aim was to control the wood quality as a final product or as raw material (Machado, 2000) and to inspect historic structures (Sandoz, 1989; Ross *et al.*, 1996; Ross *et al.*, 1999; Ross and Hunt, 2000). Some of the studies try to focus on the distinction between clear wood and decayed wood, comparing the results and creating “evaluation maps”, with experimental results in clear wood that could be adopted in future interventions (Shaji *et al.*, 2000). Other authors tried to determine residual strength of structural elements that were used in ancient constructions or that were attacked by biological agents (De Groot *et al.*, 1998), or tried to determine qualitative properties by modelling wood as a homogeneous isotropic material, assuming that the clear and the defected wood can be modelled as a fluid, neglecting bending stiffness (Fransson and Nilsson, 2001).

Among the NDE methods special attention seems to be paid to the ultrasonic technique due to its fast execution, efficiency, precision, relative simplicity of use and transportation. However, the technique requires an experience operator and coupling between probe and specimens.

Density Method – density is a current classification criterion of wood due to the relation between density and mechanical strength values. Correlations between mechanical properties and density were reported by several authors (Kollmann and Coté, 1968; Bodig and Jayne, 1993; Giordano, 1999; U. S. Forest Products Laboratory, 1999) for different species, even if often only weak correlations could be found.

The density determination can be done laboratorially in small dimension specimens extracted from the elements or can be determined using non-destructive methods (local test methods) *in situ* that could be constrained by various factors: firstly, measurements are costly in terms of manpower and money because they involve extraction and processing of cores. Another important factor is that, in many situations, density determination has to be restricted to few samples due to the

destructive testing performed to obtain the test pieces. This restriction affects the representative of the sample.

2.3 LOCAL TEST METHODS (LTM)

Drill Resistance (Resistograph Method) – the drill resistance measure by the Resistograph device is based on the resistance offered by the material to the advance of a small diameter drill bit. Rinn *et al.* (1996) found that the mean resistance levels of the Resistographic profiles closely correlate with the gross density of dry wood from X-ray density profile (with the Resistograph resolution being smaller than the X-ray resolution). Helms and Niemz (1994) previously related the resistance profile with member density and radiographic analysis.

In the past, core sampling using conventional drills ($\phi = 10$ to 40 mm) was used to determine density properties of wood products. But these methods are hardly suited for determining density variations of structural timber due to the large boreholes.

The Resistographic method is considered a quasi-non-destructive method because the size of the hole in the specimen after testing does not have any weakening effect. This test allows to obtain the density profile of specimens/elements, which is the graphical representation of the values of the drill resistance versus the penetration depth (up to 50 measuring points per mm). The profiles reveal variations in the density of earlywood and latewood layers thus indicating decayed wood. From drops in the profiles it is possible to define different stages of deterioration. Also it allows the detection of discontinuities (for instance fissures).

The equipment used in the present work, see Figure 2.3, measures the resistance of a small drilling needle ($\phi = 3$ mm) through the power consumption of the drilling device.

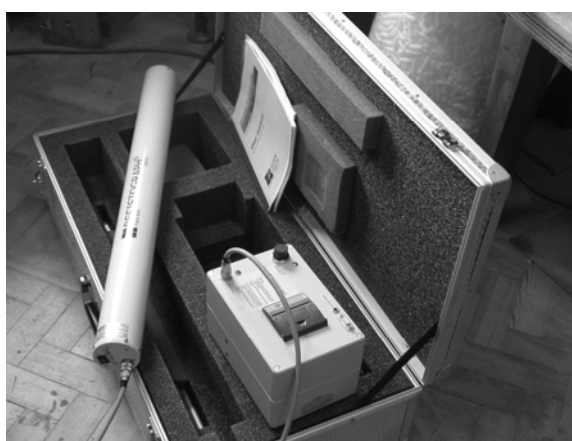


Figure 2.3 – Resistograph equipment.

Since the electronic resolution of current equipments is 12 bit (effective signal resolution of 10 bits), the ordinate values of the Resistographic chart vary from 0 to 4095 (Rinn *et al.*, 1996). The

stroke of the needle is constant and the needle rotates continuously (Rinn, 1993; Rinn, 1994a; Rinn, 1994b; Rinn *et al.*, 1996). The needle design eliminates the excessive drill energy consumption through friction in deeper penetrations: shaft diameter is 1 to 1.5 mm and maximum length is 1500 mm (maximum drilling depth is 950 mm). The tip of the needle has a special geometry and grinding. The drill resistance concentrates at the tip because its width is double the width of the shaft (2 to 3 mm). The device contains two engines: one for constant feed and one for the rotation of the needle. The needle shaft is stabilized continuously inside the drilling device by a special telescope.

This evaluation method provides information about conservation of the structural elements and (indirectly) about their structural capacity, such as beam cross section (when it is not possible to directly measure the dimensions), the residual cross section (decayed wood \approx lower penetration resistance of wood), the distribution pattern of annual growth rings (Wang *et al.*, 2003; Frattari and Pignatelli, 2005), the presence of natural defects and decayed wood not externally visible (important in architectural details such as beam butts). Some advantages of the method are the graphical resolution, the simplicity of storing data, of transporting the equipment and performing the tests (Machado and Cruz, 1997).

Some studies reveal limitations of this method, namely related to the difficulties in carrying out some inspections/tests due to the location of the element (difficulty in positioning the device perpendicularly to the element), the testing procedure itself (requires usage of both hands and the drill must be perpendicular to the surface), the measurements of only local characteristics of the elements and the invasive nature of the drill resistance technique (Bonamini, 1995a; Emerson *et al.*, 1998). Therefore, the resistographic method may be best employed if used in conjunction with NDE methods and techniques that provide qualitative condition assessment or more global condition assessment.

Some researchers (Görlacher and Hättich, 1990; Isik and Li, 2004) reported relatively moderate correlation between drilling resistance and wood density ($r^2 \approx 0.21-0.69$), showing that this correlation has not yet been adequately developed for use in *in situ* quantitative evaluation. It is noted that moisture content of wood has a large influence on the density values and Machado and Cruz (1997) observed that the drilling resistance decreases as moisture content increases. Works show that the resistance drilling data correlate well with the X-ray densitometry measurements (Rinn *et al.*, 1996).

Nowadays, the resistographic method is one of the most used methods and several campaigns were carried out using this technique (Tampone *et al.*, 2002; Augelli *et al.*, 2005a; Meade and Anthony, 2005; Branco *et al.*, 2005).

Pilodyn Method – similarly to the Resistograph the Pilodyn wood tester is an alternative for fast and non-destructive estimate of wood density (Hoffmeyer, 1978). The Pilodyn method using the Pilodyn 4JR, or similar equipment, can be understood as an adaptation and evolution of the soil's dynamic penetration test (Giuriani and Gubana, 1993; Ronca and Gubana, 1998) or the concrete sclerometer (Malhotra, 1984). The Pilodyn wood tester was originally developed in

Switzerland to obtain quantitative data on the extent of soft rot in wooden telephone poles, and was used with the aim of correlating the density of each specimen/element with the depth reached with the pin of the device. Density is a parameter well related to wood hardness, as it is fairly related with all the wood properties (Panshin and De Zeeuw, 1980; Bonamini *et al.*, 1995b). The method is widely used today for evaluating pole decays, or standing trees or sawn lumber density. It is noted that only the surface hardness or resistance to superficial penetration is measured, which represents a disadvantage.

There are several versions of this device, more powerful or simply with a different testing philosophy, that can be used in the evaluation or diagnostic inspections of wood species showing a high resistance to superficial penetration or in particular situations. These devices like the Pilodyn 12J and the Pilodyn 18J, which possess a spring with a higher stiffness (increasing strike force), or like the Pilodyn 4JR, which allows a repeating shot, are used to measure parameters related to density of the specimens. These are dynamic devices based on the action of a calibrated spring able to drive a flat-head steel pin into the surface of the specimen.

The Pilodyn model 6J for single shot (see Figure 2.4) and model 4JR for repeated shots are devices that allow to measure the penetration of a metallic pin with 2.5 mm of diameter into wood, through the release of a spring-loaded pin that transforms the elastic potential energy into impact energy. This dynamic impact is responsible for the penetration of the pin in the surface of the specimens, allowing to register the depth penetrated. The density of the wood or the degree of decay in the wood can be assessed by the different spring energy absorbed by the specimen (Zombori, 2000).



Figure 2.4 – Pilodyn 6J.

A possible broad application of Pilodyn is to sort logs into broad density classes, making the prices based not only on log size and visual grading but also on density characteristics (Graves *et al.*, 1996; Watt *et al.*, 1996). In standing trees pin penetration is likely to vary according to normal density variations patterns present in annual ring of Softwoods and ring-porous Hardwoods (Sprage *et al.*, 1983). Other applications are the genetic control of species (Aguiar *et al.*, 2003), however

there is the need to monitor some field trials for a longer period of time to confirm and support the results.

Watt *et al.* (1996) found that the Pilodyn is able to predict mean outerwood density values with reasonable accuracy, and offer an alternative to the slower and more costly core sampling. These authors calibrated the Pilodyn results in specimens of different size against X-ray densitometer values. Görlacher (1987) obtained good correlation coefficients between density and depth of penetration of the Pilodyn 6J, taking into account that the number of measurements for each specimen must be large. This author proposed empirical relations between the depth of penetration and density, showing that these empirical relations are affected by moisture content. The correlation coefficient varied from 0.74 to 0.92, and depended on number of measurements and species, therefore, species-based calibrations are required.

Studies were also carried out to define correlations with mechanical properties. Relations between resistance to superficial penetration and a three point loading test were found but more studies are needed to corroborate these results, due to its empirical nature and to the local and superficial character of the results obtained (Togni, 1995).

For the determination of the modulus of elasticity, Turrini and Piazza (1983) proposed an empirical relation correlating impact force and modulus of elasticity. The authors proposed also the adoption of a reduction factor of the modulus of elasticity based on a visual grading of the elements: 80% for non-defect elements and 50% for elements presenting knots, spiral grain, shakes or small decay portions. Again, it is noted that the penetration depth is highly affected by the moisture content (Bonamini *et al.*, 2001).

2.4 CASE STUDIES: *IN-SITU* ASSESSEMENT OF WOOD STRUCTURES

Non-destructive evaluation has been used to examine structures for over 100 years. Methods used alone, or at the same time with other NDE techniques allow to understand wood structural behaviour. Ross and Pellerin (1994) prepared a report reviewing pertinent laboratory investigations designed to explore fundamental concepts and presented several examples of how to apply these concepts to *in-situ* assessment of wood members. Machado (2000) also presented some work in this field.

Table A.1, presented in Annex 1, summarizes some research conducted on the use of several non-destructive techniques for *in situ* evaluation of wood members.

Adopted testing equipment and procedures

The present section presents relevant issues about the experimental utilization of the non-destructive techniques used in this thesis to assess mechanical properties.

3.1 DENSITY DETERMINATION

Wood density is of key importance in the evaluation and characterization of the mechanical and physical behaviour of wood. Density is correlated with strength properties and its value is determined by the ratio cell wall to cell cavity, which in turn is function of the relative proportion of different cell types present in Softwoods and Hardwoods species.

Density was measured according to EN 408 standard (CEN, 2000). Given the conditioning of the specimens, the average density ρ_m is determined for a moisture content of 12%, given by:

$$\rho_{12\%} = \frac{m_{12\%}}{V_{12\%}} \quad (3.1)$$

Here, m indicates the mass and V indicates the volume.

3.2 ULTRASONIC PULSE VELOCITY METHOD

The methodology followed was based on the transmission method (or shadow method), which is based on two transducers located in two opposite faces, one as transmitter and the other as receiver. As mentioned in Machado (2000) this is the best method for wood due to the high roughness generally associated with wood surfaces and the high attenuation coefficients.

During the tests, the ultrasonic equipment Pundit Plus (Portable Ultrasonic Non-destructive Digital Indicating Tester Plus) was used (CNS Electronics, 1995), with cylinder-shaped transducers of 150 kHz composed by piezoelectric ceramic crystals involved in a steel box. Machado (2000) found that the frequency is lower than the value indicated by the manufacturer because the final frequency response of the probe function is not only a function of the crystal resonance frequency (150 kHz) but from the assemble of steel box and crystal (as mentioned by the manufacturer).

In all tests, coupling between the transducers and specimens was ensured by a conventional hair gel. A constant pressure was applied by means of a thick (2 mm) soft rubber spring, allowing adequate transmission of the elastic wave between the transducers and the specimen under testing, and transmitting the coupling force without loading the transducer.

Conventionally wet couplants have been used (glycerine, silicone grease and water) since they assure an efficient wave transmission energy between the probe and the specimen under inspection. However, wet couplants penetration on the specimens could damage or contaminate the specimens. Dry couplants (usually elastomeric materials) and air couplant have been tested more recently with some degree of success (Machado, 2000). Still the need for a constant and controlled contact pressure (dry couplants) and field operation restrictions have limited the use of these coupling solutions. Therefore in the present research a gel is used as couplant since it assures a reliable time of flight readings (less sensible to contact conditions) and it can be easily used in practice (easy to be removed without staining the wood).

The rubber spring used allows adequate coupling pressure eliminating micro-gaps and promoting a satisfactory coupling interface (wood/transducer) making a more uniform stress distribution within the coupling interface. Theoretically and practically the increase in the surface pressure does not significantly improve coupling after a certain level (Biernacki and Beall, 1993; Divós *et al.*, 2000). Machado (2000) referred that the velocity of propagation of the ultrasonic wave is not significantly affected by the level of pressure applied (since it is merely dependent on an amplitude value – *trigger* – that determines the propagation time), affecting mostly wave shape-related parameters (total energy, amplitude, etc...).

Transducers lack of alignment can be a possible disturbance factor on repeatability of readings. Most specimens show a surface waviness or roughness that can easily affect that alignment. To avoid misalignments two wooden guides were used to set the transducers in the wood specimens surface and align them, see Figure 3.1.

The tests were conducted on samples sufficiently large, perpendicularly to the propagation direction, to avoid sample edge effects on wave propagation. Since generally the behaviour of elastic waves scales with the wavelength, sizes relate to the respective wavelengths in the direction of interest. Ideally, the dimensions perpendicular to the propagation direction would be an order of magnitude larger than in the propagation direction.

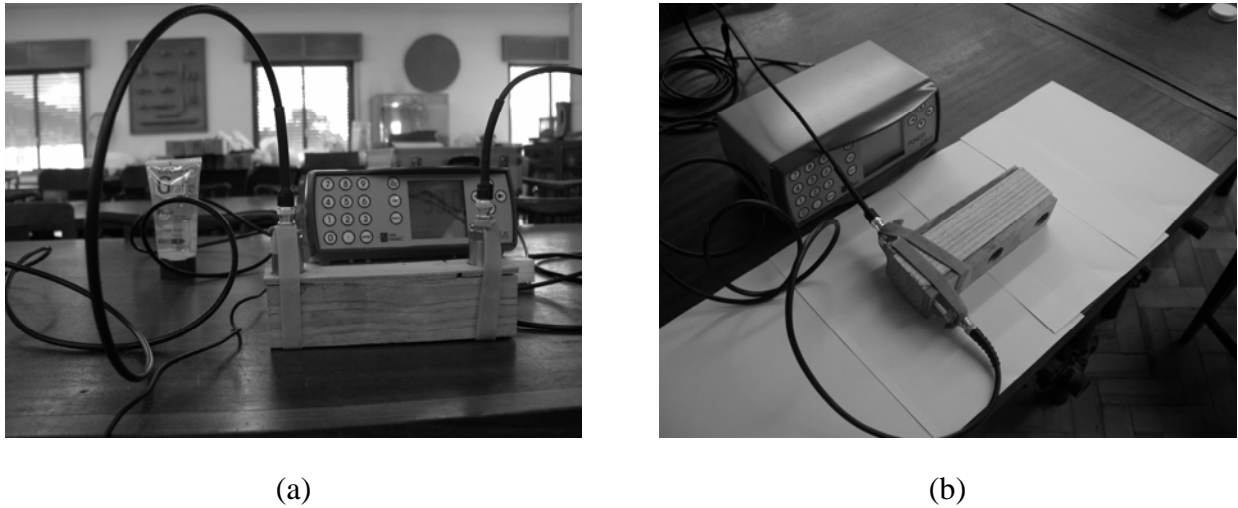


Figure 3.1 – Test set-up and alignment of the transducers: (a) front view, and (b) top view.

One correction is imperative when the dimensions of the section of the specimens are smaller than the wave length (λ). In the present work the wave frequency (f) was 150 kHz, the maximum velocity of propagation (V) was 5859.4 m/s (Direct Method, parallel to grain) and using the following relation:

$$\lambda = V \cdot \left(\frac{1}{f} \right) \quad (3.2)$$

one can obtain the wave length of 39 mm, which is smaller than all the specimens dimensions (50 mm). This can spatially be interpreted as a spherical surface, in comparison with the specimens' dimensions, which represents the shape of the front wave. In this situation one must use the follow relation:

$$E_{din} = V^2 \cdot \rho \cdot \frac{(1+\nu) \cdot (1-2\nu)}{(1-\nu)} \quad (3.3)$$

where E_{din} represents the (elasto)dynamic modulus of elasticity (N/mm²); V is the propagation velocity of the longitudinal stress waves (m/s), ρ is the density of the specimens (kg/m³) and ν is the coefficient of Poisson. However, the simplified relation:

$$E_{din} = V^2 \cdot \rho \quad (3.4)$$

was used due to the difficulties of characterizing each one of the six coefficients of Poisson. Since results obtained by this research program (reported in Chapters 4, 5 and 6) and other authors show that no significant variation of these coefficients exists within the same wood species, the equation parcel related with these coefficients can be envisage as a constant dependent only on the type of wood species.

3.2.1 *Compression perpendicular to the grain*

Although three methods were used in the framework of a more general approach, see Figure 3.2, (Indirect Method; Direct Method parallel to the grain, and Direct Method perpendicular to the grain), the Indirect Method was the only method correlated with the principal mechanical characteristics of the specimens, since it is the most appropriate in practical cases. The Indirect Method can be used for evaluating different zones of the element (global or local evaluation) and only needs a face of the element to be accessible.

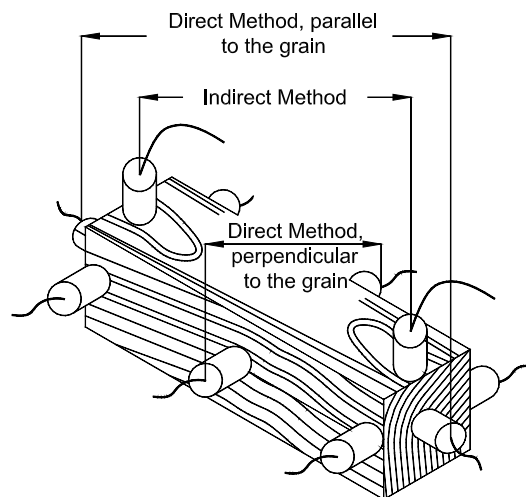
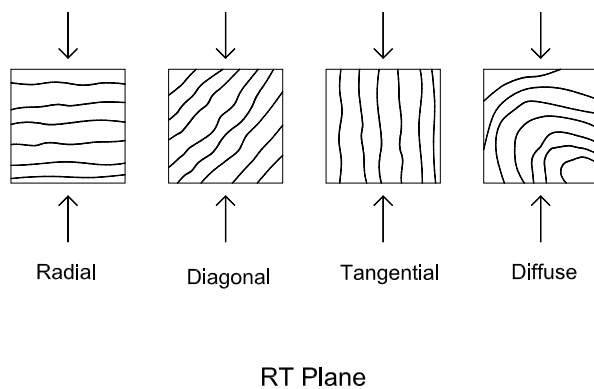
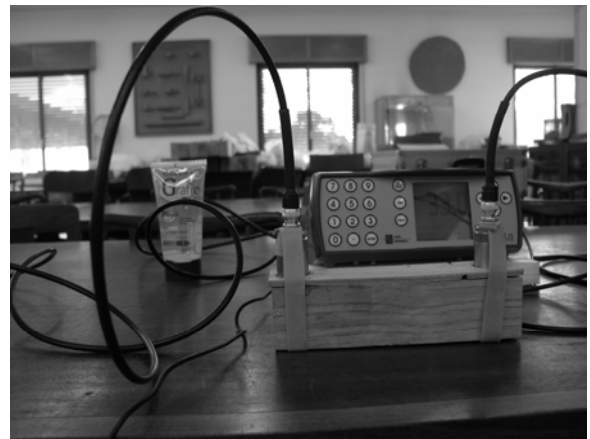


Figure 3.2 – Ultrasonic pulse velocity: all the used methods.

The transmission technique of elastic waves based on the Indirect Method was used in all the faces, for the case of diagonal and diffuse tests specimens, see Figure 3.3a. For the case of radial and tangential tests specimens, the transducers were used in two opposite faces, depending on the orientation of annual growth rings. In all cases average values were considered in all measurements and two readings per specimen were generally made but a third one was added if the two first readings differed significantly, see Figure 3.3b.



(a)



(b)

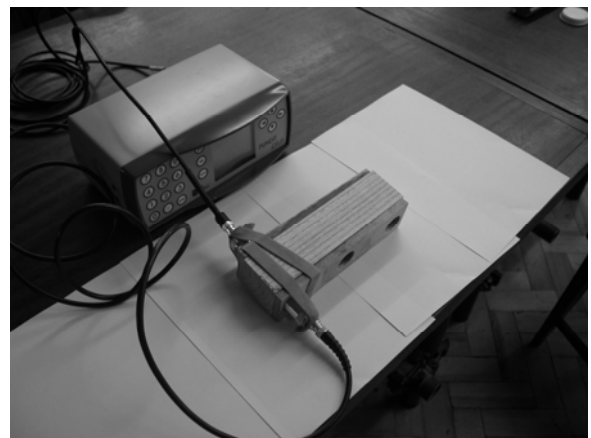
Figure 3.3 – Compression perpendicular to the grain: (a) annual growth rings orientation along the direction of the load, and (b) Indirect Method test set-up.

Regarding the Direct Method parallel to the grain, it requires access to the ends of the elements (in most cases not possible) and allows only a global evaluation of the material (it is not possible to evaluate weak or critical zones in the element), see Figure 3.4a.

Finally, the Direct Method, perpendicular to the grain, only gives a local evaluation of the element and it needs access to two opposite faces. In this method contiguous sections of the same specimen were used (the distance between each section was 6 cm), see Figure 3.4b. The results of these two last methods are presented in Annex 2.



(a)

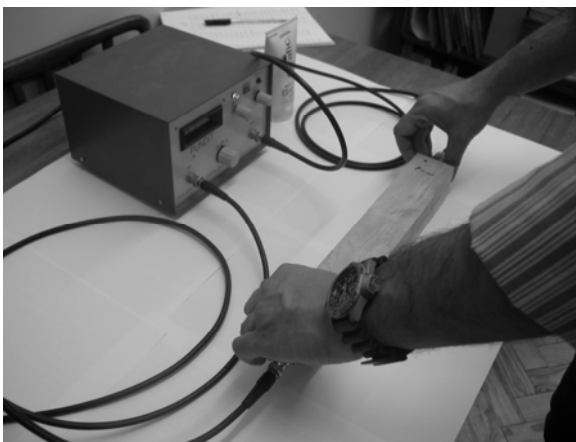


(b)

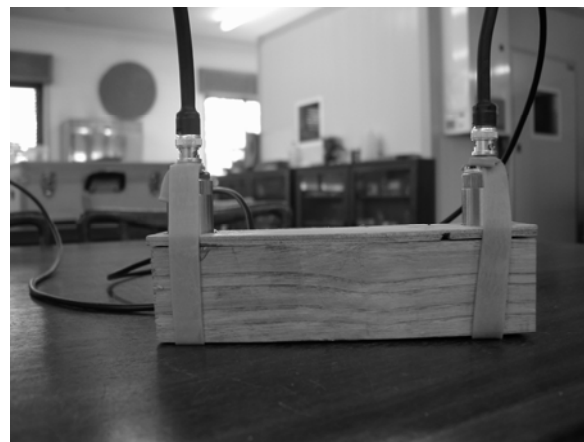
Figure 3.4 – Test set-up: (a) Direct Method, parallel to the grain, and (b) Direct Method, perpendicular to the grain.

3.2.2 Compression parallel to the grain

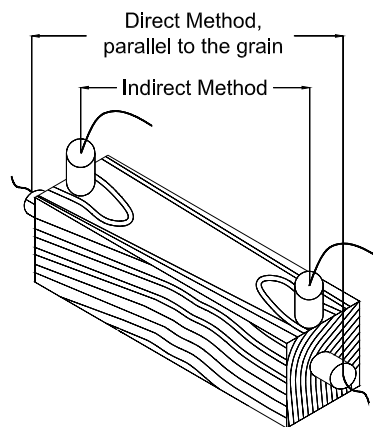
In the specimens tested in compression parallel to the grain, the ultrasonic tests were carried with two types of signal transmission: i) Direct Method, parallel to the grain, and ii) Indirect Method, see Figure 3.5. In this case, only the transmission technique of elastic waves based on the Direct Method, parallel to the grain was used. The elastic properties of wood were estimated by the measurement of stress wave propagation time and average values of the propagation velocity of the longitudinal stress wave were considered in all measurements. At least two readings per specimen were generally made but a third one was added if the two first readings differed significantly. The results of the Direct Method, parallel to the grain, are presented in Annex 3.



(a)



(b)



(c)

Figure 3.5 – Test set-up: (a) Direct Method, parallel to the grain, (b) Indirect Method, and (c) the two distinct methods used.

3.2.3 Tension parallel to the grain

Finally, in the specimens tested in tension parallel to the grain three different kinds of emission tests were realized: i) Indirect Method ($d = 20$ cm); ii) Indirect Method ($d = 45$ cm) and iii) Direct Method, parallel to grain, see Figure 3.6.

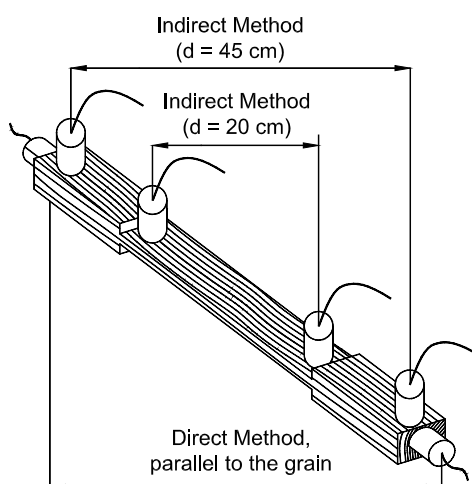
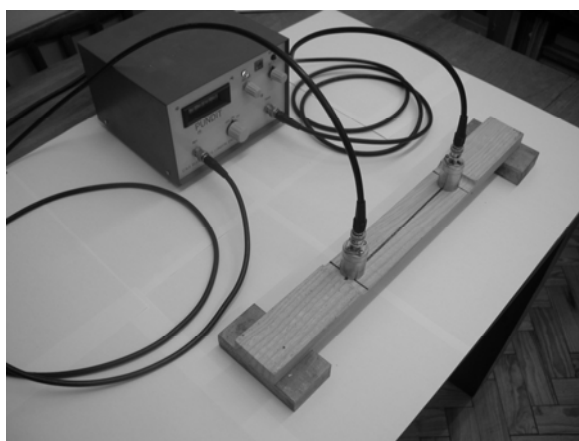
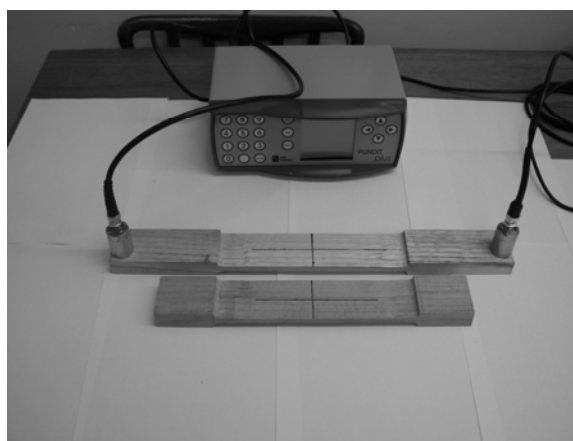


Figure 3.6 – Ultrasonic tests: the three distinct methods used.

The transmission technique of elastic waves based on the Indirect Method ($d = 20$ cm and $d = 45$ cm) was used in both faces, see Figure 3.7a and Figure 3.7b. In all methods average values were considered. In the Direct Method, parallel to grain, the measurements were made as represented in the Figure 3.8, and once more average values were considered.



(a)



(b)

Figure 3.7 – Ultrasonic tests: (a) Indirect Method ($d = 20$ cm), and (b) Indirect Method ($d = 45$ cm) and comparison between the two specimens (the standard and the adopted).

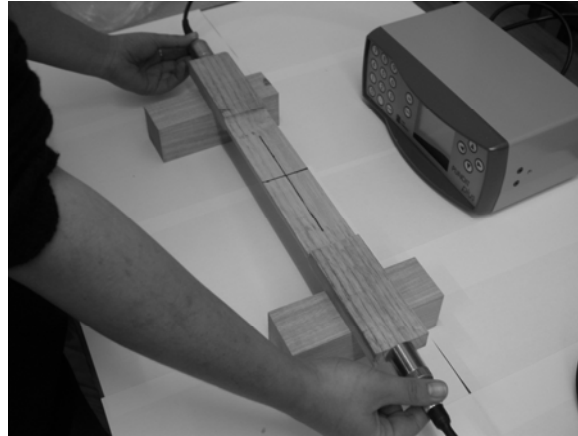


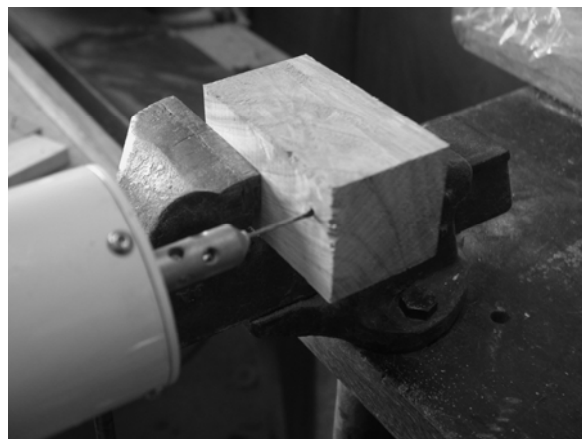
Figure 3.8 – Ultrasonic tests: Direct Method, parallel to grain.

3.3 RESISTOGRAPH METHOD

The use of the Resistograph allowed to obtain the density profile of the used tests specimens, see Figure 3.9. The Resistograph is usually adopted to obtain density profiles and, in the present testing program, drilling was made on planes TL or LR, which, in real cases, represents the accessible faces of timber elements. For each specimen, three independent profiles have been carried out and the results shown represent the average of the readings. Here, R, T and L are respectively the radial, transversal and longitudinal directions, where the grain corresponds to the longitudinal direction.



(a)



(b)

Figure 3.9 – Resistograph device: (a) global view of the equipment, and (b) drilling a specimen.

For all the specimens, as a function of the obtained graphs with the Resistograph, a resistographic measure (RM) was calculated. The ordinate of the Resistograph profiles reveals a

relative measure for the power consumption of the drilling equipment, which cannot be controlled by the user. This is acceptable in most applications because scaled values are sufficient, for detection of tree rings and decayed wood. For structural or mechanical usage, quantitative and absolute values are required.

The adopted resistographic measure represents the ratio between the integral of the area of the diagram and the height of the tests specimens (see Eq. 3.5), which is an average value. Using this quantity, the Resistograph results can be compared with the values of density and the strength values, even if the value remains scaled.

The RM value is given by:

$$RM = \frac{\int_0^h Area}{h} \quad (3.5)$$

where h is the height (drilling distance) of the specimens.

A workbench and a tripod were used to execute the drills reducing the possibility of error, by accurately controlling the specimen position and execution time.

3.4 PILODYN 6J METHOD

The dynamic impact provided by Pilodyn 6J is responsible for the penetration of the pin in the surface of the specimens, see Figure 3.10. The penetration depth is recorded while the Pilodyn 6J is still pressed against the tree. The penetration is read in millimetres (0-40 mm, without decimals) on the scale on one side of the instrument.



(a)



(b)

Figure 3.10 – Pilodyn 6J device: (a) global view of the equipment and parts, and (b) specimen under testing (the depth reached can be read from the scale).

The Pilodyn 6J was used with the aim of correlating the density of each specimen with the depth reached with the pin of the device (surface hardness or resistance to superficial penetration).

As in the case of Resistograph the tests were made on planes TL or LR, which, in most real cases, represents the accessible face of timber elements. The shot was made at an angle of 90° between the direction of penetration and the tangent to annual growth rings. This way undesirable variability of the results due to the orientation of annual growth rings is eliminated. Occasionally, it was necessary to select shot locations so that local defects would be avoided.

For each specimen, the average value of the four faces was considered. Three readings per specimen were made but a fourth one was added if the four first readings differed by more than 2 mm. Apart from regularly cleaning and occasional calibration, the pin was replaced every 500 shots. In the entire testing campaign, bending or crushing of the pin was never observed.

Chestnut wood in compression perpendicular to the grain. Evaluation by non-destructive methods

In traditional timber framed buildings the structural system is usually designed in such a way that load is transferred perpendicular to the grain using joints between walls and floors that are easy to produce and assemble (Blass and Görlacher, 2004), see Figure 4.1.

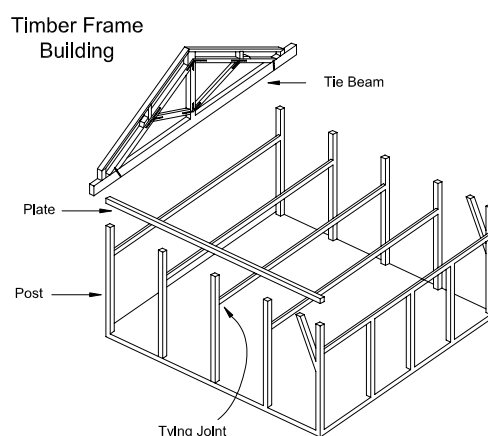


Figure 4.1 – Timber frame building.

The primary effect of compression perpendicular to the grain is compaction of the wood fibers. With higher fibers compaction, load carrying capacity increases due to density increase. Compressive stresses may be self-imposed, as in seasoning (shrinkage forces perpendicular to the axis of the tree), in drying and in pulping, or mechanically imposed, as in production of wood composites products. But such compressive stresses can generally be found in timber structures such as trusses, where tie beams, also referred to as crossbeams, anchor-beams, ties and lower chords, are transverse horizontal members that span from wall to wall, resisting the outward thrust of roof planes. Where a tie beam meets the wall framing, a tying joint is formed. Some of these joints are “mysterious” since their configuration and method of assembly are a mystery until they are disassembled. Because truss spans are often large, very substantial forces can develop in elements and mainly in joints.

Compression perpendicular to the grain is often critical in different situations of timber design. It is usually most severe at the ends of deep, narrow beams, and in the connecting members at the ends of short, heavily-loaded columns. In most cases, these compressive stresses are usually low but this does not apply to large and heavy timber beams and timber truss rafters (Korin, 1990). These stresses can occur concentrated over a portion or distributed over the surface of a specimen. Examples of concentrated loads are a post resting on a sill, sills continuously loaded in compression perpendicular to grain sliding sideways or a rail on a crosstie (which is the basis for standard tests). A final example is the intermediate support of a continuous beam, where compression perpendicular to the grain can lead to bending failure.

But there are situations where elements are transversely loaded along all its length, e.g. in mining timber, foundation elements or frame wooden (see Figure 4.2). It is then necessary to fully understand the strength capacity of these timber elements or systems in order to design adequate strengthening solutions and to eliminate possible original design misconceptions.

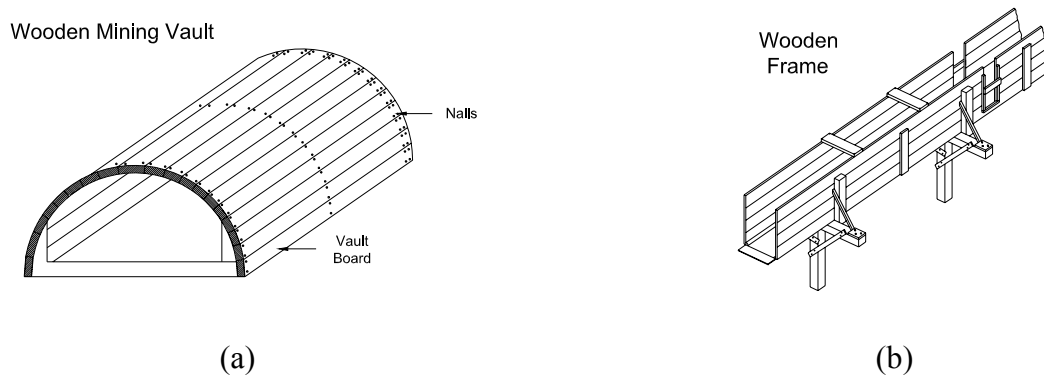


Figure 4.2 – Timber structural systems transversely loaded along their length: (a) wooden mining vault, and (b) wooden frame.

From an engineering point of view one of the most important questions is that structures are usually designed to respect simple execution, economy, adequate structural behaviour and safety of the occupants. In theory it is possible to design joints so that load transfer perpendicular to the grain is avoided, but this is not feasible considering all other aspects of the design.

When a uniaxial compressive stress is applied to a specimen, the following types of deformation may take place: elastic or plastic shortening in ductile materials, crushing and fracture in more brittle materials, sudden out-of-axis instability (buckling) in long, slender bars, or combination of all these. A material such as wood commonly fails along a diagonal plane that is not the plane of maximum compressive stress, but rather one of high shear stress, which accompanies uniaxial compression. Deformation perpendicular to grain is crucial in joints, especially for multi-storey timber frame buildings, where displacements at each level can add up to substantial movements over the building height.

It is easy to understand that these large displacements have adverse consequences in structural systems as excessive deformation damages non-structural elements such as windows, doors and renderings. In general, this situation can be controlled by imposing limits to ultimate stress but Thelandersson and Mårtensson (1997) defend a more sophisticated philosophy for the design of wood loaded perpendicular to grain.

4.1 BACKGROUND

4.1.1 Influence of wood characteristics

From the studies aiming to characterize the physical-mechanical properties of wood when loaded in compression perpendicular to the grain, some factors seem particularly relevant for the interpretation of results.

Density is one of the main factors that influence the wood behaviour. When loading parallel to grain occurs, strength tends to be linearly dependent on density. However, if loading is perpendicular to grain, it is frequent to adopt a nonlinear relation given by:

$$f_{c,90} \approx (\rho)^\alpha \quad (4.1)$$

Here, $f_{c,90}$ is the transversal compressive strength, ρ is the density and α is a constant ranging between 1.5 and 2.3. This value depends on growth rings orientation, specimen dimensions and criteria for definition of failure. In the absence of more information, a value of α equal to 1.7 is recommended (Gehri, 1998).

A criterion for definition of failure assumes a major role due to the different approaches of structural behaviour on wood constructions. Figure 4.3 shows typical stress-strain diagrams for radial and tangential compression. The letters in the graph represent notable diagram points that correspond to: A and A' – specimens after the accommodation load; B and B' – first failure at a strain around 3%; C and C' – for a strain around 10% and D and D') for a strain around 20%.

As frequently happens, the behaviour of elements with structural dimensions, when loaded in direction perpendicular to grain, is extrapolated from the behaviour of wood specimens without defects. Understanding the influence of annual ring patterns on the mechanical properties of wood, and knowing that the behaviour is characterized by a total absence of a clear failure of the material, three deformation levels may occur and be easily identified when, for example, a radial specimen is loaded: i) initial elastic deformation; ii) plastic level (buckling of cellular walls and failure) and iii) densification (Bodig, 1965; Tabarsa and Chui, 2000; Tabarsa and Chui, 2001). This failure mode is associated with relatively high displacements on wood.

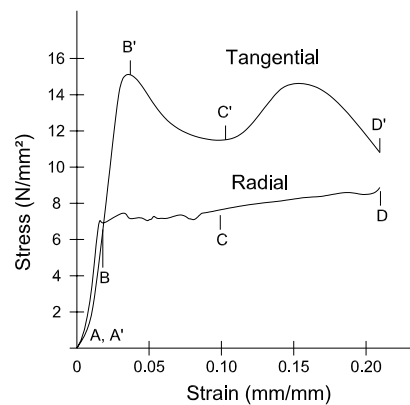


Figure 4.3 – Typical stress-strain diagrams (up to 20 percent compressive strain) of a ring porous wood in transverse compression (Bodig, 1965).

Characterization of physical-mechanical behaviour in compression perpendicular to grain, as a function of the orientation of the annual growth rings, becomes a fundamental step from a structural point of view. Taking into account the load direction towards the annual growth ring orientation, Youngs (1957) showed that normal to the grain tension behaviour of pieces with 0 to 45° inclinations (relatively to the annual growth rings) was similar, only differing for 90° angles. In compression, the behaviour it is not exactly the same, namely on the differences between failure mechanisms for orientations mentioned above. For 45° inclinations, strength is lower than in radial and tangential loads situations.

The stress-strain diagram shape can be justified by wood's anatomy. Load alignment with the three principal wood axis is mainly responsible for the different patterns found in stress-strain diagrams obtained from compression perpendicular to grain tests. This variable can be more important than differences between wood species (Bodig, 1965; Bodig, 1969).

Kollman (1959) showed that the annual growth rings properties are crucial on the transversal compression control. Porosity ratio in the hardwood rings or contrast of density between summerwood/springwood on coniferous are determinant factors on the characterization of transversal compression. Intermediate orientation of the growth rings and wood rays, between the tangential and radial position were also been identified as influence factors on the mechanical characterization process. This author concluded that strength in transversal compression was reduced to a minimum value for approximately 45° of the annual growth rings and wood rays inclination, in relation to the load direction, which is corroborated by the general composite materials elastic theory. Ethington *et al.* (1996) shown that compressive strength perpendicular to the grain depends and is related, in an approximately quadratic form, with the orientation of the annual growth rings.

Hall (1980) concluded a study in which the influence of the orientation of the annual growth rings on several species was evaluated. The author obtained the strength values of the different resinous species, as well as the correspondent modulus of elasticity, adopting a criterion based on

an extension of 0.2%. Madsen (1989) corroborated these results and presented more detailed correlations.

However, in practical situations, the influence of the annual growth rings along the direction of the load is not so clear; this is due to the absence of wooden elements with sections showing a particular orientation. Therefore, tests should be made using randomized growth orientations, taking into account that the failure mode observed for 45° inclinations (which provides lowest strength values for transversal compression), which is common in prismatic standardized specimens without apparent defects, is rarely observed when structural dimensions specimens are used and in real-life situations.

Schniewind (1959 *in* Bodig, 1965) determined the elastic properties of selected microscopic wood components – such as the wood ray – and concluded that the cause of lower modulus of elasticity in the tangential direction could not be explained only by the annual growth rings arrangement but rather by the presence of wood rays. Kunesh (1968) also justified the differences in tangential and radial inelastic behaviour of yellow poplar by the presence of wood rays, based on their influence in the increase of elastic and inelastic properties.

Depending on shape and dimensions, thickness and stressed area, different relations between strength and elastic properties of wood may be obtained. Bodig (1963) found that nearly all mechanical properties of Douglas-fir in radial compression were affected significantly by the thickness of specimens. Kunesh (1968) observed that, in radial compression for western hemlock and Douglas-fir wood, the maximum stress decreased with increasing thickness and moisture content. This author concluded that there will always be a weak portion of rays located in an earlywood layer in any specimen and with increasing thickness the probability of occurrence of an extremely weak ray, or several of them, is increased. Other elastic properties such as modulus of elasticity were also influenced by the specimen geometry, (Bodig, 1963; Bodig, 1965; Kunesh, 1968) increasing with thickness and decreasing with moisture content and stressed area.

Some authors pointed out that wood behaviour in radial compression is strongly dependent on its anatomical features (Alexiou, 1994; Tabarsa and Chui 2001; Müller *et al.*, 2003). But others authors believe that elastic behaviour is more dependent on density than on anatomical characteristics (Kennedy, 1968; Beery *et al.*, 1983). Defects as number of knots, its location and kind, grain inclination, variations on width and spacing between growth rings and presence of reaction wood, influence to great extent wood behaviour in compression perpendicular to grain. However, values given in technical standards and literature for strength and stiffness properties do not usually consider reduced sections taking into account the presence of defects. Also important factors are the long-term behaviour and moisture ratio.

4.1.2 *Influence of testing procedure*

Different issues are usually taken in consideration in experimental investigations in wood, namely mechanical and physical characteristics. As a result of the knowledge gathered it is widely

accepted that structural responses cannot be dissociated from its physical and mechanical properties. For instance, strength and stiffness, for compression parallel to the grain are severely influenced by wood density (Gindl, 2002).

Wood structural design is based on the hypothesis of a relatively fragile material, with strength influenced by natural defects that often initiate failure and might cause the collapse of the element. Experimental tests which used wood elements with structural dimensions confirmed the hypothesis of linear elastic behaviour up to failure, where it is possible to distinguish a more sensitive behaviour on higher quality wood (without apparent defects or with short term known load history) that, in compression parallel to the grain or bending, might show a stiffer behaviour.

Softwood and porous or semi-porous hardwood show a distinctive compression strength and stiffness behaviour as a function of the angle between direction of loading and annual rings. Structural differences between latewood and earlywood layers lead to significant different strength and stiffness between these layers. In the case of softwood the difference relies on the thickness of the tracheids cell walls and in the case of hardwood the difference relies on the degree of porosity (Bodig and Jayne, 1993; Damkilde *et al.*, 1998).

Technical limits imposed on wood design are not only directly associated to its high degree of anisotropy and heterogeneity but are also the result of an association of failures while trying to understand and evaluate the real properties and strength of wooden materials. As a consequence, admissible values for wood structural design are normally 10 to 15 times lower than the real strength of the material (Gehri, 1997b).

Gehri (1997b; 1998) referred that several tests were made trying to solve the issue of supplying a better understanding about wood materials behaviour. However, the global process of wood characterization as a construction material is becoming a hard task due to:

- technical reasons, related with test execution, such as the definition of clearly and consensual criteria for definition of failure;
- normative difficulties, related to the definition of a standard tests and testing procedures;
- lack of incentive, related with the preconception idea of using wood as a construction material.

For instance, and in contrast with several studies that were made with the goal of investigating the main physical and mechanical properties in compression parallel to the grain, and their relations with structural characteristics, there are not enough studies or efforts in the understanding of compression perpendicular to the grain.

4.1.2.1 Full versus partial loading test standards

Since the beginning of the XX century that investigations about the stress-strain relationship of wood in compression perpendicular to the grain are made, reporting how the stress-strain relationship in transverse compression is influenced by the anatomy of wood (Bodig, 1965;

Kennedy, 1968; Kunesh, 1968; Bodig, 1969). Presently, one of the questions that add more complexity to the problem is that several normative possibilities for the experimental tests of compression perpendicular to grain co-exist, namely:

- full load test surface: EN 408 (CEN, 2000), NBr7190 (1997);
- partially loaded test surface: ASTM D 143-94 (1994).

The results obtained by the full-surface and partial plate compression tests are quite different, due to the added edge effect of the latter, resulting in a shear effect along the perimeter of the compression plate (Bodig, 1969; Blass and Görlacher, 2004). The resistance to the shearing force is due to the bending of fibers along the edges of the compression plate, which is additional to the compressive resistance of wood. Kunesh (1968) reported a 39% increase for western hemlock and a 29% increase for Douglas-fir for the maximum strength. Stress distribution in transverse compression is very complex even with full-surface compression. Bodig (1969) suggests that multiple strip bearing-plates increase the load carrying capacity over full surface and over ASTM D143-94 (1994) values, but the increase is even better with square bearing-plates.

It is obvious that there are advantages in partial-plate compression to produce higher load-carrying capacity, so the edge effect contribution can be utilized in many engineering applications where the bearing strength of wood across the grain is required to carry load.

In practical situations, if the load is applied only to a portion of the upper surface, the bearing plate or post indents the wood, crushing the upper fibers without affecting the lower part of the member. Under this loading condition, the projecting ends of the member increases the strength of the material directly beneath the compressing weight by introducing a beam-action which helps to carry the load; however, this situation is exerted for a short distance only, as is referred in the literature.

Bodig and Jayne (1993) claim that results obtained using ASTM D143-94 (1994) are not able to be used as a definition of the compression perpendicular to grain strength. Its use has a minor interest and only for comparison between different wood species.

Stäudacher (1936 *in* Gehri, 1997b) carried out an intense experimental campaign using green wood specimens with small dimensions and defect free, showing unequivocally the difficulties in defining a consensual value that characterizes strength in transversal compression. This author, using two different specimens (one with dimensions of $50 \times 50 \times 50 \text{ mm}^3$ and other of $50 \times 50 \times 200 \text{ mm}^3$) defined two limits: a *failure limit* or *elastic limit* (specific deformation of failure rate of 1%/2 min) and an *ultimate limit* (coinciding with the intersection point of both tangential straight lines), see Figure 4.4.

On the other hand, this author also verified the influence of the orientation of the annual growth rings along the direction of the load beyond the influence of specimen length influence by using partial loading, similarly to ASTM D143-94 (1994). Depending on the specimens' sizes, different stress-strain ratios were obtained. In a partial loading situation, the author compared results of two different kinds of specimens: $50 \times 50 \times 150 \text{ mm}^3$ and $50 \times 50 \times 200 \text{ mm}^3$, three and four times the

dimension of the partially loaded central area of 50 mm, and where it was observed a light increase on the resistant capacity of the specimens with 50×50×200 mm³ dimensions, when compared to the first specimens. Another factor investigated was the influence of the moisture content.

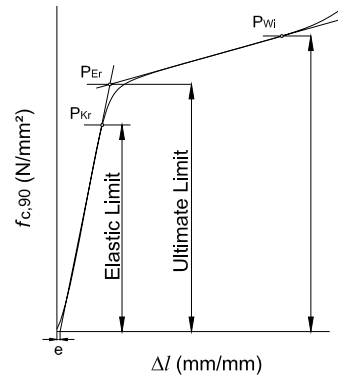


Figure 4.4 – Staudacher’s experimental campaign: stress-strain diagram interpretation (*in* Gehri, 1997b).

Rothmund (1949 *in* Gehri, 1997b) proposed as ultimate strength criteria a total deformation of 1% in wood specimens tangentially loaded, as show in Figure 4.5, obtaining the following relation between compression strength and density:

$$f_{c,90} = 18 \cdot \rho^{1.7} \text{ (N/mm}^2\text{)} \quad (4.2)$$

with ρ (g/cm³).

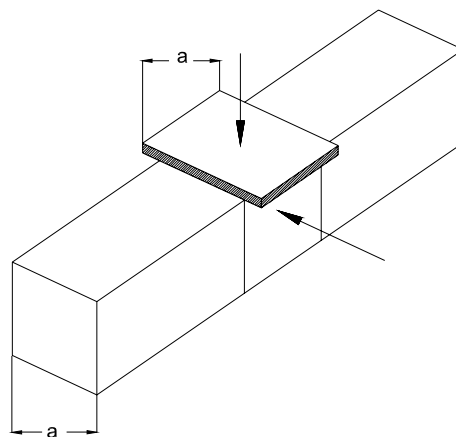


Figure 4.5 – Rothmund’s specimen and experimental procedure (*in* Gehri, 1997b).

Blass and Görlacher (2004) observed significantly different load-deformation behaviour according to the loading conditions. These authors, inspired on Madsen's work (1989), derived a mechanical model (from tests with glulam specimens) and presented a reliable and economic design method for partial loading situations in compression perpendicular to the grain adopting four different loading situations leading, obviously, to four different stress distributions.

EC5 (1998) enables an increase of design strength values depending on contact member length, calculated from the equation:

$$\sigma_{c,90} \leq k_{c,90} \cdot f_{c,90} \quad (4.3)$$

where $k_{c,90}$ is a factor to adjust the load application length.

4.1.2.2 Stress-strain diagrams and ultimate strength

In most cases, it is possible to define a linear segment on the stress-strain diagram at lower stress-levels, and also to associate this behaviour a tangent straight line on the graphic area (Bodig and Jayne, 1993). It is in this region, where it is assumed that linearity between stress and strain exists, that Hooke's law is applicable for practical purposes (Bodig, 1965). The point where the stress-strain diagram deviates from the maximum slope fitted to that diagram (tangential straight line) is defined as *proportional limit* (Y), as proportionality between stress and strain is lost after this point. Stress corresponding to this point is defined as *proportional stress* (σ_y) and the corresponding strain is called *proportional strain* (δ_y) (Bodig and Jayne, 1993), see Figure 4.6.

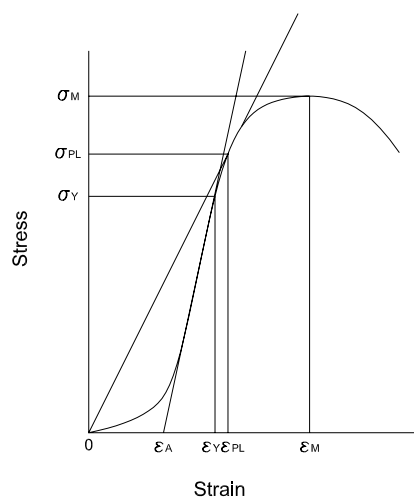


Figure 4.6 – Typical continuously recorded stress-strain diagram for wood (Bodig, 1965).

Proportional limit in radial compression is lower on softwood (generally higher on hardwood, mainly on those that have diffuse porosity) than in tangential compression (Bodig, 1963; Bodig, 1965; Kunesh, 1968). The proportional limit in radial compression is determined only by springwood, although, in tangential compression, summerwood is the control factor. Not only the proportional limit but also the modulus of elasticity behaves differently in radial and tangential compression or tension (Bodig, 1965; Bodig and Jayne, 1993).

Korin (1990) referred that the test method preconized by ASTM D143-94 (1994) does not include a clear definition of failure in compression perpendicular to grain due to the difficulties on the exact definition of the *proportional limit* in the stress-strain diagram. This author, who based his work on the extensive performed tests with small contact areas performed by Madsen *et al.* (1982), clarifies that the collapse of some cells walls may occur on the presence of low stress values, leading then to a substantial deviation from the straight imaginary line corresponding to a pure elastic behaviour. As a consequence, it is often very difficult to define a straight-line in the elastic zone, and the stress-strain diagram is nonlinear in all its length, expressing a combination of elastic behaviour of some cells with collapse of other cells.

Generally, the characteristic strength and stiffness are calculated by assuming a linear relation between stress and strain until failure, as Figure 4.7 shows. For example, characteristic strength values are normally based on random criteria of percentual extension values, which do not correspond to a real failure criterion, used for checking ultimate limit states. For Gehri (1998), a criteria for definition of failure with the goal of characterizing strength in transverse compression may be made following several perspectives. On Figure 4.7 it is possible to identify some of those approaches.

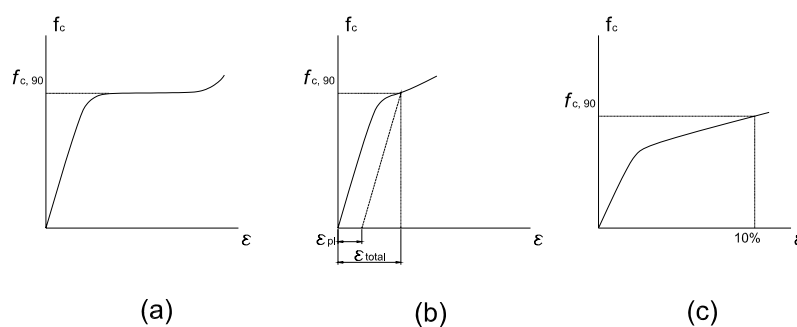


Figure 4.7 – Criteria for definition of failure: (a) pronounced plastic stage; (b) deformation criteria based on the plastic deformation ϵ_{pl} ; (c) excessive deformation, with imposed value of global deformation (e.g., 10%) (Gehri, 1998).

In usual design situations, it is unusual to observe complete structural failures. The observation of shakes, grain inclination or any kind of failure mechanism is always avoided by safety and comfort reasons adopting deformation criterion and taking into account foreseen actions and other design questions which are considered by the engineer taking into account the global structure

behaviour, see Figure 4.7c. These physical-mechanical properties are also influenced by moisture content and its variation along time, and by viscous-elasticity of the material.

The attempt of achieving an *ultimate strength criterion*, and, overall, its definition as a truth design value, has been very complex. On an early stage, the issue focused on the concept of materials densification; however this can only be used for non-porous materials and it is not applicable to wood. In fact, this definition depends mostly on the used criterion and more specifically on the plastic deformation adopted as an ultimate failure criterion. A nominal limit of 2.5% of the verified extension (based on the original size of the specimens) was used in the past on the characterization of the proportional limit (Youngs, 1957).

But the attempt to define a strength criterion unanimously accepted is still facing difficulties. Following EC5 (1998), failure by excessive deformation or loss of stability are recommended as a failure criteria; EN 1193 (CEN, 1997) recommends a plastic deformation value of 1%. In terms of total deformation, proposed values are around 2% to 5% (Bodig and Jayne, 1993).

The high anisotropic behaviour of wood at different structural levels is generally not considered and due to the lack of a clear failure of wood transversally loaded, different European standards have introduced the yield point as an easily quantifiable strength (Müller *et al.*, 2003).

4.1.2.3 Specimen size

According to the different kinds of approach, and depending on the goals of the investigation, different procedures have been used. Those differences begin on the specimens' standard type definition, for example, Bodig (1965) used 127 mm specimens with tangential and radial growth rings orientation, while DIN 52192 (1979) requires 20 mm specimens. In this standard and due to the densification effect on wood, it becomes difficult to define a characteristic strength that can only be expressed in function of a global deformation value. The strength values obtained with this standard shall not be used as design values. These considerations about DIN 52192 (1979) are also applied for ISO 3132 standard (Gehri, 1997b). Some proposes were made on CIB-W18A. One of them was made by Larsen (1987) that proposed the use of prismatic specimens, as shown on Figure 4.8.

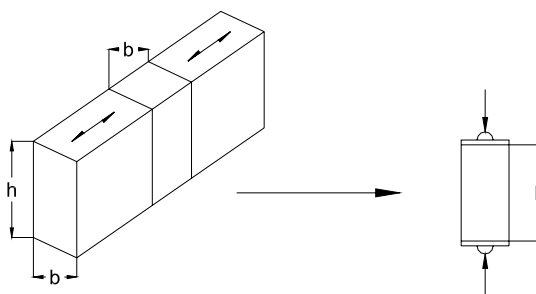


Figure 4.8 – Larsen's proposal (Larsen, 1987).

4.1.3 Conclusion

The definition of an appropriate strength model that defines the real resistance capacity based on material properties, involved actions and geometric conditions must be developed. In practical situations this criterion may be obtained based on: i) excessive deformation criterion, e.g., 10% of total deformation; ii) a random value based on the slope that the stress-strain diagram presents on the elastic domain or iii) based in an evident plastic behaviour.

Gehri (1991; 1997b) criticizes the incomprehensible situation growing with the inexistence of an uniform criterion able to represent a reliable support to the structural design: “...it is irresponsible to create standards without a retrospective knowledge of the problem...”.

EN 384 (CEN, 1995) standard proposes the following characteristic strength value in compression normal to grain:

$$f_{c,90,k} = 0.015 \cdot \rho_k \text{ (N/mm}^2\text{)} \quad (4.4)$$

with ρ_k (kg/m³). According to Gehri (1991), this value, frequently used as a design basis, doubles the real resistant capacity of wood in the direction perpendicular to grain, and points its inclusion on EN 338 (CEN, 1995) as the continuous cause for an incorrect use since the test method for the compression strength perpendicular to the grain in EN 1193 (CEN, 1997) was changed from a partial area to a full area loading test.

4.2 EXPERIMENTAL SET-UP

4.2.1 Material

The sample consisted of specimens of chestnut wood, $5 \times 5 \times 30 \pm 0.2$ cm, each taken from a clear, straight-grained portion. The ultrasonic tests were made on these original specimens and subsequently, each specimen was cut in three samples of $5 \times 5 \times 10 \pm 0.2$ cm: two for destructive testing and one for non-destructive testing (Pilodyn and Resistograph), see Figure 4.9.

In total, 164 specimens of chestnut wood were tested. The specimens were divided in two groups: new chestnut wood (NCW), which was never used structurally even so it comes from logs that could be used as such, and old chestnut wood (OCW), which was already used in structural elements from ancient constructions (date and precise origin unknown).

The two groups comprise clear wood specimens (reducing variability due to defects and allowing a better comparison of differences between samples) from the same provenance: North of Portugal.

The visual grading and inspection of the groups was carried out and in every specimen the number and dimension of knots, the slope of the grain and the colouring of the timber were investigated, being the worst specimens discarded.

The visual grading and grouping of the specimens, taking into account the orientation of the annual growth rings along the direction of the force, was not a simple task due to difficulties in visually grading all the specimens and including them in a specify group. Sometimes the orientation of the annual growth rings was not well defined, inducing an error on the grouping process. Some specimens were rejected to avoid a dual criterion. For example, it was difficult to find “truly” tangential and radial specimens for the OCW group.

The specimens were also divided in different groups taking into account the orientation of the annual growth rings in the RT plane with respect to the direction of the applied force. Therefore, four groups were considered: (a) diffuse, (b) diagonal, (c) tangential and (d) radial, as shown in Figure 3.3a (see Chapter 3).

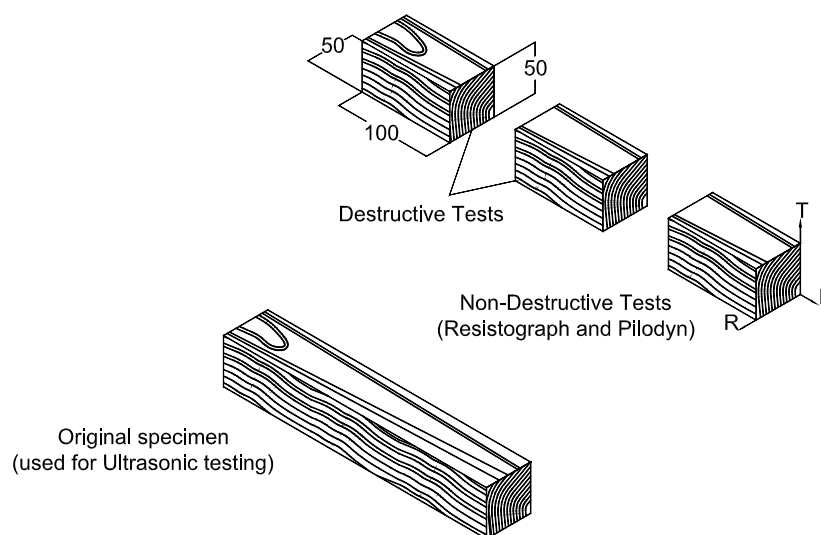


Figure 4.9 – Used specimens: nominal dimensions.

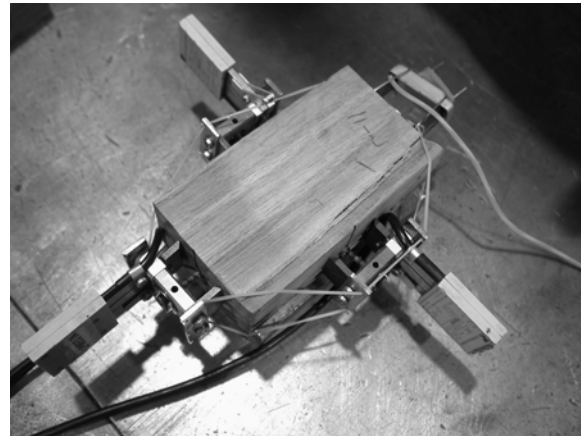
All the specimens were previously conditioned in a climatic chamber capable of keeping a temperature of $20 \pm 2^\circ\text{C}$ and a humidity of $65 \pm 5\%$. The tests specimens were considered conditioned when the density variation is smaller than 0.5% in a period of two hours, as recommended by the EN 408 standard (CEN, 2000). The weight was measured through an electronic weighing machine with a precision of 0.01 g.

4.2.2 Test set-up and equipment

The experimental research was carried out at the Structural Testing Laboratory of the National Laboratory for Civil Engineering, using a universal testing machine Baldwin, with a load cell of 300 kN (maximum) and a minimum strength of 6 kN. A power supply Schenk equipment was used, together with a HBM system (Spider 8) for data acquisition, see Figure 4.10a.



(a)



(b)

Figure 4.10 – Test set-up for destructive tests: (a) general view and (b) instrumented specimen.

The tests were carried using the NBr7190 (1997) standard with a rate of loading of 6×10^{-3} mm/s in the cyclical phase, and 6×10^{-2} mm/s in the last step (during the failure phase), being the stress-strain diagrams recorded continuously (see Figure 4.11). the loading rate applied was different from the value stated in the normative, because the tests were performed under displacement control and not under force control, as prescribed by the standard (testing machine limitation imposition). During testing, photographs were taken at different loading stages.

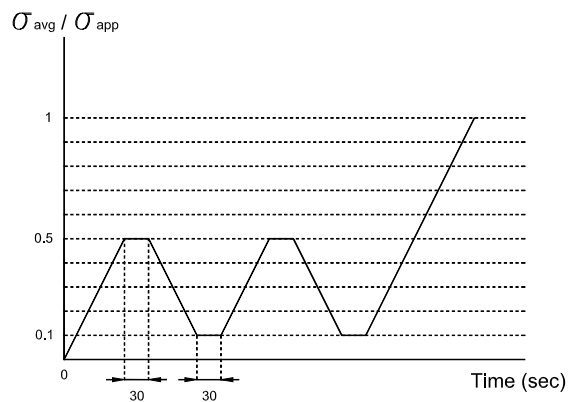


Figure 4.11 – Destructive testing procedure.

The adoption of a Brazilian standard is due to the lack of a Portuguese standard. On the other hand, European standards addressed the determination of characteristic values of mechanical properties of structural timber with defects.

Previously, a series of calibration tests of the apparatus was carried out, for the purpose of verifying the agreement between the vertical displacements in the faces of the tested specimens, measured using mechanical strain gauges, and the vertical displacements between the test machine platens, measured by LVDT's. Four mechanical strain gauges (one in each side of the faces) were used to measure the horizontal displacements and two additional LVDT's were placed in the arms of the test machine for measuring the vertical displacements, see Figure 4.12. Given the limitation on the strain gauges available at the laboratory, as shown in Figure 4.10b, three mechanical strain gauges from HBM (DD1 type) and one from Schenck were used. Problems related with insufficient adhesion made the readings from the latter not always effective.

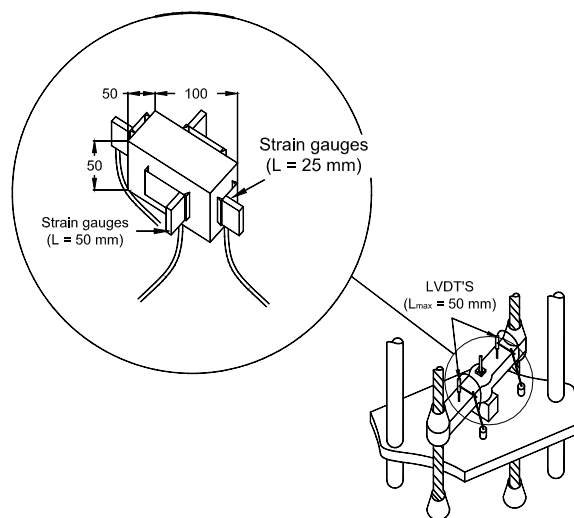


Figure 4.12 – Destructive tests apparatus.

The normal compressive strength ($f_{c,90}$) is the conventional value determined by the residual specific deformation of 2%, according to the NBr7190 standard (1997). The modulus of elasticity is equal to the slope of the linear part on the stress-strain curve (Figure 4.13), defined by the points ($\sigma_{10\%}; \varepsilon_{10\%}$) and ($\sigma_{50\%}; \varepsilon_{50\%}$) corresponding respectively to 10% and 50% of the conventional stress, in compression perpendicular to the grain, and it is given by:

$$E_{c,90} = \frac{\sigma_{50\%} - \sigma_{10\%}}{\varepsilon_{50\%} - \varepsilon_{10\%}} \quad (4.5)$$

where $\sigma_{10\%}$ and $\sigma_{50\%}$ are the normal stresses corresponding to 10% and 50% of the conventional stress ($f_{c,90}$), and $\varepsilon_{10\%}$ and $\varepsilon_{50\%}$ are the specific strains corresponding to the values of $\sigma_{10\%}$ and $\sigma_{50\%}$.

The relative moisture and the temperature during the tests were registered by an electronic device. During the tests, the average values of temperature and relative moisture were $24 \pm 2^\circ\text{C}$ and $52 \pm 12\%$, respectively.

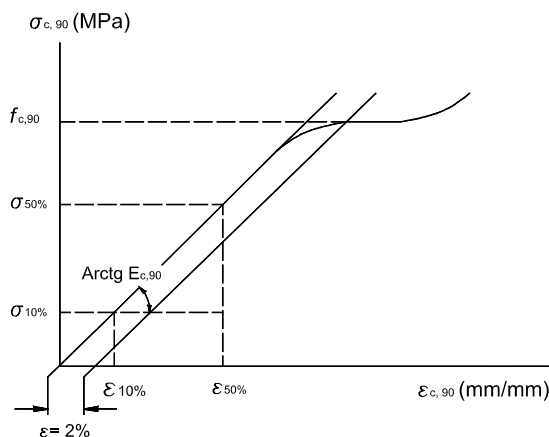


Figure 4.13 – Stress-strain relationship: definition of the normal compressive strength ($f_{c,90}$) following the NBr7190 (1997) standard.

4.3 RESULTS

4.3.1 Density determination

Table 4.1 shows the results obtained, where CV is the coefficient of variation.

Table 4.1 – Average and limit values of density (forty one specimens for each group).

	Density (kg/m ³)	
	NCW	OCW
Average	586.2	596.2
Max.	682.7	653.7
Min.	532.6	530.2
CV (%)	7	6

Table 4.2 presents the results for the characteristic and average density and the coefficient of variation organized according to two group types (loading orientation and age). The sample 5-percentile density ρ_k was calculated from the equation:

$$\rho_k = (\bar{\rho} - 1.64s) \text{ (kg/m}^3\text{)} \quad (4.6)$$

where $\bar{\rho}$ and s are the mean and standard deviation, in kilograms per cubic metre, of all specimens in the sample.

On average and for the complete 160 specimens sample, the densities of OCW and NCW groups are similar (differences smaller than 2%). Density differences between the smaller groups defined by loading orientation are larger, but still with a maximum of 5%: the maximum average density of a group is 607.9 kg/m³ for radial OCW and the minimum density of a group is 567.9 kg/m³ for tangential NCW. This indicates that, optimally, a larger sample would be required in each group.

Table 4.2 – Characteristic and average density (kg/m³).

	Radial		Diagonal		Tangential		Diffuse		Total	
	NCW	OCW	NCW	OCW	NCW	OCW	NCW	OCW	NCW	OCW
no. specimens	19	12	22	30	19	12	20	26	80	80
ρ_k (kg/m ³)	566.0	599.4	581.3	576.7	557.1	592.3	593.0	583.6	574.2	587.9
ρ_m (kg/m ³)	579.8	607.9	593.8	587.2	567.9	599.8	600.2	594.1	585.4	597.2
CV (%)	8.4	5.2	7.6	6.4	6.6	4.6	4.4	6.4	6.8	5.7

4.3.2 Destructive tests

The results of the destructive tests are presented taking into account the orientation of the annual growth rings along the direction of the force. Table 4.3 to Table 4.6 provide the values obtained for all groups and summarize the test statistics.

Table 4.3 – Radial specimens: NCW and OCW.

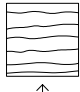
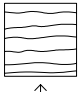
Radial (NCW)						Radial (OCW)					
	$E_{c,90}$ (N/mm ²)	Poisson			$f_{c,90}$ (N/mm ²)		$E_{c,90}$ (N/mm ²)	Poisson			$f_{c,90}$ (N/mm ²)
		ν_{RL}	ν_{TR}	ν_{LT}				ν_{RL}	ν_{TR}	ν_{LT}	
Average	783	0.04	0.33	0.13	7.45	Average	794	0.05	0.32	0.16	7.74
Max.	1015	0.06	0.39	0.18	10.84	Max.	1059	0.08	0.45	0.22	12.11
Min.	518	0.03	0.21	0.10	3.77	Min.	538	0.04	0.23	0.11	5.17
No.	19					No.	12				
CV (%)	15	17	11	13	22	CV (%)	19	27	18	18	28

Table 4.4 – Diagonal specimens: NCW and OCW.

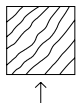
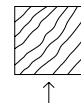
Diagonal (NCW)						Diagonal (OCW)					
	$E_{c,90}$ (N/mm ²)	Poisson			$f_{c,90}$ (N/mm ²)		$E_{c,90}$ (N/mm ²)	Poisson			$f_{c,90}$ (N/mm ²)
		ν_{RL}	ν_{TR}	ν_{LT}				ν_{RL}	ν_{TR}	ν_{LT}	
Average	612	0.06	0.36	0.18	6.99	Average	601	0.06	0.35	0.17	6.67
Max.	752	0.08	0.44	0.22	9.93	Max.	712	0.08	0.43	0.24	8.74
Min.	516	0.04	0.30	0.11	3.69	Min.	505	0.04	0.29	0.11	3.73
No.		22				No.		30			
CV (%)	12	16	9	13	19	CV (%)	9	17	8	16	16

Table 4.5 – Tangential specimens: NCW and OCW.

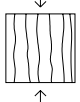
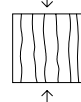


Tangential (NCW)						Tangential (OCW)					
	$E_{c,90}$ (N/mm ²)	Poisson			$f_{c,90}$ (N/mm ²)		$E_{c,90}$ (N/mm ²)	Poisson			$f_{c,90}$ (N/mm ²)
		ν_{RL}	ν_{TR}	ν_{LT}				ν_{RL}	ν_{TR}	ν_{LT}	
Average	526	0.05	0.28	0.19	6.58	Average	569	0.06	0.33	0.17	7.47
Max.	695	0.07	0.39	0.25	8.62	Max.	688	0.06	0.38	0.18	9.20
Min.	383	0.04	0.22	0.16	5.17	Min.	483	0.05	0.29	0.14	6.39
No.		19				No.		12			
CV (%)	14	18	13	13	14	CV (%)	10	8	9	7	10

Table 4.6 – Diffuse specimens: NCW and OCW.

Diffuse (NCW)						Diffuse (OCW)					
	$E_{c,90}$ (N/mm ²)	Poisson			$f_{c,90}$ (N/mm ²)		$E_{c,90}$ (N/mm ²)	Poisson			$f_{c,90}$ (N/mm ²)
		ν_{RL}	ν_{TR}	ν_{LT}				ν_{RL}	ν_{TR}	ν_{LT}	
Average	552	0.04	0.26	0.16	6.22	Average	607	0.04	0.27	0.15	6.81
Max.	673	0.05	0.32	0.19	7.34	Max.	911	0.05	0.32	0.22	10.10
Min.	466	0.02	0.13	0.11	5.23	Min.	422	0.02	0.21	0.09	3.39
No.		20				No.		26			
CV (%)	11	22	16	13	10	CV (%)	21	22	12	18	21

The CV values can be interpreted optimistically. The large heterogeneity of wood does not allow usually a good statistical interpretation of the results: the variations between the elastic and strength properties are sometimes considerable, but taking into consideration the obtained results (average CV of 16% and large samples), the values do seem representative. Higher values of CV,

for the elastic and strength properties, are obtained for Radial (OCW) orientation due the few number of specimens tested.

In general, the OCW group shows higher values, for the elastic and strength properties, than the NCW group, i.e., the mechanical characteristics of old wood are slightly higher than the new wood (4-11%). A reason for this it not clear but it is likely that old specimens have been obtained from larger trees. But a firm conclusion is that time, acting alone, did not change the mechanical and physical properties of wood. The design of new timber structures and rehabilitation projects can be done in the same way, using similar mechanical data for new and old wood. These conclusions have been reported earlier by Kuipers (1986) and Togni (1995).

As a first approach, wood's microstructure in the radial direction can be regarded usually as a sandwich construction consisting of alternating layers with completely different mechanical properties (Müller *et al.*, 2003). From the results it is easy to infer that transverse compressive strength decreases to a minimum in the diffuse orientation for the NCW group, followed by the tangential and diagonal orientations. For the OCW group, diagonal specimens present the lowest values of compressive strength; followed by the diffuse and tangential specimens. In both cases the radial specimens present higher values indicating that perpendicular to the grain compressive strength decreases to a minimum at an annual ring orientation of 45° with respect to the direction of loading that is corroborated by the OCW group. However the compressive strength perpendicular to the grain is minimal in NCW group when loaded "diffusely".

The radial behaviour can be explained by the relations between earlywood and latewood percentages: higher radial strength corresponds to a low properties of latewood layers. These layers have a supporting effect in the radial direction and a weakening effect when stressed across their long axes. In the OCW group the percentage of latewood layers is higher (working tangentially as continuous parallel elements that transfer the force between layers) the radial stress ratio decrease. In radial compression, in which the dense latewood layers are arranged in series between weak earlywood bands the limiting factor is the "weak-layered" earlywood. The initial failure is caused by this earlywood "weak-layer" and follows by others with increasing load, decreasing the cross section height, see Figure 4.14. As a limit, and as a result of the large compaction of the earlywood layers, the final aspect of the specimen can be compared to a "thin" global layer.

Due to the early collapse of these layers when compressed perpendicularly, some precautions will have to be carried out concerning the evaluation of the earlywood/latewood percentage ratio in specific design situations or industrial manufacturing of wood products. Nevertheless, the differences observed between radial and tangential compressive strength are small (13% in NCW and 3.5% in OCW).

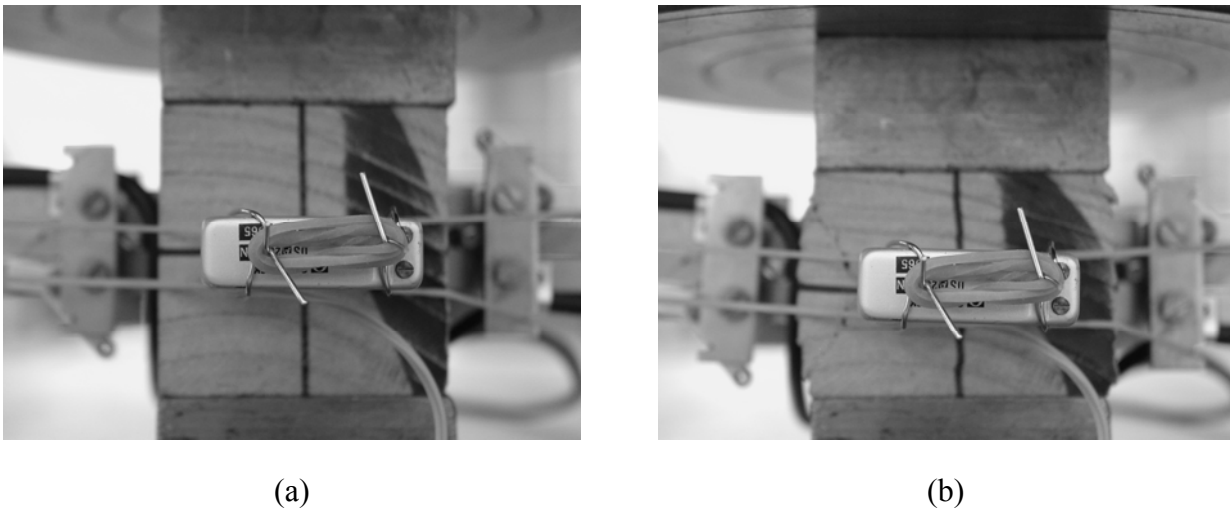


Figure 4.14 – Typical radial behaviour: (a) unloaded test specimen, and (b) test specimen at failure.

The diagonal behaviour can be classified as an intermediate situation: i) the initial failure is caused by an initial earlywood “weak-layer” and follows by others with increasing load, decreasing the cross section height, similar to the radial behaviour (see Figure 4.15), and ii) failure is caused by the early bond failure between earlywood and latewood layers. With increasing load, separation (slope) between these layers can be observed, similar to the tangential behaviour.

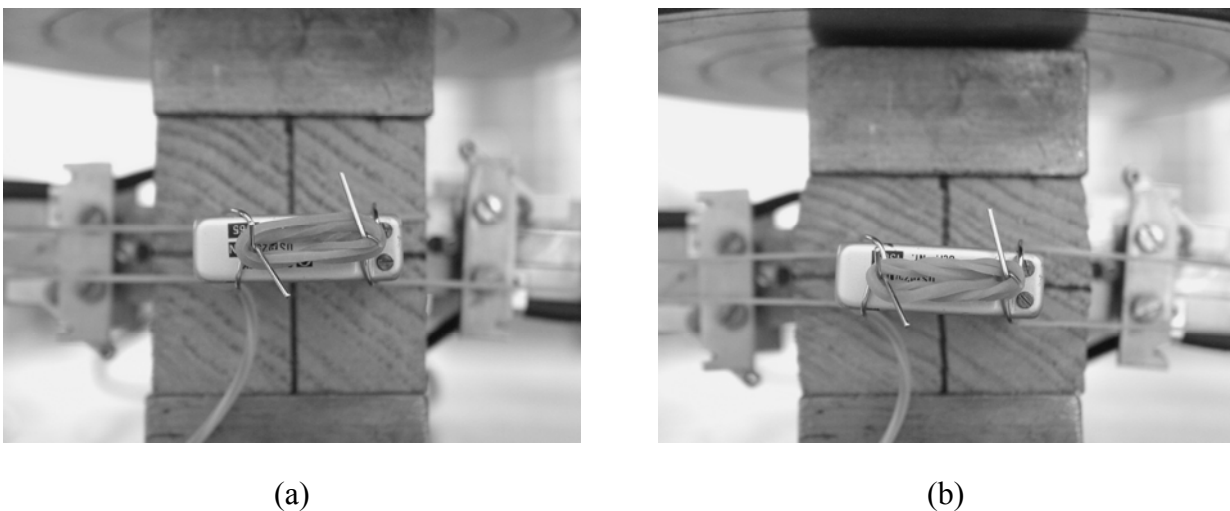


Figure 4.15 – Typical diagonal behaviour: (a) unloaded test specimen, and (b) test specimen at failure.

The tangential behaviour can be explained by the early bond failure between earlywood and latewood layers. With increasing load one can observe a separation (slope) between these layers, see Figure 4.16. Also, buckling failure can be observed as a result of the low slenderness that individual earlywood and latewood layers show along their axes.

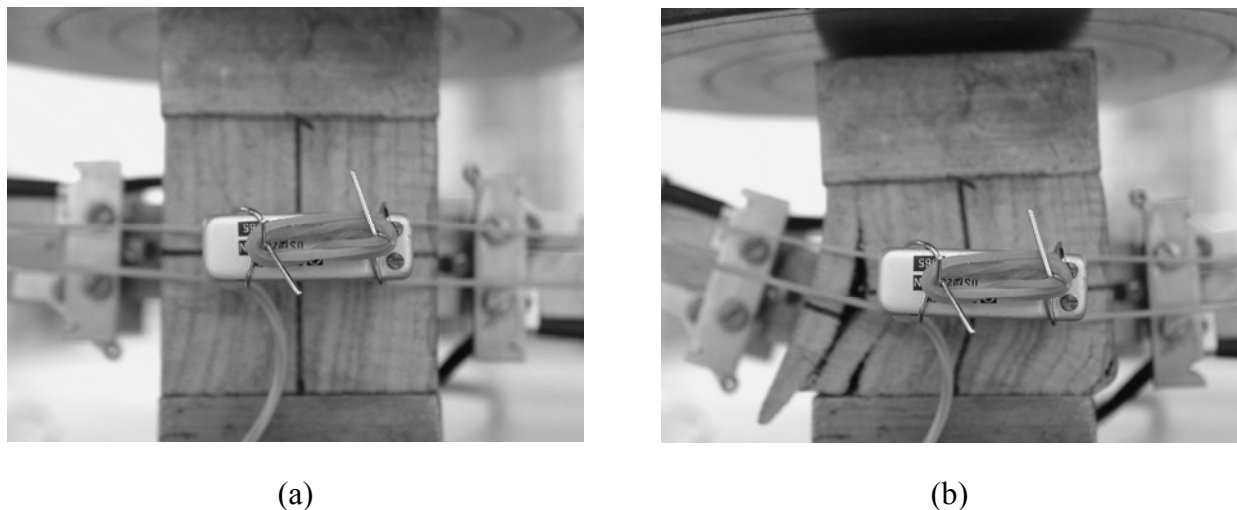


Figure 4.16 – Typical tangential behaviour: (a) unloaded test specimen, and (b) test specimen at failure.

The diffuse orientation must be considered as an attempt to simulate what would happen in real structures, in which load is often not aligned with the annual growth ring orientation. The arbitrary distribution of the annual growth ring orientation can make the task of property identification rather complex due to the ilimited possible failures modes. In the tests, a diffuse specimen could have an orientation and a failure mode similar to the radial direction but also similar to the tangential or diagonal directions.

Experimental measurements of Poisson's ratios for wood have traditionally been tedious and difficult, partly due to equipment limitations. As a result, very few data is available and difficulties are frequently encountered in structural analysis.

Zink *et al.* (1997) reported that Poisson's ratios are not constant during the loading process, which is true due the nonlinear behaviour of the material. In the present work, Poisson's ratios were calculated as the ratio of expansion strain perpendicular to the load (ε_x) over the compression strain parallel to the load (ε_y) due to the compressive load, and were calculated using strains obtained within the elastic portion of the stress-strain diagram:

$$\nu_{xy} = -\frac{\varepsilon_{x,50\%} - \varepsilon_{x,10\%}}{\varepsilon_{y,50\%} - \varepsilon_{y,10\%}} \quad (4.7)$$

Expansion strain and compressive strain used to calculate a given Poisson's ratio for a test specimen was the average of strains for either the expansions strains or the compressive strains, as recommended by NBr7190 (1997). Poisson's ratios present low values in the RT plane (ν_{RL}). It is noted that the strength results presented in Table 4.3 to Table 4.6 reveal good agreement with the literature values (Bucur and Archer, 1984; U.S. Forest Products Laboratory, 1999). However, limited data are available for comparison of Poisson's ratios.

Basic characteristic compression strength values according to EN 384 (CEN, 1995) and to the destructive tests are summarized in Table 4.7. As shown, there are significant differences between the values proposed by the EN 384 (CEN, 1995), calculated using Eq. 4.4, and the experimental results. The main conclusion is that the normative values are, approximately, 70% higher than the real strength of wood. These results have been pointed by Gehri (1991), which found normative values around 100% higher than experimental values.

For each group a 5-percentile value $f_{c,90,05}$ was determined by ranking all the test values for a group in ascending order. The 5-percentile value is the test value for which 5% of the values are lower, as recommended by EN 384 (CEN, 1995). The average values ($f_{c,90,mean}$) are also given in Table 4.7.

Table 4.7 – Compression perpendicular to the grain: proposed and obtained results.

		Characteristic compressive strength values (N/mm ²)							
		Radial		Diagonal		Tangential		Diffuse	
		NCW	OCW	NCW	OCW	NCW	OCW	NCW	OCW
EN 384	$f_{c,90,k}$	7.49	8.34	7.79	7.88	7.59	8.32	8.35	7.96
Exp.	$f_{c,90,05}$	4.70	4.21	4.10	4.75	5.10	6.28	5.21	4.43
Tests	$f_{c,90,mean}$	7.45	7.74	6.99	6.67	6.58	7.47	6.22	6.81

Figure 4.17 through Figure 4.20 show selected results of the experimental programme; the complete results are given in Annex 2. This sequence shows typical stress-strain diagrams (up to 10% total deformation in the diagonal group, up to 20% total deformation in the tangential and diffuse group and up to 30% total deformation in the radial group) for NCW and OCW in the several annual growth rings orientation considered.

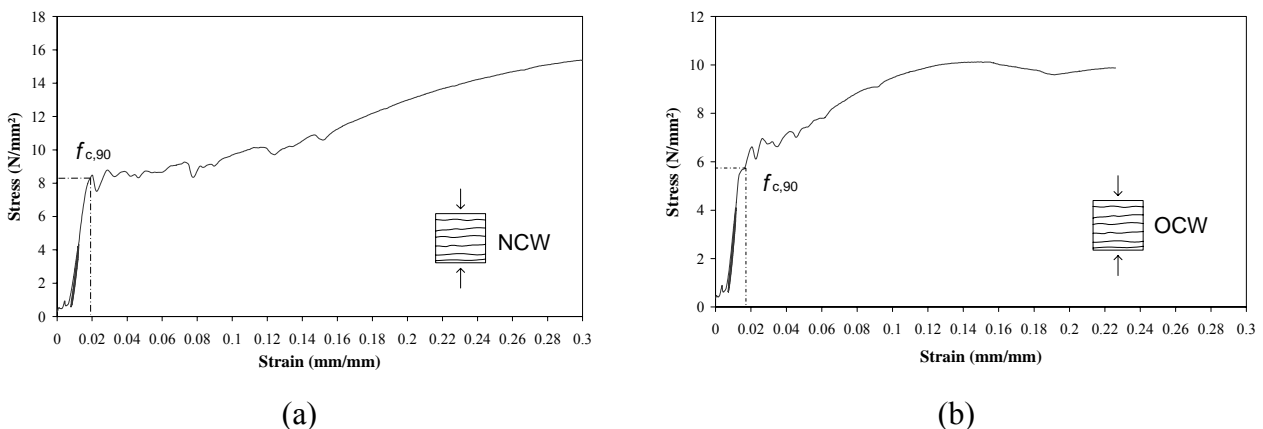


Figure 4.17 – Typical stress-strain diagrams for compression perpendicular to the grain and radial orientation of annual growth rings: (a) NCW; (b) OCW.

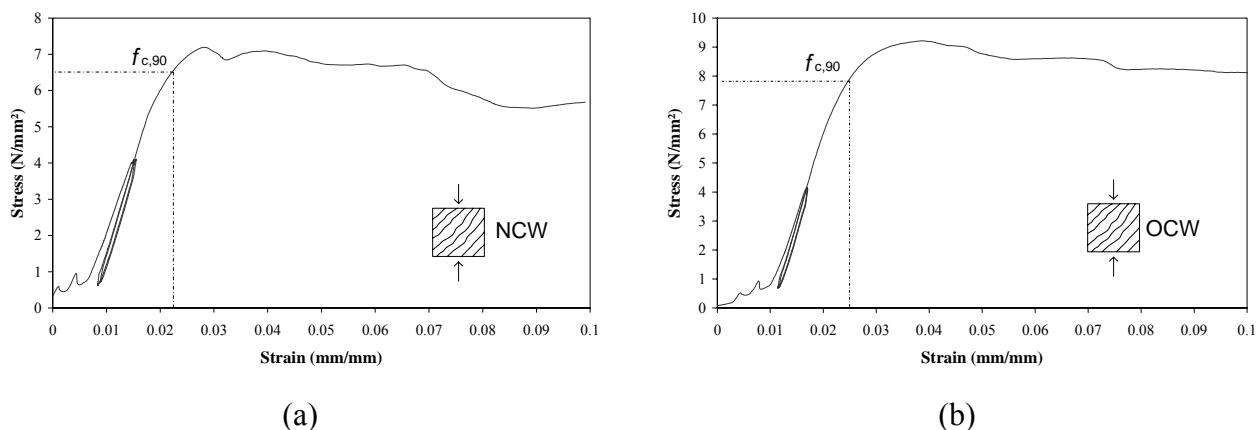


Figure 4.18 – Typical stress-strain diagrams for compression perpendicular to the grain and diagonal orientation of annual growth rings: (a) NCW; (b) OCW.

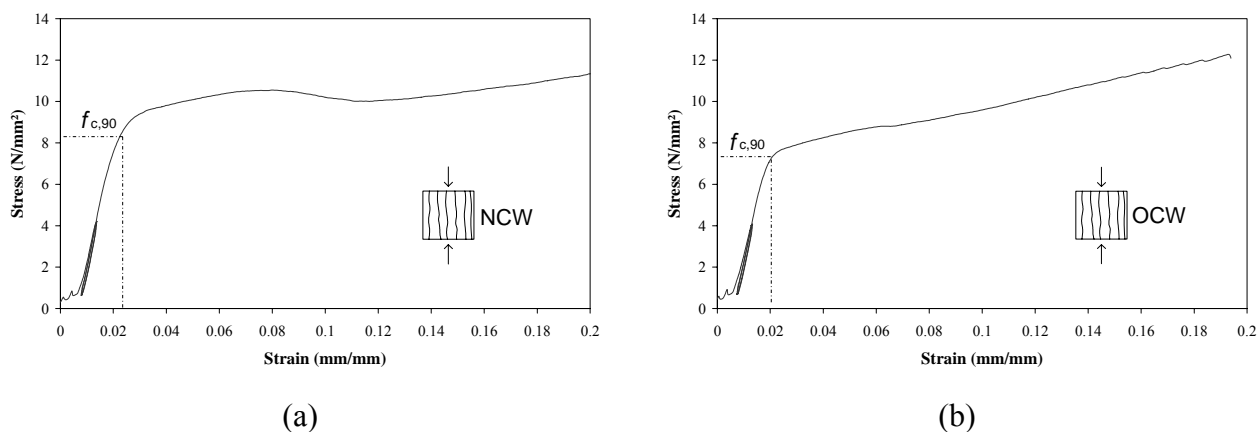


Figure 4.19 – Typical stress-strain diagrams for compression perpendicular to the grain and tangential orientation of annual growth rings: (a) NCW; (b) OCW.

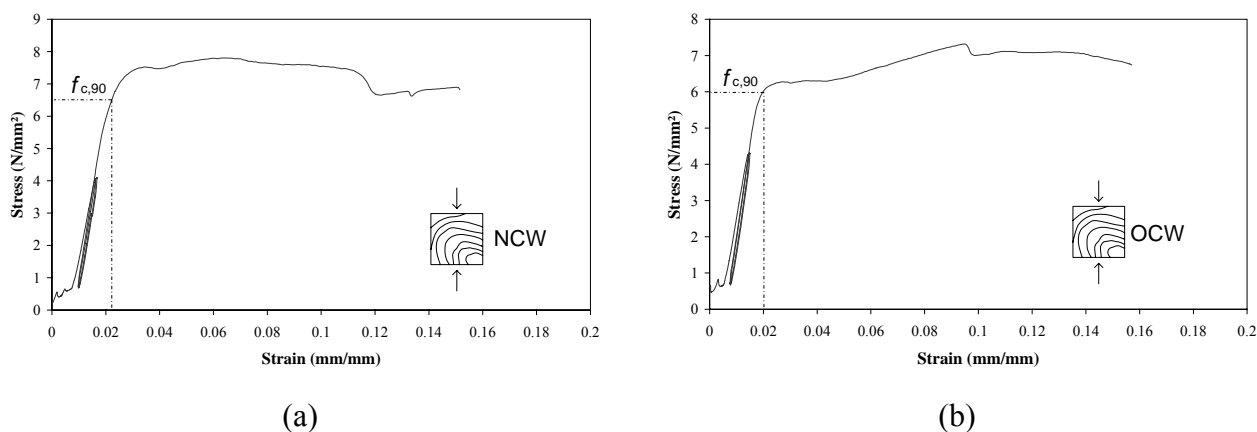


Figure 4.20 – Typical stress-strain diagrams for compression perpendicular to the grain and diffuse orientation of annual growth rings: (a) NCW; (b) OCW.

The stress-strain diagrams obtained along the various orientations of the annual growth rings considered are rather different. In radial compression the stress-strain diagrams show some particularities that may be analyzed:

- in a first phase, the diagrams always start with an upward curvature which also occurs in the other species types and is due to the adjustment of the specimen to the plates, followed by a straight line and finalized by a downward curve. The change from initial linear elastic deformation to the first failure of wood, located in the weakest earlywood layer (buckling of a portion of rays located in a growth ring), as observed by Bodig (1965), occurs with a sudden load drop. According to several authors (Bodig, 1963; Kunesh, 1968; Tabarsa and Chui, 2000; Tabarsa and Chui, 2001) and corroborated by this work, the initial maximum stress value is determined by the weakest earlywood layer (created naturally by various anatomical elements), and the strength of the latewood and other earlywood layers add very little to this value. Rays act as spaced columns and fail simultaneously as a single unit. As pointed out by Courtney (2000) when the cell wall material is brittle, failure corresponds to the fracture of cell-walls;
- in a second phase, a plateau is obtained, graphically represented by irregular saw-tooth shapes, reported by Bodig (1965) as “micro-stress-strain diagrams”, corresponding to the fracture of individual cell walls (initial average plateau stress lies below the initial failure stress) follow by a densification zone where the additional failures occur in the same or in several other earlywood layers as the compression progresses (Bodig, 1965; Tabarsa and Chui, 2000; Tabarsa and Chui, 2001). This densification zone is responsible for the redistribution of stress and strain to growth rings that have not failed, corresponding graphically to a stress increase;
- in a third phase, the strain increases rapidly, due to the compaction of the material.

In conclusion, radial compression initial failure occurs at the weakest layer by compression and lateral deformation. With increasing deformation, the global stability governs failure.

In tangential compression the stress-strain diagrams do not show a marked maximum stress value as in radial compression (elastic phase gradually merges into a plateau zone until a region where the strain increases rapidly to the same load value), and the failure will be characterized by the buckling of the latewood bands. It is noted that maximum strength could not be reached up to a strain level of 20%, because the rays are normal to the load direction and are just compressed.

In accordance to the literature (Bodig, 1965; Müller *et al.*, 2003), it is observed that minor differences exist between the proportional limit stresses in radial compression or in tangential compression. The assumed 0.2% total strain threshold can be seen easily in the stress-strain diagrams of the different directions. Even if in some situations wood fails at this strain level, usually this level corresponds still to the elastic portion of the stress-strain diagram, denoting the conservative character of the NBr7190 (1997).

Figure 4.21 illustrates the good relation between the normal compressive stress and the compressive modulus of elasticity and represents the upper and lower 95% confidence limit, which have an important role in practical purposes.

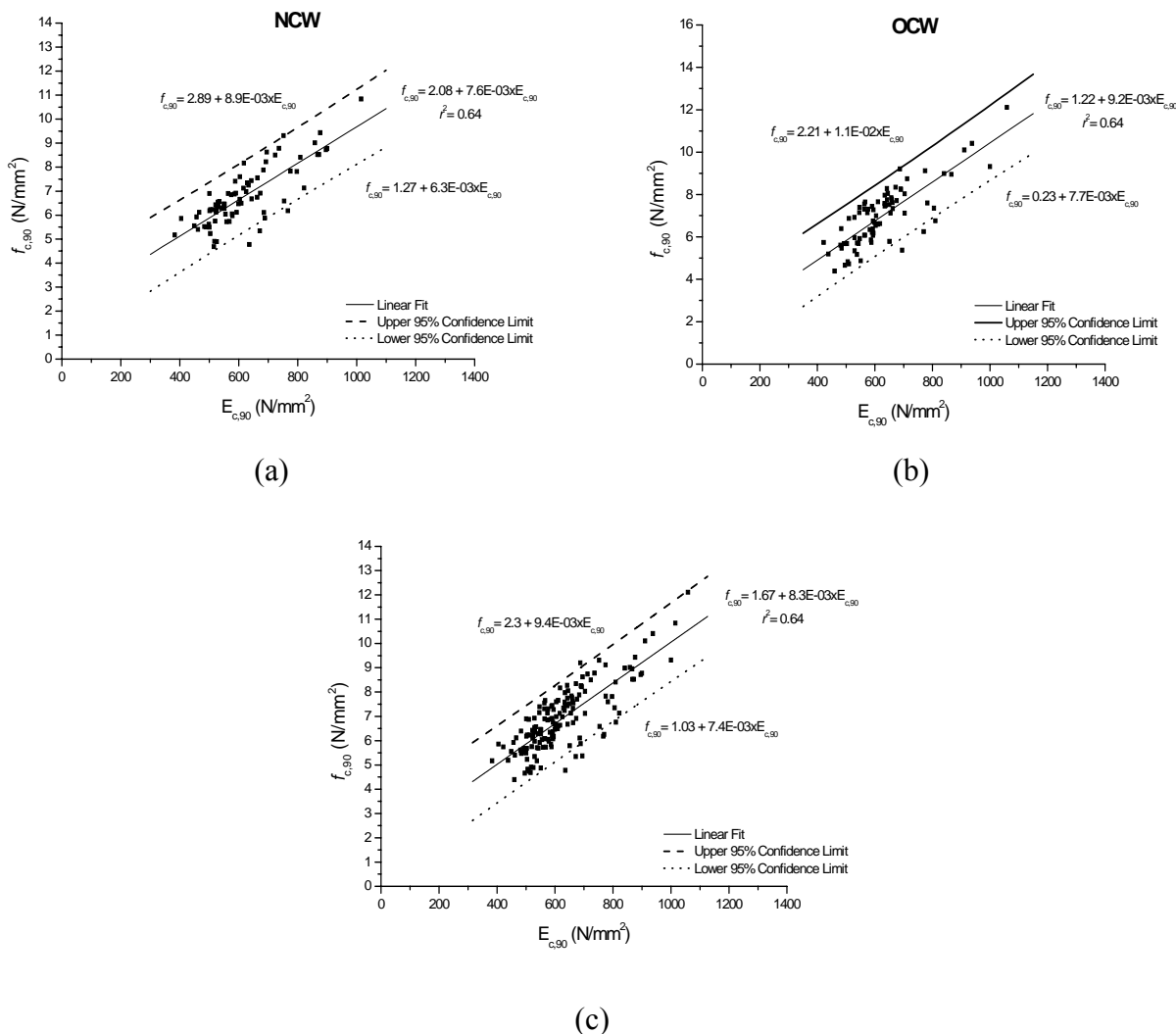


Figure 4.21 – Relation between $f_{c,90}$ and $E_{c,90}$: (a) for the NCW group, (b) for the OCW group, and (c) for both considered groups.

4.3.3 Ultrasonic pulse velocity method

Table 4.8 to Table 4.10 provides the values measured for all specimens. The values obtained with ultrasonic testing emphasize the relation between the dynamic and static moduli of elasticity. The data found indicate that the acoustic wave transmission preferably follows the direction of larger stiffness, showing a dependence of the wave propagation on the elastic properties of material, which takes into account the directions of the annual growth rings, as reported by Green (1991).

The results confirm the better mechanical properties of the OCW group, already observed in the destructive tests. The ultrasonic wave transmission characteristics are very similar in the Direct Method, parallel to the grain, and in the Indirect Method.

In these two methods the layers of latewood/earlywood are parallel to the direction of transmission, justifying the similar results, see Figure 4.22. Again, the diffuse group shows better results for NCW specimens than OCW specimens but the random distribution of the annual growth rings does not allow a final conclusion in this case.

Table 4.8 – Direct method, perpendicular to the grain: NCW and OCW.

Dynamic modulus of elasticity (N/mm²)								
Direct Method, perpendicular to the grain								
	Radial		Diagonal		Tangential		Diffuse	
	NCW	OCW	NCW	OCW	NCW	OCW	NCW	OCW
Average	2946	3009	1878	1821	1408	1692	1618	1901
No.	19	12	21	30	19	12	20	26
CV (%)	10	6	10	10	14	10	9	22

Table 4.9 – Indirect method: NCW and OCW.

Dynamic modulus of elasticity (N/mm²)								
Indirect Method								
	Radial		Diagonal		Tangential		Diffuse	
	NCW	OCW	NCW	OCW	NCW	OCW	NCW	OCW
Average	11798	13063	11782	11501	12004	14196	12385	11710
No.	19	12	21	30	19	12	20	26
CV (%)	12	15	13	11	8	6	10	7

Table 4.10 – Direct method, parallel to the grain: NCW and OCW.

Dynamic modulus of elasticity (N/mm²)								
Direct Method, parallel to the grain								
	Radial		Diagonal		Tangential		Diffuse	
	NCW	OCW	NCW	OCW	NCW	OCW	NCW	OCW
Average	13739	12588	12735	15769	13320	12588	15181	14027
No.	19	12	21	30	19	12	20	26
CV (%)	15	2	19	17	14	2	22	13

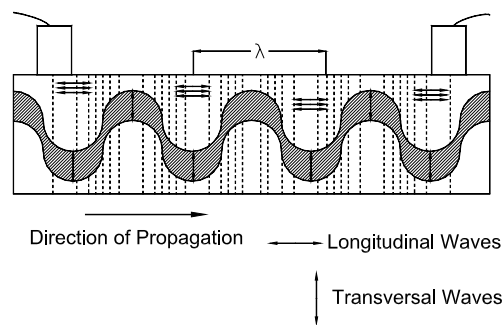


Figure 4.22 – Propagation of the ultrasonic waves.

In the Direct Method, perpendicular to the grain, the results are very different in comparison with the two methods above mentioned. This difference is due to the anatomical characteristics of wood. The dissipation of energy occurs in the boundary of earlywood/latewood layers, and naturally, part is reflected and the remaining part is transmitted to the next layer (depending on the acoustic impedance). Because of this, and taking into account the natural disposition of wood elements, the ultrasonic wave propagation will be faster in longitudinal direction (Direct Method, parallel to the grain, and Indirect Method) than in transversal direction.

Machado (2000) studied several parameters related with the wave energy and form, and observed that, in propagation perpendicular to the grain, the energy transference in the radial plane is 50% higher than in the tangential plane, which is also supported by the present work. These results were also observed by other authors (Bucur, 1995; Tiita *et al.*, 1998; Machado, 2000). A possible explanation of this phenomenon is the presence, in the radial direction, of continuity elements (wood rays) that do not exist in the tangential direction (Machado, 2000). Bucur (1995) found differences between the velocities of propagation in these two directions, for ring porous wood, around 17%; in the present work the difference was of 22%.

4.3.4 Correlations based in the NDE methods

4.3.4.1 Correlations with density

A linear correlation between density, normal compressive stress and modulus of elasticity perpendicular to the grain seems adequate to represent the test results, as shown in Figure 4.23 to Figure 4.25.

The agreement between density and normal compressive stress is good and shows clearly the relation between these two properties. However, the agreement between density and elasticity modulus is not so good. The variations of density observed in the specimens are a plausible reason: the percentage of latewood/earlywood layers has a considerable influence in the results.

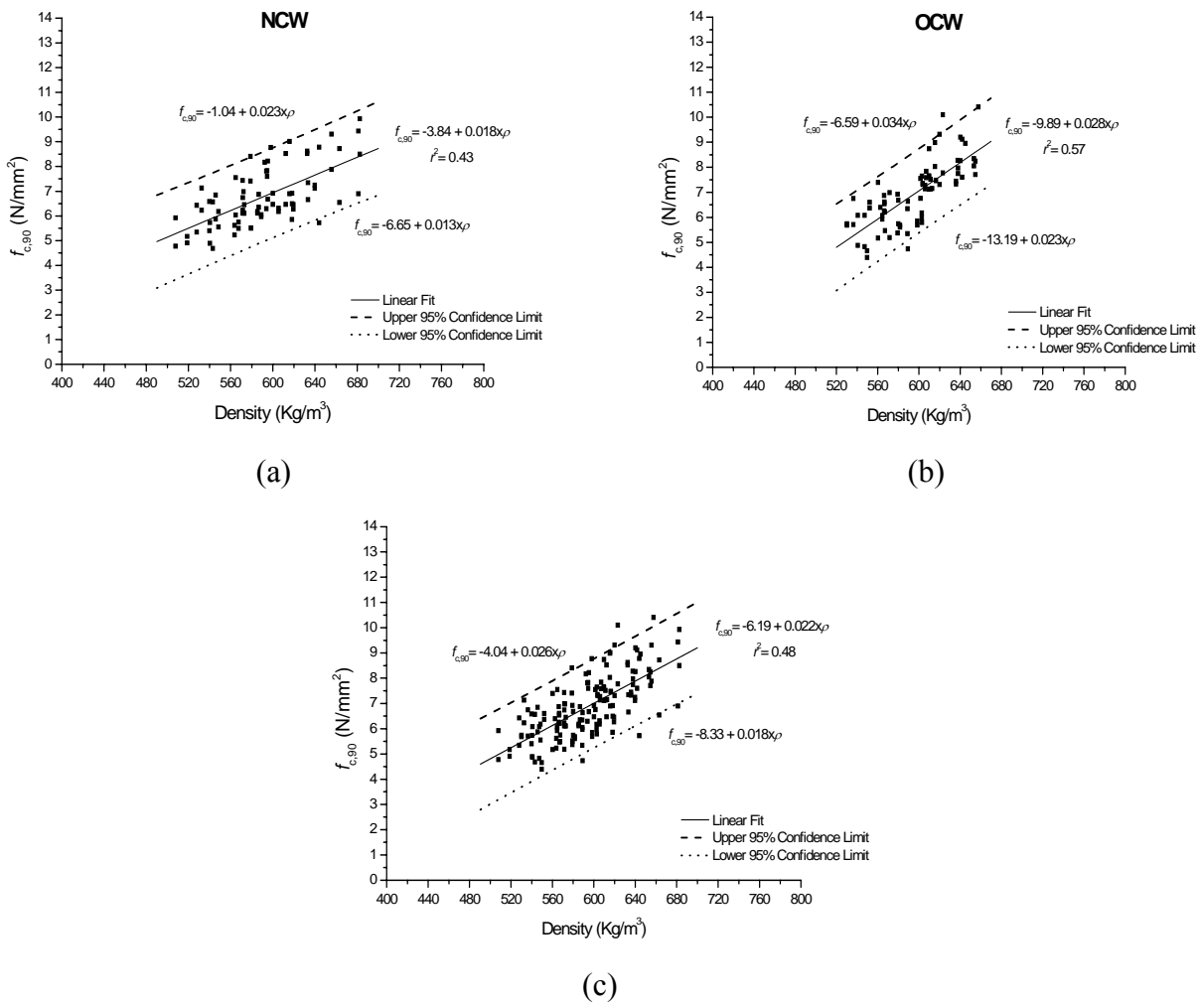


Figure 4.23 – Relation between $f_{c,90}$ and density for the: (a) NCW group, (b) OCW group, and (c) NCW and OCW groups.

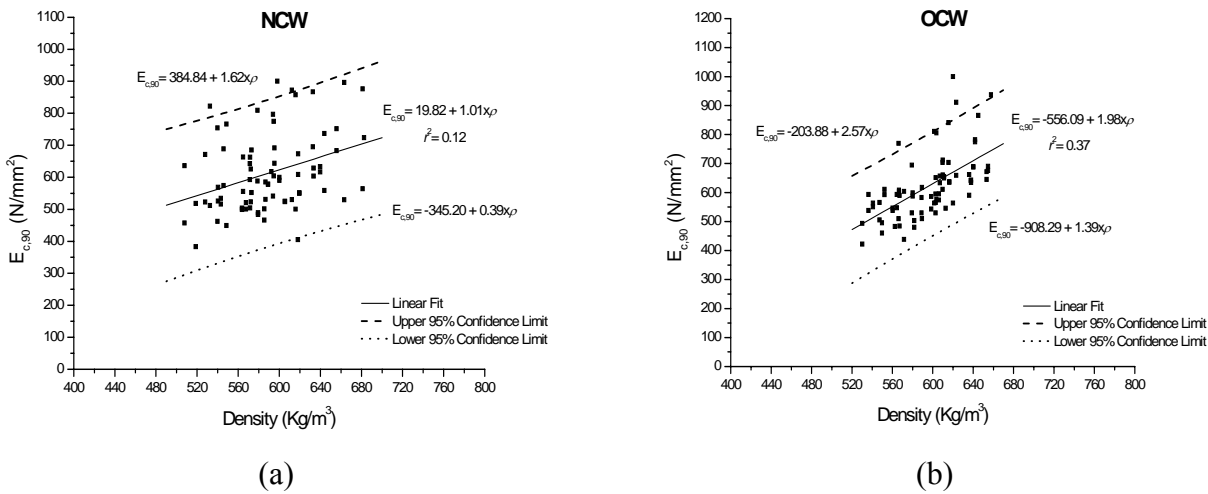


Figure 4.24 – Relation between $E_{c,90}$ and density: (a) for the NCW group, (b) for the OCW group.

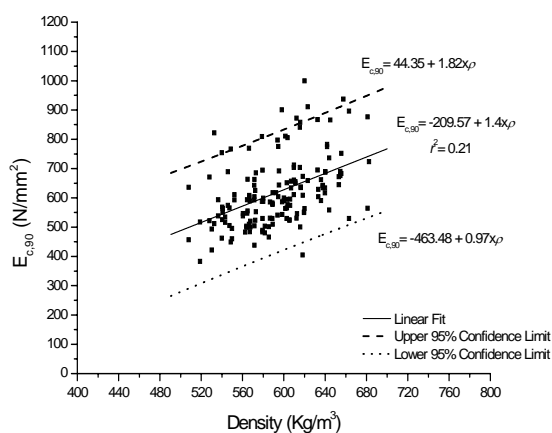


Figure 4.25 – Relation between $E_{c,90}$ and density for both considered groups.

Figure 4.26 and Figure 4.27 show the correlations between resistographic measure and density of each specimen for the NCW group and for the OCW group, and for both groups.

The scatter in the results is too high and no correlation can be found between the two quantities. In addition, the difference between the groups of NCW and OCW is also too large. Generally, the resistographic measure values are slightly higher for the NCW group than for the OCW group: this is explained by the presence of a higher percentage of latewood in the NCW group, despite the average density of the OCW group being higher than the density of the NCW group. For practical purposes, it is not recommended to use this measure as a quantitative indicator. Considering all tests together, a lower 95% confidence limit is given by the following expression:

$$\rho = 456.8 + 0.27 \cdot RM \tag{4.8}$$

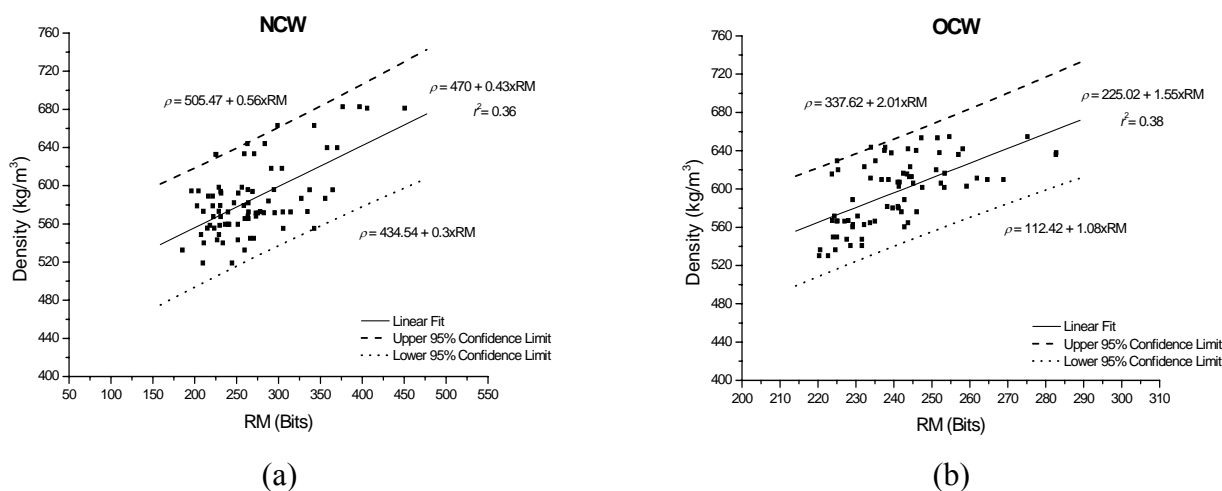


Figure 4.26 – Relation between RM and density: (a) NCW, and (b) OCW.

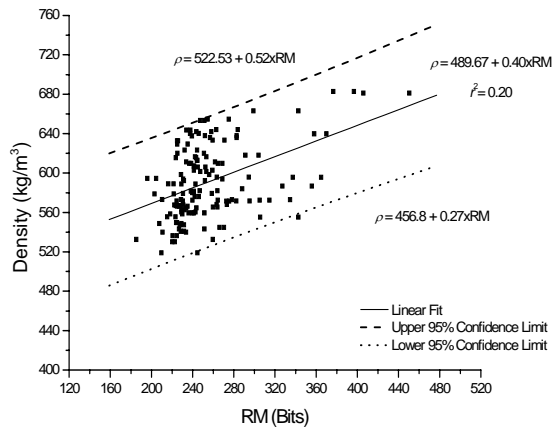


Figure 4.27 – Relation between RM and density for NCW and OCW groups.

Figure 4.28 and Figure 4.29 show the correlations between the pin depth of the Pilodyn and the density for the NCW and OCW groups, and for both groups. The scatter in the results is moderate and a reasonable correlation between the two quantities is found. The results are independent of the orientation of the annual growth rings and the wood age.

Considering all tests together, the average correlation is given by the following expression (r^2 is equal to 0.78):

$$\rho = 1115.16 - 60.1 \cdot \text{Depth} \tag{4.9}$$

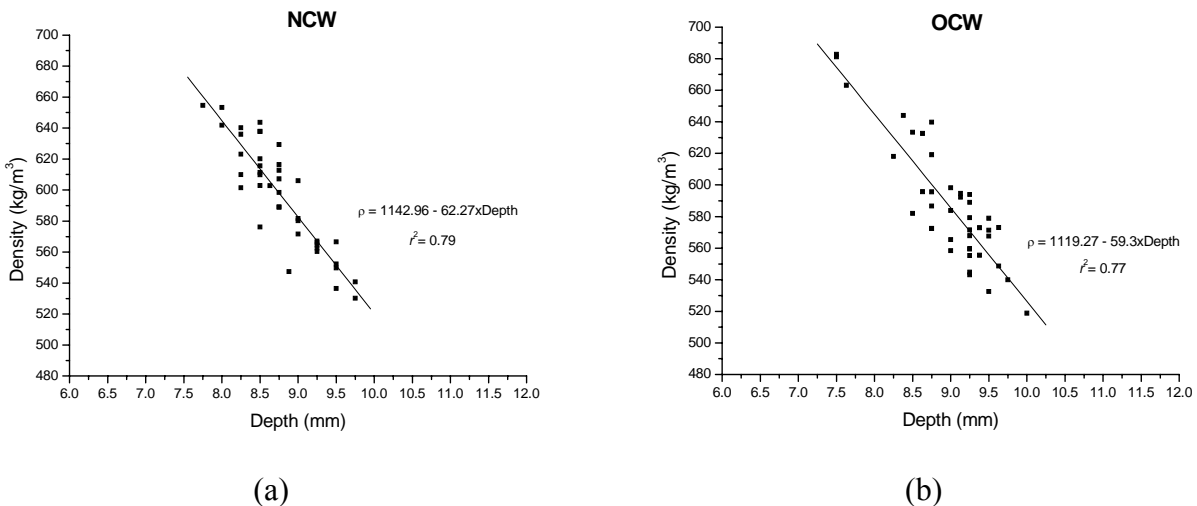


Figure 4.28 – Relation between pin depth (Pilodyn) and density: (a) NCW group, and (b) OCW group.

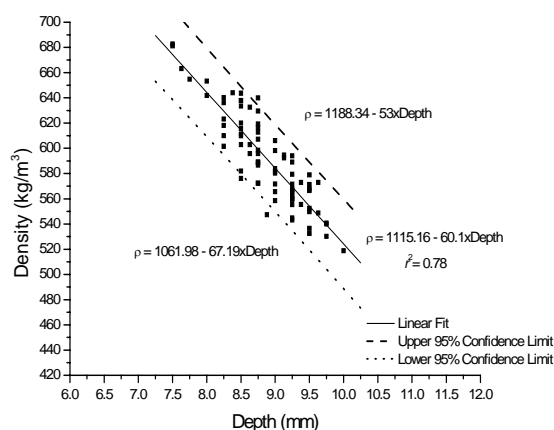


Figure 4.29 – Relation between pin depth (Pilodyn) and density for both groups.

It is noted that the pin penetrates only 6 to 14 mm into wood. This means that it penetrates only between one and three annual growth rings. Therefore, the result is only superficial and care must be taken in practical applications, taking into account if the outer surface is deteriorated due to biological attack.

4.3.4.2 Correlations with the elasticity modulus

Figure 4.30 shows the results between $E_{c,90}$ and E_{din} using the Indirect Method (the results of the two other methods are less relevant for practical purposes and are given in Annex 2). The inclusion of the Indirect Method is related with the further utilization of this method in the evaluation of the elastic properties of traditional wooden-wooden joints.

As expected, very good linear correlations were found but it is necessary to use different correlations according to the load orientation and wood age. In the comparison of the same loading direction but different ages, it is striking that the slope of the linear correlations is equal in the case of the radial specimens, it is similar in the case of the diagonal and tangential specimens (analysed separately), and it is totally different in the case of the diffuse specimens. This is obviously due to the possibility of rather different configurations of the annual growth rings for the diffuse specimens. Also, these results are in agreement with the discussion provided in the previous section.

It is noted that the correlations with E_{din} are much better than with the UPV, meaning that the knowledge of the wood density is of utmost importance for obtaining reliable correlations.

Considering all tests together, a lower 95% confidence limit is given by the following expression:

$$E_{c,90} = -74.4 + 0.035 \cdot E_{din} \tag{4.10}$$

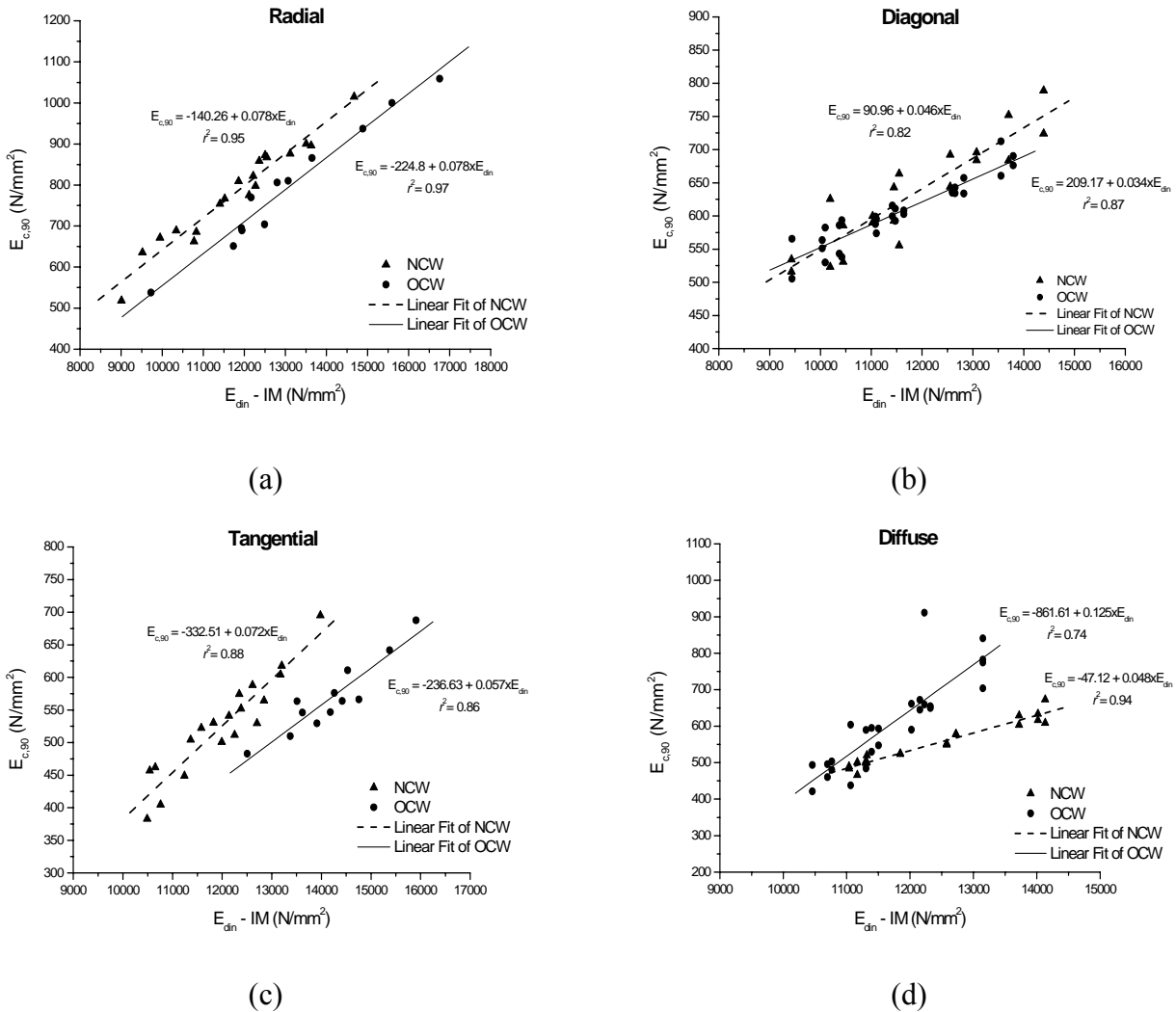


Figure 4.30 – Relation between E_{din} and $E_{c,90}$, using the Indirect Method, for the: (a) radial group, (b) diagonal group, (c) tangential group, and (d) diffuse group, for both NCW and OCW groups.

Some authors tried to find correlations between strength and stiffness characteristics, and punctual hardness or drill resistance properties. The results show that these methods are reliable only for an early evaluation of basic density of the wood, rather than for mechanical grading of the wood elements.

Figure 4.31 show the correlations between the resistographic measure and the elasticity modulus for the NCW and OCW groups. Weak linear correlations were found and it is necessary to use

different correlations according to the load orientation and wood age. For practical purposes, it is not recommended to use this measure as a quantitative indicator.

Considering all tests together, a lower 95% confidence limit is given by the following expression:

$$E_{c,90} = 68.11 + 0.98 \cdot RM \tag{4.11}$$

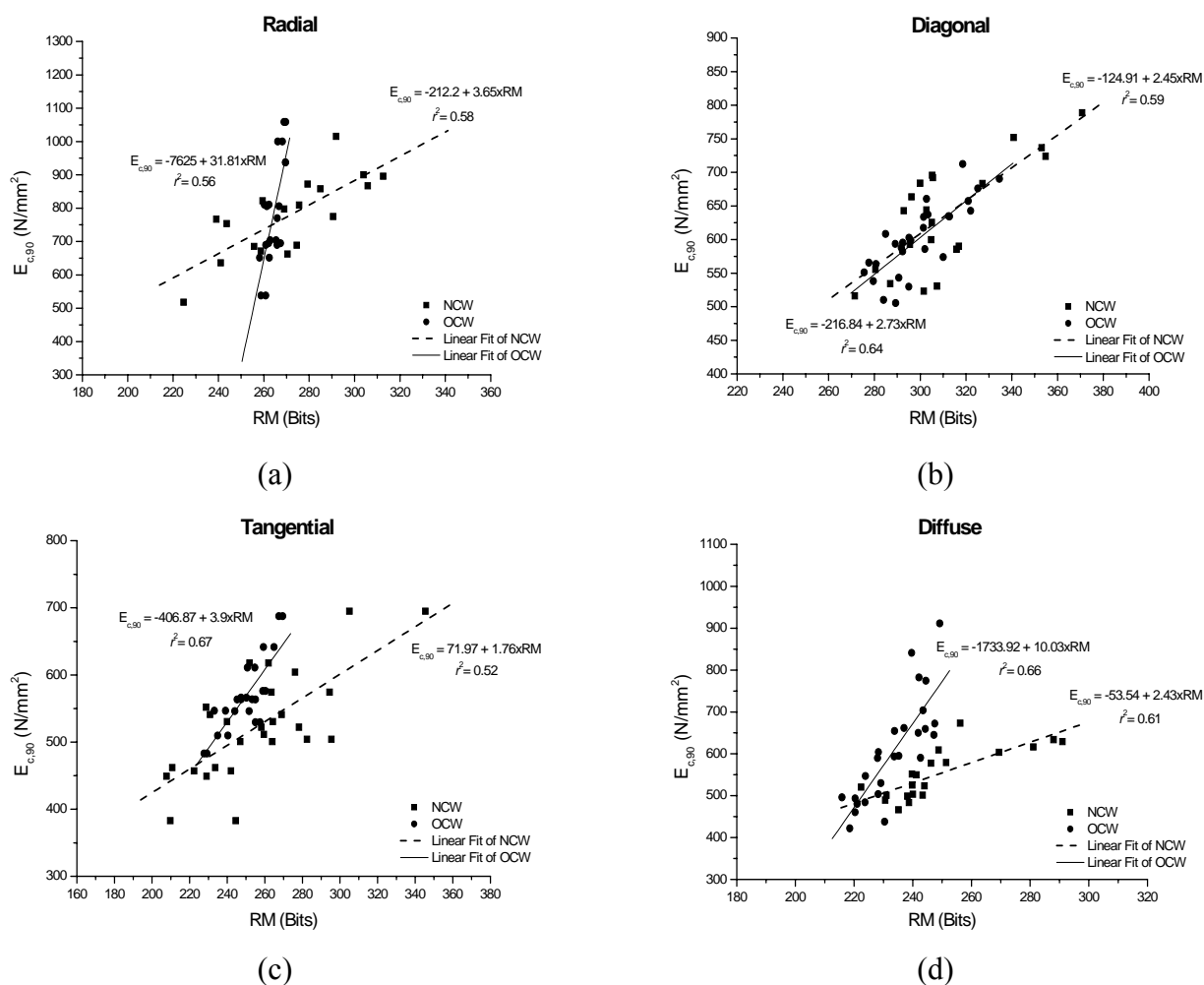


Figure 4.31 – Relation between RM and $E_{c,90}$ for the: (a) radial group, (b) diagonal group, (c) tangential group, and (d) diffuse group. Both NCW and OCW are considered.

Figure 4.32 shows the correlation between the depth reached with the needle of the Pilodyn device and the elasticity modulus for the NCW and OCW groups. No correlation was found and it is not recommended to use this measure as a quantitative indicator.

Still, a lower 95% confidence limit is given by the following expression:

$$E_{c,90} = 714.36 - 82.46 \cdot Depth \tag{4.12}$$

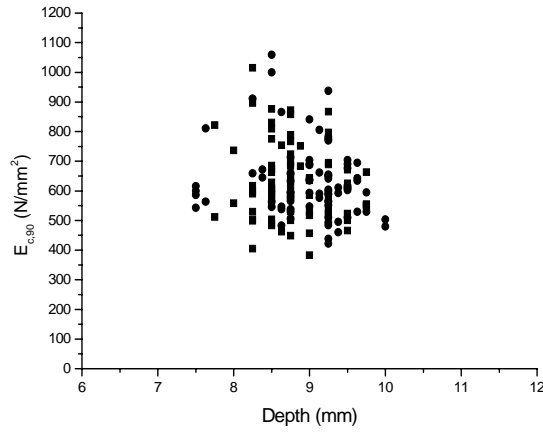


Figure 4.32 – Relation between pin depth (Pilodyn) and $E_{c,90}$ for the NCW and OCW groups.

4.3.4.3 Correlations with the strength

Figure 4.33 and Figure 4.34 show the correlations between E_{din} and $f_{c,90}$ using the Indirect Method. Good linear correlations were found but, again, it is necessary to use different correlations according to the load orientation and wood age.

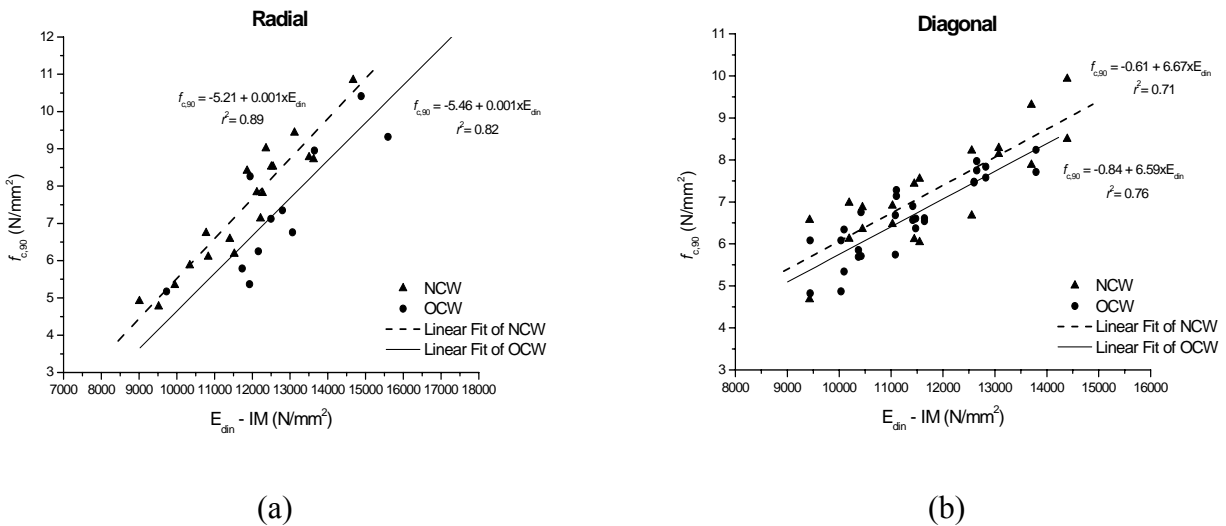


Figure 4.33 – Relation between E_{din} and $f_{c,90}$, using the Indirect Method, for the: (a) radial group, and (b) diagonal group. Both NCW and OCW are considered.

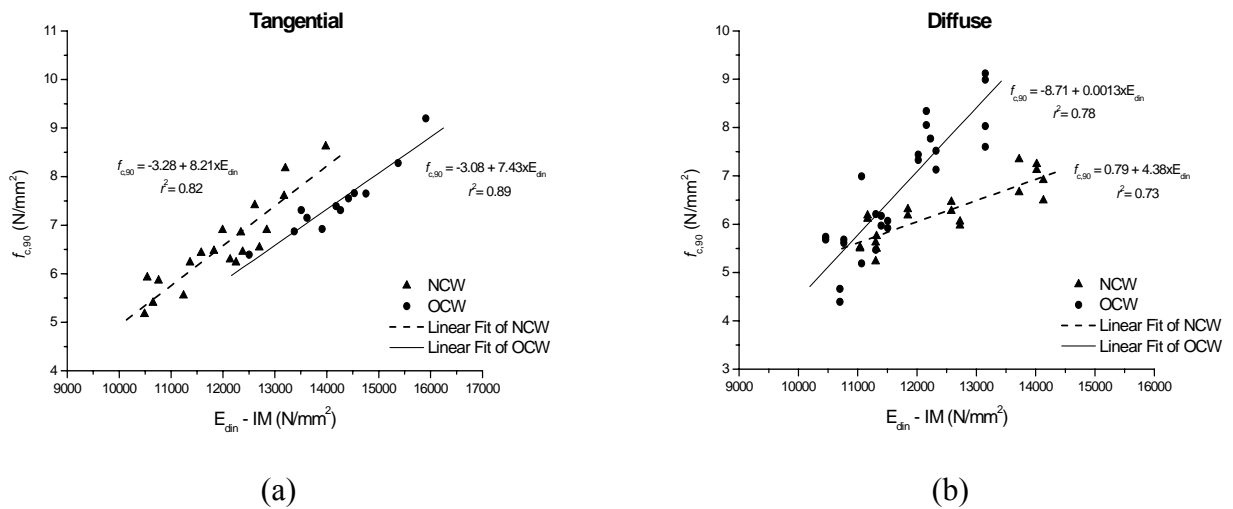


Figure 4.34 – Relation between E_{din} and $f_{c,90}$, using the Indirect Method, for the: (a) tangential group, and (b) diffuse group. Both NCW and OCW are considered.

If the comparison is made for the same loading direction but different ages, it is even more striking that the slope of the linear correlations is equal in the case of the radial, diagonal and tangential specimens (analysed all separately), and it is totally different in the case of the diffuse specimens.

Considering all tests together, a lower 95% confidence limit is given by the following expression:

$$f_{c,90} = -2.33 + 5.82 \cdot E_{din} \quad (4.13)$$

Figure 4.35 show the correlations between the resistographic measure and the uniaxial compressive strength for the NCW and OCW groups.

Moderate linear correlations were found but it is necessary to use different correlations according to the load orientation and wood age. For practical purposes, it is not recommended to use this measure as a quantitative indicator.

Considering all tests together, a lower 95% confidence limit is given by the following expression:

$$f_{c,90} = 0.67 + 0.011 \cdot RM \quad (4.14)$$

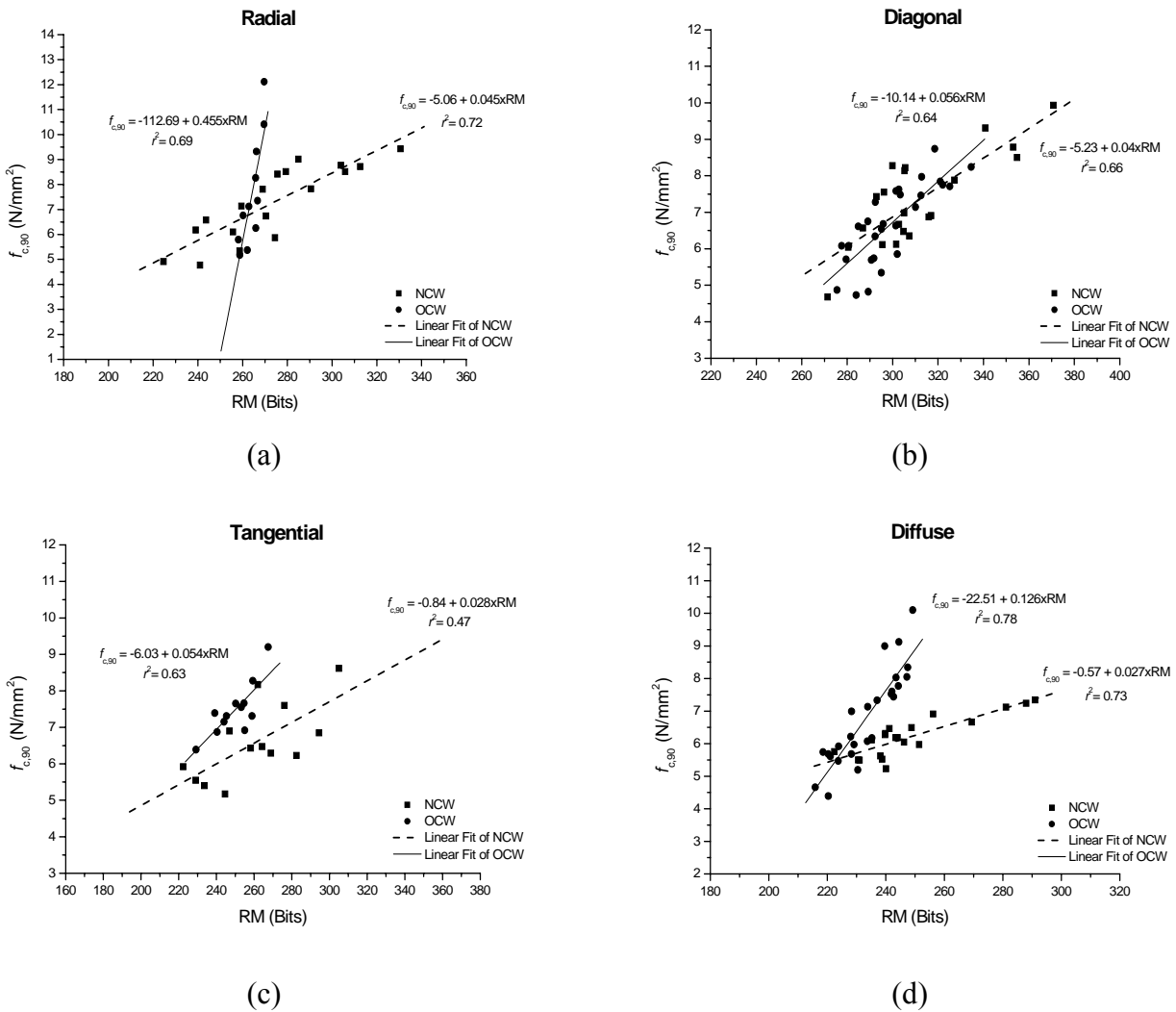


Figure 4.35 – Relation between RM and $f_{c,90}$ for the: (a) radial group, (b) diagonal group, (c) tangential group, and (d) diffuse group. Both NCW and OCW are considered.

Figure 4.36 shows the correlation between the depth reached with the needle of the Pilodyn device and the elasticity modulus for the NCW and OCW groups. Again, no correlation was found and it is not recommended to use this measure as a quantitative indicator.

Still, a lower 95% confidence limit is given by the following expression:

$$f_{c,90} = 7.67 - 0.85 \cdot Depth \tag{4.15}$$

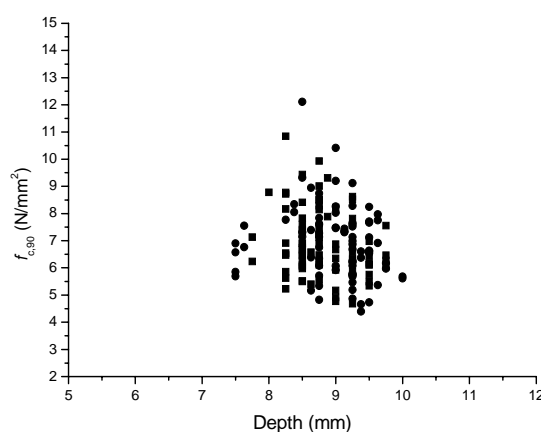


Figure 4.36 – Relation between pin depth (Pilodyn) and $f_{c,90}$ for the NCW and OCW groups.

4.4 CONCLUSIONS

The analysis of the tests carried out in timber specimens indicates that results must take into account the orientation of the annual growth rings, not only in terms of numerical values but also in terms of observed failure modes. Both new and old sound chestnut wood are considered in the testing program.

As a first conclusion, it is possible to confirm that no mechanical damage was presented in the timber beams (from which OCW specimens were obtained) due to service loads. The design of new timber structures and rehabilitation projects can be carried out using similar mechanical and physical values for new and old chestnut wood. A second conclusion is that transverse elasticity modulus and compressive strength reach a maximum for radial orientation of loading, and the global behaviour can be explained by the relation between earlywood and latewood.

Finally, novel correlations have been proposed for density, elasticity modulus and compressive strength perpendicular to the grain, using the Resistograph, Pilodyn and ultrasonic testing. With respect to density, the Resistograph must be used carefully because no correlation could be found, while the results for the Pilodyn provide good correlations that are independent of the wood age. With respect to mechanical characteristics, reasonable correlations have been obtained in general taking into account the wood age and loading orientation. As this is not reasonable for practical purposes, expressions with a lower 95% confidence have been proposed.

The correlations obtained with the dynamic modulus of elasticity via ultrasonic testing were very good but this requires the knowledge of the density, which adds complexity to the non-destructive testing technique.

The following conclusions can also be obtained from the present chapter:

- transverse compressive strength decreases to a minimum to the diffuse and tangential orientation, followed by the diagonal and radial orientations;

- compressive strength values predicted through EN 384 (CEN, 2004) are significantly higher (70%) than the experimental values;
- ultrasonic wave transmission characteristics are similar in Direct Method, parallel to the grain, and Indirect Method;
- the Indirect Method proved to be a reliable method in the evaluation of the elastic properties of chestnut wood, since it can be used for evaluating different zones of the element and only needs one face of the element to be accessible;
- Resistograph method showed to have moderate correlations with elastic mechanical properties;

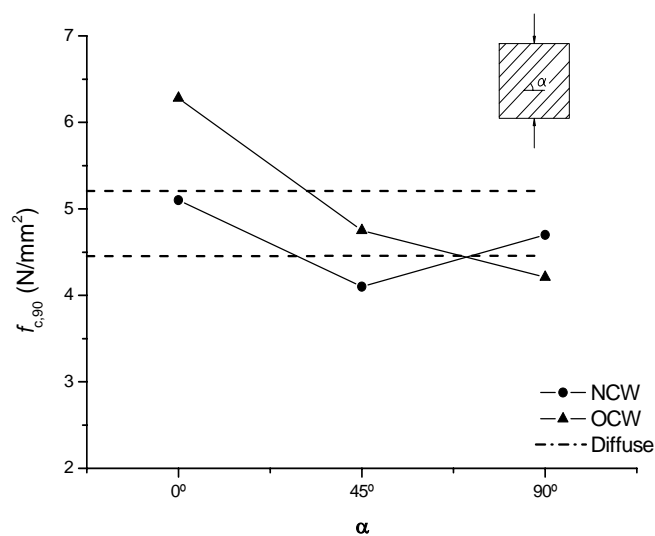


Figure 4.37 – Compressive strength versus annual ring orientation, for the NCW and OCW group.

Chestnut wood in compression parallel to the grain. Evaluation by non-destructive methods

Every material is distinguished by characteristics peculiar to itself. Knowledge of them are a necessary prerequisite for processing the material appropriately and the design of timber structures usually considers the exceptional capacity of wood to withstand loading parallel to the grain. Therefore, understanding of the wood behaviour parallel to the grain is of crucial importance for design and safety assessment purposes, see Figure 5.1.

Compressive strength parallel to the grain ($f_{c,0}$) of clear wood is between 40 and 60 percent of the bending strength in that direction and between 30 and 50 percent of the tensile strength (U.S. Forest Products Laboratory, 1999). The ratio of strength properties varies depending upon density and tracheids length which have a strong positive correlation with compressive strength parallel to the grain (Gong and Smith, 2000; Gong and Smith, 2004).

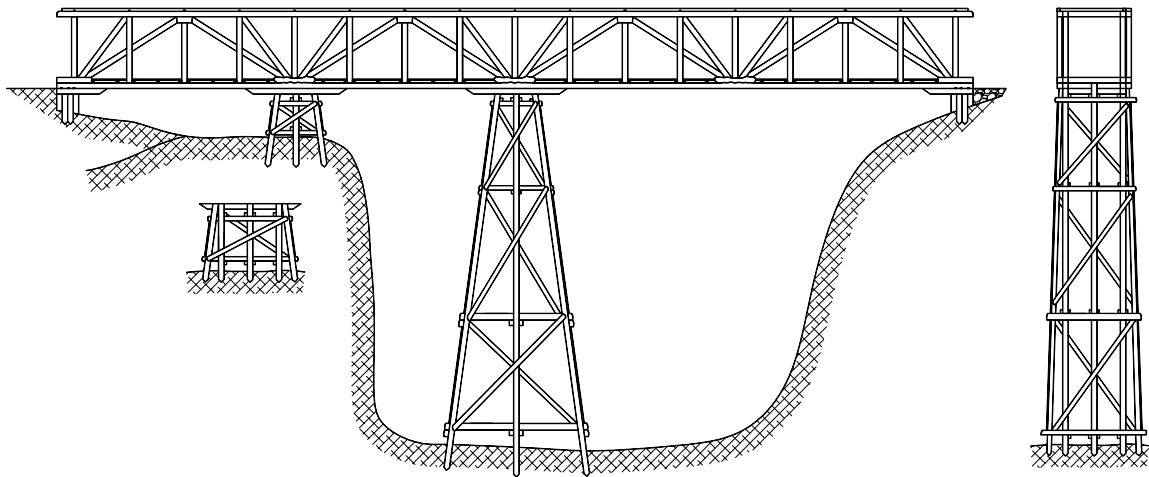


Figure 5.1 – Typical wooden structure where studs have an important role.

Static compressive strength of clear wood is usually characterized via tests on prismatic specimens taking into account that to subject these specimens to pure compression it is needed that the axial length of the specimens be minor than the dimensions of the base. If the condition:

$$\lambda = \frac{l}{r} \leq 10 \quad (5.1)$$

where λ represents the slenderness ratio, l is the length of the specimen and r is the minimum radius of gyration, is verified a pure compressive state occurs otherwise a punctual load situation could be considered.

5.1 EXPERIMENTAL SET-UP

5.1.1 Material

Visual inspection of chestnut wood specimens in their final testing dimensions was carried out, being removed specimens showing knots and significant slope of grain (superior to 1:10). In total, 94 specimens were selected and divided into two distinct groups (NCW and OCW). As for the other mechanical tests the provenance of the specimens was the Northern region of Portugal.

Specimen dimension of $50 \times 50 \times 200$ mm were used with the longitudinal (long) axis being oriented in the parallel to the grain direction, see Figure 5.2. These specimens have the dimensions recommended by ASTM standard D143-94 (1994).

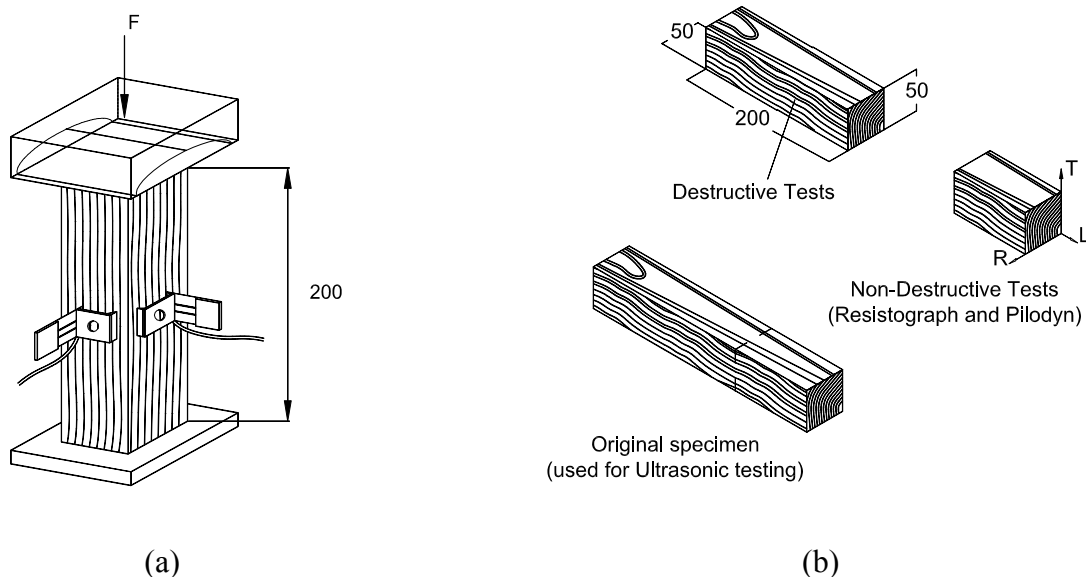


Figure 5.2 – Specimens used in the testing program (nominal dimensions in mm): (a) prismatic test specimen, and (b) compressive and non-destructive tests.

All the specimens were previously conditioned in a climatic chamber capable of keeping a temperature of $20 \pm 2^\circ\text{C}$ and a humidity of $65 \pm 5\%$. The tests specimens were considered

conditioned when the density variation is smaller than 0.5% in a period of two hours, as recommended by the EN 408 standard (CEN, 2000). The densities were measured through an electronic weighing machine with a precision of 0.01 g.

Before testing, the top of the specimens were slightly dried, to guarantee that failure initiates and develops away from the ends of each specimen, as recommended by ASTM standard D143-94 (1994). This causes a slight local straightening, which is enough to avoid failure in the tops.

5.1.2 Test set-up and equipment

The tests were carried taking into account the method specified in the standard Nbr7190 (1997) and were conducted in a universal testing machine (Baldwin), with a loading cell of 300 kN. An acquisition system (HBM – Spider 8) capable of measuring the load with an accuracy of 1% and the deformation with an accuracy of 0.001 mm was setting up (see Figure 5.3a and Figure 5.3b). Although Nbr7190 (1997) was used to rule the test procedure, the test specimens geometry are similar to the recommended by ASTM standard D143-94 (1994).



Figure 5.3 – Compression testing: (a) general view, and (b) test piece under testing.

The rate of loading was force controlled (test's machine limitation imposition) and the load was applied at a constant rate ($v = 4 \times 10^{-2}$ mm/s) so that the maximum load was attained within the range 5 min \pm 2 min as imposed by the standard, see Figure 5.4. Compressive failure parallel to the grain is a progressive and stable process, and the failure mechanism has been found to be insensitive to the loading rate. However, this does not mean that other mechanical properties are unaffected by it (Renaud *et al.*, 1996; Gong and Smith, 2004).

In order to improve alignment of the specimens and promote uniform stress distribution over the top surfaces one of the platens was equipped with a spherical bearing.

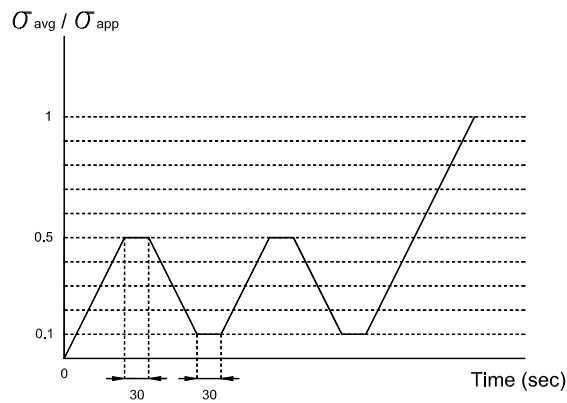
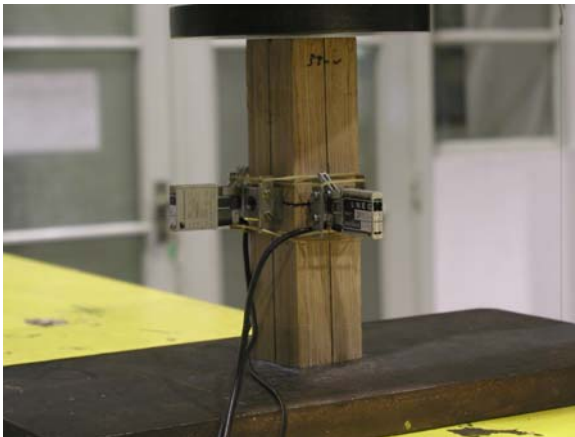


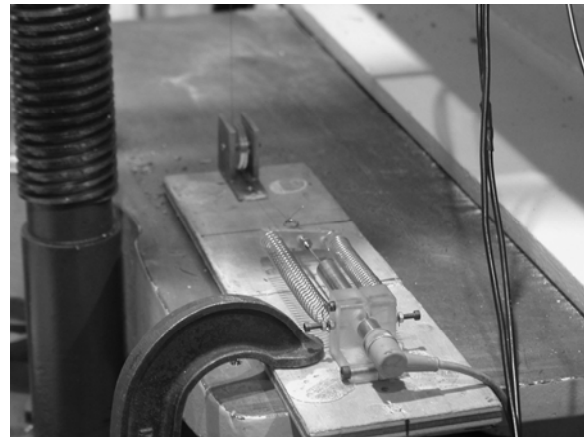
Figure 5.4 – Loading procedure.

The horizontal strains in the specimens were measured by two pairs of mechanical strain gauges (HBM_DD1 type, one in each one of the faces), placed on opposing faces of the specimens to eliminate the effect of bending (if any), see Figure 5.5a.

The vertical strains in the specimens were measured by using a pair of LVDT's placed in the arms of the test machine. Previously, a series of calibration tests of the apparatus was carried out, for the purpose of verifying the agreement between the vertical displacements in the faces of the tests specimens, measured using mechanical strain gauges, and the vertical displacements test machine platens and arms, measured by means of LVDT's, confirming a good agreement, see Figure 5.5b.



(a)



(b)

Figure 5.5 – Test set-up for destructive tests: (a) instrumented specimen, and (b) vertical strain measurements in the arms of the test machine.

The compressive strength parallel to the grain is the conventional value determined by the maximum load applied to the specimen, according to the NBr7190 standard (1997). The modulus of

elasticity is equal to the slope of the linear part on the stress-strain relationship (Figure 5.6), defined by the points $(\sigma_{10\%}; \varepsilon_{10\%})$ and $(\sigma_{50\%}; \varepsilon_{50\%})$ corresponding respectively to 10% and 50% of the conventional stress, in compression perpendicular to the grain, and it is given by:

$$E_{c,0} = \frac{\sigma_{50\%} - \sigma_{10\%}}{\varepsilon_{50\%} - \varepsilon_{10\%}} \quad (5.2)$$

where $\sigma_{10\%}$ and $\sigma_{50\%}$ are the compressive stresses corresponding to 10% and 50% of the conventional stress ($f_{c,0}$), and $\varepsilon_{10\%}$ and $\varepsilon_{50\%}$ are the specific strains corresponding to the values of $\sigma_{10\%}$ and $\sigma_{50\%}$. During the tests, strain in the longitudinal direction is accompanied by transverse expansion in the Radial-Tangential plane. The Poisson ratios were calculated equally as secant values for the same stress range of the conventional failure stress.

The relative humidity and temperature of the air during the tests were registered by an electronic device. During the tests, the average values of temperature of the air and relative humidity were $21 \pm 2^\circ\text{C}$ and $48 \pm 6\%$, respectively. The time elapsed between the tests and withdraw of the specimens from the climatic chamber did not affect the conditions of the test specimens (less than 24 hours, 65% of relative humidity and 20° of temperature).

In the preload cycle no information (strain or load) was recorded. The standards specify the preload cycle with the purpose of assuring that loading and support points and measuring equipment were properly aligned and fully contacted.

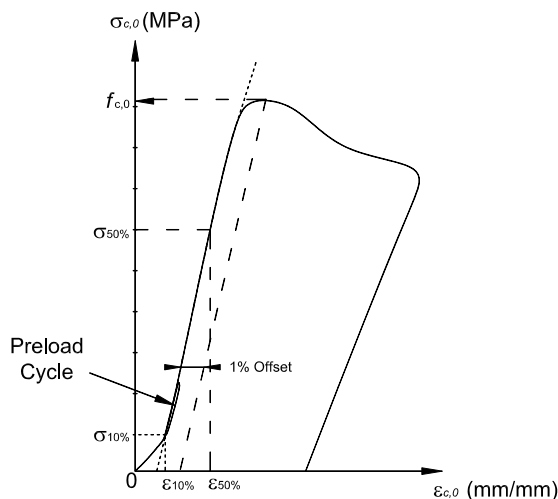


Figure 5.6 – Stress-strain relationship: definition of the compressive strength parallel to the grain following the NBr7190 standard (as based upon an offset of 1%).

5.2 RESULTS

5.2.1 Density determination

As a result of many years of investigation and observation, researchers recognise that there is a straight positive relation between density and compressive strength parallel to the grain, which following some authors could be expressed by:

$$f_{c,0} = \alpha + \beta \cdot \rho \quad (5.3)$$

where ρ is the density, and α and β are constants. On the other hand, some researchers considered that this relation could be represented by:

$$f_{c,0} = \frac{(\beta' \cdot 100)}{\rho} \Leftrightarrow \beta' = \frac{f_{c,0}}{100} \cdot \rho \quad (5.4)$$

where $f_{c,0}$ is the compressive strength, in kg/m², ρ is the density, in g/m³, and β' is the Monnin coefficient (1919) or static quality coefficient, which is very important when different species were compared, usually ranging between 7 and 9.5. This relation represents a length (in km) which is designated failure length, and represents the maximum height that a singular structural element, with constant cross section, could have in a way of sustain its own weight. Giordano (1999) refers an American study which gives the following relation:

$$f_{c,0} = 75.8 \cdot \sqrt[4]{\rho^5} \text{ (MPa)} \quad (5.5)$$

Table 5.1 shows the results for the average density and the coefficient of variation organized according to age. On average and for the complete 94 specimens sample, the densities of OCW and NCW groups are similar. Therefore the density of NCW was found to be 8% higher than OCW.

Table 5.1 – Average and limit values of density (Kg/m³).

	NCW	OCW
Average	647.8	581.8
Max.	658.5	607.2
Min.	624.7	570.9
CV (%)	3	3

To a better comprehension of the results presented in this chapter the characteristic density values are given in Table 5.2.

Table 5.2 – Characteristic density (kg/m³).

	NCW	OCW
ρ_k	612.7	548.8

5.2.2 Destructive tests

Figure 5.7 illustrates the typical failure patterns that could be observed in compression parallel to the grain. Gross shear band(s) run approximately perpendicular to the longitudinal axis on the radial plane and obliquely, at an angle between 45° and 70° with respect to the longitudinal axis, on the tangential plane, as observed by Gong and Smith (2000). These bands reach depths ranging between 0.2 mm and 1.1 mm deep.

What determines the angle of inclination of a single gross shear band has not been clearly elucidated. It is known that for brittle materials the fractured surface, produced by normal stresses, is normal to the longitudinal axis. For ductile materials the fractured surface has an angle of ≈ 45° to the longitudinal axis (Bodig and Jayne, 1993). Because wood is a natural fibre reinforced composite exhibiting moderate ductility under parallel to the grain compressive stress, and taking into account that for unidirectional fibrous glass-epoxy composite, the angle of a shear failure band is determined by the minimum combination of shear and compressive strength, gross shear band(s) orientation in wood specimens could be explained based on this.

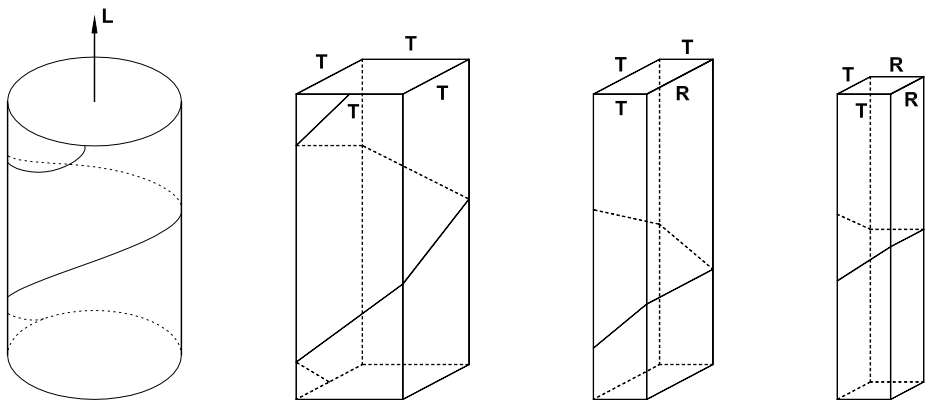


Figure 5.7 – Cleavage theory in wood adapted from (Tampone, 1996a).

As a first conclusion, as can be seen in Figure 5.8, it was observed that the limit of proportionality occurred at a considerable higher stress level ($\approx 75\%$), as reported by Gong and Smith (2000). Another factor is the inexistence of a straightforward definition of the transition point between regions of linear and nonlinear response. Once more, this indicates the arbitrariness of the limit of proportionality. Beyond the linear range, the stress-strain diagram exhibits distinct nonlinearity with reduction in stress carrying capacity beyond the strain at which the maximum stress is attained.

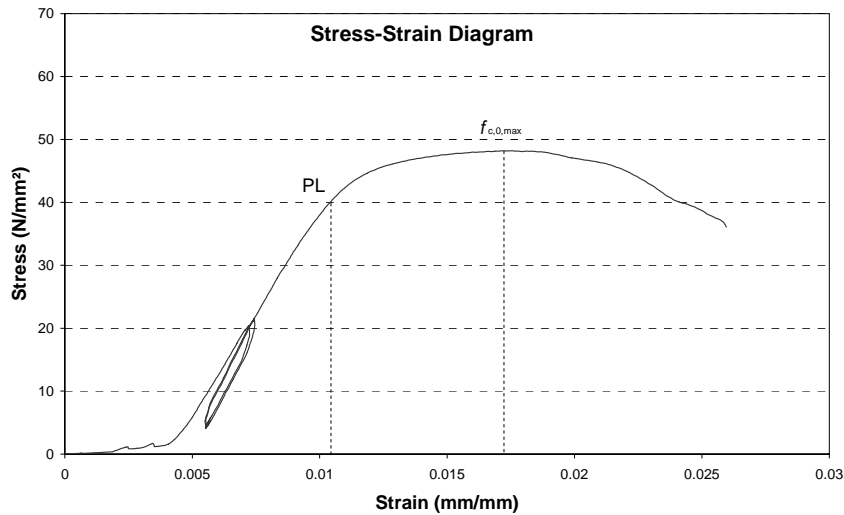


Figure 5.8 – Stress-Strain diagram.

A summary of the compression tests results are shown in Table 5.3. As referred above, compressive failure parallel to the grain is a progressive and stable process, usually deemed to be a result of shear stresses.

Table 5.3 – Compressive parallel to the grain results (average values): NCW and OCW.

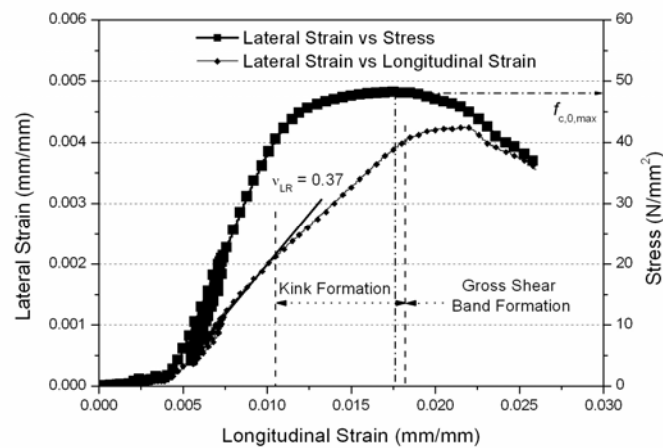
	NCW					OCW					
	$E_{c,0}$ (N/mm ²)	Poisson			$f_{c,0}$ (N/mm ²)	$E_{c,0}$ (N/mm ²)	Poisson			$f_{c,0}$ (N/mm ²)	
		ν_{LR}	ν_{LT}	ν_{TR}			ν_{LR}	ν_{LT}	ν_{TR}		
Média	7700	0.31	0.31	0.71	42.9	Average	8800	0.31	0.28	0.72	47.6
Máx.	10200	0.43	0.49	0.92	57.0	Max.	10300	0.44	0.47	0.91	57.7
Mín.	5100	0.23	0.14	0.47	31.7	Min.	6800	0.23	0.15	0.50	28.2
No.	47					No.	47				
CV	16	14	30	13	15	CV	8	14	27	13	14

The values for the coefficient of variation CV are relatively large (average CV of 15% for the strength values and values ranging between 8 and 16% for the elasticity modulus) but within the

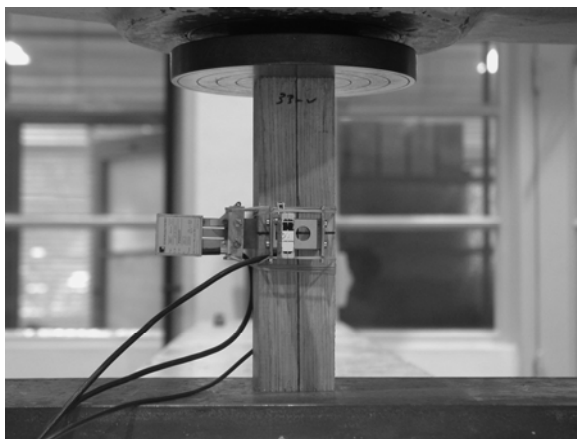
variability range usually found for wood species tested in compression parallel to the grain. The main conclusion is that the difference in the results between old and new wood is moderate to very low.

Nevertheless, it is interesting to observe that, in this particular sample, the compressive strength of old chestnut wood $f_{c,0}$ is 11% higher than new chestnut wood. This is opposition with the density values, where the density of OCW is 10% lower than NCW (Table 5.1).

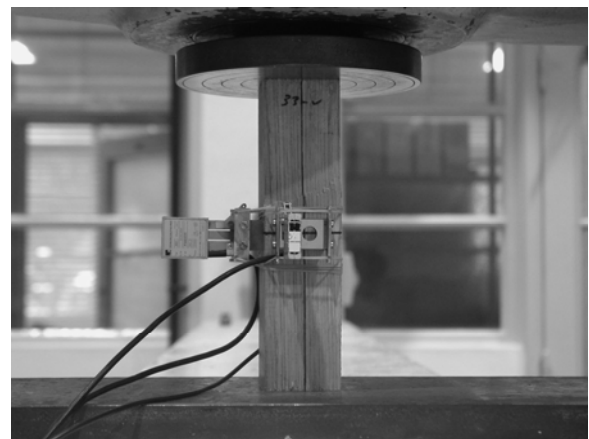
Figure 5.9 illustrates the stress and radial-longitudinal strain diagram, for a specimen in compression parallel to the grain, and different steps of the test procedure. It can be observed, in Figure 5.9a, that initially, the response is linear elastic and the limit of proportionality occurs at a longitudinal strain of about 0.01 and at a longitudinal strain of about 0.018, a gross shear band formed.



(a)



(b)



(c)

Figure 5.9 – Compression parallel to the grain: (a) stress and radial-longitudinal strain diagram, for a specimen in compression parallel to the grain, (b) initial specimen, and (c) end of the test procedure.

Poisson's ratios found reveal good agreement with the literature values (Sliker and Yu, 1993; U.S. Forest Products Laboratory, 1999). Poisson's ratios show, in the three considered planes, higher CV values. This could be justified due the inherent inhomogeneity of wood. Under parallel to the grain compression, structural change initiates as the stress level and instability increased with formation of kinks in cell walls (Dinwoodie, 1989; Gong and Smith, 2000). These authors referred that it seems reasonable to infer, at least for practical purposes, that kinks do not form unless the limit of proportionality is exceeded.

It was observed that each specimen develops one or, at maximum, two principal gross shear band(s) at relatively large strain, i.e. at a strain beyond the maximum stress ($f_{c,0,max}$), observable with the naked eye, see Figure 5.10. This/these shear band(s) formed at a strain of 1.6-2.1% over the specimen length. It is clear that the radial-tangential strain is sensitive to formation and development of shear band(s) in wood specimens.

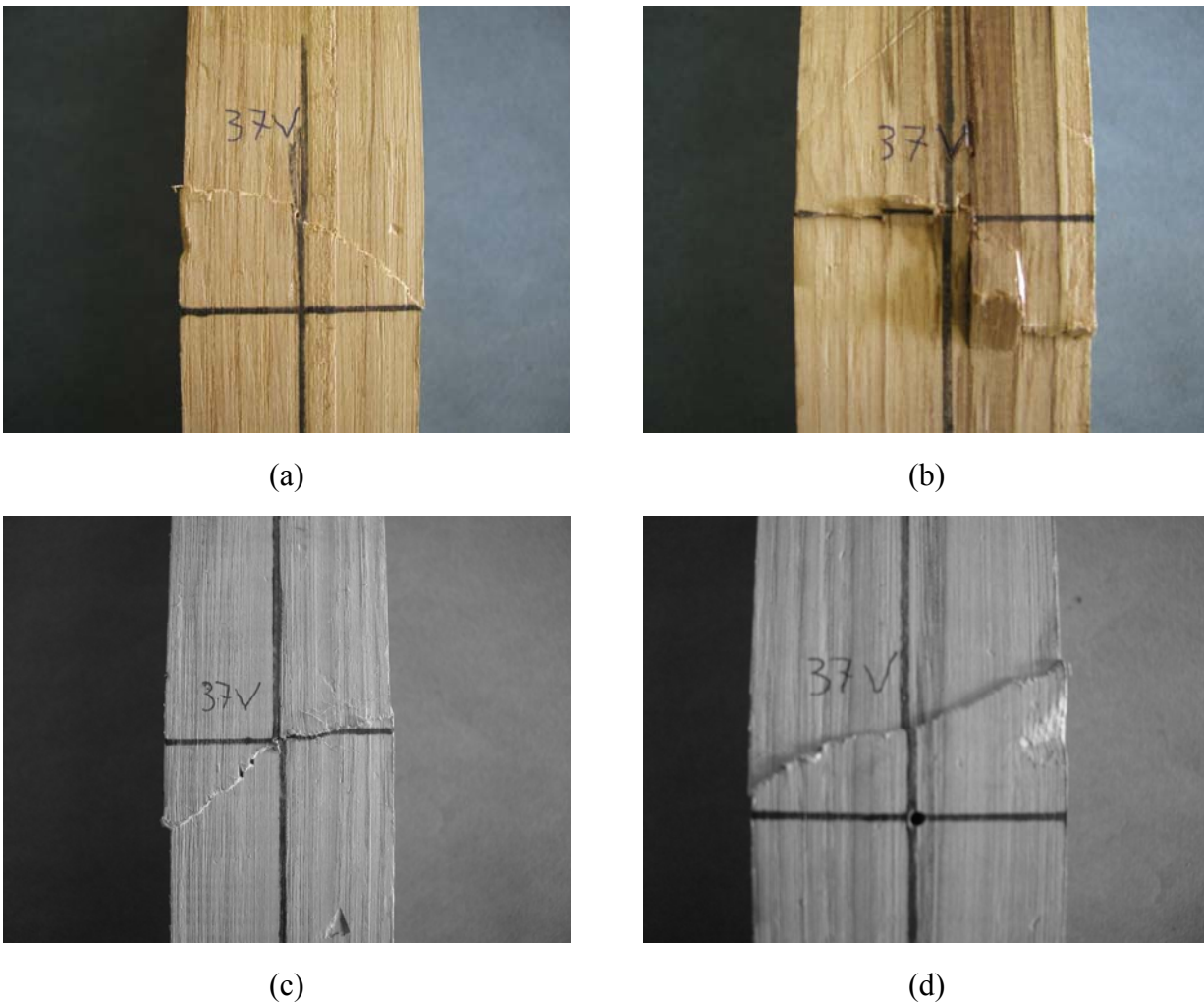


Figure 5.10 – Compression parallel to the grain: (a) to (d) failure in the four faces, where is visible at the naked the gross shear band.

Daniel and Ishai (1994) referred two main microbuckling (macroscopically characterized by wrinkling of the fibres) modes in unidirectional fibre reinforced composites: the “out-of-phase” or extensional mode (occurs at lower fibre volumes ratios) and the “in-phase” or shear mode (occurs at higher fibre volumes ratios), see Figure 5.11. Because the tracheids volume ratio is very high in softwoods ($\approx 90\%$), mechanics considerations imply that the “in-phase” microbuckling mode will be dominant.

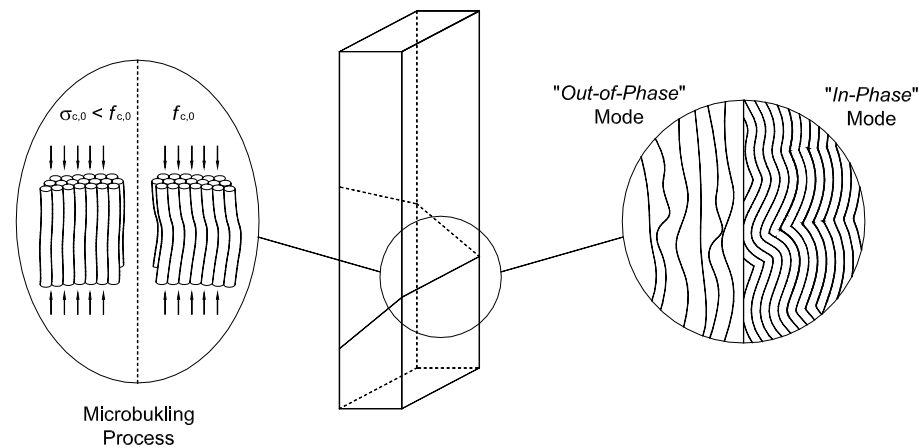


Figure 5.11 – Microbuckling modes.

The OCW group (see Table 5.4) show higher values, for the characteristic compression parallel to the grain characteristics, than NCW group, i.e., the compression strength and modulus of elasticity values of the old wood are, usually, slightly higher than the new wood (varies in the range 12%-33%).

Table 5.4 – Compression parallel to the grain: proposed and obtained results.

Characteristic values			
NCW		OCW	
$E_{c,0,05}$ (N/mm ²)	$f_{c,0,05}$ (N/mm ²)	$E_{c,0,05}$ (N/mm ²)	$f_{c,0,05}$ (N/mm ²)
5700	32.2	7600	36.2

Table 5.5 gives the relation between characteristic strength values and average strength values. This table proves the existence of a very good relation between the obtained results and the presented in ASTM D2555-88 standard (ASTM, 1992), which expresses the statistical variation of the tests results in clear wood specimens.

Table 5.5 – Relation between characteristic strength and average strength.

	NCW		OCW	
	$E_{c,0,05} / E_{c,0,mean}$	$f_{c,0,05} / f_{c,0,mean}$	$E_{c,0,05} / E_{c,0,mean}$	$f_{c,0,05} / f_{c,0,mean}$
ASTM D2555	0.74	0.75	0.86	0.76
	0.64	0.74	0.64	0.74

Comparing the characteristic tensile strength and modulus of elasticity values with the characteristic compressive results one can conclude that the characteristic strength values are slightly higher in tension parallel to the grain than in compression parallel to the grain ($\approx 32\%$). The elastic moduli results are also slightly higher in tension parallel to the grain than in compression parallel to the grain ($\approx 25\%$), which is in agreement with Gehri works (1997a). Table 5.6 gives the comparison results.

Table 5.6 – Comparison between compression and tension parallel to the grain characteristic values.

NCW		OCW	
$E_{t,0,05} / E_{c,0,05}$	$f_{t,0,05} / f_{c,0,05}$	$E_{t,0,05} / E_{c,0,05}$	$f_{t,0,05} / f_{c,0,05}$
1.32	1.41	1.18	1.23

Figure 5.12 and Figure 5.13 illustrate the correlation between $f_{c,0}$ and $E_{c,0}$.

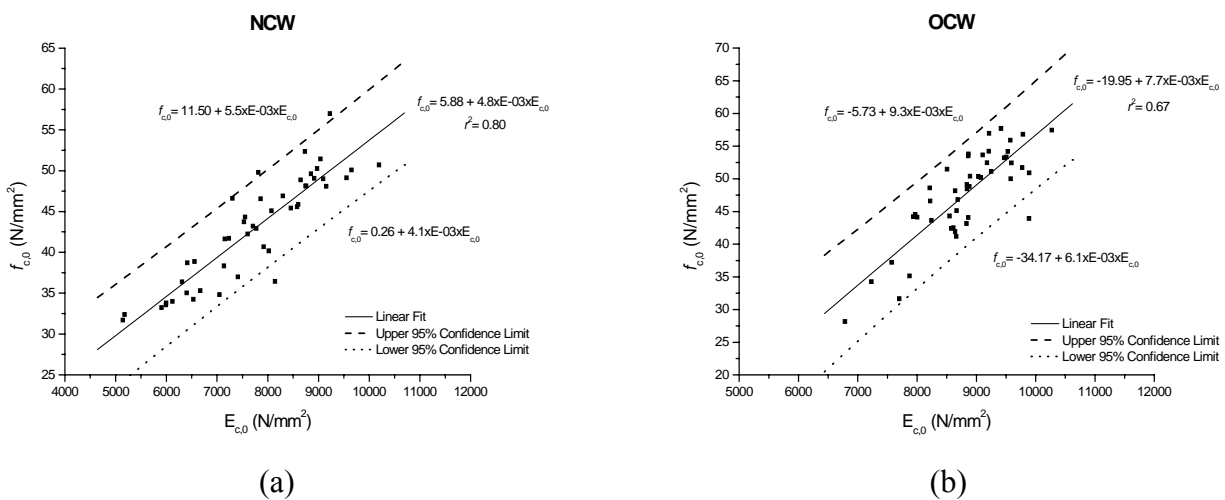


Figure 5.12 – Correlation between $f_{c,0}$ and $E_{c,0}$: (a) NCW, and (b) OCW.

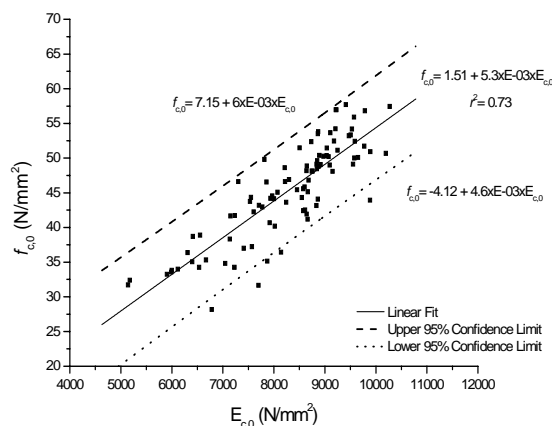


Figure 5.13 – Correlation between $f_{c,0}$ and $E_{c,0}$, for both considered groups.

5.2.3 Ultrasonic pulse velocity method

Table 5.7 provides the values measured for all specimens and stresses the importance of the age of wood in the propagation of stress waves. For each specimen, three independent ultrasonic tests have been carried out and the results shown represent the average of the readings.

In propagation velocity domain analysis, the OCW group present higher values (+12%) when compared with the NCW group. This can be justified from the density values given in Table 5.1 and the elasticity modulus values given in Table 5.3. Assuming E_{din} proportional to E , the ratio $(E/\rho)_{new}$ reads $11.9 \times 10^9 \text{ mm}^2/\text{s}^2$ and $(E/\rho)_{old}$ reads $15.1 \times 10^6 \text{ mm}^2/\text{s}^2$, confirming that the $UPV_{old} \approx (15.1/11.9)^{0.5} = 1.13 UPV_{new}$.

Table 5.7 – Indirect and Direct method, parallel to the grain: NCW and OCW.

Dynamic modulus of elasticity (N/mm ²)			Dynamic modulus of elasticity (N/mm ²)		
	Indirect Method		Direct Method, parallel to the grain		
	NCW	OCW	NCW	OCW	
Average	13000	15000	Average	15000	18000
No.	47	47	No.	47	47
CV	22	8	CV	21	9

5.2.4 Correlations based in the NDE methods

5.2.4.1 Correlations with density

The results presented in Figure 5.14 shows that the higher the density, the greater the strength of wood specimens. Figure 5.15 leads to the same conclusion, but referred to the modulus of elasticity: the higher the density, the greater the modulus of elasticity of wood specimens.

These two figures illustrate the good relation between density and the studied mechanical properties.

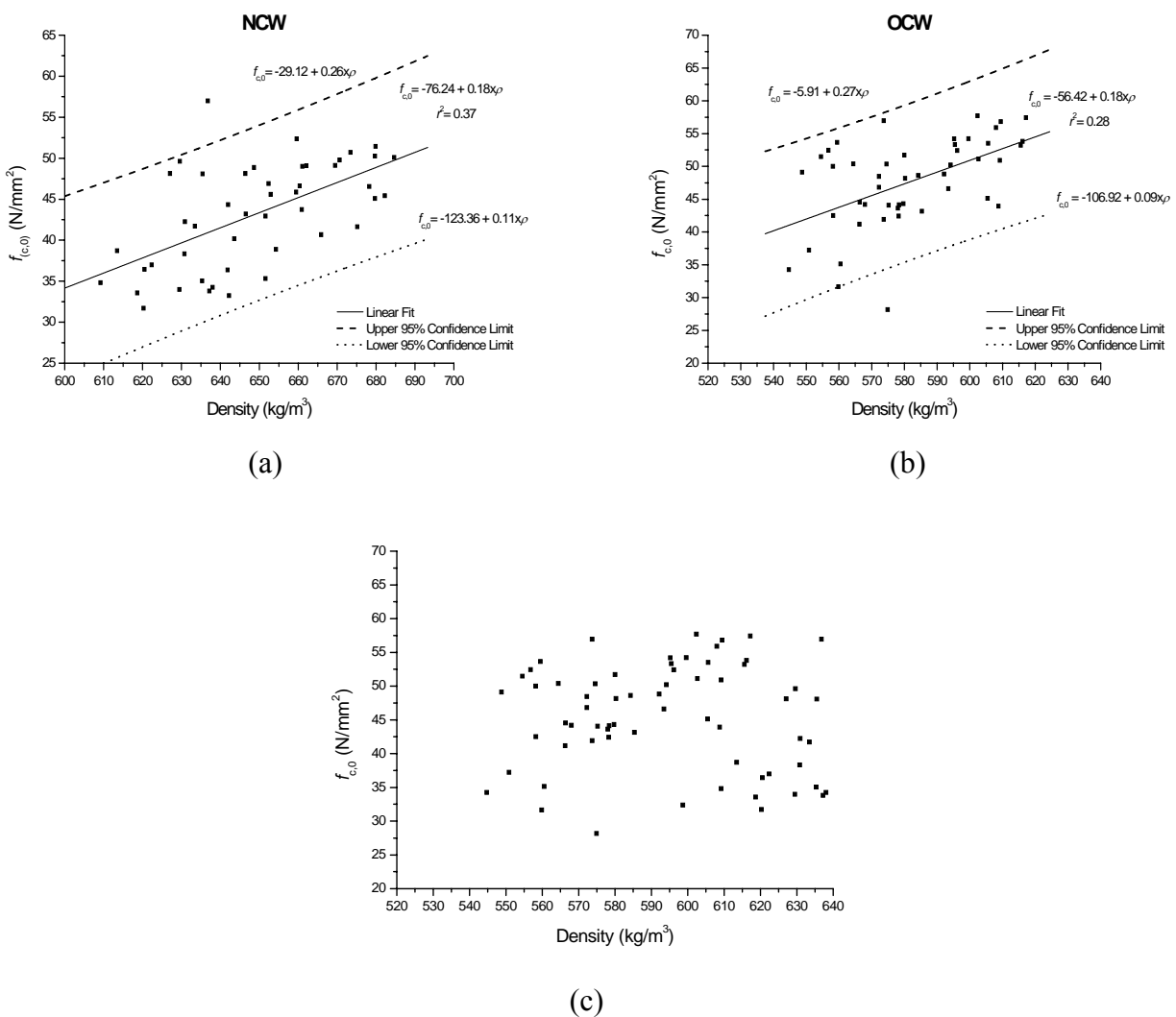


Figure 5.14 – Relation between $f_{c,0}$ and density: (a) for the NCW group, (b) for the OCW group, and (c) for both considered groups.

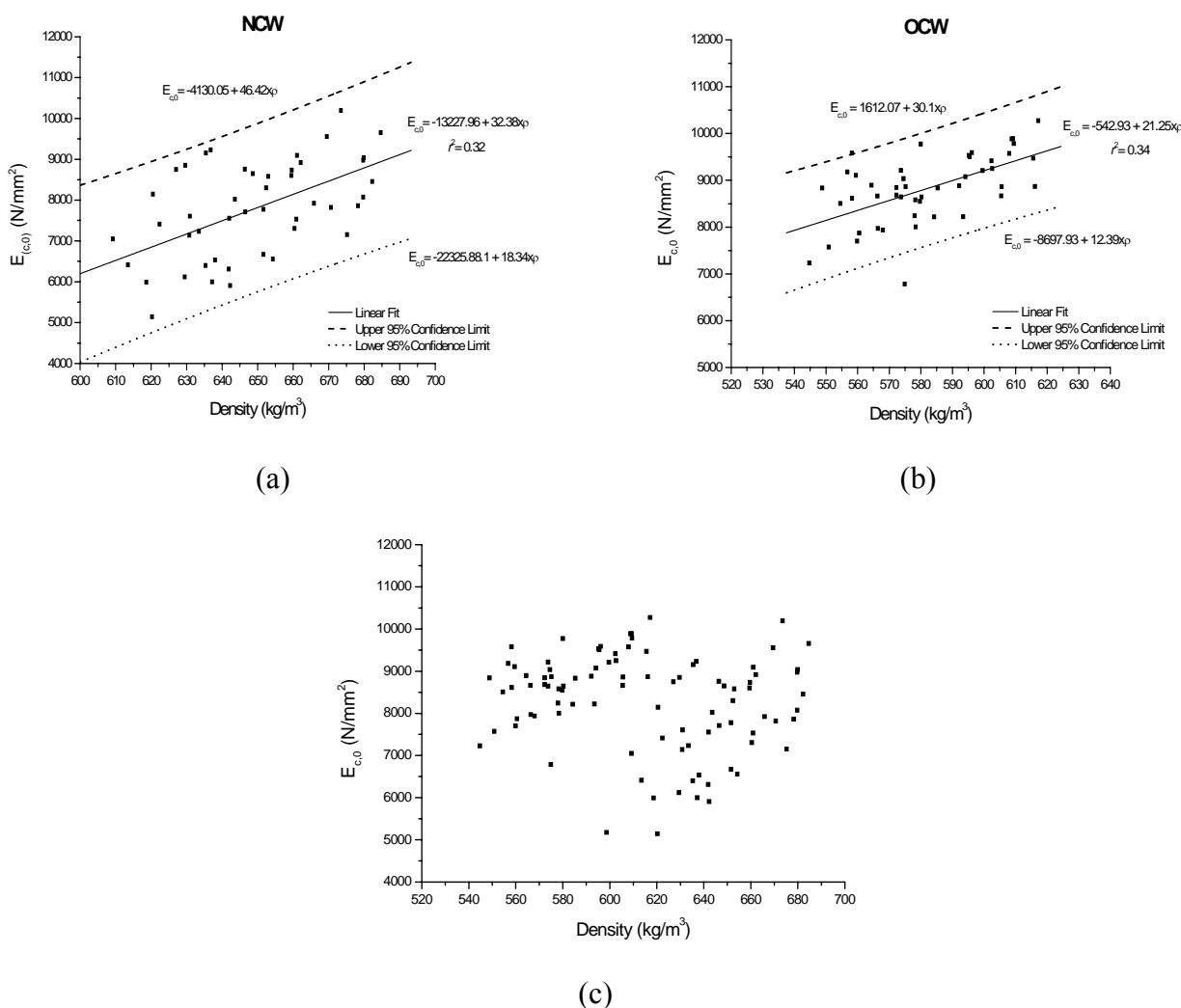


Figure 5.15 – Relation between $E_{c,0}$ and density: (a) for the NCW group, (b) for the OCW group, and (c) for both considered groups.

Figure 5.16 shows the correlations between the RM and the density for NCW and OCW. Moderate correlations are found between the two quantities when the results are analysed separately.

However, when the results are analysed together, good correlations are obtained. For practical purposes, it is recommended to use this measure carefully as a quantitative indicator. Considering all tests, a lower 95% confidence limit is given by:

$$\rho = 224.29 + 1.06 \cdot RM \tag{5.6}$$

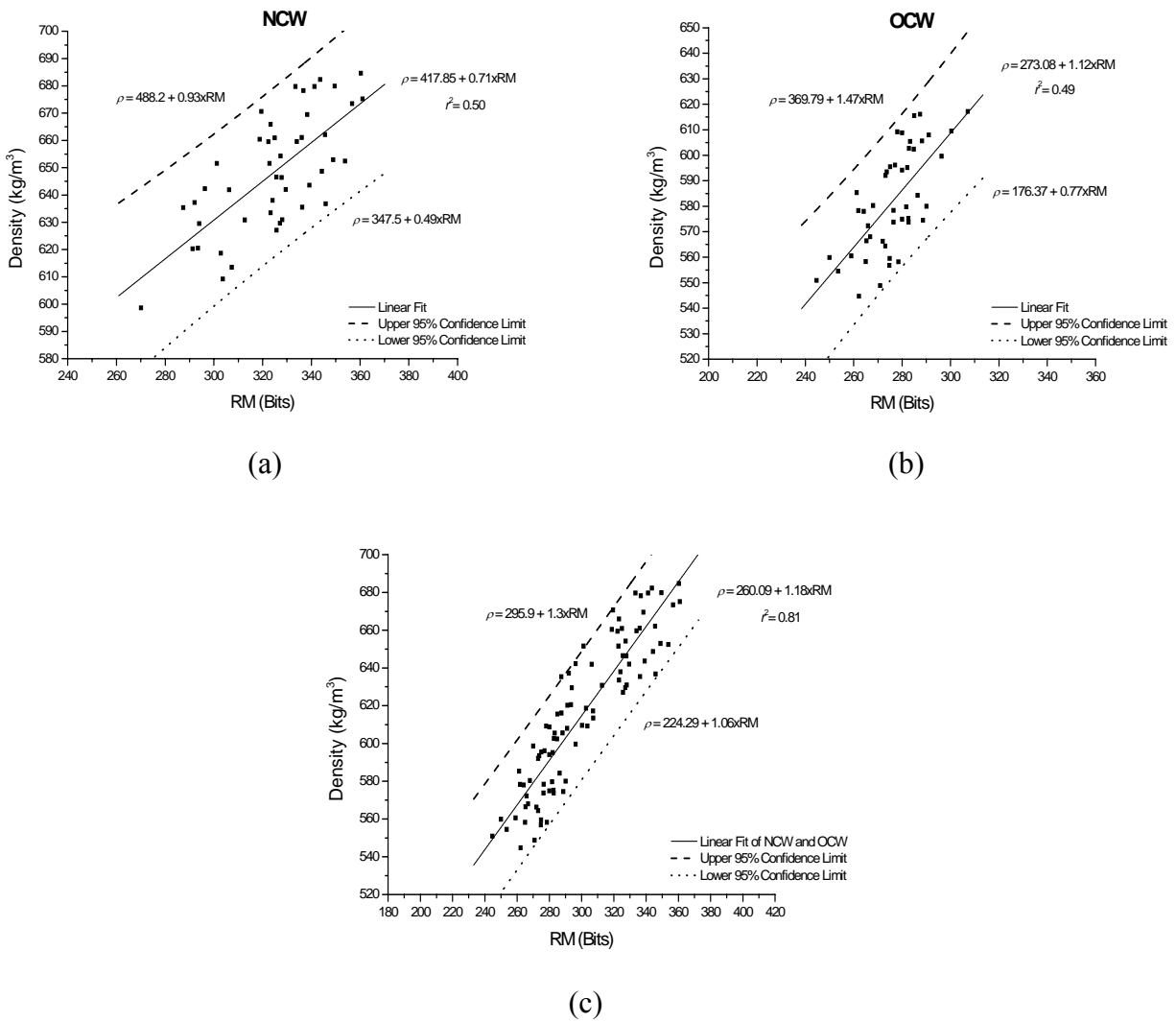


Figure 5.16 – Relation between RM and density: (a) NCW group, (b) OCW group, and (c) for both considered groups.

Figure 5.17 shows the correlations between the needle penetration and the density for NCW and OCW. The scatter in the results is low and a good correlation between the two quantities is found. Once again, when the results are analysed together the correlations improve.

The results show some dependency on the wood age. Considering all tests, a lower 95% confidence limit is given by:

$$\rho = 1001.99 - 51.81 \cdot \text{Depth} \tag{5.7}$$

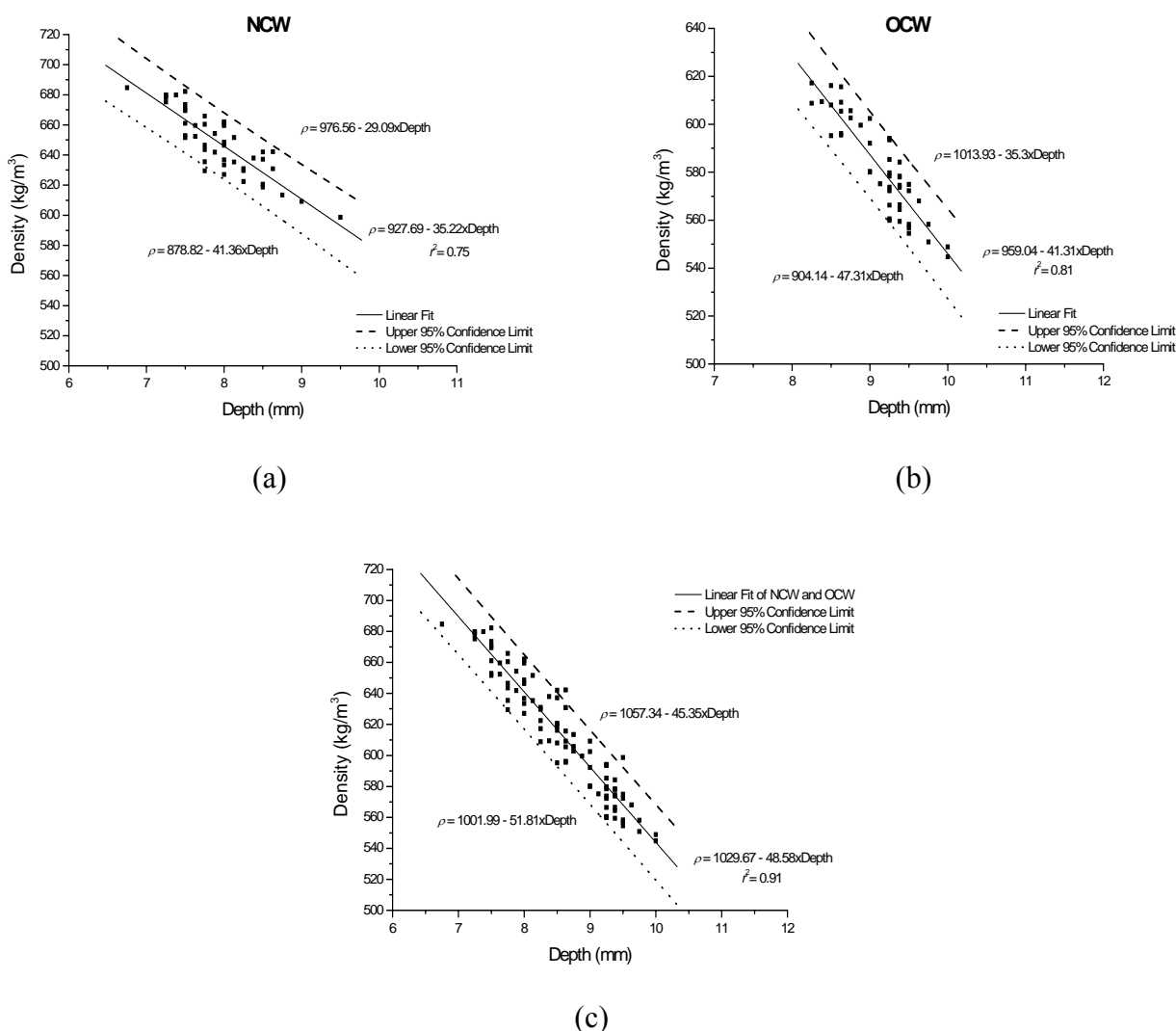


Figure 5.17 – Relation between pin depth (Pilodyn) and density: (a) NCW group, (b) OCW group, and (c) for both considered groups.

It is noted that the needle penetrates only 6.5 to 10 mm, or between one and three annual growth rings. Therefore, the result is superficial and care is needed in practical applications, verifying if the outer surface is deteriorated due to biological attack.

5.2.4.2 Correlations with the elasticity modulus

Figure 5.18 illustrates the results between $E_{c,0}$ and E_{din} using the Indirect Method. Again, it should be stressed that Indirect Method results are more meaningful in terms of application in practice since the Direct Method requires at least partial access to the ends of timber beams.

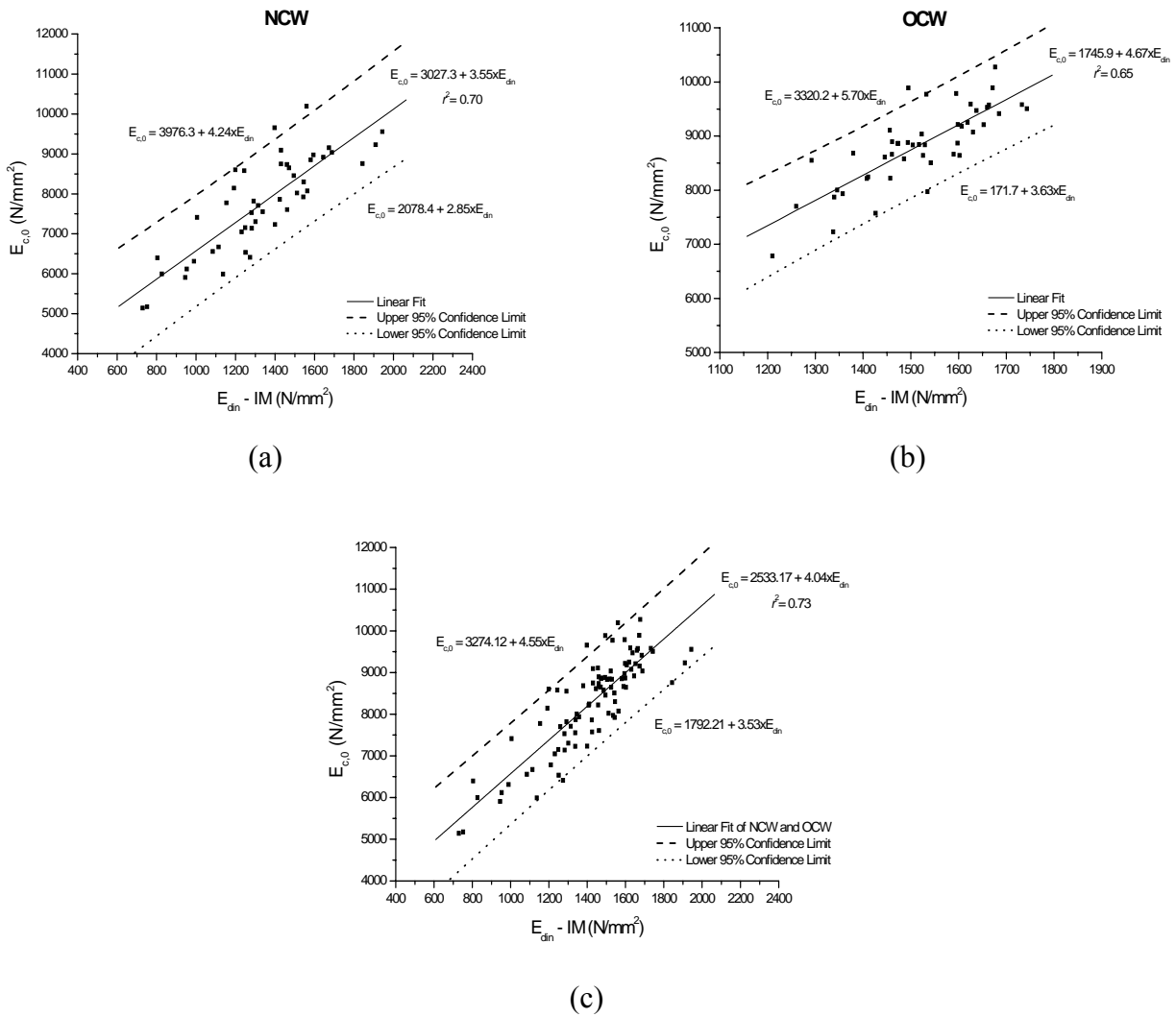


Figure 5.18 – Relation between $E_{c,0}$ and E_{dn} using the Indirect Method: (a) NCW group, (b) OCW group, and (c) for both groups.

Only moderate linear correlations are found with a very large difference between NCW and OCW. Also, these results are in agreement with Table 5.7 and the discussion provided in the previous section. Considering all tests, a lower 95% confidence limit is given by:

$$E_{c,0} = 1792.21 + 3.53 \cdot E_{dn} \tag{5.8}$$

Figure 5.19 shows the correlations between the RM and the elasticity modulus for NCW and OCW. Moderate linear correlations were found. For practical purposes, it is not recommended to use this measure as a quantitative indicator. Considering all tests together, no significant correlation is obtained.

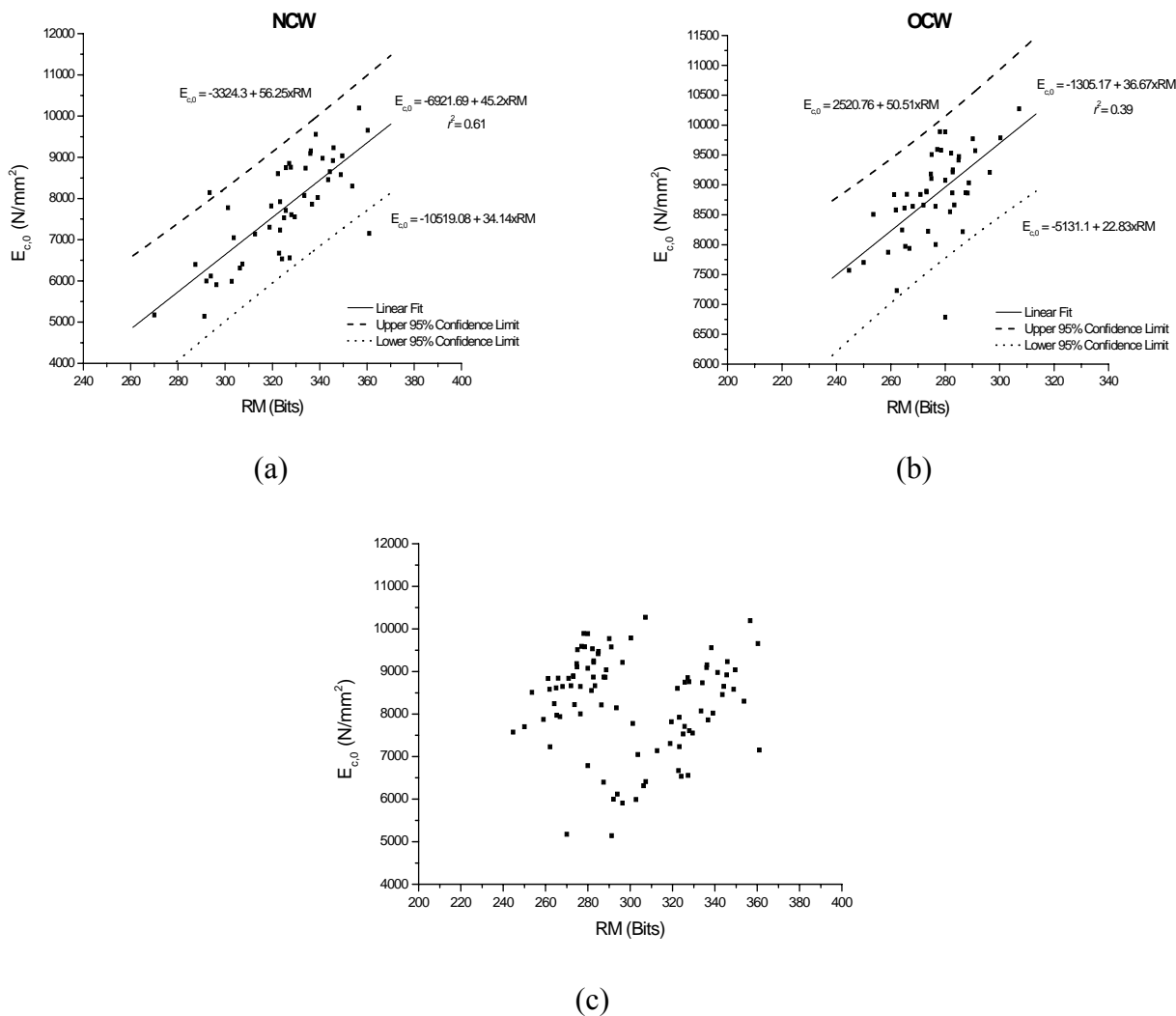


Figure 5.19 – Relation between RM and $E_{c,0}$: (a) NCW, (b) OCW, and (c) for both considered groups.

Figure 5.20 shows the correlations between the penetration reached with the needle of the Pilodyn device and the elasticity modulus for NCW and OCW, which were found to be moderate. Again, the global results present no significant correlation.

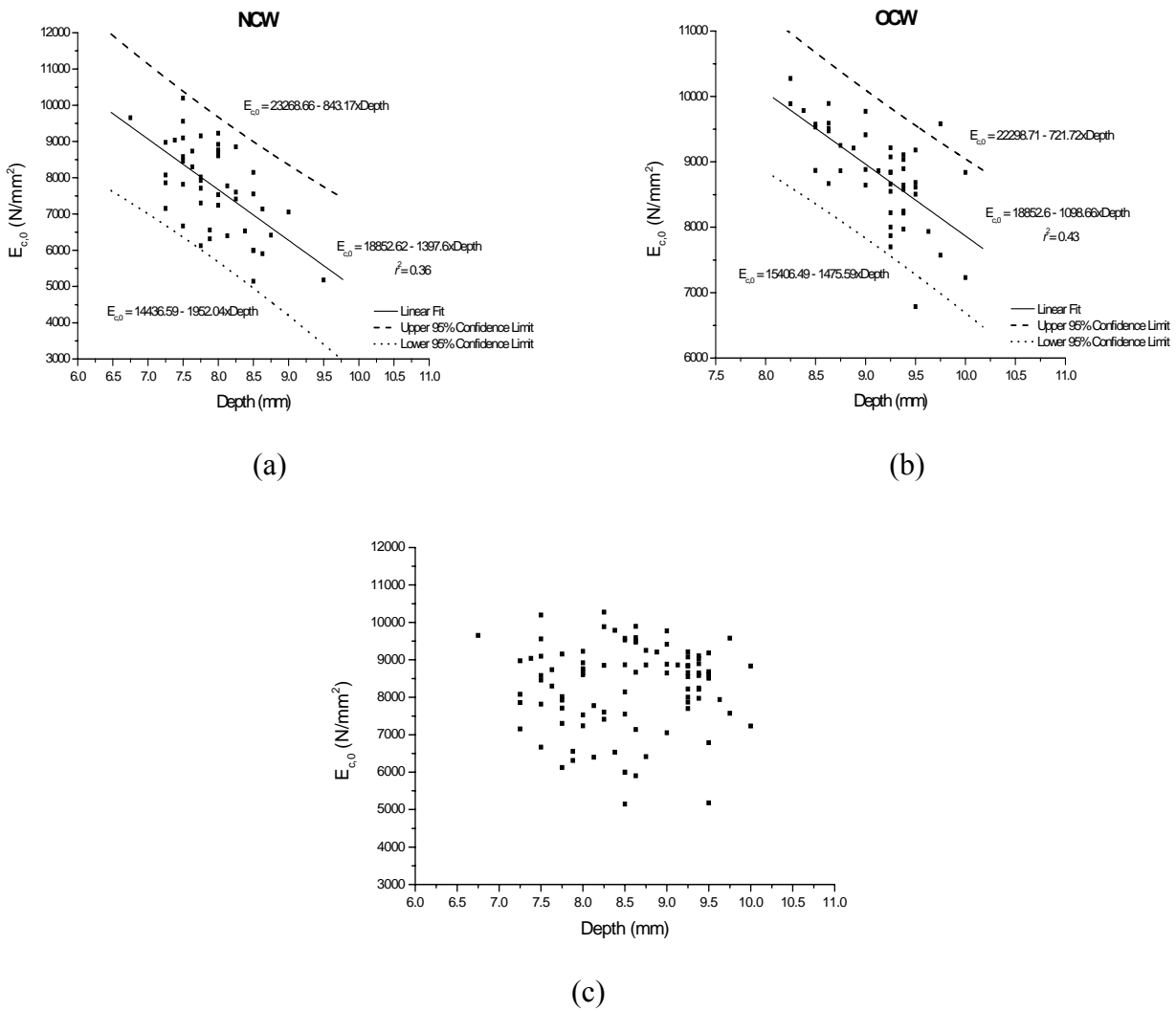


Figure 5.20 – Relation between pin depth (Pilodyn) and $E_{c,0}$: (a) NCW, (b) OCW, and (c) for both considered groups.

5.2.4.3 Correlations with the strength

Figure 5.21 shows the moderate linear correlations between the dynamic elasticity modulus (E_{din}) and the uniaxial compressive strength ($f_{c,0}$), using the IM. Considering all tests together, a lower 95% confidence limit is given by:

$$f_{c,0} = 7.15 + 0.019 \cdot E_{din} \tag{5.9}$$

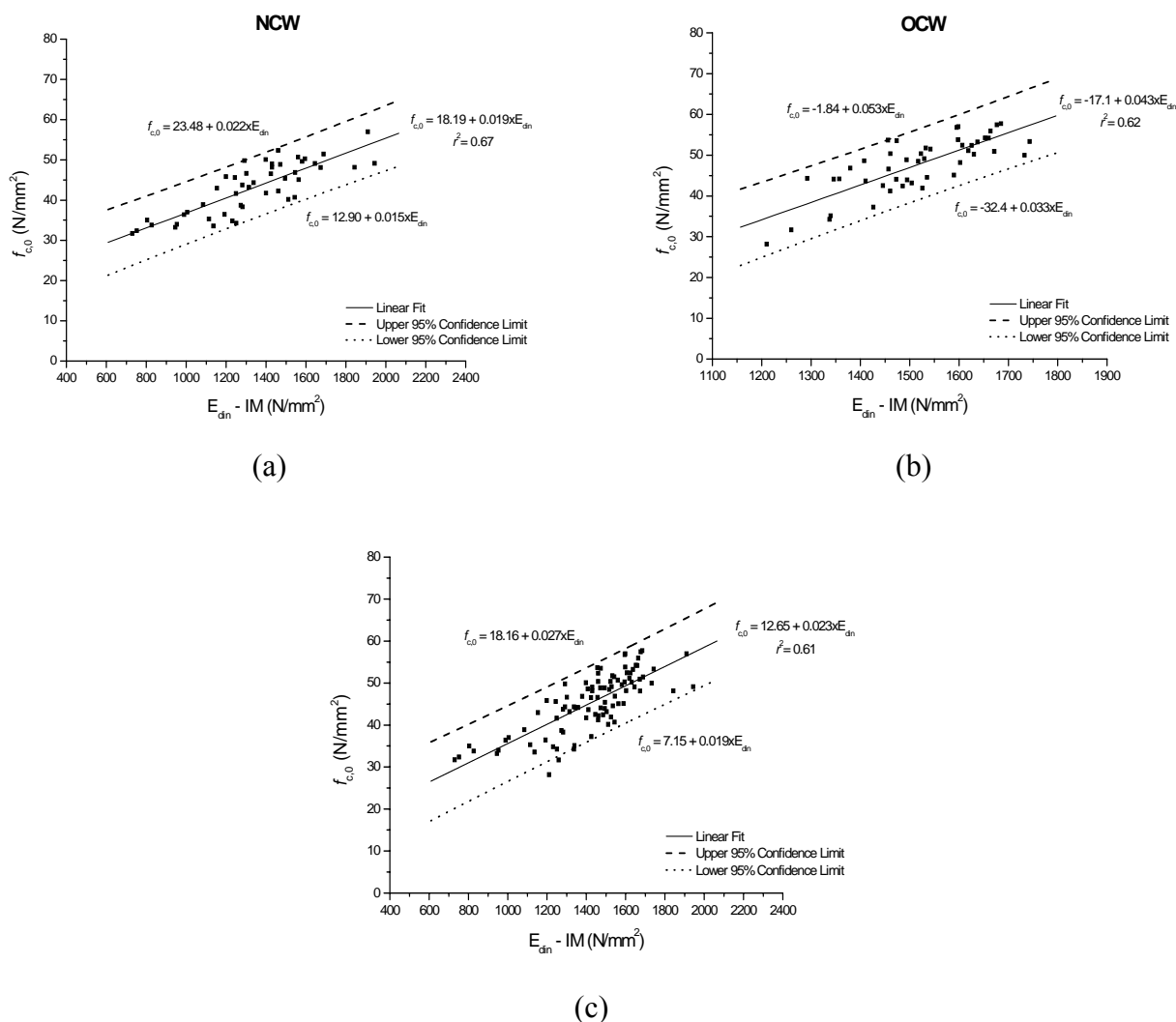


Figure 5.21 – Relation between $f_{c,0}$ and E_{din} using the Indirect Method: (a) NCW, (b) OCW, and (c) for both considered groups.

Figure 5.22 shows the correlations between the resistographic measure and the uniaxial compressive strength for NCW and OCW. Moderate linear correlations were found. For practical purposes, it is not recommended to use this measure as a quantitative indicator. Considering all tests together, no significant relations were obtained.

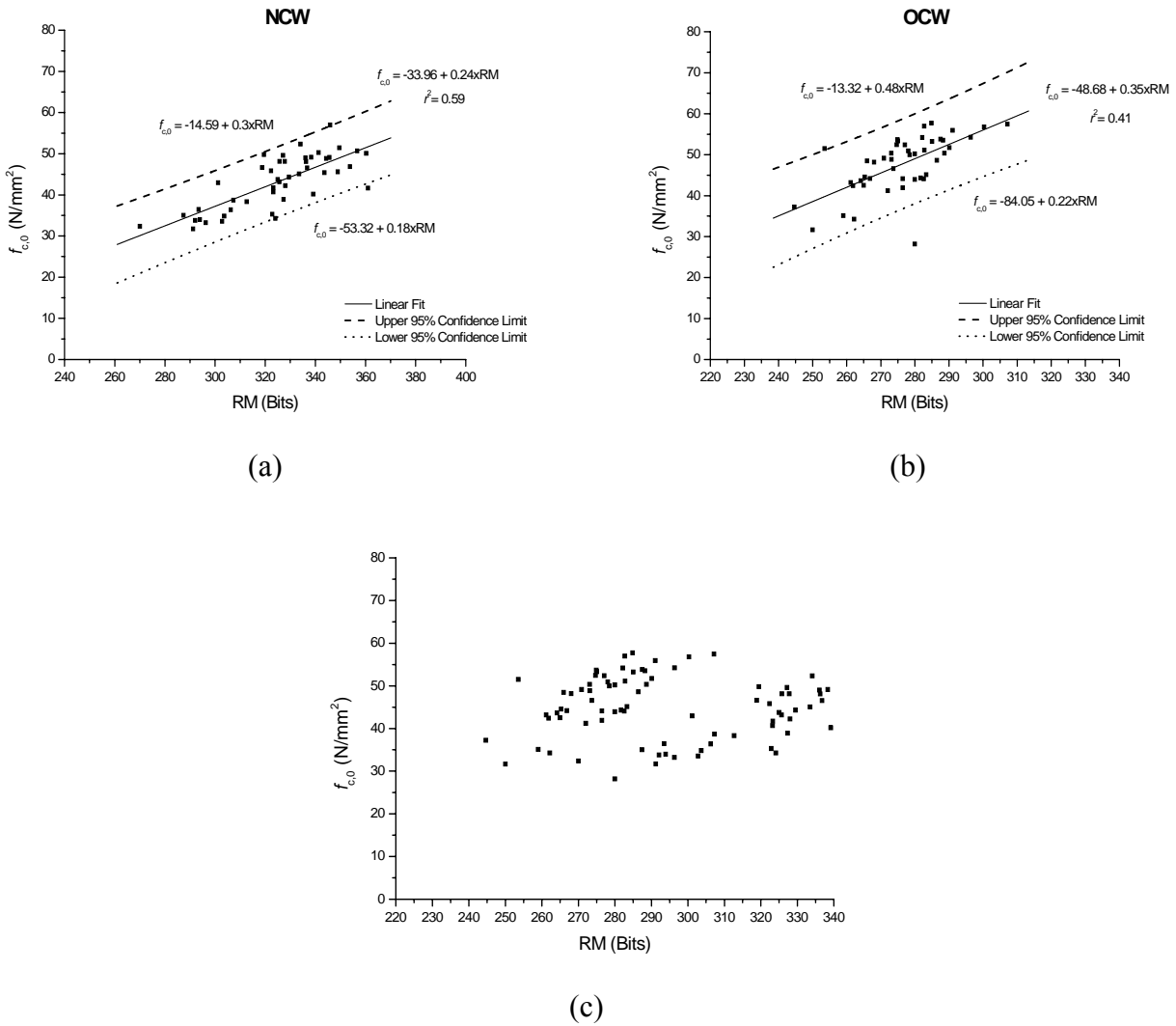


Figure 5.22 – Relation between $f_{c,0}$ and RM: (a) NCW, (b) OCW, and (c) for both considered groups.

Figure 5.23 shows that the correlation between the penetration reached with the needle of the Pilodyn device and the elasticity modulus for NCW and OCW is not significant. Again, the global results present no significant correlation.

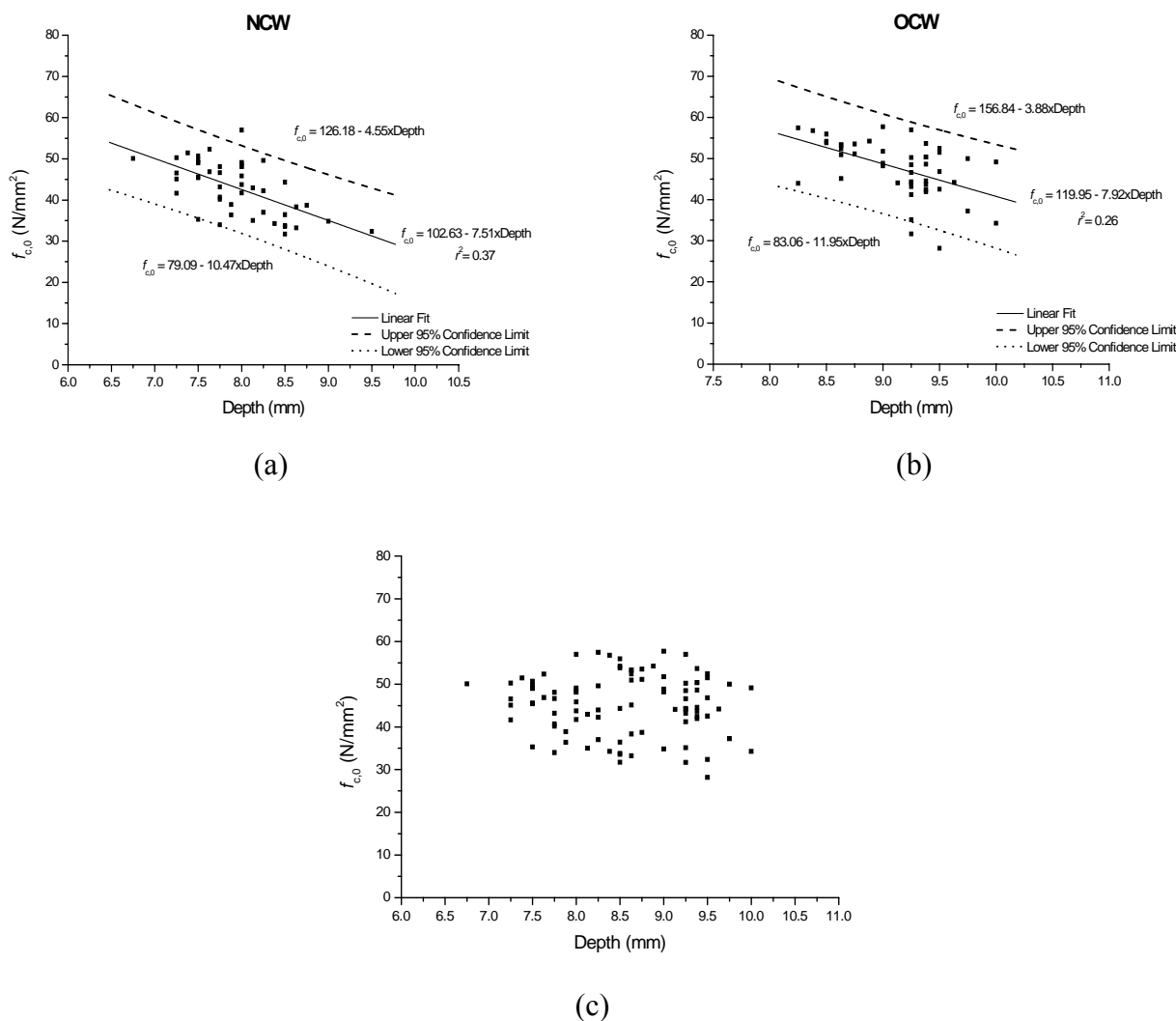


Figure 5.23 – Relation between $f_{c,0}$ and pin depth (Pilodyn): (a) NCW, (b) OCW, and (c) for both considered groups.

5.3 CONCLUSIONS

The present chapter aims at characterizing the density and mechanical properties of new and old chestnut wood in compression parallel to the grain. In addition, the performance of different NDT for assessing strength and stiffness is also evaluated.

The average strength values are slightly higher in the OCW group than in the NCW group ($\approx 11\%$), and the elasticity modulus is much higher in the OCW group than in the NCW group ($\approx 15\%$), see Table 5.3. The results confirm that no mechanical damage was presented in the timber beams (from which OCW specimens were obtained) due to service loads. Thus, safety assessment of new and existing timber structures can be made with similar mechanical data.

The experimental campaign shows that beyond the linear range, the stress-strain diagram exhibits distinct nonlinearity with reduction in stress carrying capacity beyond the strain at which the maximum stress is attained. It was observed that each specimen develops one or, at maximum, two principal gross shear band(s) at relatively large strain observable with the naked eye. It is clear that the radial-tangential strain is sensitive to formation and development of shear band(s) in wood specimens. Poisson's ratios presented reveal good agreement with the literature values.

Novel single-parameter linear regressions have been proposed for density, elasticity modulus and compressive strength parallel to the grain, using the Resistograph, Pilodyn and ultrasonic testing. The conclusions are that, with respect to density, the Resistograph and the Pilodyn provide reasonable correlations. With respect to mechanical characteristics, correlations can only be obtained taking into account the wood age, which in fact means a re-calibration with the wood sample. As this is not reasonable for practical purposes, expressions with a lower 95% confidence of the mechanical parameters have been proposed for the ultrasonic testing. For the Resistograph and the Pilodyn such expressions are not possible due to the dispersion found, and the use of these methods for quantitative mechanical data is not recommended.

It is possible to conclude that no significant differences were observed between the two methods.

Chestnut wood in tension parallel to grain. Evaluation by non-destructive methods

Wood as a ligneous material without defects presents considerable higher strength capacity parallel to grain than perpendicular to the grain. Therefore, the present chapter addresses the mechanical and physical properties of chestnut wood in tension parallel to grain. In the last decades several researchers addressed this issue, with a focus on the determination of the modulus of elasticity in the RT plane (Bodig and Goodman, 1973; Sliker, 1988). Usually it is assumed that a uniaxial and uniform state of tension exists in the referential of orthotropic symmetry of the specimens, which is the base for almost all structural timber design standards, e.g., EN 408 (CEN, 2000) and ASTM D143-94 (1994). The tension strength parallel to grain is therefore determined by:

$$f_{t,0} = \frac{F}{A_{Tot}} \quad (6.1)$$

where F is the tension load applied and A_{Tot} is the average area of the cross section of the specimens. Other studies try to compare and adjust experimental tests and numerical simulations including phenomena such as the annual growth ring direction influence and the introduction of correction coefficients aiming to represent the complexity of the stress-strain field, obtaining more accurate results (Pereira *et al.*, 2003).

It is obvious that the values of the elasticity modulus parallel to grain are needed for the design of timber structures. It is also known that the modulus of elasticity for wood parallel to grain is independent of the type of loading: tension, compression or even bending. Therefore, the European standards for timber adopt a uniform modulus of elasticity parallel to grain (E_0).

Burger and Glös (*in* Gehri, 1997a) reported that the modulus of elasticity in bending ($E_{m,0}$) is higher than the corresponding modulus of elasticity in tension ($E_{t,0}$). These authors found the following relationship from a database of tests:

$$E_{m,0} = 88 + 1.077 \cdot E_{t,0} \quad (N / mm^2) \quad (6.2)$$

In this work, Gehri (1997a) present the work done by Thunell (1941) and explain that the modulus of elasticity on tension and compression ($E_{c,0}$) “...are quite the same...”. Following his thoughts, he referred that the modulus of elasticity on bending should correspond to the middle value of $E_{t,0}$ and $E_{c,0}$:

$$E_{c,0} \leq E_{m,0} \leq E_{t,0} \quad (6.3)$$

The two above investigations are in contradiction, but it is clarified that the modulus of elasticity on bending and on tension should be the same.

Tensile strength parallel to grain is strongly affected by material defects (namely knots and local grain deviations). Although few results of single wood species are available, tensile strength can be significantly reduced (four or five times) in comparison with a “perfect” specimen and, the $E_{t,0}$ can be reduced up two thirds of the nominal value.

Temperature and shakes have not a strong influence in the strength; however the slope grain angle has a strong influence on $f_{t,0}$. Giordano (1999) proposed the strength reduction coefficients show in Table 6.1:

Table 6.1 – Coefficients of reduction of the tensile strength parallel to grain as a function of the slope angle, for load application (Giordano, 1999).

Slope angle	0°	5°	10°	15°	20°	45°	90°
Reduction Coefficient	1	0.91	0.70	0.46	0.35	0.14	0.07

Based on the above results the design values for timber members loaded in tension parallel to grain were gradually reduced in almost all structural timber design standards. Taking into account the difficulties in carrying out the tests described in EN 408 (CEN, 2000), the tensile strength, according to EN 384 (CEN, 1995), is derived from the bending strength. However, the large influence of material defects (knots and local grain deviations) in tension parallel to grain is responsible by a reduction of 40% of the characteristic bending strength ($f_{m,k}$):

$$f_{t,0,k} = 0.6 \cdot f_{m,k} \quad (6.4)$$

The ratio of tension to bending strength tends to increase with rising timber quality and decreasing dimensions (Burger and Glös, 1996; Burger and Glös, 1997).

6.1 EXPERIMENTAL SET-UP

6.1.1 Material

In total, 84 specimens were considered. In these tests, visual inspection was particularly careful to ensure, as far as possible, that the test length was kept clear of usual defects. To prevent fracture at the grips care was taken avoiding large knots at the transition from test length to the clamped section.

According to the standard Nbr7190 (1997), the specimens adopted must possess a geometry as the one represented in Figure 6.1. Their overall length is 330 mm while the “gauge section” is 210 mm long and 7 mm in thickness. Preliminary tests carried out indicated that failure occurred with crushing of the specimens at the grip zone, if the original normalized dimensions were used. Therefore the tensile specimens were modified, taking into account the effective grip area of the testing equipment. Ultrasonic tests were carried out in these specimens before testing them up to failure.

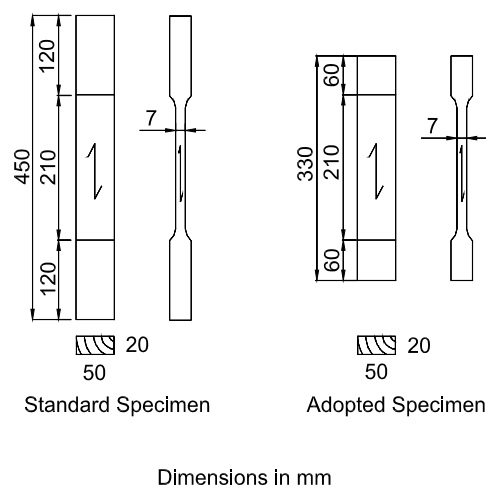


Figure 6.1 – Specimens geometry: standard specimen and experimental/adopted specimen (dimensions in mm).

All the specimens were previously conditioned in a climatic chamber capable of keeping a temperature of $20 \pm 2^\circ\text{C}$ and a humidity of $65 \pm 5\%$.

The tests specimens were considered conditioned when the density variation is smaller than 0.5% in a period of two hours, as recommended by EN 408 (CEN, 2000) standard. The densities were measured through an electronic weighing machine with a precision of 0.01 g.

6.1.2 Test set-up and equipment

Mechanical testing was carried out using a mechanical universal testing machine (INSTRON – Model 4483), with a loading cell of 100 kN. Additionally a feed, acquisition and amplification data system was defined for testing, which allows to obtain and to register all the data.

The measurements of the vertical and horizontal strains in the specimens were done by two pairs of bonded strain gauges, placed on opposite faces of the specimens to eliminate the effect of bending (if any) due to load eccentricities. This measured strain is considered to represent strain at a point acceptable from a macro-mechanics perspective, considering wood as a homogeneous material in a microscopic basis. The strain gauges are based on the resistance variation of a conductor when deformed (see Figure 6.2).

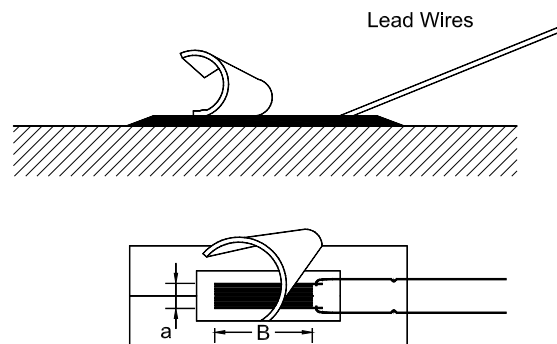


Figure 6.2 – Strain gauges.

TML's – Tokyo Sokki Kenkyujo Co., Ltd – B-1 adhesive, which is highly resistant to moisture, was used to bond all strain gauges to the specimens. The recommended curing temperature for the adhesive is +36°. All bonded strain gauges were wired to full bridge transducers with one dummy gauge as the temperature compensation strain gauge and compensating the bending resultants strains (load eccentricities). The compensating strain gauges were of the same lot as the active strain gauges and were mounted on similar specimens.

The pair of vertical strain gauges (parallel to grain; TML – L-60-11) and the pair of horizontal strain gauges (perpendicular to the grain; TML – L-20-11) were mounted (each distinct pair in each face) in the central section of the specimens, see Figure 6.3.

All the specimens were previously prepared: first grease and rust were removed from the bonding surface, then they were lightly polished with an abrasive paper of #120~180. After these two operations the specimens were wiped with acetone and the strain gauges installation position was marked, see Figure 6.3b.

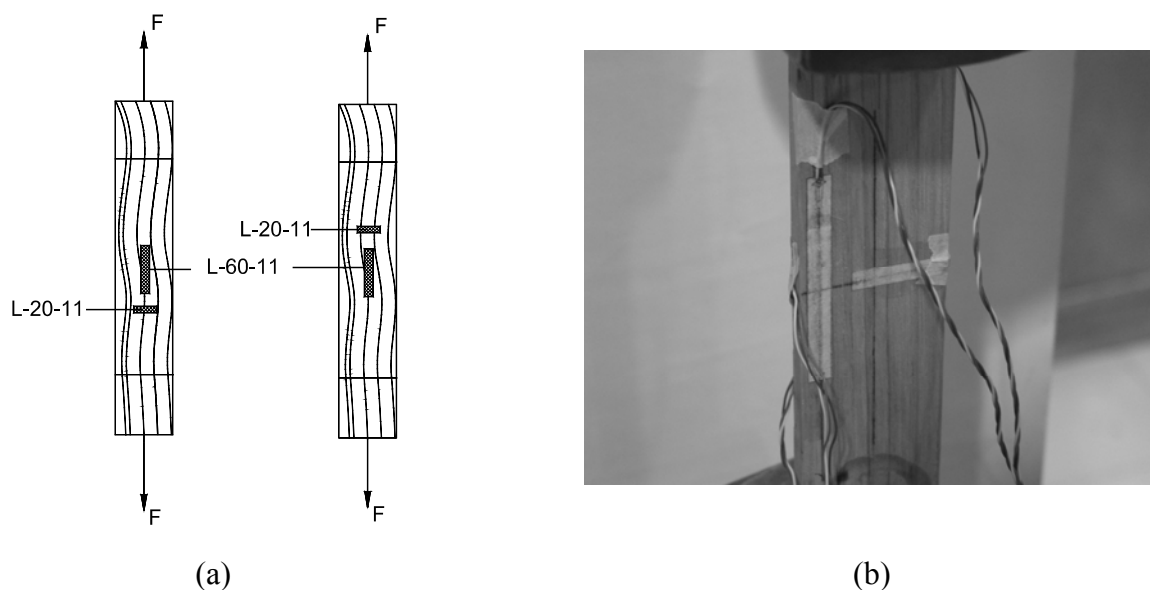


Figure 6.3 – Bonded strain gauges: (a) scheme in the two opposite faces; and (b) bonded in a specimen.

The adopted test procedure follows the Nbr7190 (1997) standard and the rate of loading was fixed at 5×10^{-2} mm/s for the entire test. This normative change was necessary, because the tests were performed under displacement control and not under force control, as prescribed by the standard. Two preliminary loading cycles were performed and no information (strain or load) was recorded. The requirement of this preload cycle was to permit and homogenize a perfect accommodation of the material avoiding slacks, see Figure 6.4.

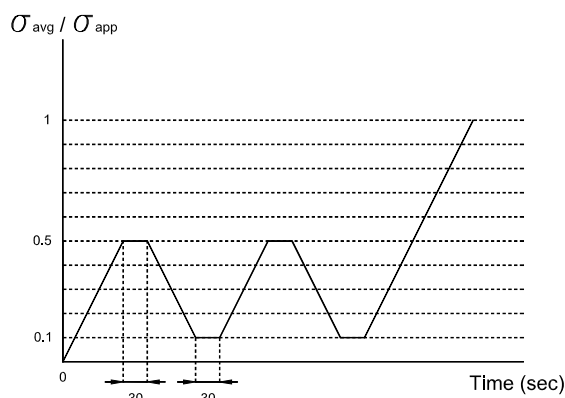


Figure 6.4 – Destructive testing loading procedure.

Additionally a mechanical strain gauge was used in the first testing campaign (INSTRON 2630_100 Strain Clip-On Extensometer – 50 mm) to compare the results between the two different strain measuring equipments used: the mechanical and the bonded (see Figure 6.5). This mechanical strain gauge was used only in the first 30 tests: 15 specimens of NCW and 15 specimens of OCW.



Figure 6.5 – Bonded strain gauges and mechanical strain gauge.

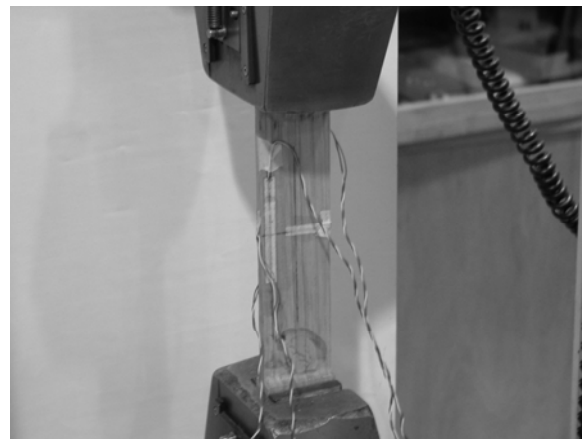
The moisture content and the temperature were controlled and recorded by a thermo-hydrophanous instrument. The recorded average values during the test campaigns are given in Table 6.2. The time elapsed between the tests and removal of the specimens from the climatic chamber did not affect significantly the conditions of the test specimens (less than 24 hours, 65% of relative humidity and 20° of temperature).

Table 6.2 – Average values of relative humidity and temperature of the air during the tests.

Relative Humidity	44-58%
Temperature of the air	20-23°C



(a)



(b)

Figure 6.6 – Destructive tests: (a) global view; and (b) location of the strain gauges.

The stiffness of wood, in tension parallel to the grain, is determined by its modulus of elasticity, $E_{t,0}$. This is equal to the slope of the linear part on the stress-strain relationship, defined by the

points $(\sigma_{10\%}; \varepsilon_{10\%})$ and $(\sigma_{50\%}; \varepsilon_{50\%})$ corresponding respectively to 10% and 50% of the conventional stress, in tension parallel to grain, and it is represented by:

$$E_{t,0} = \frac{\sigma_{50\%} - \sigma_{10\%}}{\varepsilon_{50\%} - \varepsilon_{10\%}} \quad (6.5)$$

where $\sigma_{10\%}$ and $\sigma_{50\%}$ are the normal stresses corresponding to 10% and 50% of the conventional stress, and $\varepsilon_{10\%}$ and $\varepsilon_{50\%}$ are the strains corresponding to the values of $\sigma_{10\%}$ and $\sigma_{50\%}$.

Finally, the Poisson ratios were calculated, in the longitudinal-tangential plane (ν_{LT}), equally as secant values for the same stress range of the conventional failure stress.

$$\nu_{xy} = \frac{\varepsilon_{x,50\%} - \varepsilon_{x,10\%}}{\varepsilon_{y,50\%} - \varepsilon_{y,10\%}} \quad (6.6)$$

For each group, a 5-percentile value ($f_{t,0,05}$ - characteristic strength value) was determined by ranking all the test values for a group in ascending order. The 5-percentile value is the test value for which 5% of the values are lower, as recommended by EN 384 (CEN, 1995). The average values are also represented ($f_{t,0,mean}$).

6.2 RESULTS

6.2.1 Density determination

Table 6.3 presents the results for the average density, the coefficient of variation and the characteristic density organized according to the age. On average and for the complete 84 specimens sample, the densities of OCW and NCW groups are similar. The high coefficients of variation found are justified by the complex shape of the specimens that introduces additional uncertainty to the volume determination.

Table 6.3 – Average and limit values of density (kg/m³).

	NCW	OCW
Average	604.3	597.5
Max.	743.75	715.63
Min.	518.75	496.66
CV	10	10
ρ_k	518.0	505.7

6.2.2 Destructive tests

In general, failure in tension parallel to the grain follows one of the patterns shown in Figure 6.7, namely shear, a combination of shear and tension, pure tension and splinter mode. After the destructive tests, and confirming the theoretical results expected, the patterns observed on Figure 6.8 and Figure 6.9 were observed.

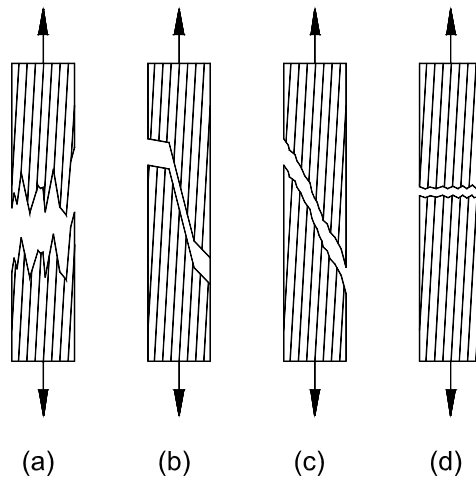


Figure 6.7 – Theoretically possible failure patterns: (a) splinter; (b) shear and tension failure; (c) shear failure; and (d) pure tension failure.

The parallel to grain tensile strength is the conventional value determined by the maximum strength applied to a specimen, following the NBr7190 (1997) standard. Each load-extension curve was reduced to a true stress-true strain plot; from these, yield strengths were determined using a strain displacement that was equivalent to a 0.3% offset in the usual terminology.



Figure 6.8 – Typical failure patterns observed: (a) splinter, and (b) shear and tension failure.

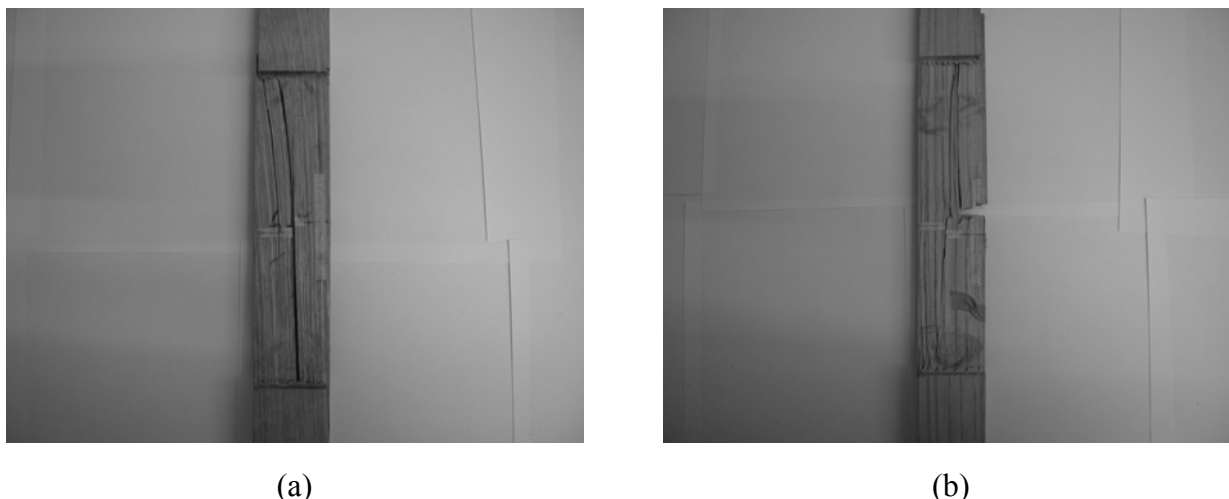


Figure 6.9 – Other typical failure patterns observed in tensile tests: (a) shear failure, and (b) pure tension failure.

Figure 6.10 shows the typical tensile stress-strain diagrams (average values for the NCW and OCW groups are given). These diagrams are related with the observed failure patterns. The test result presented in Figure 6.10a, where the yield strength for a 0.3% offset is indicated, could be associated to a pure shear failure or to a shear and tension failure: after the initial failure the specimen as a considerable plastic deformation.

On the other hand, the results given in Figure 6.10b could be associated with the aforementioned failure patterns (plastic behaviour) or to a pure tension failure or to a splinter failure of the specimen (elastic behaviour).

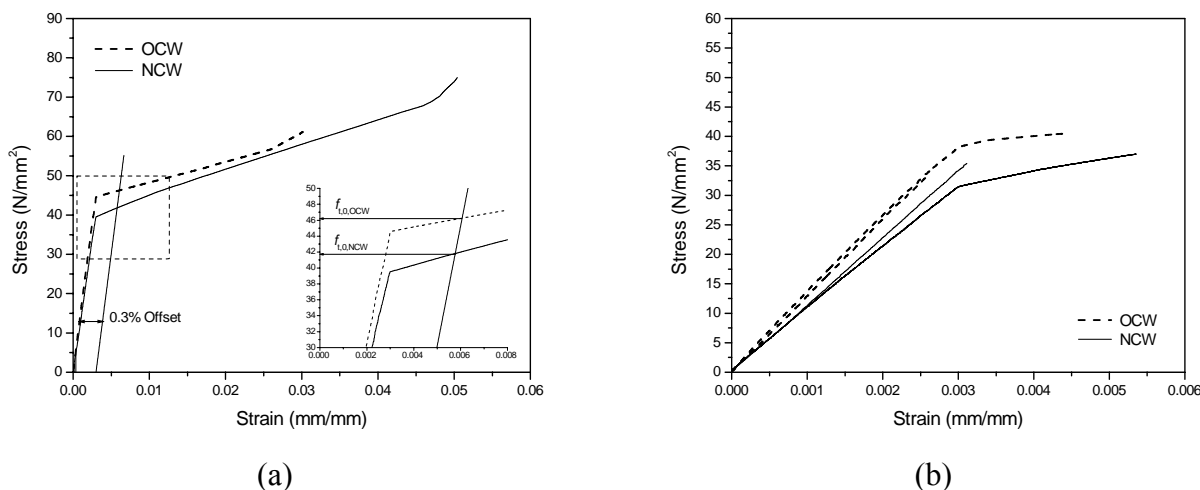


Figure 6.10 – Typical tensile stress-strain diagrams: (a) illustrates the selection of $f_{t,0}$ as based upon an offset of 0.3% (i.e. a plastic strain of 0.003).

The envelope tensile stress-strain diagrams are shown in Figure 6.11. Three different shapes were observed: linear deformation, plastic deformation with small yield plateau and plastic deformation with large yield plateau.

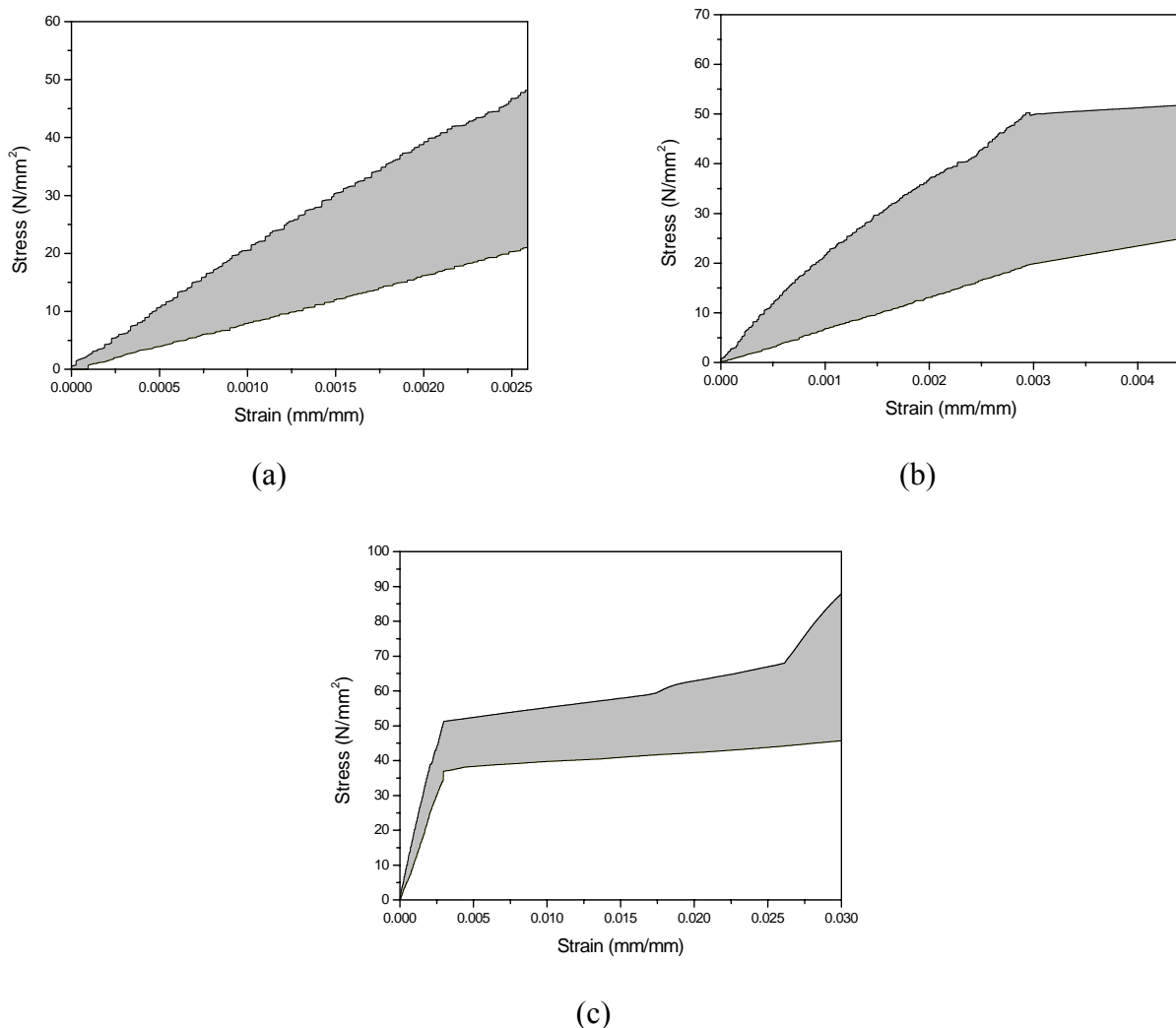


Figure 6.11 – Envelope tensile stress-strain diagrams: (a) to (c) three different situations.

Table 6.4 and Table 6.5 summarize the average results of the mechanical and bonded strain gauges. Once again, the coefficients of variation are relatively large (ranging between 19 and 29%) but within the variability found for wood species and the presence of small material defects (namely local grain deviations).

Another explanation is that the global analysis of the results should give particular attention to the observed failure pattern groups, which obviously had a great influence in the strength of the specimens. However, this could be a good solution because in practical situations one can not guarantee which kind of failure pattern will occur. It was assumed that the reason for the different failure behaviour and the different tensile strengths were mainly caused by slope grain deviations. The maximum slope angle observed in the test specimens was $\approx 6^\circ$.

The difference in the results between old and new wood is very low, which seems in agreement with the values of density found for the sample, see Table 6.3. The average values for the main elastic properties are similar when used the two aforementioned gauges.

Table 6.4 – Results obtained with the bonded strain gauges.

Destructive Tests (Bonded Strain Gauges)						
	NCW			OCW		
	$E_{t,0}$ (N/mm ²)	ν_{LT}	$f_{t,0}$ (N/mm ²)	$E_{t,0}$ (N/mm ²)	ν_{LT}	$f_{t,0}$ (N/mm ²)
Average	11.5E+03	0.45	47.4	13.7E+03	0.44	48.1
No.	42			42		
Max.	16.1E+03	0.58	61.3	18.9E+03	0.54	64.1
Min.	6.5E+03	0.31	33.6	8.0E+03	0.34	28.4
CV	19	12	29	19	13	23

Table 6.5 – Results obtained with the mechanical strain gauge.

Destructive Tests (Mechanical Strain Gauge)				
	NCW		OCW	
	$E_{t,0}$ (N/mm ²)	$f_{t,0}$ (N/mm ²)	$E_{t,0}$ (N/mm ²)	$f_{t,0}$ (N/mm ²)
Average	11.7E+03	45.4	13.8E+03	50.8
No.	15		15	
Max.	15.7E+03	52.9	17.8E+03	57.7
Min.	8.0E+03	38.2	10.4E+03	44.2
CV	21	10	17	8

Table 6.6 shows the characteristic tensile strength and modulus of elasticity values. According to EN 384 (CEN, 1995) the 5-percentile values for elastic properties have to be determined from at least 40 tests using order statistics by a non-parametric method or by interpolation, when necessary.

Table 6.6 – Characteristic values obtained with the bonded and mechanical strain gauges (N/mm²).

		NCW	OCW
Bonded Gauges	$f_{t,0,05}$	40.1	41.4
	$E_{t,0,05}$	8.9E+03	10.6E+03
Mechanical Gauges	$f_{t,0,05}$	37.8	43.7
	$E_{t,0,05}$	7.6E+03	9.9E+03

Figure 6.12 illustrates the correlations between the modulus of elasticity calculated with the bonded strain gauges and the mechanical strain gauge for the NCW and OCW groups. In a first analysis one may conclude that exist a good relation between the values obtained with the bonded strain gauges and the mechanical strain gauge (r^2 range between 0.83 and 0.82).

These results indicate that bonded strain gauges may be avoided in future campaigns. In fact, such devices are costly, non-reusable, and are very difficult to bond to preservative-treated or wet specimens. These bonded strain gauges also present problems with bonding handle and alignment.

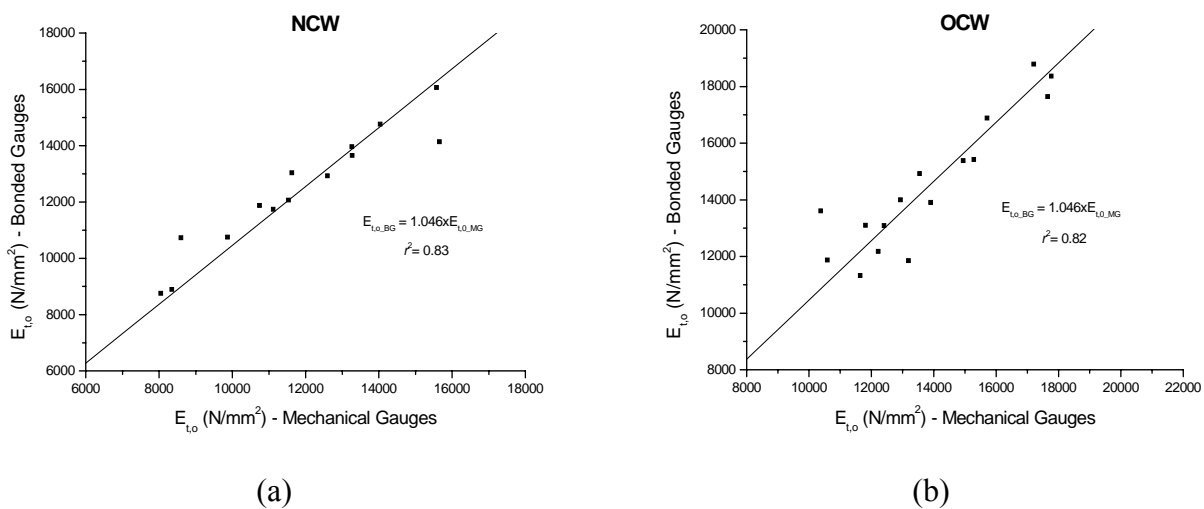


Figure 6.12 – Correlation between the modulus of elasticity calculated with the bonded strain gauges and the mechanical strain gauge: (a) NCW; and (b) OCW.

The Poisson's ratios obtained using bonded strain gauges are very similar in both groups: NCW and OCW. In the NCW group, the Poisson's ratios, in the LT plane, range between 0.58 and 0.31, the CV found was 16% and the average value 0.45. In the OCW group, Poisson's ratios, in the LT plane, range between 0.54 and 0.34, the CV found was 12% and the average value 0.44.

A number of linear regression equations were attempted between pairs of elastic constants and also between elastic constants and density. No significant relationships were found for the Poisson's ratios as function of density, strength or modulus of elasticity. This agrees with Bodig and Goodman's (1973) conclusions. These authors have found Poisson's ratios average values, for hardwoods, of 0.50 (CV = 23%). Sliker and Yu (1993) found Poisson's ratios using tension specimens (off-axis tension test with an angle between load and grain axis of 20°) made from 18 eastern hardwoods logs selected to provide a range of densities and elastic constants (selection was based on wood's reputation for straightness of grain) of 0.43 (CV = 19%). These authors also refer the work of Yu (1990) and Weigel (1991) that using compression specimens and combining the results of both campaigns, obtained average values equal to 0.45 (CV = 11%).

Other important observation was that the gauge length must to be just large enough to record an average macroscopic strain under the gauge representative of the deformation of the specimen

around the point of interest. In many specimens the region where the strain gauges were really effective was not coincident with the “failure region” and the values were continuously recorded despite failure of the specimen. The sensibility of the strain gauges is excellent in a certain region/length of the specimen, but if the rupture was localized in other region that is not covered by the strain gauge, the interpretation of the results is very complicated. On the other hand this region of the specimen could be yet in an elastic field despite of others regions are in plastic failure. The mechanical gauge by showing a greater gauge length than the bonded gauge have a higher probability of overlap the failure region therefore more prone to record the true global stress-strain curve on the weakest region. One problem arises when only the mechanical gauge was used: when this gauge reached a predefined strain value ($\approx 0.5\%$), the test procedure was aborted because of security reasons of the equipment. Figure 6.13 presents the correlation between $f_{t,0}$ and $E_{t,0}$. Moderate linear correlations were found and the results are in agreement with Table 6.4.

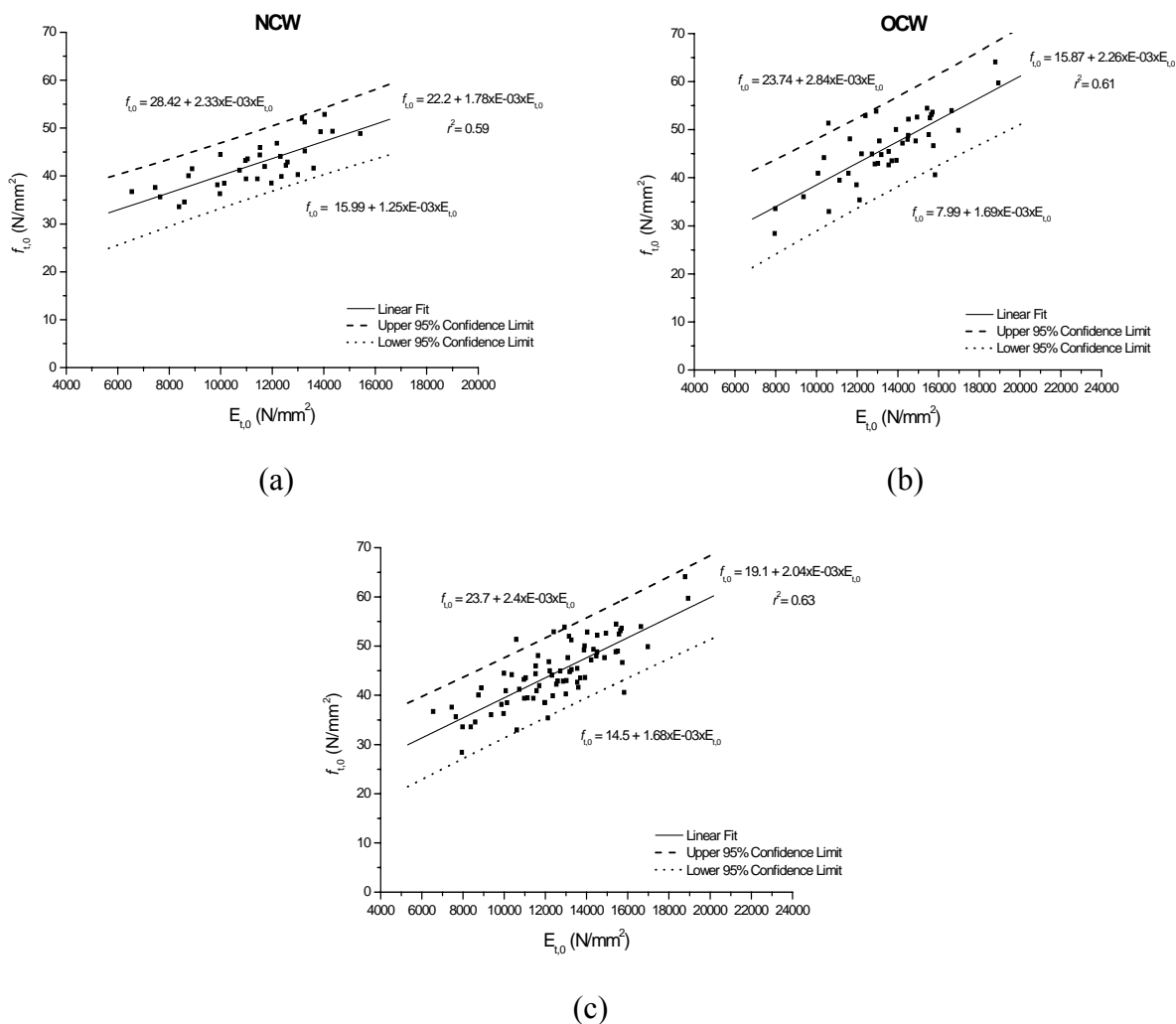


Figure 6.13 – Correlation between $f_{t,0}$ and $E_{t,0}$: (a) NCW, (b) OCW, and (c) both groups.

6.2.3 Ultrasonic pulse velocity method

Again, for each specimen, three independent ultrasonic tests have been carried out and the results shown represent the average of the readings. The only method reported here is the Indirect Method, since it is the most appropriate in practice. The measuring length has considerable relevance in the ultrasonic pulse velocity (UPV) and the Indirect Method larger measuring base provides values comparable to the Direct Method. Therefore, only the smaller measuring base is presented in this paper.

Table 6.7 gives the results of the ultrasonic tests and shows the differences between the two considered groups in terms of wood age. The main conclusion is again that the OCW group show slightly higher values (+10%) when compared with the NCW group. The difference found between OCW and NCW is not corroborated by the density and elasticity modulus values found for this sample, which are almost equal, see Table 6.3 and Table 6.4.

The highest modulus of elasticity values were obtained to the Indirect Method ($d = 20$ cm). This fact is directly related with the uniform section presented by the measured region: there were no narrow or contract zones in the specimen, such as happens in the other two methods, see Table 6.7.

Table 6.7 – Ultrasonic pulse velocity method results.

	Direct Method		Indirect Method (d = 20 cm)		Indirect Method (d = 45 cm)	
	E_{din_DM} (N/mm ²)		E_{din_IM} (N/mm ²)		E_{din_IM} (N/mm ²)	
	NCW	OCW	NCW	OCW	NCW	OCW
Average	14600	16200	20000	21900	15000	17000
No.	39	45	39	45	39	45
Max.	20300	20400	27500	27700	20600	21300
Min.	9900	10900	13800	16500	10600	9900
CV	18	15	17	16	17	16

6.2.4 Correlations based in the NDE methods

6.2.4.1 Correlations with density

Figure 6.14 to Figure 6.16 show the relation between density and the studied mechanical properties. Because of the similar properties of the two groups and the unrealistic separation of the specimens into different failure pattern classes, the overall values are more realistic than the separated failure pattern values. These results show a clear positive correlation between density and the studied mechanical properties. The dissimilarity of coefficients of correlation found might be caused by the presence of defects not detected visually (for instances small deviations of the grain or microscopic fissures).

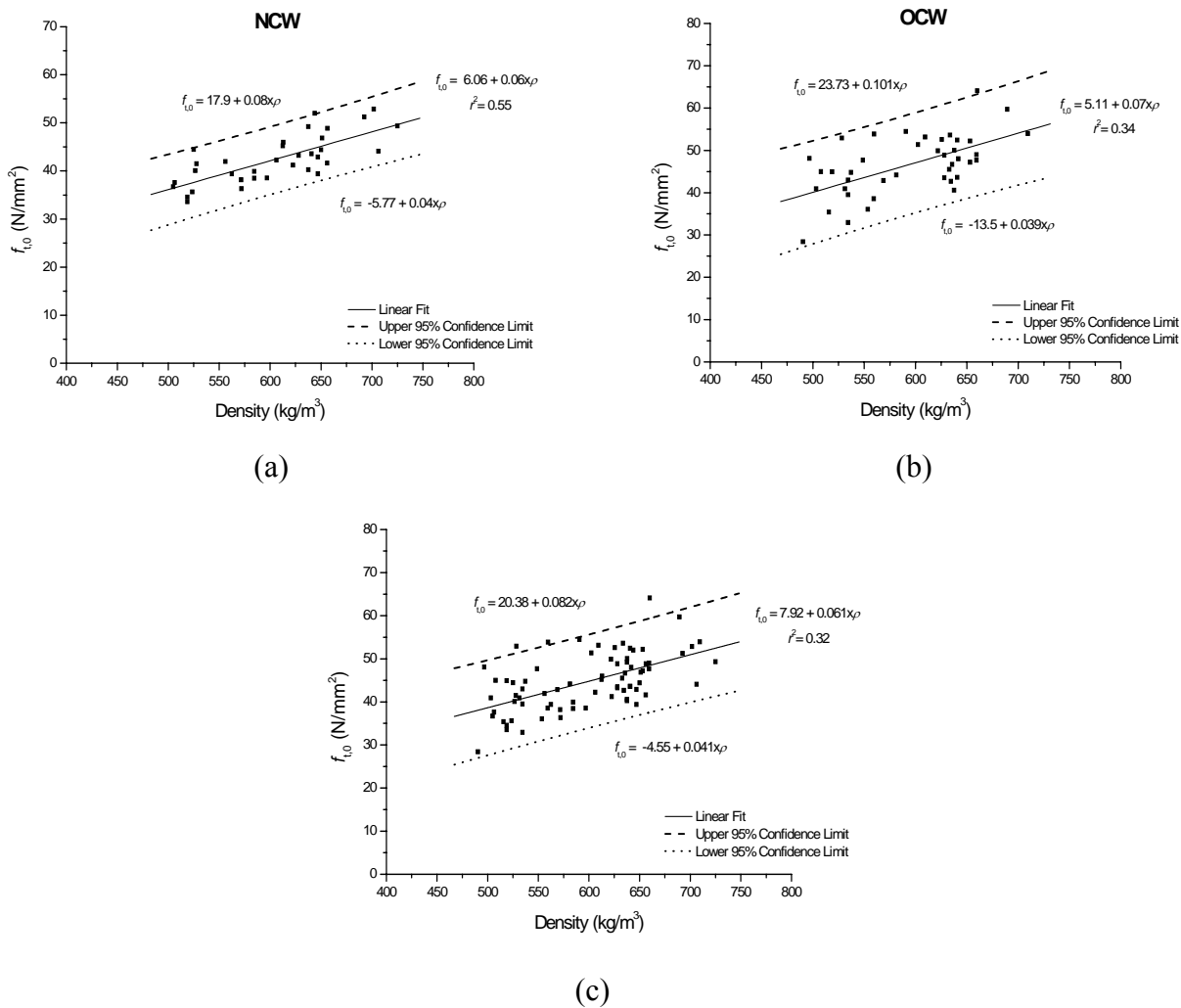


Figure 6.14 – Relation between $f_{t,0}$ and density: (a) NCW group, (b) OCW group, and (c) both groups.

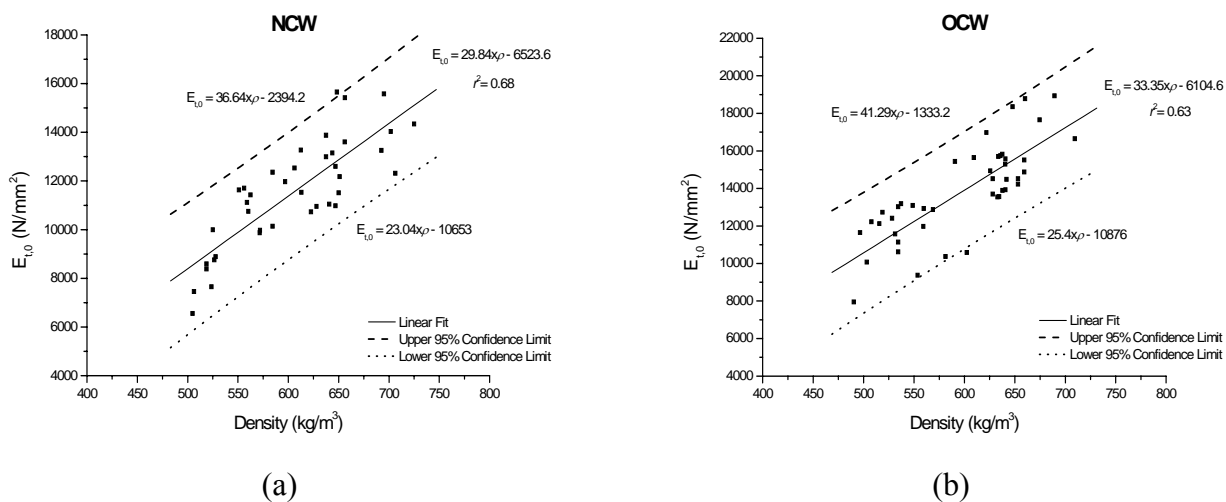


Figure 6.15 – Relation between $E_{t,0}$ and density: (a) for the NCW group, and (b) for the OCW group.

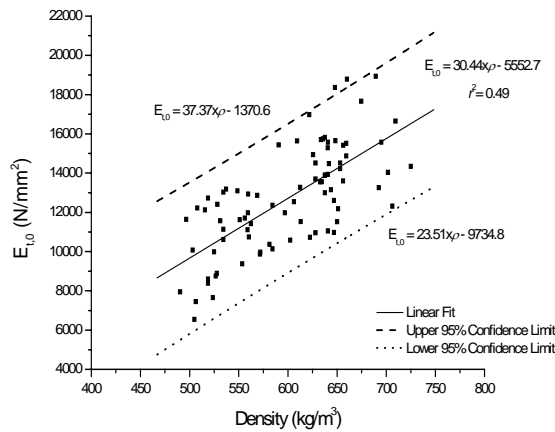


Figure 6.16 – Relation between $E_{t,0}$ and density, for both considered groups.

6.2.4.2 Correlations with the elasticity modulus

Figure 6.17 and Figure 6.18 show the correlations between the $E_{c,0}$ and E_{din} using the Indirect Method ($d = 20$ cm). Moderate linear correlations were found and the results are in agreement with Table 6.7. Considering all tests, a lower 95% confidence limit is given by:

$$E_{t,0} = -2212.82 - 0.52 \cdot UPV \tag{6.7}$$

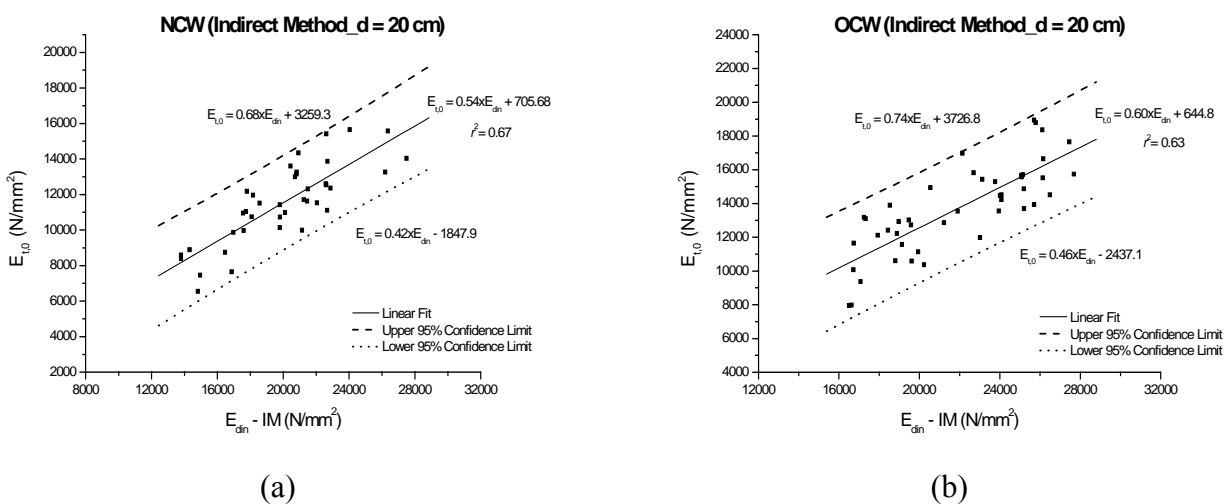


Figure 6.17 – Relation between $E_{t,0}$ and E_{din} : (a) for the NCW group, and (b) for the OCW group.

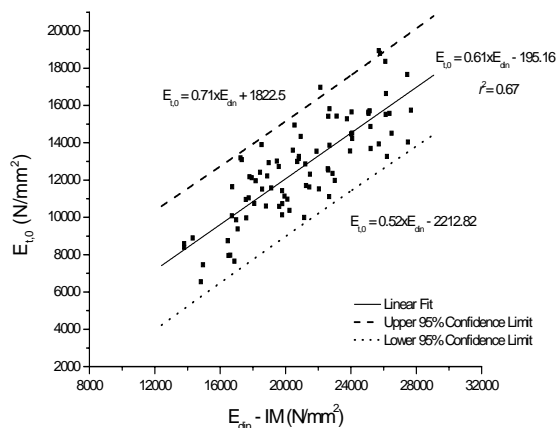


Figure 6.18 – Relation between $E_{t,0}$ and E_{din} for the NCW and OCW groups.

6.2.4.3 Correlations with the strength

Figure 6.19 and Figure 6.20 show the weak linear correlations between the E_{din} and $f_{c,0}$ using the Indirect Method ($d = 20$ cm). Considering all tests, a lower 95% confidence limit is given by the following expression:

$$f_{t,0} = 13.07 + 8.28 \times E - 04 \cdot E_{din} \tag{6.8}$$

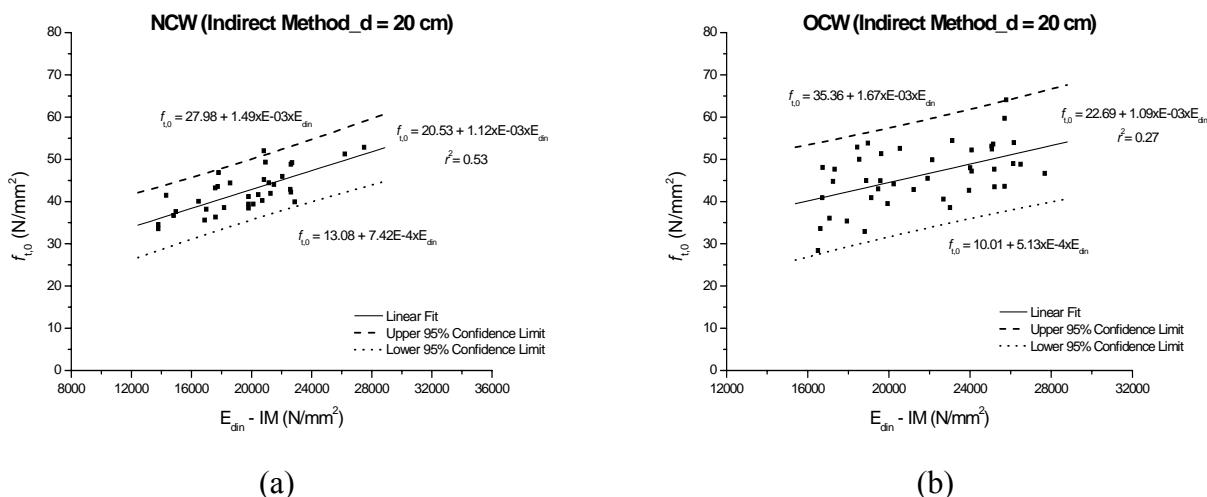


Figure 6.19 – Relation between $f_{t,0}$ and E_{din} : (a) for the NCW group, and (b) for the OCW group.

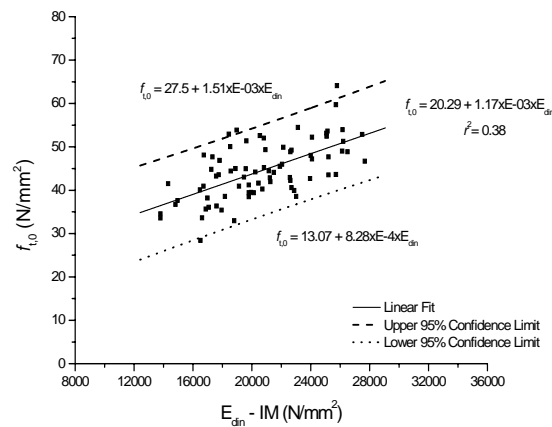


Figure 6.20 – Relation between $f_{t,0}$ and E_{din} for both considered groups.

6.3 CONCLUSIONS

The aim of the present chapter is to evaluate the tensile properties of chestnut wood specimens in tension parallel to the grain, using destructive and non-destructive methods (ultrasonic pulse velocity method), and to assess the suitability of the non-destructive methods in the evaluation of these properties.

The experimental campaign shows that tension strength parallel to the grain is strongly affected by material defects, namely local grain deviations. Taking into account the values presented in Table 6.1, it is observed that the results were affected by a coefficient of reduction of about 0.87 (corresponding to a grain slope of $\approx 6^\circ$). Aiming at a better test performance, the tension specimens were modified at the ends. This modification was based on the difference between the effective grip area and the original grip area.

It is possible to confirm that apparently no mechanical damage was present in the timber beams (from which OCW specimens were obtained) due to load-history while in service. Novel single-parameter linear regressions have been proposed for elasticity modulus and tensile strength perpendicular to the grain, using ultrasonic testing. The Poisson's ratios obtained using bonded strain gauges are very similar in both groups: NCW and OCW.

The following conclusions can also be obtained from the present chapter:

- the criteria found to determine the modulus of elasticity was found to be accurate. Each load-extension curve was reduced to a true stress-true strain plot; from these, yield strengths were determined using a strain displacement that was equivalent to a 0.3%;
- a good relation between the values obtained with the bonded strain gauges and the mechanical strain gauge (r^2 range between 0.83 and 0.90) was found. These results allow to think in future campaigns without the necessity of use bonded strain gauges which are costly, non-reusable, and are very difficult to bond to preservative-treated or wet

specimens. These bonded strain gauges also present problems with bonding handle and alignment;

- the high CV's obtained can be explained taking into account the global analysis of the results without giving any particular attention to the observed failure pattern groups, which obviously had a great influence in the strength of the specimens;
- the mechanical gauge by showing a greater gauge length than the bonded gauge have a higher probability of overlap the failure region therefore more prone to record the true global stress-strain curve on the weakest region;
- the highest modulus of elasticity was obtained using the Indirect Method ($d = 20$ cm). This fact is directly related with the uniform section presented by the measured region: there were no narrow or contract zones in the specimen, such as happens in the other two methods;
- the results indicate a marginal (5%) difference between average compressive and tensile strength but a significant difference in terms of the modulus of elasticity ($E_{c,0} = 0.66 E_{t,0}$).

Evaluation of load carrying capacity of a traditional timber joint

“The function of a loadbearing structural wood joint in terms of the construction is to join together pieces of timber permanently and securely in such a way that the required structural interaction of the constructional element or the construction itself is enabled...” (Zwerger, 2000).

In the past, timber structural design was dominated by the carpenter know-how which in turn was based upon his previous works or upon the works of others both supported on timber trusses solutions that performed reasonable well (did not fall). Although carpenters awareness that some members were subjected to tension and others to compression stresses is evident from the observation of old timber structures, the lack of scientific understanding about the global structural behaviour of timber trusses led sometimes to structural anarchy which is also perceptible on joints. Joints assure important functions as holding on the truss and sustaining the stresses imposed on it. In traditional timber constructions load distribution through joints was made with empirical knowledge, transmitted and improved through generations. The early design rules or standards were built upon this empirical evidence, see Figure 7.1.

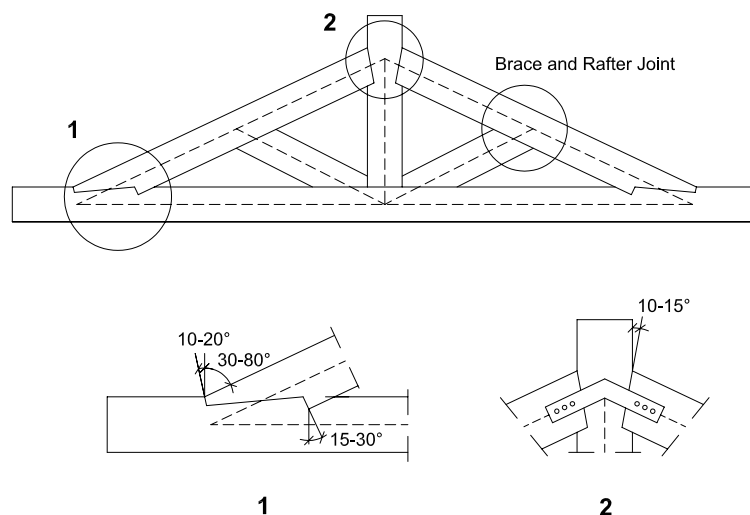


Figure 7.1 – Typical timber roof structure in traditional constructions, with details: connection between rafter and chord (1) and between rafter and king post (2).

The geometric configuration of old timber joints varies, depending on the structural elements connected and on the skills of ancient builders. But, often joints exhibit sophisticated and reasonable structural understanding (Erman, 1999).

There is a large number of timber joint types, such as the butt-joints, the halved and lapped joints, the notched joints and the birdsmouth joint, see Figure 7.2. These traditional timber joints rely on direct contact and friction, plus nails, pins or both often used to increase the joint resistance.

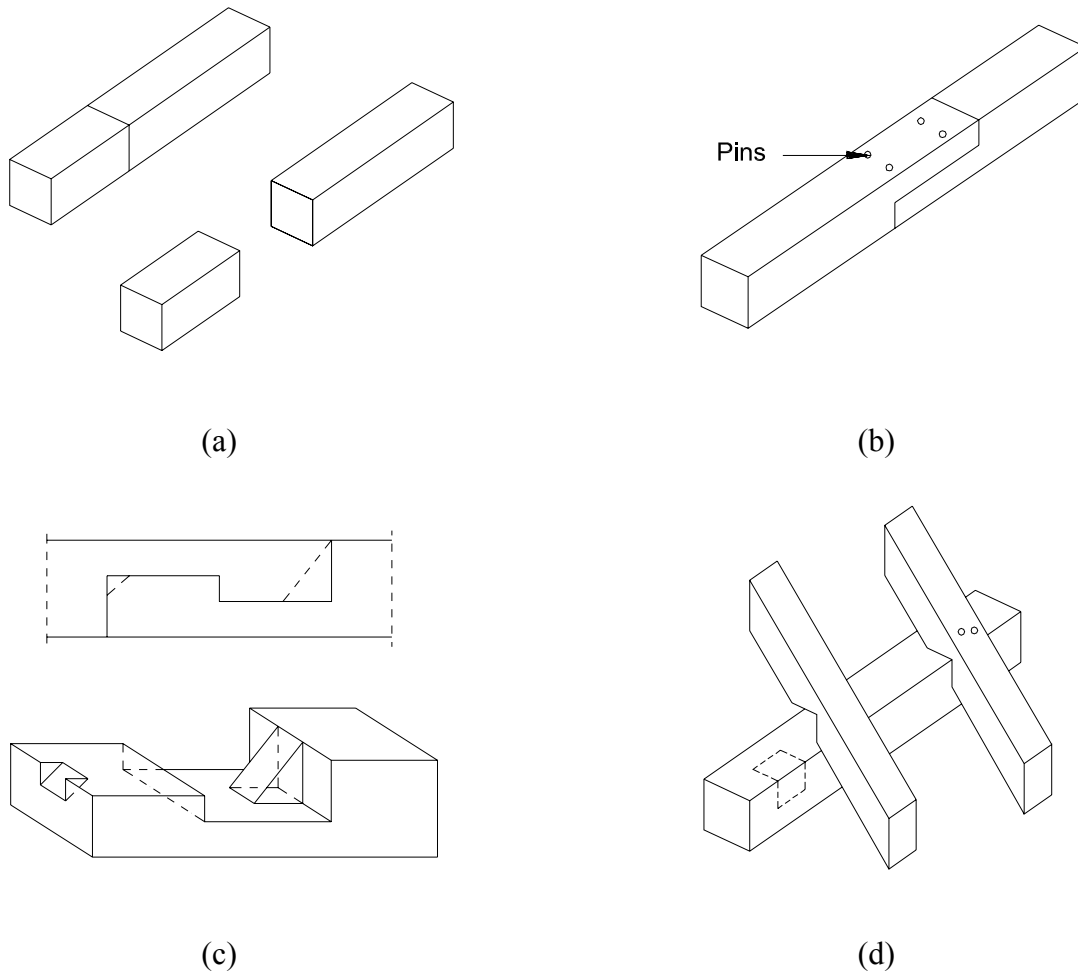


Figure 7.2 – Typical timber joints: (a) butt-joint, (b) lap joint, (c) notched joint, and (d) birdsmouth joint.

Another typical timber joint is the mortise and tenon, which solved a major problem by carrying the shear and compressive force on its tenon. The lack of knowledge about this joint has become particularly important to predict the load carrying capacity of existing constructions. Therefore, the present work addresses this type of joints. In particular, the objective is to investigate the correlations between non-destructive investigations and the strength of a typical mortise and tenon joint, considering both new and old chestnut wood. The adopted NDT's for the joints are the Pilodyn, Resistograph and ultrasonic tests.

7.1 THE MORTISE AND TENON JOINT

The mortise and tenon joint, see Figure 7.3, was selected because it is one of the most commonly used and a typical example of an interlocking joint. Mortise and tenon joints were the basic components of joint craftery in Portugal and connect two or more linear components, forming a “L” or “T” type configuration. The key problem found in these joints is the possible premature failure caused by large displacements. Unlike most timber joints, the load-displacement behaviour of these joints is generally very ductile.

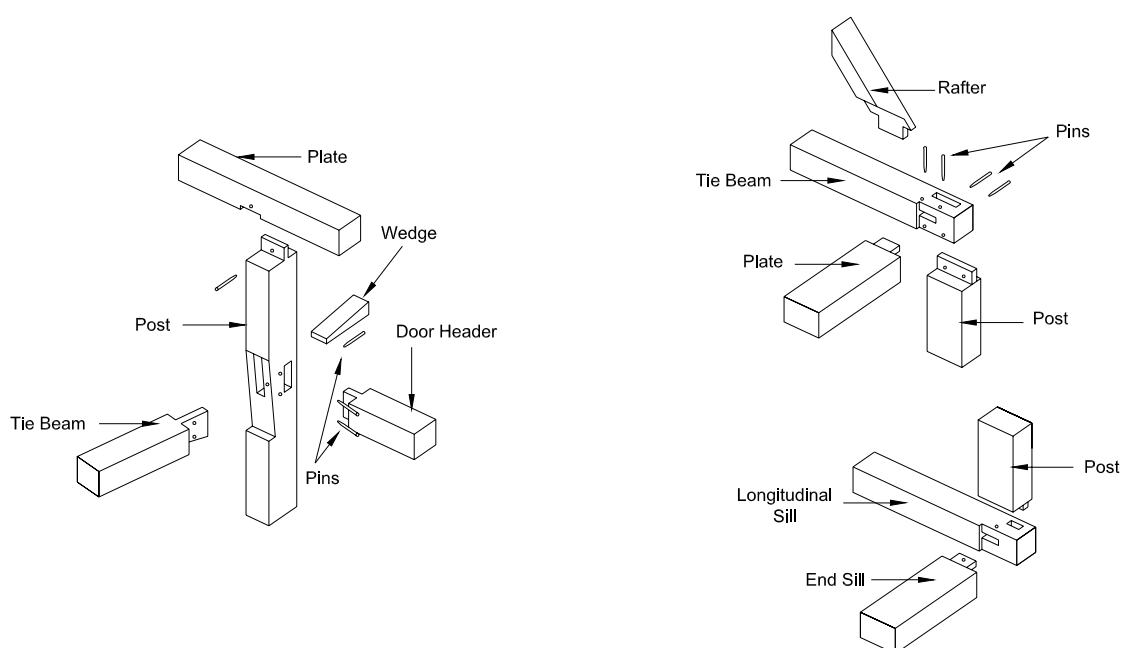


Figure 7.3 – Details of typical tenon and mortise joints.

The bearing capacity of mortise and tenon joints is a function of the angle of the connection, and length of the toe and mortise depth. According to the European building codes, joints are of crucial importance for the seismic design of timber structures. However, there are no recommendations on the design codes about general dimensions, such as length of the toe and the mortise depth in order to avoid structural failure of the connections, and the joints in existing structures are based on empirical rules.

The tenon is the piece of wood that slots inside the mortise, which has a hole that matches the size of the tenon. Some practical issues have to be ensured when the joint is made:

- the width and depth of the mortise is equal to the width and depth of the tenon. If the tenon is y cm width, then the mortise will be y cm width;
- the width of the mortise is around $1/3$ of the wood element thickness.

Generally, the bearing capacity of these joints is controlled by the following aspects:

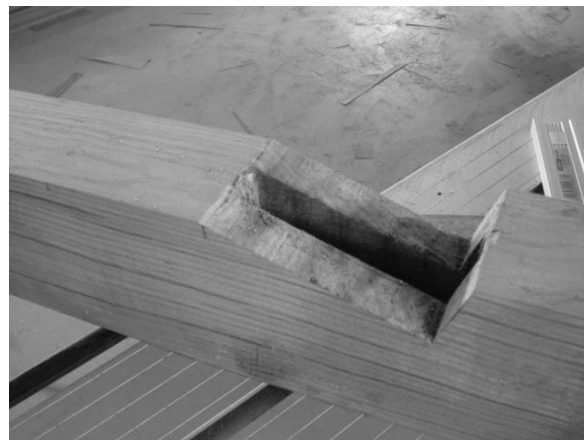
- the type of tenons and their geometry;
- the length and location of tenons;
- the number of tenons;
- the types of fasteners used in the joint.

7.2 DESCRIPTION OF TEST SPECIMENS

The specimens were produced by a specialist contractor to replicate old timber structures, see Figure 7.4.



(a)



(b)



(c)

Figure 7.4 – Test specimens production: (a) general view of the joint, (b) aspect of the mortise, and (c) aspect of the tenon.

The main goals of the present testing campaign were to:

- investigate the static behaviour of real scale replicates of old timber connections (wood-wood connections);

- characterize the ultimate strength and, the global deformation of the joint, as well as the respective failure patterns.

Each specimen consists of two timber elements, with a cross section of 92×150 mm, connected with a mortise and tenon joint without any pins. The angle between the elements is 65° , see Figure 7.5. Eight wooden specimens of chestnut wood, again divided in two distinct groups, were tested: NCW (New Chestnut Wood) and OCW (Old Chestnut Wood).

The old logs have been obtained from a specialist contractor claiming that the wood has been in service for over 100 years (date and precise origin unknown). The OCW specimens were made using original beams obtained from rehabilitation works carried out in the Northern of Portugal, using specimens with the least possible damage. The NCW specimens were prepared using recent sawn wood showing minor defects.

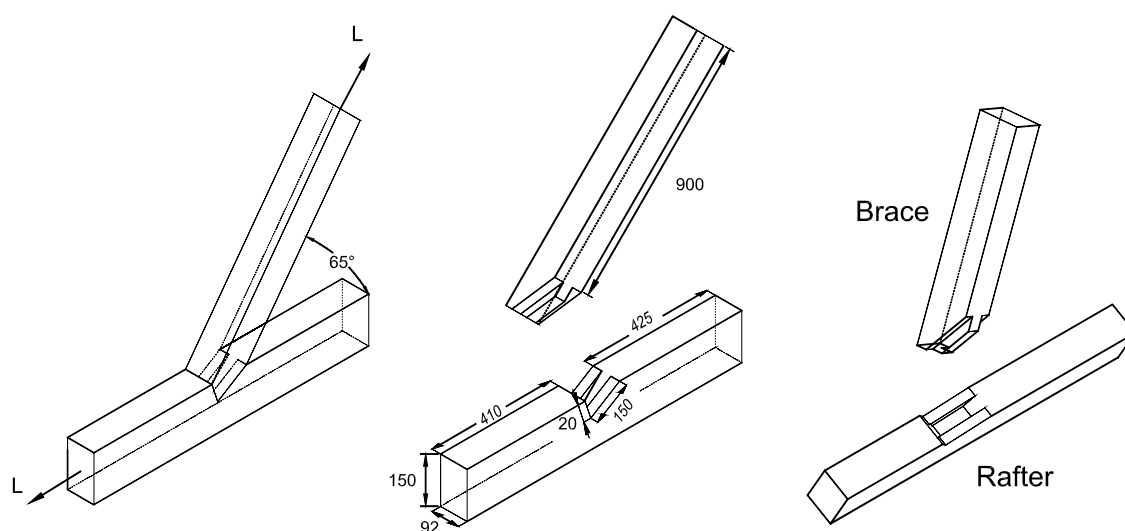


Figure 7.5 – Geometry of the test specimens (dimensions in mm).

Figure 7.6 presents the results from visual grading of the test specimens. Specimens J_1 to J_4 are made with NCW and specimens J_5 to J_8 are made with OCW. It is stressed that in the production of the specimens with old wood (OCW), special attention to the presence of defects and/or biologically attacked zones was given, particularly for the tenon region. Visual grading and inspection was carried out and in every specimen/element the knottiness, the slope of the grain and the colouring of the timber were investigated, being the worse specimens/elements discarded.

Attention was paid to the conditioning of the timber before and after the manufacture of the joints, avoiding great variations of moisture content and temperature. The conditioning was conducted in such a way that the test conditions correspond in a realistic manner to adequate in situ conditions as regards the influence of moisture content and the occurrence of gaps induced by shrinkage.

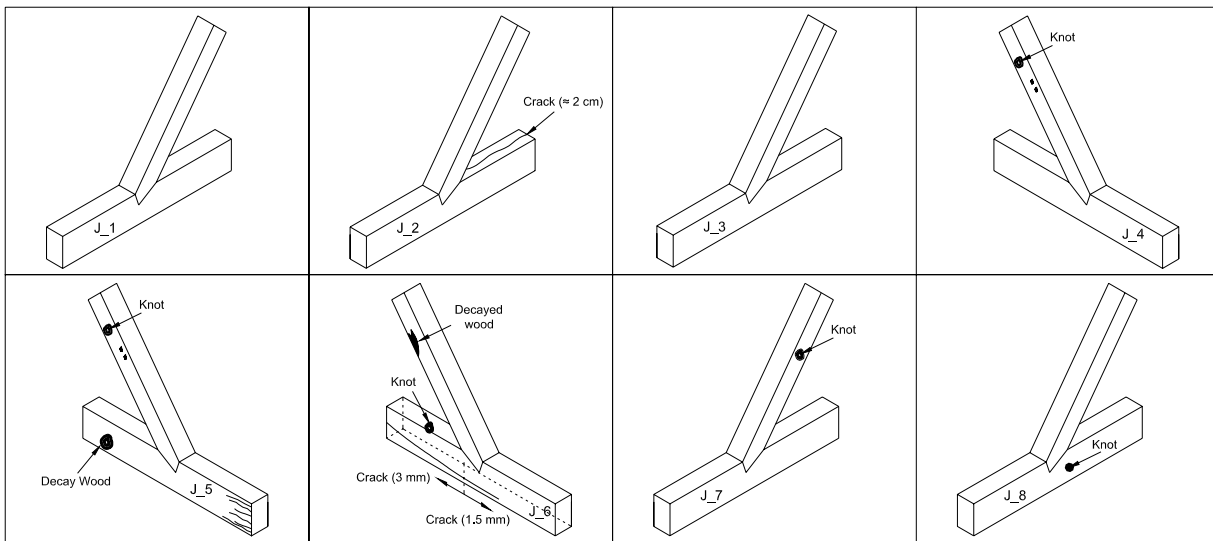


Figure 7.6 – Visual grading of the test specimens (J_1-J_4 NCW; J_5-J_8 OCW).

The joints were produced to avoid any shear in the tenon and to avoid the formation of the so called “Shear Block”. Preliminary calculations indicated that the area of the $[ABCD]$ should be larger than 50 cm^2 , see Figure 7.7.

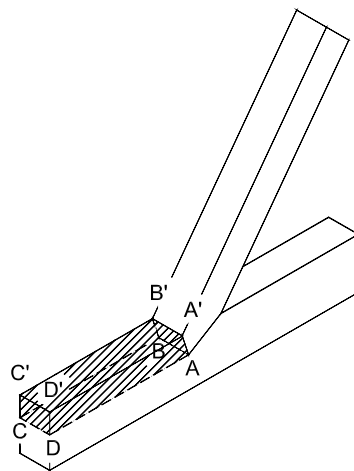


Figure 7.7 – “Shear Block” formation.

7.2.1 Density determination

Before the mechanical characterization of the connections, the density of the specimens was characterized, see Table 7.1. The density tests were carried out in samples removed from the specimens ends. Even if the sample size is very low, the NCW group presents slightly higher values of average density ($\approx 4\%$) than OCW group. The values encountered for the density are in accordance with the requirements of the ISO 8970 (1989) standard.

Table 7.1 – Average values of density (one specimen for each timber element).

Density (kg/m ³)					
	Brace	Rafter	Average	Std. Dev.	Group
J_1	584.2	602.1			
J_2	584.9	544.2	593.6	25.4	NCW
J_3	604.0	605.5			
J_4	590.2	633.3			
J_5	575.1	605.6			
J_6	598.9	574.7	568.8	31.4	OCW
J_7	507.1	545.7			
J_8	561.7	581.8			

7.3 DESTRUCTIVE TESTS

7.3.1 Test set-up

A test set-up was built to test the specimens under compression. One hydraulic jack was used to apply a compression force aligned with the rafter, with a programmed loading cycle. The system includes a support plate with stiffeners, able to rotate and ensure verticality of the brace. The support plate includes a toe so that the rafter does not suffer a displacement along its axis. The brace is hold in the original alignment with a horizontal bar, connected to a load cell. The jack has a maximum loading capacity of 300 kN and a maximum extension of 200 mm. Additionally a feed (Schenk system), acquisition and amplification data system (both from HBM – Spider 8) was used, to obtain and to register all the data.

Displacements were continuously recorded until failure using linear variable differential transducers (LVDT). The accuracy of the LVDT's is ± 0.025 mm and the location is shown in Figure 7.8a.

The measurements of the vertical and horizontal displacements in the specimens were done by two pairs of LVDT's placed on opposite faces of the specimens to eliminate the effect of bending (if any), see Figure 7.8b. Previously, a series of calibration tests of the set-up was carried out for the purpose of assessing its performance. For more details see Annex 5.

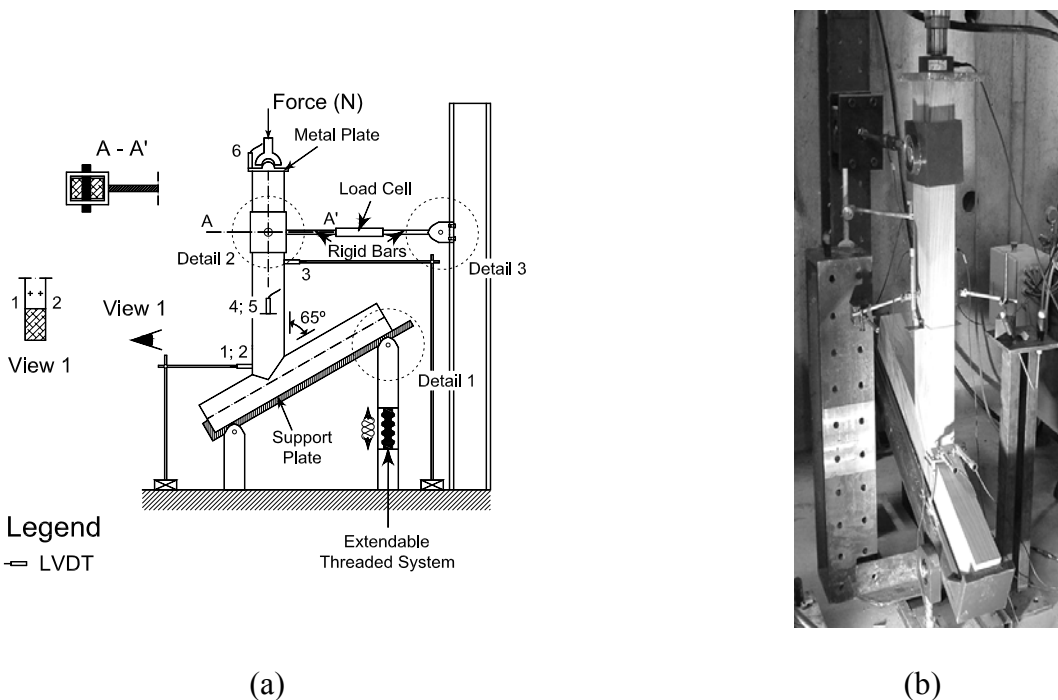


Figure 7.8 – Aspects of the destructive test set-up: (a) front view with location of LVDT’s 1-6, and (b) perspective inside the laboratory.

It should be noted that the force was imposed in the test specimens by using a metal bearing platen promoting uniform stress distribution on the top surface. The loading procedure consisted of the application of two monotonic load stages: firstly, the load was applied up to 50% of the estimated maximum load (determined on the basis of the preliminary tests) and was maintained for 30 s. The load was then reduced to 10% of the estimated maximum load and maintained for 30 s., as shown in Figure 7.9. This procedure was repeated once again and, thereafter, the load was increased until ultimate load or until a maximum slip of 15 mm between the two timber elements was reached. This procedure is based on the EN 26891 (CEN, 1991) requirements.

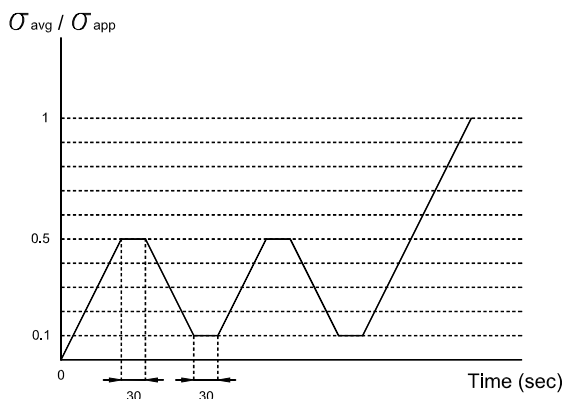


Figure 7.9 – Load testing procedure.

A constant rate of loading corresponding to about 20% of the estimate maximum load per minute was used, in such a manner that the ultimate load or slip of 15 mm was reached in about five minutes of additional testing time in the final loading procedure. The total testing time is about 9 to 12 minutes.

Each load-displacement curve was reduced to a true force-true displacement plot. The ultimate load of the joint ($F_{ult, joint}$) is defined as the conventional value corresponding to a strain equal to a 2% offset in the usual terminology, as shown in Figure 7.10.

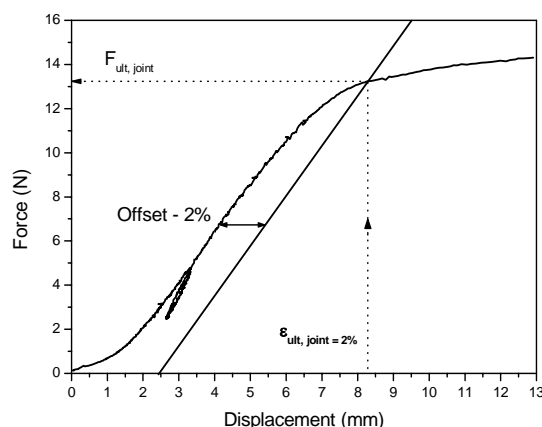


Figure 7.10 – Definition of the ultimate load from the force-displacement diagram.

7.4 NON-DESTRUCTIVE TESTS

In order to investigate possible correlations and the validity of using NDE as a tool to assess the joint strength, different non-destructive techniques (NDT's) have been carried out. The adopted NDT's are the Pilodyn, the Resistograph and the ultrasonic tests, which were carried out in both timber elements, see Figure 7.11.

Average values were considered in all measurements and two readings per specimen, per side, were generally made but a third one was added if the two first readings differed significantly.

Here, it is noted that Pilodyn and Resistograph have been carried out in samples removed from the elements ends, in order not to affect (even if marginally) the local strength of the joint, and the ultrasonic tests have been carried out at the exact joint location.

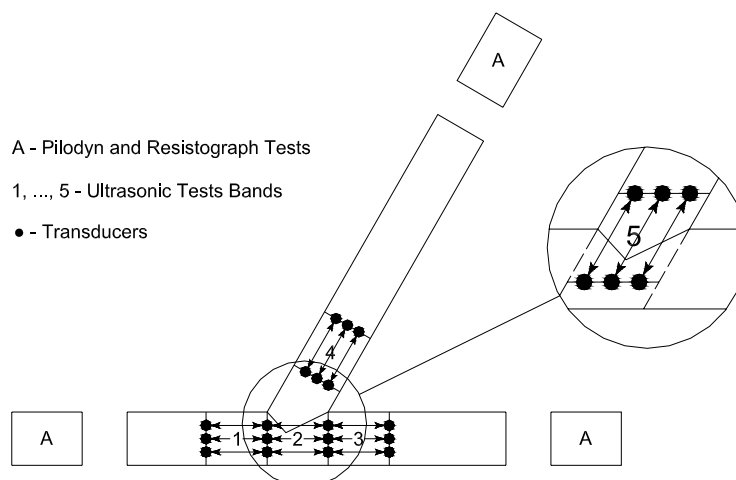


Figure 7.11 – Location of NDT tests.

7.4.1 Pilodyn and Resistograph tests

In the case of Pilodyn and Resistograph, for each element three independent measurements have been carried out. The results shown represent therefore the average of the readings permitting to reduce the scatter related to local measurements. In the present testing program, drilling penetration was made on planes TL and LR, which, in real cases, represents the accessible faces of timber elements.

The resistographic drills were made by using the Resistograph 3450-S. For all the specimens, a resistographic measure (RM) was calculated from the diagram obtained with the Resistograph, as the ratio between the integral of the area of the diagram and the length l of the drilled perforation. The average results are presented in Table 7.2. The Pilodyn 6J can measure the penetration of a metallic needle with 2.5 mm of diameter, which is inversely proportional to the density of the wood, evaluating the surface hardness or resistance to superficial penetration. The average results are presented in Table 7.3.

Table 7.2 – Average results of the Resistograph Tests (values in bits/mm).

	Brace	Rafter	Group
J_1	449.5	464.1	NCW
J_2	367.7	471.7	
J_3	365.0	424.5	
J_4	463.6	412.3	
J_5	391.7	474.3	OCW
J_6	332.0	495.2	
J_7	396.6	390.5	
J_8	323.1	432.0	

Table 7.3 – Average results of the Pilodyn Tests (values in mm).

	Brace	Rafter	Group
J_1	8.0	8.0	NCW
J_2	7.8	8.8	
J_3	8.0	7.3	
J_4	8.0	7.3	
J_5	8.0	8.2	OCW
J_6	8.0	7.3	
J_7	9.0	8.8	
J_8	8.7	8.2	

7.4.2 Ultrasonic tests

Given the dimensions of the wood elements and the diameter of the transducers used ($\phi = 25$ mm), a reference testing mesh was defined on the central mid-third of each element, as shown in Figure 7.11. Five distinct locations were defined, corresponding to three distinct zones of testing:

- three locations in the brace;
- one locations in the rafter;
- one location in the joint.

The tests in the brace and rafter aimed at characterizing the mechanical properties of the elements in zones nearby the joint. The test across the joint tried to evaluate in a qualitative way the effectiveness of the assembly between the two elements. A through-transmission technique was adopted measuring the wave propagation velocity parallel to the grain in each element and joint.

A Pundit/Plus device (ultrasound generator) and a pair of cylinder-shaped transducers (150 kHz) were used. In all tests, coupling between the transducers and specimens was assured by a conventional hair gel, and a constant coupling pressure was applied on top of the transducers by means of a rubber spring, allowing adequate transmission of the elastic wave between the transducers and the specimen under testing. The transducers were fixed into a special purpose assembly jig to ensure their alignment. The average and the standard deviation results for the ultrasonic pulse velocity, for each considered joint, are presented in Table 7.4.

Table 7.4 – Results of the Ultrasonic Tests (average and standard deviation values in m/s).

NCW Joints							
		Brace		Joint		Rafter	
		Side 1	Side 2	Side 1	Side 2	Side 1	Side 2
J_1	Average	4160.9	4291.8	3960.5	3960.5	4459.5	4760.5
	Std. Dev.	76.4	243.6	55.3	55.3	0	80.1
	Average (Total)	4226.3		3960.5		4610	
	Std. Dev. (Total)	160.0		55.3		40.0	
		Brace		Joint		Rafter	
		Side 1	Side 2	Side 1	Side 2	Side 1	Side 2
J_2	Average	4834.3	4814.8	3992.5	4091.5	5000.0	4809.5
	Std. Dev.	258.1	219.6	55.3	58.1	0	165
	Average (Total)	4824.6		4042.0		4904.8	
	Std. Dev. (Total)	238.9		56.7		82.5	

	Brace		Joint		Rafter		
	Side 1	Side 2	Side 1	Side 2	Side 1	Side 2	
J_3	Average	4652.2	4792.2	4024.4	4024.4	4855.7	4585.7
	Std. Dev.	237.8	98.7	0	0	142.9	127.4
	Average (Total)	4722.2		4024.4		4720.7	
	Std. Dev. (Total)	168.2		0		135.2	

	Brace		Joint		Rafter		
	Side 1	Side 2	Side 1	Side 2	Side 1	Side 2	
J_4	Average	4276.1	4049.4	3722.2	3750.0	4976.2	4760.5
	Std. Dev.	205.1	118.1	48.1	0	453.6	80.1
	Average (Total)	4162.7		3736.1		4868.3	
	Std. Dev. (Total)	161.6		24.1		266.8	

OCW Joints

	Brace		Joint		Rafter		
	Side 1	Side 2	Side 1	Side 2	Side 1	Side 2	
J_5	Average	4650.7	4550.7	3587.0	3837.2	4763.1	4763.1
	Std. Dev.	124.8	322.1	0	0	155.7	155.7
	Average (Total)	4600.7		3712.1		4763.1	
	Std. Dev. (Total)	223.5		0		155.7	

	Brace		Joint		Rafter		
	Side 1	Side 2	Side 1	Side 2	Side 1	Side 2	
J_6	Average	4824.9	4904.8	4024.4	3960.5	4951.0	4902.0
	Std. Dev.	135.7	146.0	0	55.3	84.9	84.9
	Average (Total)	4864.9		3992.5		4926.5	
	Std. Dev. (Total)	141.0		27.7		84.9	

	Brace		Joint		Rafter		
	Side 1	Side 2	Side 1	Side 2	Side 1	Side 2	
J_7	Average	3928.6	3928.6	3666.7	3666.7	3928.6	3837.2
	Std. Dev.	0	0	0	0	0	0
	Average (Total)	3928.6		3666.7		3882.9	
	Std. Dev. (Total)	0		0		0	

	Brace		Joint		Rafter	
	Side 1	Side 2	Side 1	Side 2	Side 1	Side 2
J_8						
Average	4777.1	4910.0	3904.1	3963.6	4812.1	4951.0
Std. Dev.	156.0	344.5	196.2	147.1	211.3	84.9
Average (Total)	4843.5		3933.8		4881.5	
Std. Dev. (Total)	250.2		171.6		148.1	

7.5 EXPERIMENTAL RESULTS AND OBSERVATIONS

The main characteristic of the adopted joint is that the direction of the grain of the two assembled pieces it is not coincident, forming an acute angle. The rafter is loaded in the direction parallel to the grain, whereas the brace is loaded at an oblique angle inducing large stresses perpendicular to the grain. Due to the anisotropic behaviour of wood, wood stressed parallel to the grain assumes the highest values of strength. Therefore, the rafter, stressed in compression parallel to the grain, easily penetrates the brace.

The compressive damage in the brace occurred either localized at the toe or distributed along the full contact length. Often, out-of-plane bulging of the rafter under the contact length was observed. In some cases, compressive damage was accompanied with shear failure in the rafter in front of the toe. Figure 7.12 and Figure 7.13 illustrate the typical damage observed at ultimate load and gives the experimental results in terms of ultimate force.



Figure 7.12 – Typical experimental failure patterns observed: (a) joint collapsed in compression, with damage localized at the toe, and (b) joint collapsed in compression, with uniform distribution of damage.

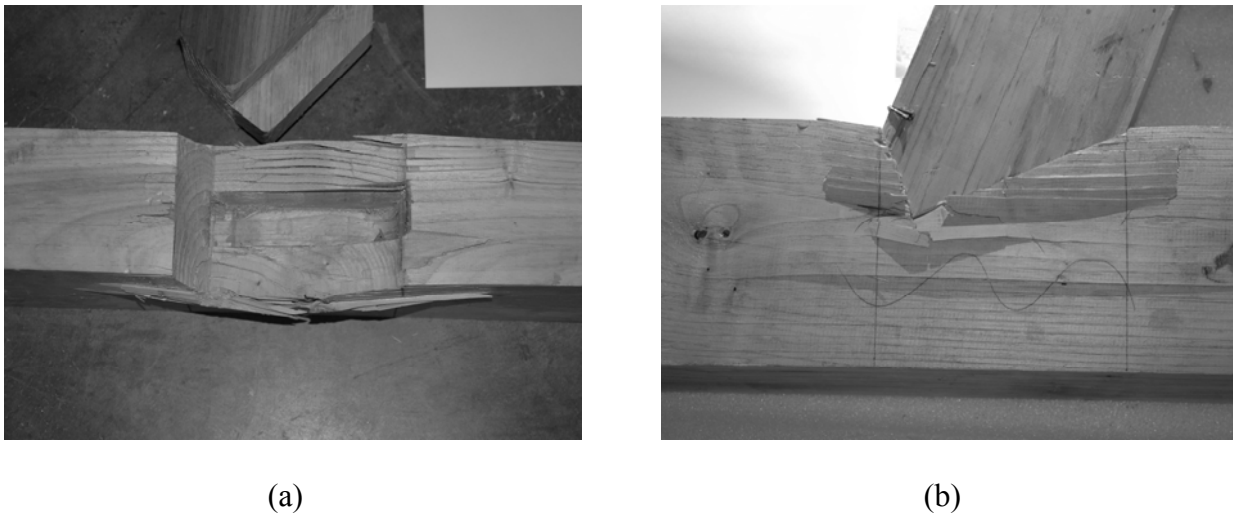


Figure 7.13 – Typical experimental failure patterns observed: (a) joint collapsed in compression, with out-of-plane bulging, and (b) combined failure in compression and shear parallel to the grain at the toe.

Table 7.5 presents the results for the average ultimate force, and the standard deviation, organized according to age. Here, it can be seen that the results presents a huge scatter, ranging from an ultimate force of 98.5 kN up to a force of 161.5 kN. Even if the number of specimens is rather low, the average force in terms of groups NCW and OCW exhibits a difference lower than 10%. Specimen J_7 can possibly be discarded because the value found is too low and is controlled by a local defect: the large longitudinal crack in the rafter. In this case, the average ultimate force values of the groups NCW and OCW are almost the same.

Table 7.5 – Test results: ultimate force.

	Ultimate Force (kN)	Average	Std. Dev.	Group
J_1	121.6			
J_2	161.5	145.4	18.9	NCW
J_3	159.7			
J_4	138.9			
J_5	126.4			
J_6	157.1	133.8	27.2	OCW
J_7	98.5	(145.5*)	(16.7*)	
J_8	153.0			

(*) average discarding specimen J_7

The specimens were executed avoiding the presence of large defects but some small defects were present. During the tests it was observed that the longitudinal and radial cracks of moderate width in the rafter did not have a considerable influence in the ultimate strength and in the global

behaviour of the joints. The longitudinal cracks show the tendency to close their thickness and the radial cracks show the tendency to open. This effect is more salient when the cracks are close to the joint. On the other hand, the cracks present in the brace, namely the longitudinal ones, show a tendency to propagate and to open during the tests. Nevertheless, it seems difficult to quantify the influence of these cracks in the ultimate strength of the joint. Because damage at ultimate stage is much localized at failure, the relevant defects are concentrated close to the joint. This “influence zone” of the joint according to the Saint-Venant principle is shown in Figure 7.14, and the cracks are of relevance only if located in this area.

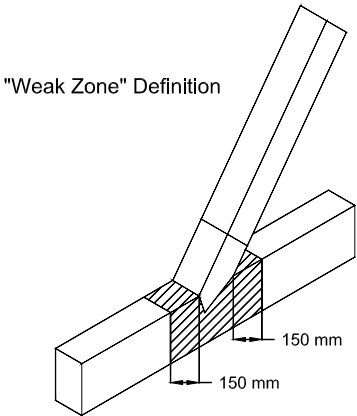


Figure 7.14 – Definition of a “influence zone” for the joint.

The influence of other defects, namely knots, in the ultimate strength capacity and global behaviour of the joints is also of relevance according to their location, see Figure 7.15.

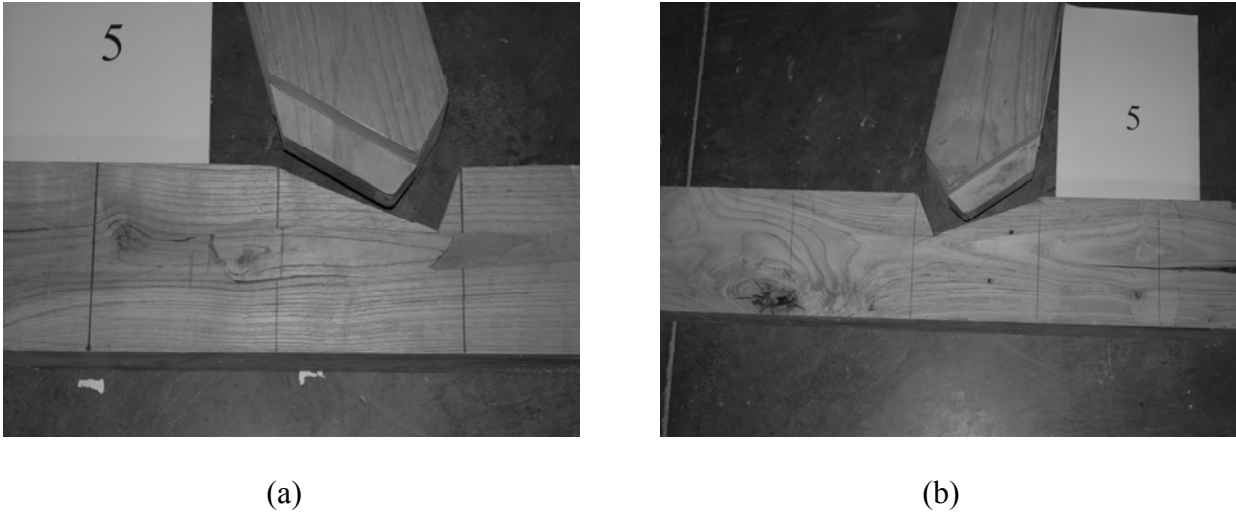


Figure 7.15 – Relevance of defects: (a) knot located inside the “influence zone”, influencing the ultimate load, and (b) knot located outside the “influence zone”.

7.5.1 Load-displacement diagrams

The present campaign shows that, considering all tests, the average strength values are slightly higher in the NCW group ($\approx 8\%$) than in the OCW group, see Table 7.6. The difference in the results between old and new wood is very low, which seems in agreement with the values of density found for the sample, where the NCW group present slightly higher values of density ($\approx 5\%$) in comparison with the OCW group, see Table 7.6. This should be expected, as shown before in Chapters 4 to 6, but it seems to be further confirmed here with real scale (and larger) specimens.

Table 7.6 – Comparison between destructive tests and density: average results.

	NCW	OCW
Strength Average (kN)	145.4	133.8
		145.5*
Density Average (kg/m³)	593.6	568.8

(*) average discarding specimen J_7

The results of all tests in terms of load-displacement diagrams, given by the vertical force vs. vertical displacement, are given in Annex A.5. Here, the vertical load is measured by the load cell located between the vertical actuator and the brace and the vertical displacement is given by the average of the LVDT's located in the mid third of the brace, see Figure 7.8.

Figure 7.16 and Figure 7.17 show typical individual load-displacements diagrams and envelopes of load-displacement diagrams. It is evident as addressed before, that the scatter of the OCW group is much larger than the scatter of NCW group, due to J_7 specimen. From the load-displacement diagrams obtained the following relevant remarks can be drawn:

- in a first phase, the diagrams always start with an upward curvature, exhibiting a nonlinear, non-recoverable, “bedding” response, which is due to the adjustment of the tenon and the mortise;
- in a second phase, within working stress levels, the response exhibits an approximately linear branch up to the conventional maximum load, which occurred at an average displacement of 8 mm for the NCW group and 7 mm for the OCW group. The value of the displacement associated with the maximum load is lower for the NCW group joints in comparison with the OCW group joints, possibly indicating a slightly larger deterioration of the timber of the OCW specimens;
- it is noted that unloading-reloading cycles within working stress levels provide a constant stiffness, which is higher than the loading stiffness. The justification of this behaviour is probably attributed to the nonlinear behaviour of the interface between rafter and brace, which exhibits a closure phenomenon;

- finally, after the conventional maximum load the displacement increases rapidly with a much lower stiffness, due essentially to the compressive failure of the wood in the rafter around the joint.

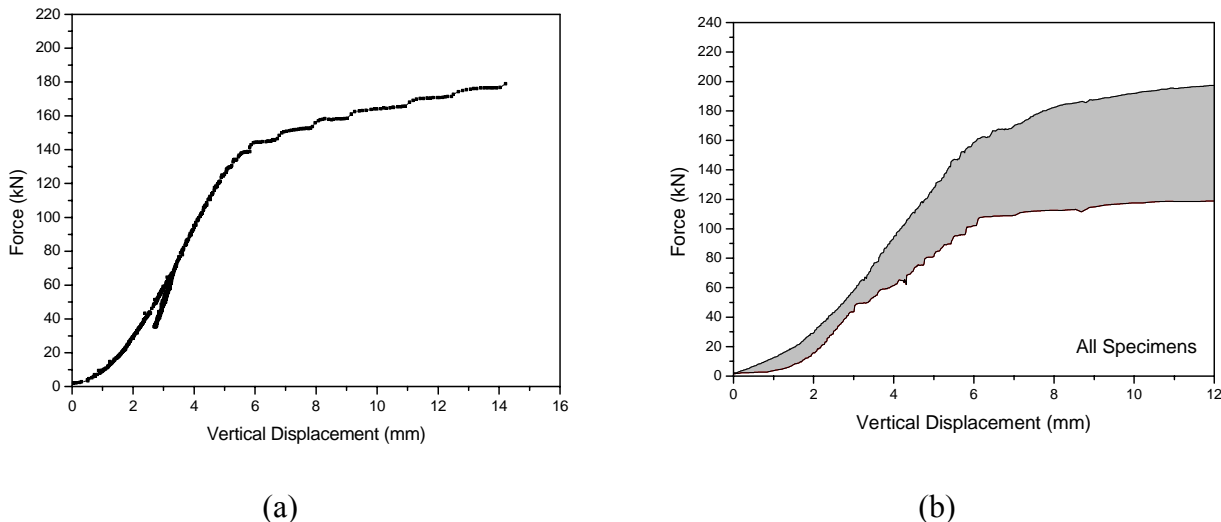


Figure 7.16 – Load-displacement diagrams: (a) typical individual load-displacement diagram (specimen J_4), and (b) envelope of load-displacement diagram for all tests (NCW group and OCW group joints).

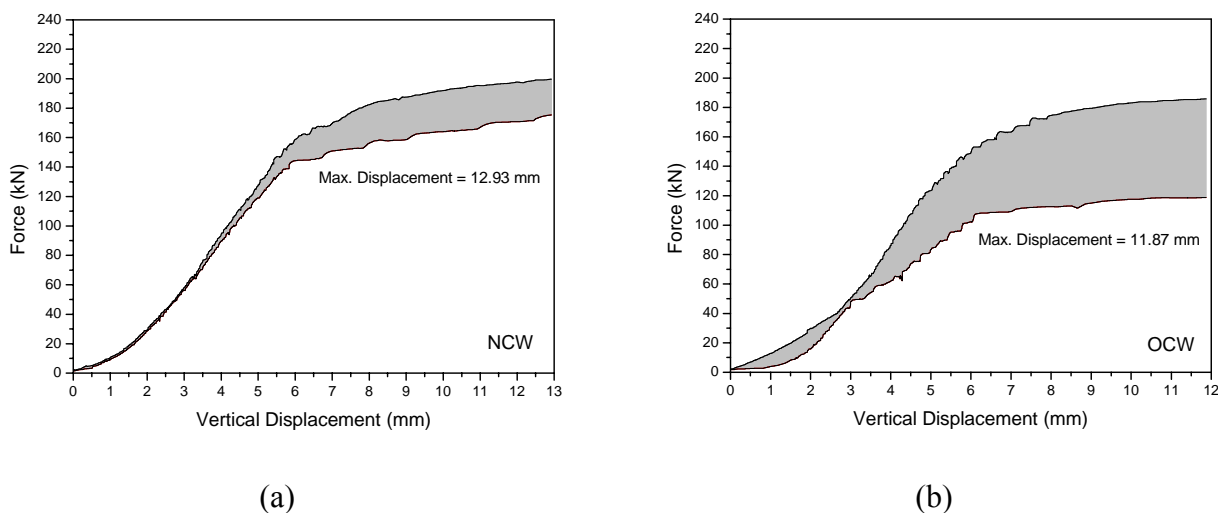
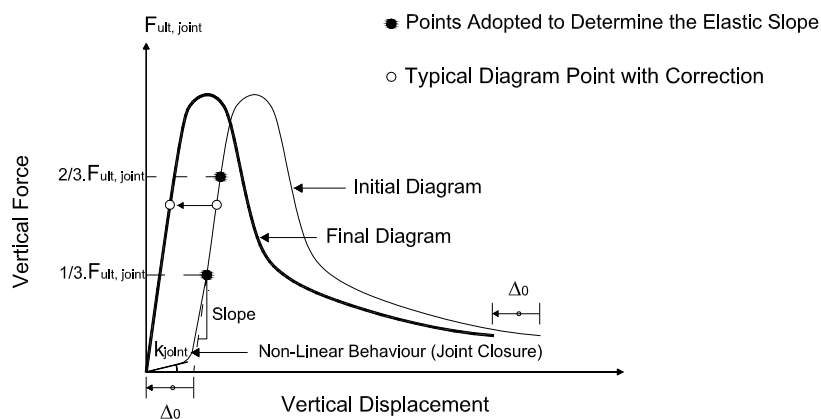


Figure 7.17 – Envelope of load-displacement diagrams for the: (a) NCW group, and (b) OCW group.

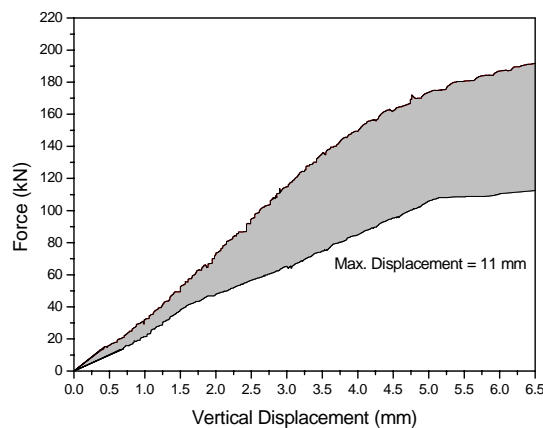
For the purpose of a more refined analysis in Chapter 8, the true load-displacement diagrams were corrected with an offset that eliminates the upward curve related to the nonlinear behaviour of the joint previous to full contact (joint closure), see Figure 7.18.

Due to the nature of load-displacement diagrams for mortise and tenon joints, choosing the linear portion of the curve includes some subjectivity. To reduce the subjectivity the elastic stiffness was calculated between 1/3 and 2/3 of the ultimate load, as represented in Figure 7.18a. The line plotted between these two points to visually analyse the quality of the fit to the linear portion of the plot, indicated that the proposed procedure is adequate.

Figure 7.18b shows the new envelope for all tests after individual correction for each load-displacement diagram.



(a)



(b)

Figure 7.18 – Load-displacement diagrams: (a) definition of removal of initial joint closure, and (b) corrected envelope diagram for all tests.

Figure 7.19 shows the relation between the vertical load and the horizontal load (reaction load measured in the horizontal load cell), for all specimens and for the two main studied groups. It can be observed that the horizontal reaction varies between 0% and 3.5% of the vertical load. Such low values are in the range of values usually adopted for bracing members and indicate that the

horizontal effects in the testing set-up can be neglected for practical purposes. From the results it is possible to conclude that the NCW group presents slightly higher reaction forces, when compared with the OCW group.

Figure 7.20 shows the load-horizontal displacement diagram, for the LVDT placed near the horizontal load cell, see Figure 7.8. Again, the horizontal displacements are very small, with a maximum around 3% of the maximum vertical displacements.

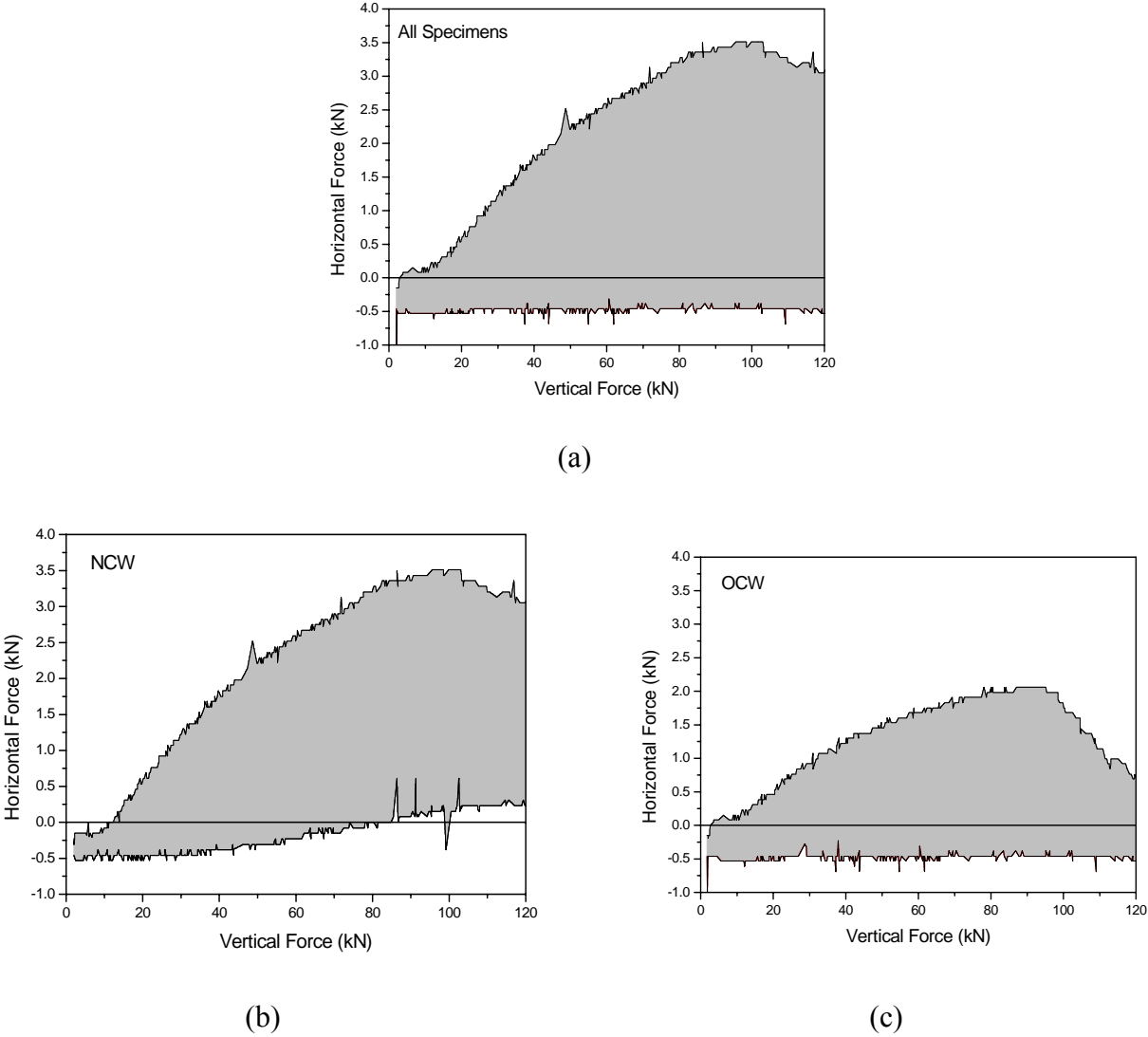
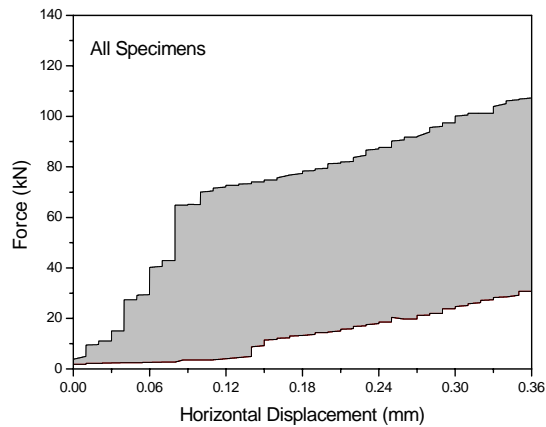
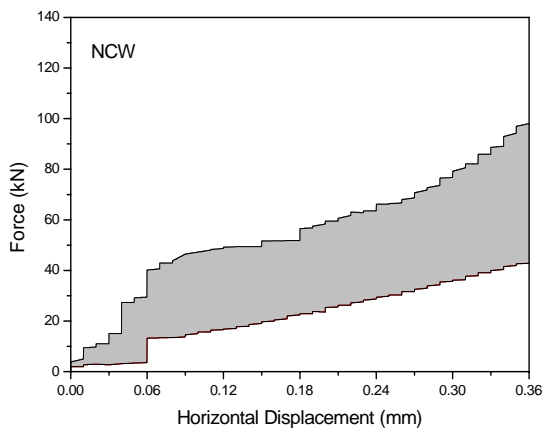


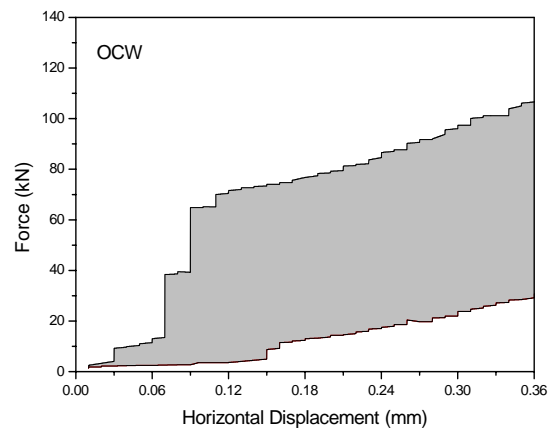
Figure 7.19 – Envelope of the relation between horizontal reaction and vertical force: (a) all specimens, (b) NCW group joints, and (c) OCW group joints.



(a)



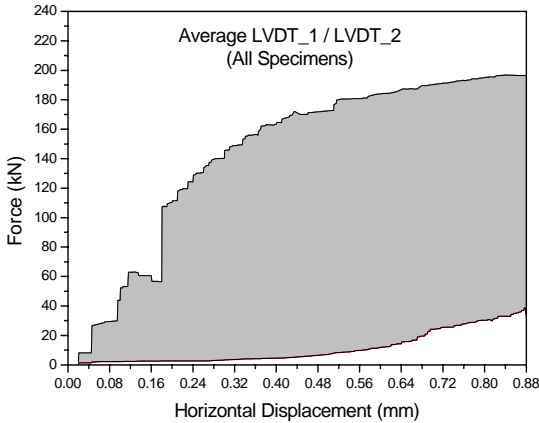
(b)



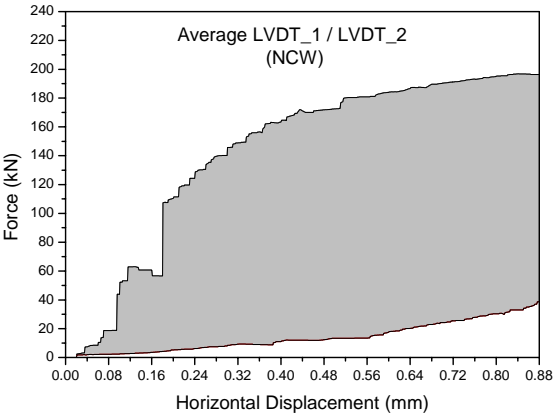
(c)

Figure 7.20 – Load vs. horizontal displacement diagram, measured at the top of the brace: (a) all specimens, (b) NCW group joints, and (c) OCW group joints.

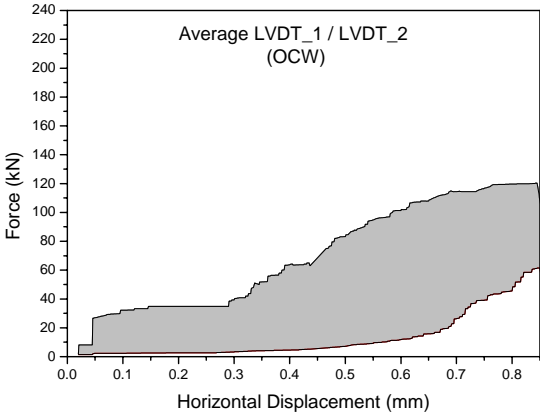
The horizontal displacements near the contact zone between the brace and the rafter were also monitored. Figure 7.21 shows the load-displacement diagrams of the average from the LVDT's placed on the bottom of the brace, see Figure 7.8, which measure the horizontal displacement of the joints. From the results, it is possible to observe that the maximum horizontal displacement reaches around 7% of the maximum vertical displacement. This is obviously due to the angle between the timber elements, but the value is still very low, indicating the excellent performance of the joint to withstand large compression forces without slipping.



(a)



(b)



(c)

Figure 7.21 – Load vs. horizontal displacement diagram, measured at the bottom of the brace: (a) all specimens, (b) NCW group joints, and (c) OCW group joints.

7.5.2 Correlations with ultimate load and stiffness

It is well known for wood that higher density means usually higher stiffness. Figure 7.22 shows the relations between density and ultimate load, in case of the joint and of the rafter only, as the structural response is controlled by the rafter. It is clear that the correlation is very weak. A possible reason for this result is that the structural response is controlled by the local characteristics of wood and density was measured at the specimens ends.

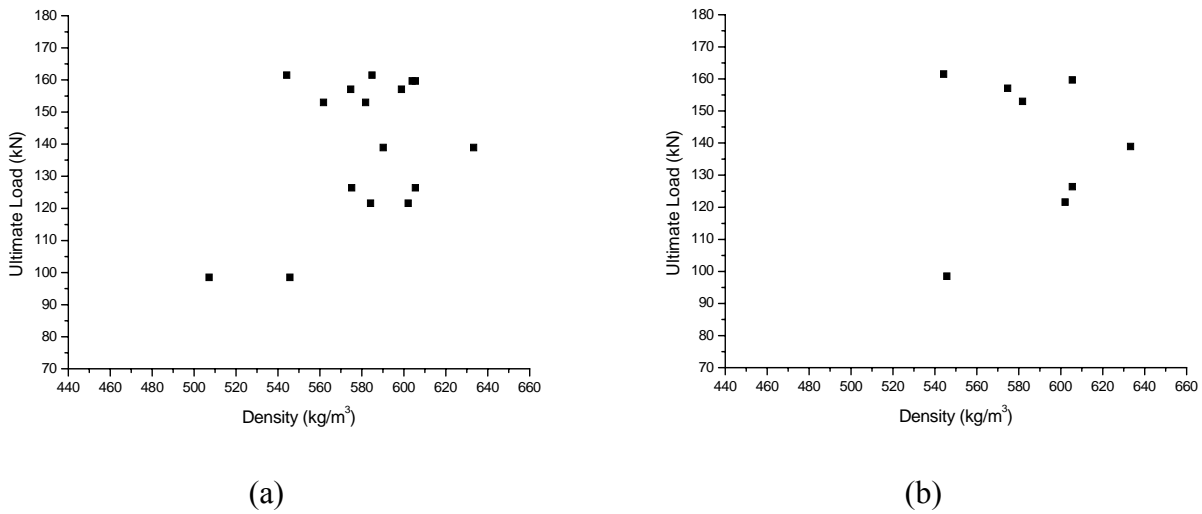


Figure 7.22 – Ultimate load vs. density for all tests: (a) total (brace and rafter); and (b) only rafter.

Figure 7.23 and Figure 7.24 show the correlations between ultimate load and two non-destructive techniques. The results indicated that these non-destructive techniques (Pilodyn and Resistograph method) are not good indicators for predicting the joint strength. Again, a definitive conclusion cannot be made because the measurements have been made in specimens ends and not at the joint location. However, taking into account also the previous Chapters, these non-destructive techniques seem more adequate to make a preliminary estimation of density, rather than mechanical grading of wood.

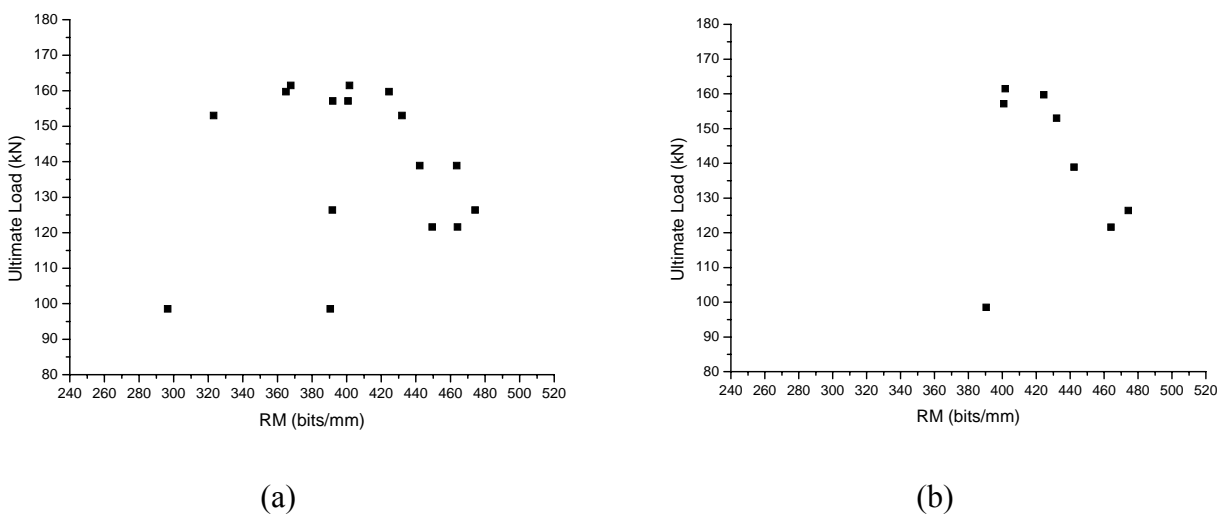


Figure 7.23 – Ultimate load vs. resistographic measure for all tests: (a) total (brace and rafter); and (b) only rafter.

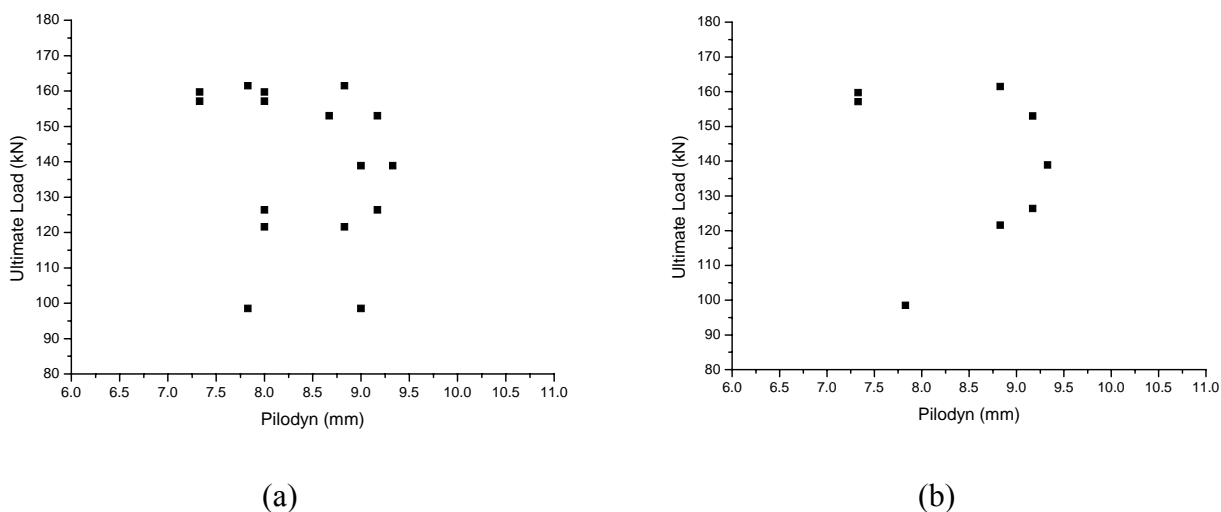


Figure 7.24 – Ultimate load vs. Pilodyn for all tests: (a) total (brace and rafter); and (b) only rafter.

Figure 7.25a illustrates the relation between the ultimate load and the ultrasonic pulse velocity. The results show that ultrasonic pulse velocity could be a good indicator for the prediction of the ultimate load. Here, it is noted that the results using local measurements only in the rafter, or rafter and brace together provide better correlations that measurements across the joint. In the latter, also the stiffness of the joint is taken into account, meaning that the ultrasonic pulse velocity is much lower. The joint stiffness is a relevant parameter for the estimation of deformations and, sometimes, resistance of timber structures, see Figure 7.18a. Therefore, Figure 7.25b illustrates the correlation between joint stiffness k_{joint} and ultrasonic pulse velocity across the joint. A clear linear correlation was found, indicating that it is possible to estimate joint stiffness from ultrasonic testing.

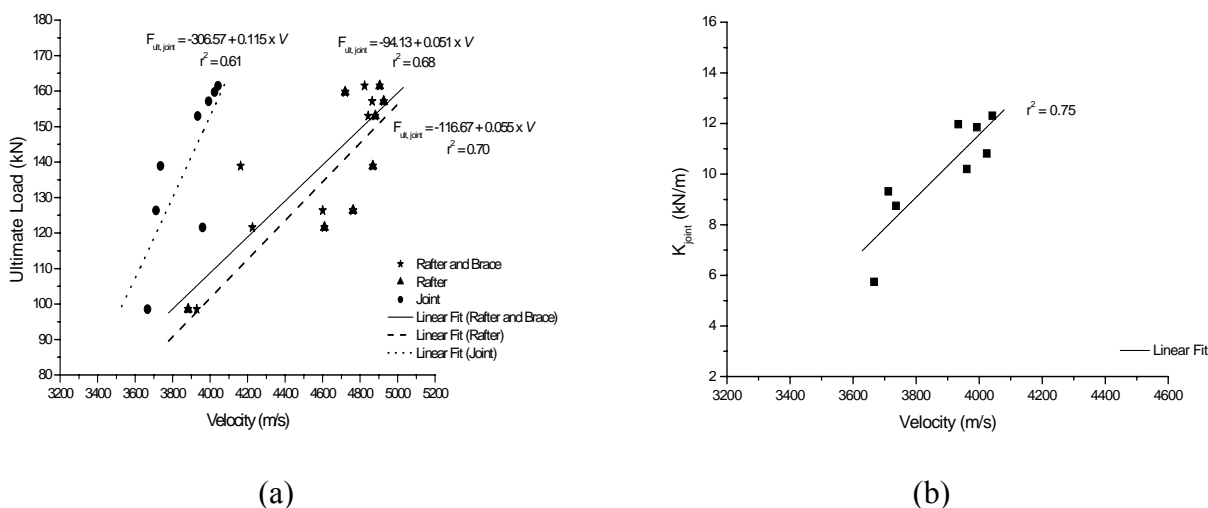


Figure 7.25 – Ultrasonic pulse velocity method for all tests: (a) relation between the ultimate load and the ultrasonic pulse velocity, and (b) joint stiffness vs. ultrasonic pulse velocity.

7.6 CONCLUSIONS

Despite the wide use of mortise and tenon joints in existing timber structures scarce information is available for design and “in situ” assessment. The objective of the present study was to quantify the strength capacity of wood-wood mortise and tenon joint by physical testing of full-scale specimens. In addition, the performance of different NDT for assessing global joint strength is also evaluated. For these purposes, old (OCW) and new (NCW) chestnut wood is used.

The difference in the results for the ultimate load between the two groups (NCW and OCW) is very low, which is in agreement with the values of density found for the sample. Therefore, the results consent to consider that no mechanical damage was forced upon timber beams (from which OCW specimens were obtained) due to load-history while in service. Thus, safety assessment of new and existing timber structures can be made with similar mechanical data.

With respect to the usage of non-destructive techniques for the prediction of the ultimate strength of the joint, the dispersion found for the density, Resistograph and Pilodyn do not recommend the usage of the related parameters for quantitative mechanical assessment. On the contrary, ultrasonic testing provides good correlations. The results also show that measuring the ultrasonic pulse velocity near the joint is a reliable way of evaluating in a qualitative manner the effectiveness of the assembly between the two elements. Novel linear regressions have been proposed in this study.

Modelling of a traditional timber mortise and tenon joint under compression

For the purpose of numerical analysis wood is often considered as a homogenous and isotropic material. This is certainly not the case as: (a) wood exhibits anisotropic elastic and inelastic behaviour; (b) natural growth characteristics such as knots, slope grain and other defects are always present. Defects can be included in numerical simulations but this requires a thorough investigation of the specimens and fine tuning, being of moderate interest for practical purposes. On the contrary, the usage of orthotropic failure criteria is essential for accurate numerical simulations.

Failure criteria that describe orthotropic inelastic behaviour offer the opportunity to perform adequate analyses of wood elements and structures, beyond the elastic limit. This can be especially valuable in the detailed analysis of timber joints and other details with complex stress distribution.

Here, the finite element method (FEM) is adopted to simulate the structural behaviour and obtain a better understanding of the failure process. Calculations are performed using a plane stress continuum model, which can capture different strengths and softening/hardening characteristics in orthogonal directions. The failure criterion is based on multi-surface plasticity, comprising an anisotropic Rankine yield criterion for tension, combined with an anisotropic Hill criterion for compression.

The adopted failure criterion is based on the available software package, Diana 8.2 (TNO, 2002; De Witte and Wolthers, 2002). It is noted that a large number of anisotropic failure criteria have been proposed to model wood and other composite materials. Conceptually, most of these criteria are phenomenological, in the sense that they do not derive from a micro-structural analysis but represent experimental data in a mathematical way.

Hill (1950) was the first to conduct studies on anisotropic plasticity proposing the following yield surface:

$$f = A \cdot (\sigma_y - \sigma_z)^2 + B \cdot (\sigma_z - \sigma_x)^2 + C \cdot (\sigma_x - \sigma_y)^2 + D \cdot \tau_{xy}^2 + E \cdot \tau_{yz}^2 + F \cdot \tau_{xz}^2 - 1 = 0 \quad (8.1)$$

where A, B, \dots, F are material parameters. His work was later extended to account for non-proportional hardening, different strengths for tension and compression (Shih and Lee, 1978; Gotoh, 1978) and softening behaviour (Lourenço *et al.*, 1997).

Hoffman (1967) proposed an empirical expression assuming different tensile and compressive strengths along the material axes, as:

$$A \cdot (\sigma_y - \sigma_z)^2 + B \cdot (\sigma_z - \sigma_x)^2 + C \cdot (\sigma_x - \sigma_y)^2 + \\ + D \cdot \sigma_x + E \cdot \sigma_y + F \cdot \sigma_z + G \cdot \tau_{xy}^2 + H \cdot \tau_{yz}^2 + I \cdot \tau_{xz}^2 = 1 \quad (8.2)$$

where A, B, \dots, I are material coefficients.

Tsai and Wu (1971) presented a strength tensor theory that is often referred to as a Tsai-Wu Theory. The basic assumption of their strength criterion is that there exists a complex failure surface in the stress-space in the following scalar form:

$$f(\sigma_k) = F_i \cdot \sigma_i + F_{ij} \cdot \sigma_i \cdot \sigma_j = 1 \quad (8.3)$$

where the contracted notation is used, and $i, j, k = 1, 2, \dots, 6$; F_i and F_{ij} are strength tensors of the second and fourth rank, respectively. This failure criterion that is believed to yield results closer to reality (Tsai and Wu, 1971; Williams *et al.*, 2000), but it is of very complex application.

Tsai and Wu (1971) assumed that the interaction terms in Eq. (8.3) are independent. This means that terms such as F_{ij} cannot be expressed as a function of uniaxial strengths.

Wu (1972) suggested an experimental method of measuring strength tensor components that involves biaxial loading. Some authors argue that removing higher-order terms from Eq. (8.3) reduces accuracy. Others argue that if higher-order terms are kept, the failure criterion becomes too complicated and question whether accuracy is truly gained (Labossiere and Neale, 1987).

Here, the failure criteria from Lourenço *et al.* (1997) is used in the analysis of the particular mortise and tenon joint detailed in chapter 7, see also Figure 8.1. The global behaviour of this joint is governed by biased compression. The influence of compression perpendicular and parallel to the grain and elastic stiffness on the response is here addressed in detail.

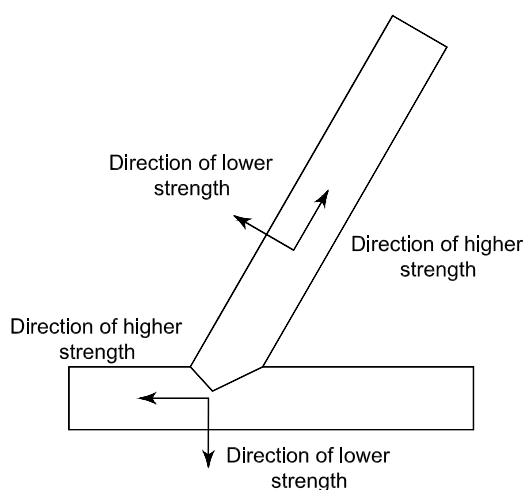


Figure 8.1 – Mortise and tenon joint under analysis, with the orientation of material axes.

8.1 ADOPTED FINITE ELEMENTS AND SOLUTION STRATEGIES

In structural mechanics, a problem is usually considered to be nonlinear if the stiffness matrix or the load vector depends on displacements (Cook *et al.*, 1989). Nonlinearities in a structure can be typically classified as material nonlinearity or as geometric nonlinearity. Material nonlinearity is related to changes in material properties, as in a nonlinear stress-strain relationship. Geometric nonlinearity is related to changes in configuration of the structure, where the strain-displacement relationship is nonlinear and equilibrium is satisfied for the deformed state of the structure.

Nonlinear analysis is used to trace the equilibrium path up to and beyond the first critical point, at which the structure becomes unstable. There is one algorithm commonly used in the incremental iterative solution of nonlinear problems: the Newton-Raphson method. The full Newton-Raphson method, with stiffness matrix update in each iteration is used in the analyses carried out in this work.

Two different finite elements were considered in the plane stress analyses carried out in this work: continuum elements (8-noded) to represent wood and line interface elements (6-noded) to represent the interface between rafter and brace, see Figure 8.2. The integration schemes used are 2×2 Gauss integration points for the continuum elements and 3 Lobatto integration points for the interface elements.

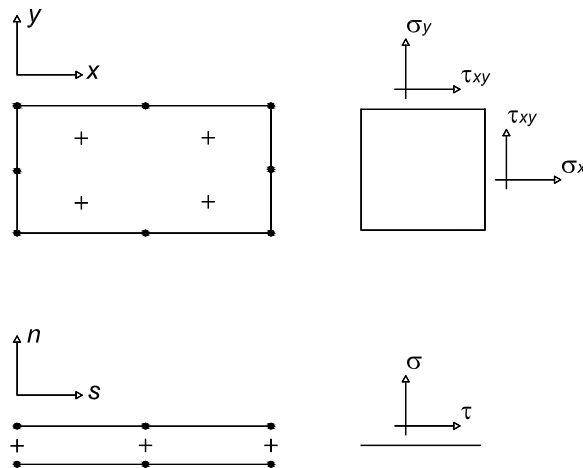


Figure 8.2 – Examples of the used finite elements: eight-noded plane stress element with Gauss integration, and six-noded line interface element with Lobatto integration.

For continuum elements the relation between the stress and strain tensors, defined by the stress vector σ and the strain vector ε , is given by:

$$\sigma = D \cdot \varepsilon \quad (8.4)$$

where

$$\sigma = \{\sigma_x \quad \sigma_y \quad \tau_{xy}\}^T \quad (8.5)$$

$$D = \begin{bmatrix} E_x & -\frac{E_x}{\nu} & 0 \\ -\frac{E_y}{\nu} & E_y & 0 \\ 0 & 0 & G_{xy} \end{bmatrix} \quad (8.6)$$

$$\varepsilon = \{\varepsilon_x \quad \varepsilon_y \quad \gamma_{xy}\}^T \quad (8.7)$$

Here, E_x and E_y are the Young's moduli in the directions parallel and perpendicular to the grain, respectively, G_{xy} is the shear modulus and ν is the Poisson's ratio.

Interface elements allow discontinuities in the displacement field and establish a direct relation between the tractions t and the relative displacements along the interface Δu , as:

$$t = k \cdot \Delta u \quad (8.8)$$

$$t = \{\sigma \quad \tau\}^T \quad (8.9)$$

$$\Delta u = \{\Delta u_n \quad \Delta u_s\}^T \quad (8.10)$$

$$k = \begin{bmatrix} k_n & 0 \\ 0 & k_s \end{bmatrix} \quad (8.11)$$

Here k_n and k_s are the linear stiffness moduli: k_n sets the relation between the normal traction t_n and the normal relative displacement Δu_n ; k_s sets the relation between the shear traction t_t and the shear relative displacement Δu_t . For detailed information about finite element formulation see Zienkiewicz and Taylor (2000a; 2000b).

8.2 THE ADOPTED ANISOTROPIC FAILURE CRITERIA

A plane stress continuum model, which can capture different strengths and softening characteristics in orthogonal directions, was formulated by Lourenço (1996). The proposed failure criterion consists of an extension of conventional formulations for isotropic quasi-brittle materials to describe orthotropic behaviour. It is based on multi-surface plasticity, and wood is an example of a material for which this criterion applies, having different strengths in the directions parallel and perpendicular to the grain.

Formulations of isotropic quasi-brittle materials behaviour consider, generally, different inelastic criteria for tension and compression. In this formulation, and in order to model orthotropic material behaviour, a Hill yield criterion for compression and a Rankine yield criterion for tension were adopted, see Figure 8.3. The formulation of this model (Lourenço, 1996) will be only briefly reviewed here.

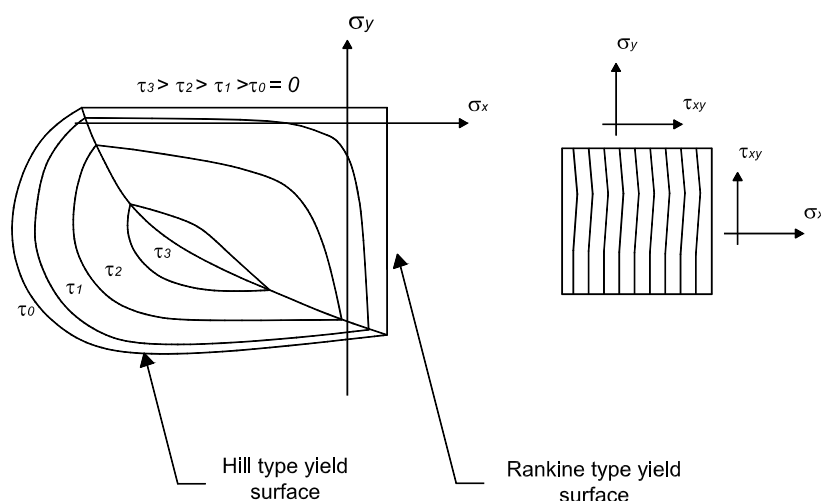


Figure 8.3 – Adopted anisotropic Rankine-Hill composite yield criterion, with different strength values for tension and compression.

8.2.1 Rankine type yield criterion

The formulation of the model is an extension of the Rankine Principal Stress model. A suitable formulation of the Rankine yield criterion is given by De Borst and Feenstra (1990). A Rankine type yield surface for an orthotropic material, with different tensile strengths along the x , y directions reads:

$$f_t = \left(\frac{1}{2} \cdot \xi^T \cdot P_t \cdot \xi \right)^{1/2} + \frac{1}{2} \cdot \pi^T \cdot \xi \quad (8.12)$$

where the projection matrix P_t and the vector π read:

$$P_t = \begin{bmatrix} \frac{1}{2} & -\frac{1}{2} & 0 \\ -\frac{1}{2} & \frac{1}{2} & 0 \\ 0 & 0 & 2\alpha_T \end{bmatrix} \quad (8.13)$$

$$\pi = \{1 \quad 1 \quad 0\}^T \quad (8.14)$$

The parameter α_T controls the shear stress contribution to failure and can be expressed as:

$$\alpha_T = \frac{f_{t,x} \cdot f_{t,y}}{\tau_u^2} \quad (8.15)$$

where $f_{t,x}$ and $f_{t,y}$ are the tensile strengths in the x and y direction respectively, and τ_u is the shear strength at zero normal stress. The usual Rankine value is $\alpha_T = 1$. The reduced stress vector ξ is given by:

$$\xi = \sigma - \eta \quad (8.16)$$

with

$$\sigma = \{\sigma_x \quad \sigma_y \quad \tau_{xy}\}^T \quad (8.17)$$

$$\eta = \{\sigma_{t,x} \quad \sigma_{t,y} \quad 0\}^T \quad (8.18)$$

Exponential tensile softening is assumed in the orthogonal directions, described by:

$$\sigma_{t,x} = f_{t,x} \cdot e^{\left(\frac{h \cdot f_{t,x}}{G f_x} k_t \right)} \quad (8.19)$$

$$\sigma_{t,y} = f_{t,y} \cdot e^{\left(\frac{h \cdot f_{t,y} \cdot k_t}{G f_y}\right)} \quad (8.20)$$

where k_t is the equivalent plastic strain. The inelastic work g_f is defined by the integral:

$$g_f = \int \sigma^T \varepsilon = \int \sigma^T \varepsilon^p \quad (8.21)$$

this corresponds to the area under the stress-strain diagram for uniaxial loading. Assuming that the inelastic work g_f is uniformly distributed over the equivalent length h , the relation between the fracture energy G_f and the work g_f is given by:

$$g_f = \frac{G_f}{h} \quad (8.22)$$

where h is related to the area of a finite element A_e

$$h = \alpha_h \cdot \sqrt{A_e} \quad (8.23)$$

It is noted that α_h is equal to 1 for quadratic elements and $\sqrt{2}$ for linear elements (Rots, 1988). In order to avoid snap-back at constitutive level, the condition of maximum equivalent length is given by:

$$h \leq \frac{G_{f_t} \cdot E_i}{f_{ii}^2} \quad (8.24)$$

where E_i is the Young's modulus and the subscript i refers to the material axis. If this condition is violated, for any of the material axes, the tensile strength f_{ii} is reduced according to:

$$f_{ii} = \left(\frac{G_{f_t} \cdot E_i}{h}\right)^{1/2} \quad (8.25)$$

8.2.2 Hill type yield criterion

Hill (1950) postulated the form of a yield surface as an extension to the Von Mises criterion for isotropic materials, in a plane-stress situation, as:

$$f_c = A \cdot \sigma_x^2 + B \cdot \sigma_x \cdot \sigma_y + C \cdot \sigma_y^2 + D \cdot \tau_{xy}^2 = 1 \quad (8.26)$$

where A, B, C and D are four material parameters. Eq. (8.26) represents a rotated centered ellipsoid in the stress space if the constraints are defined. Some authors (e.g. Jones, 1975) recommend Eq. (8.26) for wood, even if tensile and compression strengths are equal. This equation can be recast in terms of the yield values along the material axes x and y , $\bar{\sigma}_{c,x}$ and $\bar{\sigma}_{c,y}$ respectively, as:

$$f_c = \left(\frac{1}{2} \cdot \sigma^T \cdot P_c \cdot \sigma \right)^{1/2} - \bar{\sigma}_c \cdot k_c \quad (8.27)$$

if the material parameters A to D are replaced by:

$$\begin{aligned} A &= \frac{1}{(\bar{\sigma}_{c,x})^2} \\ B &= \frac{\beta}{(\bar{\sigma}_{c,x} \cdot \bar{\sigma}_{c,y})} \\ C &= \frac{1}{(\bar{\sigma}_{c,y})^2} \\ D &= \frac{\gamma}{(\bar{\sigma}_{c,x} \cdot \bar{\sigma}_{c,y})} \end{aligned} \quad (8.28)$$

Here, the projection matrix P_c reads:

$$P_c = \begin{bmatrix} 2 \frac{\bar{\sigma}_{c,y}}{\bar{\sigma}_{c,x}} & \beta & 0 \\ \beta & 2 \frac{\bar{\sigma}_{c,x}}{\bar{\sigma}_{c,y}} & 0 \\ 0 & 0 & 2\gamma \end{bmatrix} \quad (8.29)$$

and the yield value $\bar{\sigma}_c$ is given by:

$$\bar{\sigma}_c = \sqrt{\bar{\sigma}_{c,x} \cdot \bar{\sigma}_{c,y}} \quad (8.30)$$

It is noted that the β and γ values introduced in Eq. (8.27) are additional material parameters that determine the shape of the yield surface: β rotates the surface around the shear stress axis and can be determined from biaxial compression tests (Lourenço, 1996), and γ controls the shear stress contribution to failure and is calculated from:

$$\gamma = \frac{f_{c,x} \cdot f_{c,y}}{\tau_u^2} \quad (8.31)$$

where the $f_{c,x}$ and $f_{c,y}$ are the compressive strengths along the material axes and τ_u is the pure shear strength.

Parabolic hardening is assumed for the yield strength. In the absence of additional information, a value of β equal to 1.0 and a value of γ equal to 3.0 is suggested (Lourenço, 1996).

8.3 ADOPTED MATERIAL PARAMETERS

A characteristic of the adopted model is that the tension strength, in a given direction, must be equal or lower to the compression strength in the same direction (Lourenço, 1996). This does not hold for wood. In the present case, the tensile part of the yield criterion was ignored due to the irrelevant contribution of the tensile strength in the global behaviour of the joint. This means that the yield surface reduces to the standard Hill criterion.

The adopted elastic and inelastic materials properties used in the analyses are detailed in Table 8.1. The values for chestnut wood have been obtained from the experimental tests, see Chapters 4, 5 and 6, and represent average values.

Table 8.1 – Adopted elastic and inelastic material properties.

E_x	E_y	G_{xy}	ν_{xy}
800 N/mm ²	8500 N/mm ²	1500 N/mm ²	0.3
$f_{c,x}$	$f_{c,y}$	β	γ
7 N/mm ²	45 N/mm ²	-1.0	3.0

Figure 8.4 shows the stress-strain diagrams obtained in uniaxial compression along the two orthogonal directions. The values chosen for the material parameters illustrate the fact that completely different behaviour along the two main directions can be reproduced, agreeing with the experimental results, see Chapters 4, 5 and 6.

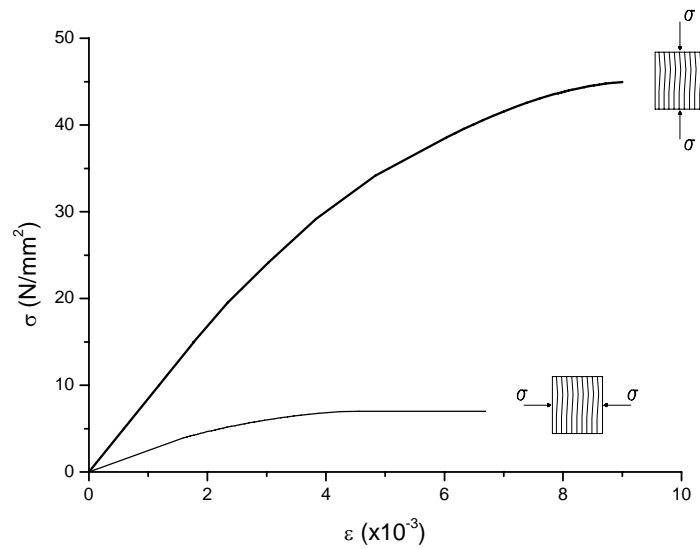


Figure 8.4 – Uniaxial load-displacement diagrams in compression parallel and perpendicular to the grain.

Finally, Figure 8.5 illustrates the shape of the adopted yield criterion in the compression-compression regime, which features an extreme degree of anisotropy with a ratio $f_{c,x} / f_{c,y} = 0.156$.

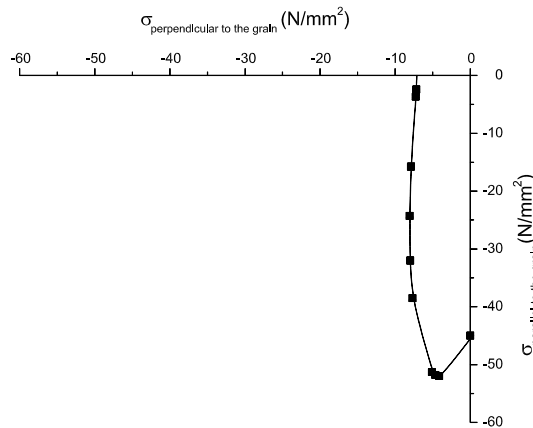


Figure 8.5 – Shape of the proposed yield criterion for chestnut wood. Material parameters: $f_{c,x} = 7.0 \text{ N/mm}^2$; $f_{c,y} = 45 \text{ N/mm}^2$; $\beta = -1.0$; $\gamma = 3.0$.

8.4 NUMERICAL VS. EXPERIMENTAL RESULTS

The use of the numerical anisotropic model for the analysis of the wood-wood joint is validated next by a comparison with the experimental results. Figure 8.6a shows the test set-up, including loading, boundary conditions and material axes. Additional boundary conditions are given in the

bottom of the tie beam by constraining the translations. Initially, the joint is subjected to a vertical pressure uniformly distributed over the cross section of the diagonal with a resultant F . It is noted that the self-weight of the wood elements is considered in the analyses. Figure 8.6b shows the adopted finite element mesh, which consists of two members of chestnut wood with cross section of $150 \times 93 \text{ mm}^2$.

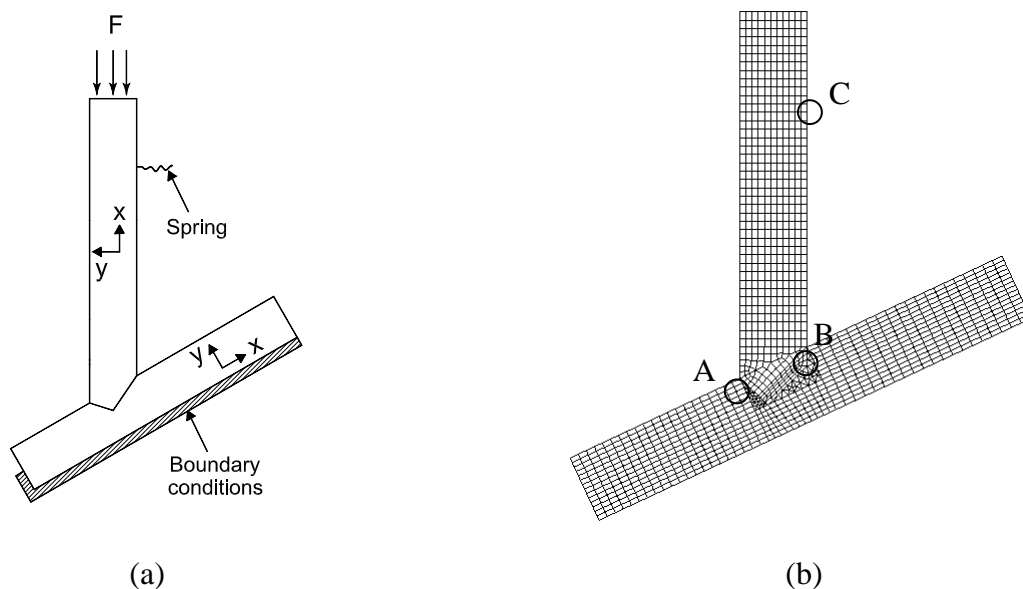


Figure 8.6 – Adopted finite element mesh: (a) boundary conditions and material axes, (b) global view and singular points.

A structured mesh is used for the rafter and the brace, whereas an irregular transition mesh is used in the vicinity of the connection between rafter and brace. Interface elements are also used between the rafter and the brace. The thickness ranges from 62 mm to 93 mm, as shown in Figure 8.7. This aims at representing the thickness of the mortise.

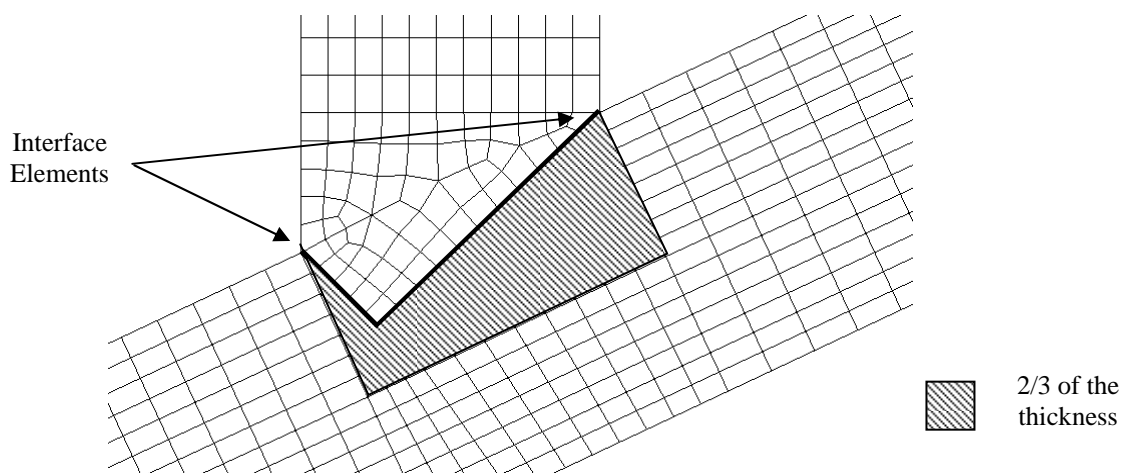


Figure 8.7 – Localization of the interface elements.

The comparison between numerical and experimental load-displacement diagrams is given in Figure 8.8. A preliminary analysis with an infinite stiffness of the interface, assuming a fully rigid connection, indicated that such an assumption provided far too stiff results. Therefore, the stiffness of the interface elements was obtained by inverse fitting.

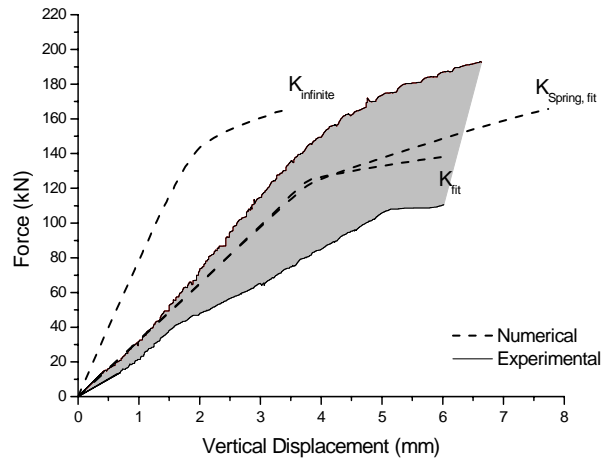


Figure 8.8 – Comparison between numerical and experimental load-displacement diagrams.

A first conclusion is that the stiffness of the interface elements has considerable influence in the yield strength of timber joints. In Figure 8.8, three distinct situations are presented:

- a numerical simulation with infinite stiffness of the interface elements ($k_{\text{infinite}} = k_n = k_s = 10^9 \text{ N/mm}^3$);
- a numerical simulation with an adjusted stiffness of the interface elements obtained by inverse fitting of the experimental results (k_{fit}): $k_n = 6000 \text{ N/mm}^3$ and $k_s = 2308 \text{ N/mm}^3$. The value of the transverse stiffness results from the elastic relation shown next, where G is the transversal deformation modulus, E is the modulus of elasticity and ν is the coefficient of Poisson:

$$G = \frac{E}{2 \cdot (1 + \nu)} \quad (8.32)$$

- a numerical simulation with a spring ($k_{\text{spring}} = 10^6 \text{ N/m}$) located in point C, see Figure 8.9, to simulate the reaction cell used in the experimental sets. The stiffness of the spring was again obtained by inverse fitting of the experimental results, keeping the adjusted stiffness of the interface elements.

The numerical results, in terms of force-displacement diagrams, with the adjusted stiffness for the interface elements, provide very good agreement with the experimental results both in the linear and nonlinear parts. The influence of the experimental horizontal restraint, simulated by a linear spring, is only marginal. The usage of infinite stiffness for the interface (rigid joint) results in an increase of the slope of the first part of the response, from 30 kN/mm to 80 kN/mm (+ 266.7%).

The ultimate strength of the joint, given by an offset of the linear stretch by 2% in terms of strain values, also changes from 130 kN to 152 kN (+ 17%), once the joint becomes fully rigid.

The behaviour of the joint is depicted in Figure 8.9 in terms of deformed meshes. Initially, the joint shows a tendency to rotate around point A (see Figure 8.9a) but with increasing load this tendency shifts, and the joint finally rotates around point B, see Figure 8.9b. These results are corroborated by the observations made in the experimental results. Figure 8.9c and Figure 8.9d illustrates the experimental and numerical load-displacement diagram in point A and the experimental and numerical load-displacement diagram in point C, respectively. The numerical trend appears within the experimental range of results.

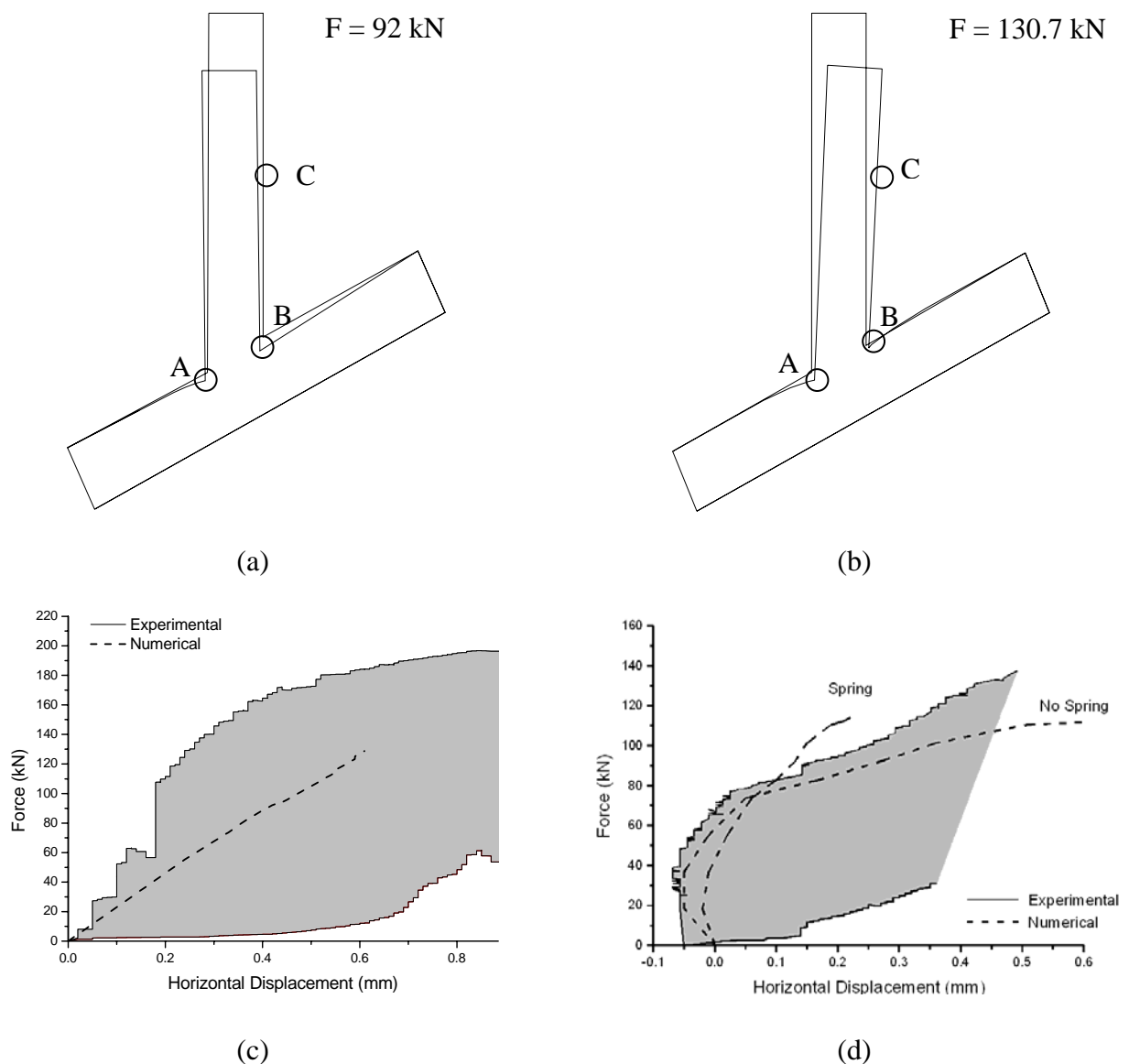


Figure 8.9 – Results of the analysis: (a) deformed mesh for a force of 92 kN, (b) deformed mesh for a force of 130.7 kN, (c) experimental and numerical load-displacement diagram in point A, and (d) experimental and numerical load-displacement diagram in point C.

Figure 8.10 shows the contour of minimum principal stresses at different stages of the analysis. It is possible to observe a concentration of stresses in a narrower band with peak stresses at the joint (zone where the interface elements were placed), upon increasing loading. With this concentration of stresses one may say that failure is clearly governed by wood crushing where, for a late stage of the analysis, the compressive strength of the wood in the joint is completely exhausted. This situation is also confirmed in the experiments, see Chapter 7.

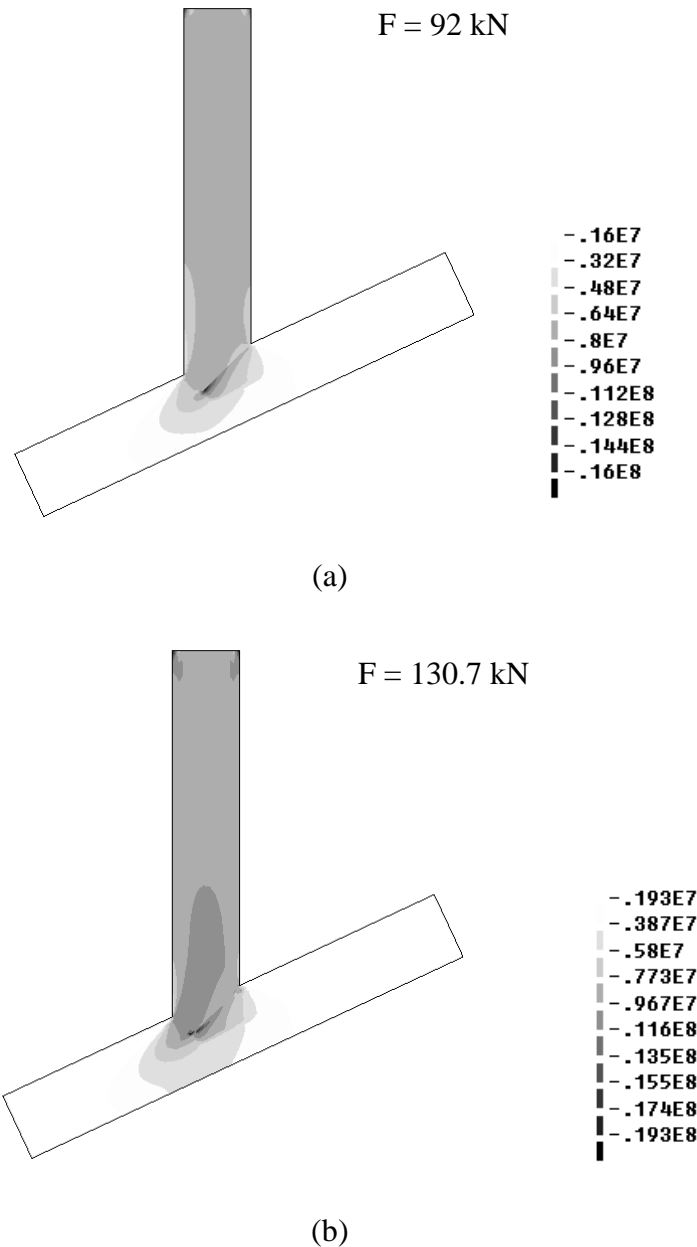


Figure 8.10 – Minimum principal stresses (values in N/m^2): (a) for a force of 92 kN, and (b) for a force of 130.7 kN.

8.5 EFFECTS OF THE MATERIAL PARAMETERS

A strong benefit of using numerical simulations is that parametric studies can be easily carried out and the sensitivity of the response to the material data can be assessed. This allows a better understanding of the structural response. There are a total of six key parameters in the present model and the effect of each parameter on the global response will be analyzed separately. Table 8.2 shows the default values and the variations considered for each parameter, namely k_n (normal stiffness of the interface), k_s (tangent stiffness of the interface), E_x and E_y (Young's moduli in the directions parallel and perpendicular to the grain, respectively) and f_x and f_y (compressive strengths in the directions parallel and perpendicular to the grain, respectively). It is noted that moderate variations ($\pm 25\%$) are considered for the strengths and large variations (division/multiplication by two) are considered for the stiffness values. These assumptions are rooted in the fact that strength is usually better known than stiffness.

Table 8.2 – Multiplication values used in the parametric study, with respect to the original default data.

k_n	k_s	E_x	E_y	$f_{c,x}$	$f_{c,y}$
0.5	0.5	0.5	0.5	0.75	0.75
1.0	1.0	1.0	1.0	1.0	1.0
2.0	2.0	2.0	2.0	1.25	1.25

8.5.1 Normal stiffness of the interface

Figure 8.11 shows a comparison between the results of the variation of the k_n parameter: with a reduction of 50% in k_n , the ultimate strength of the joint, given by an offset of the linear stretch by 2%, decreases from 127.2 kN to 120 kN (-6%); multiplying k_n by a factor of two the ultimate strength of the joint, given by an offset of the linear stretch by 2%, increases from 127.2 kN to 135.0 kN (+7%).

The reduction/increase of the normal stiffness of the interface also affects the global stiffness of the joint: the global stiffness of the joint decreases as the normal stiffness of the interface decreases, being more sensitive to this variation when compared with the ultimate strength. The reduction of 50% of the k_n parameter, results in a decrease of the slope of the first part of the response, from 32 kN/mm to 26 kN/mm (-23%).

On the other hand, the multiplication by a factor of 2 of this parameter results in an increase of the slope of the first part of the response, from 32 kN/mm to 41 kN/mm (+28%). Because this parameter sets the relation between the normal traction and the normal relative displacement, the obtained results were expected *a priori*.

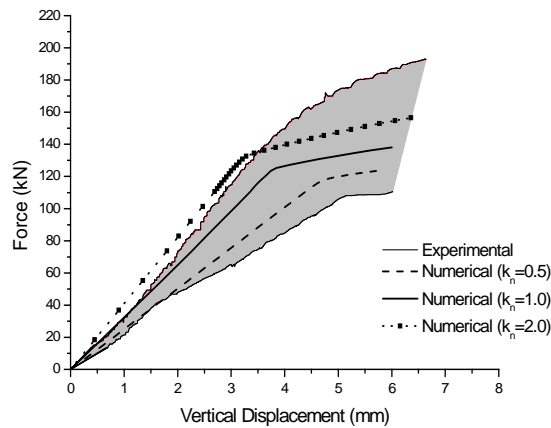


Figure 8.11 – Effect of the variation of parameter k_n on the model response.

8.5.2 Tangential stiffness of the interface

Figure 8.12 shows a comparison between the results of the variation of the k_s parameter. The ultimate strength is insensitive to a k_s variation, whereas the reduction/increase of the k_s parameter affects the global stiffness of the joint: the global stiffness of the joint decreases as the k_s parameter decreases. The reduction of 50% of the k_s parameter, results in a decrease of the slope of the first part of the response, from 32 kN/mm to 28 kN/mm (-14%).

On the other hand, the multiplication by a factor of 2 of this parameter results in an increase of the slope of the first part of the response, from 32 kN/mm to 37 kN/mm (+16%).

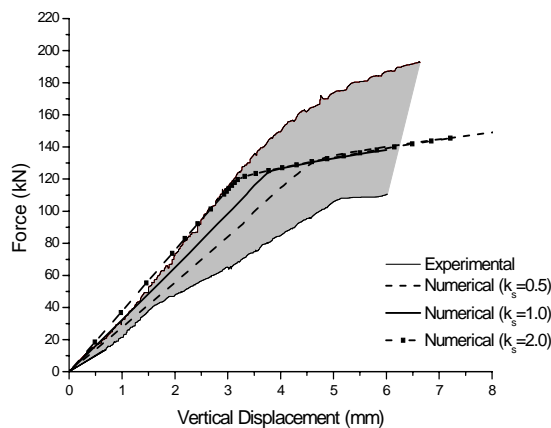


Figure 8.12 – Effect of the variation of parameter k_s on the model response.

8.5.3 Elastic modulus

The effect of the variation of the elastic modulus parallel and perpendicular to the grain was considered individually. Figure 8.13 indicates that the ultimate strength is almost insensitive to the variation of the elastic modulus of elasticity for wood ($\pm 4\%$), in both considered directions.

The inclusion of the effects of the elastic modulus of elasticity does change significantly the elastic stiffness of the joint. Therefore, decreasing the parameter E decreases the global stiffness of the joint. The reduction of 50% of the E_x parameter, results in a decrease of the slope of the first part of the response, from 32 kN/mm to 28 kN/mm (-14%). On the other hand, the multiplication by a factor of 2 of this parameter results in an increase of the slope of the first part of the response, from 32 kN/mm to 36 kN/mm (+13%).

The reduction of 50% of the E_y parameter, results in a decrease of the slope of the first part of the response, from 32 kN/mm to 28 kN/mm (-14%). On the other hand, the multiplication by a factor of 2 of this parameter results in an increase of the slope of the first part of the response, from 32 kN/mm to 36 kN/mm (+13%).

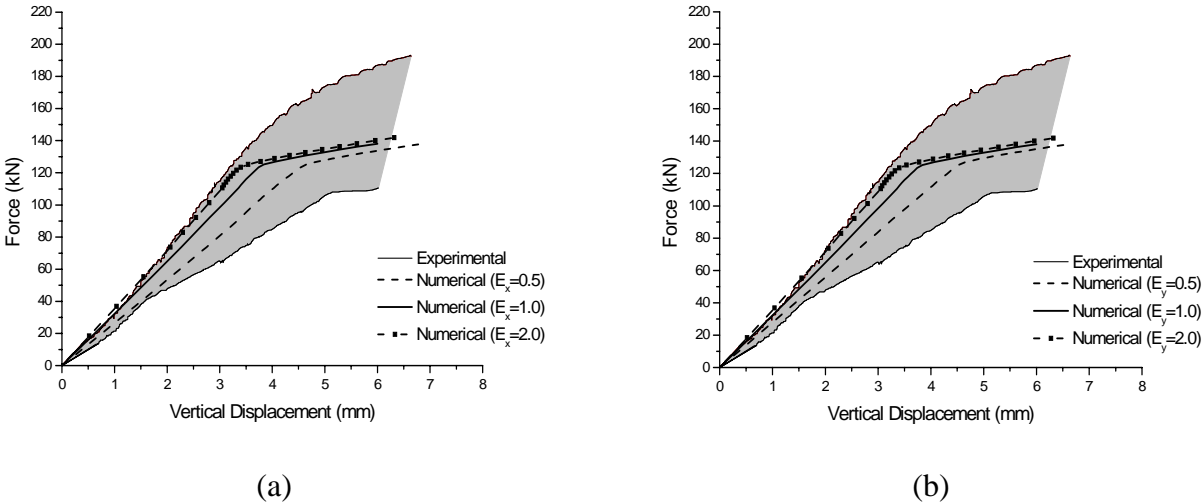


Figure 8.13 – Effect of the variation of the elastic modulus of elasticity on the model response: (a) E_x , and (b) E_y .

8.5.4 Compressive strength

The relationship between the global behaviour of the joint and the compressive strength of wood in both considered directions is shown in Figure 8.14. It is apparent in Figure 8.14a that the ultimate strength and the global stiffness of the joint are insensitive to the variation of the compressive strength of wood in the direction parallel to the grain.

Figure 8.14b indicates higher sensitivity of the ultimate strength of the joint to the variation of the compressive strength of wood in direction perpendicular to the grain, as expected: with a reduction of 50%, the ultimate strength of the joint, given by an offset of the linear stretch by 2%, decreases from 130 kN to 100 kN (-30%); multiplying by a factor of 2 the ultimate strength of the joint, given by an offset of the linear stretch by 2%, increases from 130 kN to 160 kN (+23%). However, the global stiffness of the joint is insensitive to the variation of the compressive strength perpendicular to the grain.

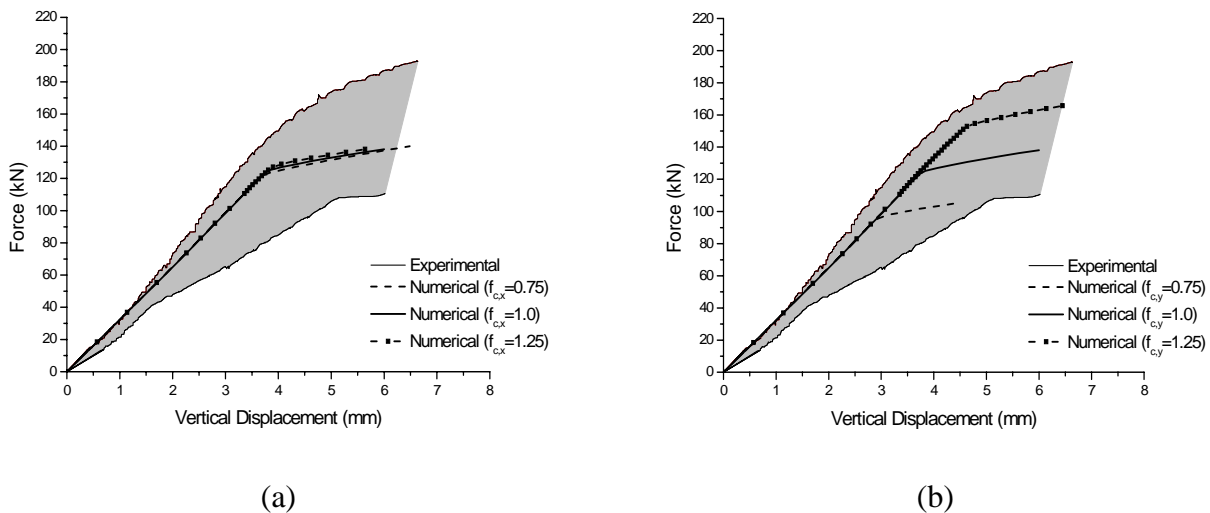


Figure 8.14 – Effect of the variation of the compressive strength on the model response: (a) $f_{c,x}$, and (b) $f_{c,y}$.

8.6 CONCLUSIONS

The adequacy of an anisotropic failure criterion to represent the behaviour of a traditional mortise and tenon joint is assessed from the comparison between experimental and numerical results.

A structured finite element mesh is used for the rafter and the brace, whereas an irregular transition mesh is used in the vicinity of the joint and interface elements are used between the wood elements. The different failure mechanisms observed in the experiments are well captured by the model, which is the most important validation of any simulation. It is striking that such excellent agreement is obtained also in the load-displacement diagrams.

A preliminary analysis considering an infinite stiffness of the interface, assuming a fully rigid connection, indicates that such an assumption provides too stiff results. Another conclusion is that the normal stiffness of the interface elements has considerable influence in the yield strength of timber joints. The numerical results, in terms of force-displacement diagrams, with the adjusted stiffness for the interface elements, provide very good agreement with the experimental results both

in the linear and nonlinear parts. The influence of the experimental horizontal restraint, simulated by a linear spring, is only marginal.

The model incorporates four elastic parameters and four inelastic parameters. It has been shown that the parameters that affect most the ultimate load of the adopted mortise and tenon joint are the compressive strength of wood perpendicular to the joint and the normal stiffness of the interface elements representing the contact between rafter and brace. The tangential stiffness of interfaces and the Young's moduli of wood have only very limited influence in the response. The compressive strength of wood parallel to the grain has almost no influence in the response.

Conclusions

In recent years, large investments have been concentrated in the area of historical structures, leading to significant developments in the areas of inspection, non-destructive testing, monitoring and structural analysis of monuments. Nevertheless, understanding, analysing and repairing historical constructions remains one of the most significant challenges to the technicians involved.

In the case of historical timber constructions, additional complexity comes from the usage of a natural material that exhibits high natural variability and complex time-dependent behaviour. In addition, ancient timber constructions have suffered significant changes during their lifetime and the architectural heritage we face today is indeed built from a variety of materials and techniques, resulting from different periods in history. The assessment of the mechanical properties of the structural elements becomes difficult as it is usually not possible to remove large samples from an ancient structure for direct testing, as it would be advisable. The common procedure is to determine average properties by visual grading and then to refer to tables.

Of course, safety assessment of existing structures is usually not addressed by the codes, which are conceptually oriented to new buildings. In fact, it seems obvious that the design requirements of a member in an existing structure need to be re-defined because the uncertainty about the mechanical properties and the structural behaviour can be reduced based on non-destructive testing.

Mechanical properties of chestnut and non-destructive correlations

A key conclusion of the present study is that there are no significant differences between clear wood specimens from “old-growth” forest and new wood. Therefore, no mechanical damage was found in “old-growth” wood specimens, due to load-history while in service or time span. These results only apply to the strength and elastic properties of clear wood zones, with no visible chemical, biological or physical damage.

The extensive testing carried out allows to conclude that density has a significant influence on wood mechanical properties but cannot explain their variability and should not be relied upon as a predictor for mechanical properties. The correlations obtained between density and mechanical properties are rather poor.

In addition, the results indicated that a clear definition for the conventional compressive strength perpendicular to the grain is required. In particular, the characteristic value proposed by the EN 384 (CEN, 1995), and used as a design basis, seems to be unsafe and unable to provide a true indication of the compressive strength. Finally, an appropriate test method for tension parallel to the grain, defining the geometry and loading conditions, must be developed and standardized. Difficulties were found when using the Brazilian standard NBr 7190 (1997).

Novel single-parameter linear regressions have been proposed for density, elasticity modulus and tensile/compressive strength parallel and perpendicular to the grain, using the Resistograph, Pilodyn and ultrasonic testing. The global conclusions are that, with respect to density, the Resistograph and the Pilodyn provide reasonable correlations. With respect to mechanical characteristics, correlations need a re-calibration with the wood population. As this is not reasonable for practical purposes, expressions with a lower 95% confidence of the mechanical parameters have been proposed for the ultrasonic testing. The usage of the Resistograph and the Pilodyn to obtain quantitative mechanical data is not recommended, due to the high dispersion found.

Evaluation and modelling of a traditional timber mortise and tenon joint

The behaviour of a traditional mortise and tenon joint has been investigated experimentally and numerically under monotonic loading conditions, and a good agreement has been found between the numerical results and the experimental data. The experimental analysis allowed to better understand the behaviour of the connection and discuss the influence of defects in the mechanical behaviour. The numerical approach allowed to identify the sensitivity of the results to the various material parameters, such as the normal and tangential stiffness of the interface, the elastic modulus of elasticity and the compressive strength. In particular, the influence of the interface stiffness between the two timber members is significant for the response. The proposed compressive constitutive material model improved the predictions of local and global behaviour, and was shown to be effective in the prediction of strength and stiffness properties of the tested specimens.

The investigation led to an improvement of the global structural analyses of traditional timber structures, providing valuable information for the transition from classical schemes (hinged or fixed joints) to more sophisticated analysis with semi-rigid joints. In addition, the failure modes and the better understanding of the behaviour of the joint provide a clear guidance for strengthening strategies in this type of traditional timber joints.

Finally, the usage of non-destructive testing confirmed the good correlations between ultrasonic testing and the ultimate strength of the joint or the stiffness of the joint. Even if, the usage of the novel correlations in engineering applications is questionable due to the small sample of joints tested, the results indicate clearly that, at least, adequate condition survey of existing joints using non-destructive testing is possible.

Suggestions for future work

The present work showed the limitations on the methods for collection of data on existing timber structures. In particular, it showed that the development of new non destructive techniques is fundamental to a full understanding of historical timber structures. Current existing NDT do not characterize, with the required detail, the mechanical properties of timber, as their focus is on the physical properties (density, humidity, and geometry). New techniques, as X-rays and thermographic inspections, could result in a significant improvement in data available to the structural engineer, resulting in more accurate analysis of the structures. These tests should also be applied to other typical timber populations in Portugal, namely oak (*Quercus robur* L.), which is present in a large number of ancient buildings.

Additional investigations are needed in traditional wood-wood joints. For mortise-and-tenon joint tested it is relevant to assess the influence of the geometry of the tenon and of the mortise, as well as the influence of the angle of the connection. Another important issue is the evaluation of the influence of localized defects in the neighbourhood of the joint. Finally, the introduction of horizontal loads in the connections (needed to analyse the behaviour under cyclic loading) also requires further studies.

References

- AGUIAR, A.; ALMEIDA, M.; BORRALHO, N.; 2003 – “Genetic Control of Growth, Wood Density and Stem Characteristics of *Pinus pinaster* in Portugal”. *Silva Lusitana*, Vol. 11(2): pp. 131-139.
- ALEXIOU, P.; 1994 – “Elastic properties of *Eucalyptus pilularis* Sm. perpendicular to the grain”. *Holzforschung – International Journal of the Biology, Chemistry, Physics and technology of Wood*, 48 (1): pp. 55-66.
- AMERICAN SOCIETY FOR TESTING AND MATERIALS (ASTM); 1989 – Standard practice measuring ultrasonic velocity in materials. ASTM Designation: E494-89. ASTM, West Conshohocken, PA.
- AMERICAN SOCIETY FOR TESTING AND MATERIALS (ASTM); 1992 – Standard test for establishing clear wood strength values. ASTM Designation: D2555-88. ASTM, West Conshohocken, PA.
- AMERICAN SOCIETY FOR TESTING AND MATERIALS (ASTM); 1994 – Standard methods of testing small clear specimens of timber. ASTM Designation: D143-94. ASTM, West Conshohocken, PA.
- ANTHONY, A.; 2005 – “Investigation of Historic Timber Structures Using Portable X-Ray Technology”. *Proceedings of the International Conference The Conservation of Historic Wooden Structures*, Florence, Vol. I: pp. 289-293.
- ANTHONY, R.; 2003 – “Examination of connections and deterioration in timber structures using digital radiography”. *Proceedings of the 3rd Forensic Engineering Congress*, San Diego, California: pp. 320-328.
- AUGELLI, F.; COLLA, C.; MASTROPIRRO, R.; 2005a – “Inspection & NDT to verify structural reliability of historic wooden roofs in the ex-Meroni spinning-mill”. *Structural Analysis of Historical Structures*, Modena – Italy, Vol. I: pp. 377-386.
- AUGELLI, F.; GRIMOLDI, A.; JURINA, L.; MERONI, D.; ZANZANI, S.; 2005b – “Il Palazzo Silva-Persichelli a Cremona: La Diagnostica e la Schedatura delle Membrature Lignee per il Progetto di Conservazione e Consolidamento”. *Proceedings of the International Conference The Conservation of Historic Wooden Structures*, Florence, Vol. I: pp. 307-321.
- BEALL, F.; 1987 – “Fundamentals of acoustic emission and acousto-ultrasonics”. *Proceedings of the 6th Non-destructive Testing of Wood Symposium*. Washington: pp. 3-28.
- BEERY, W.; IFJU, G.; McLAIN, T.; 1983 – “Qualitative wood anatomy – relating anatomy to transverse tensile strength”. *Wood and Fiber Science*, 15(4): pp. 395-407.
- BERGLIND, H.; DILLENZ, A.; 2003 – “Detection of glue deficiency in laminated wood with pulse thermography”. *Journal of Wood and Science*, Vol. 49: pp. 216–220.

- BERGSTEN, U.; LINDEBERG, J.; RINDBY, A.; EVANS, R.; 2001 – “Batch measurements of wood density on intact or prepared drill cores using x-ray microdensitometry”. *Wood Science and Technology*, Vol. 35: pp. 435-452.
- BERNABEI, M.; 2005 – “Ricerche Dendrocronologiche in Trentino: La Chiesa dei SS. Ippolito e Cassiano a Castello Tesino (TN)”. Proceedings of the International Conference *The Conservation of Historic Wooden Structures*, Florence, Vol. I: pp. 24-28.
- BERNDT, H.; SCNIEWIND, A.; JOHNSON, G.; 1999 – “High-resolution ultrasonic imaging of wood”. *Wood Science Technology*, Vol. 33: pp. 185-198.
- BERTOLINI, C.; BRUNETTI, M.; CAVALLARO, P.; MACCHIONI, N.; 1998 – “A non destructive diagnostic method on ancient timber structures: some practical application examples”. Proceedings of the 5th World Conference on Timber Engineering, Montreux, Vol. I: pp. 456-465.
- BIERNACKI, J.; BEALL, F.; 1993 – “Development of an acousto-ultrasonic scanning system for non-destructive evaluation of wood and wood laminates”. *Wood and Fiber Science*, 25 (3): pp. 289-297.
- BLANCHET, L.; 2005 – “Applying Engineering to Rescue the Heritage Integrity of Historic Timber Structures”. Proceedings of the International Conference *The Conservation of Historic Wooden Structures*, Florence, Vol. II: pp. 10-20.
- BLASS, H; GÖRLACHER, R.; 2004 – “Compression perpendicular to the grain”. Proceedings of the 8th World Conference on Timber Engineering, Finland. Vol. II: pp. 435-440.
- BODIG, J.; 1963 – “The peculiarity of compression of conifers in radial direction”. *Forest Products Journal*. 13: pp. 438-446.
- BODIG, J.; 1965 – “The effect of anatomy on the initial stress-strain relationship in transverse compression”. *Forest Products Journal*. 14: pp. 197-202.
- BODIG, J.; 1969 – “Improved load-carrying capacity of wood in transverse compression”. *Forest Products Journal*, 19 (12): pp. 39-44.
- BODIG, J.; GOODMAN, J.; 1973 – “Prediction of elastic parameters for wood”. *Wood Science*, 5 (4): pp. 249-264.
- BODIG, J.; JAYNE, B.A.; 1993 – *Mechanics of wood and wood composites*. 2^aed: Krieger Publishing Company: 712 pp.
- BODIG, J.; 2000 – “The process of NDE research for wood and wood composites”. *NDT.net* – March 2001, Vol. 6, No. 03.
- BONAMINI, G.; 1995 – “Restoring timber structures – inspection and evaluation”. *STEP/EUROFORTECH*. Vol. 2.
- BONAMINI, G.; NOFERI, M.; TOGNI, M.; UZIELLI, L.; 2001 – *Il Manuale del Legno Strutturale – Vol.I – Ispezione e diagnosi in opera*. Mancosu Editore, Roma.
- BRANCO, J.; CRUZ, P.; DIAS, S.; 2005 – “Old Timber Beams – Diagnosis and Reinforcement”. Proceedings of the International Conference *The Conservation of Historic Wooden Structures*, Florence, Vol. I: pp. 417-422.
- BROWNE, C.; KUCHAR, W.; 1985 – “Determination of material properties for structural evaluation of TRESTLE”. Proceedings of the 5th international Non-destructive testing of wood symposium. Washington State University: pp. 361–384.

- BUCUR, V.; ARCHER, R.; 1984 – “Elastic Constants for wood by an ultrasonic method”. *Wood Science and Technology*, 18: pp. 255-265.
- BUCUR, V.; 1995 – *Acoustics of wood*. 1st Ed. CRC Press Inc., NY, 284 pp.
- BUCUR, V.; GARROS, S.; NAVARETTE, A.; De TROYA, M.; GUYONNET, R.; 1997 – “Kinetics of wood degradation by fungi with x-ray microdensitometric technique”. *Wood Science and Technology*. Vol. 31: pp. 383-389.
- BURGER, N.; GLÖS, P.; 1996 – “Effect of size on tensile strength of timber”. CIB-W18A/29-6-1.
- BURGER, N.; GLÖS, P.; 1997 – “Strength relationship in structural timber subjected to bending and tension”. CIB-W18A/30-6-1.
- CAI, Z.; HUNT, M.; ROSS, R.; SOLTI, L.; 2002 – “Screw Withdrawal – A means to evaluate densities of *in-situ* wood members”. *Proceedings 13th International Symposium on Non-destructive Testing of Wood*: pp. 277-281.
- CECCOTTI, A.; UZIELLI, L.; 1989 – “Sul grado di affidabilità strutturale sulle strutture in legno antiche”. *Atti del 2^o Congresso Nazionale sul Restauro del Legno*. Nardini, Firenze: 14 pp.
- CECCOTTI, A.; TOGNI, M.; 1996 – “NDT on ancient timber beams: assessment of strength/stiffness properties combining visual and instrumental methods”. *Proceedings of the 10th International Symposium on Non-destructive Testing of Wood*. Lausanne, Switzerland: pp. 379-388.
- CEN; 1991 – “EN 26891 – Timber structures. Joints Made With Mechanical Fasteners General principles for the determination of strength and deformation characteristics”. Office for Official Publications of the European Communities. Brussels, Belgium.
- CEN; 1994 – “EN 350-1: Durability of wood and wood-based products. Part 1: Guide to the principles of testing and classification of the natural durability of wood”. Office for Official Publications of the European Communities. Brussels, Belgium.
- CEN; 1994 – “EN 350-2: Durability of wood and wood-based products. Natural durability of solid wood. Part 2: Guide to natural durability and treatability of selected wood species of importance in Europe”. Office for Official Publications of the European Communities. Brussels, Belgium.
- CEN; 1995 – “EN 338 – Structural timber – Strength classes”. Office for Official Publications of the European Communities. Brussels, Belgium.
- CEN; 1997 – “EN 1193 – Structural timber – Structural and glues laminated timber – Determination of additional physical and mechanical properties”. Office for Official Publications of the European Communities. Brussels, Belgium.
- CEN; 2000 – “EN 408 – Timber structures – Structural timber and glued laminated timber – Determination of some physical and mechanical properties”. Office for Official Publications of the European Communities. Brussels, Belgium.
- CEN; 2004 – “EN 384 – Structural timber – Determination of characteristic values of mechanical properties and density”. Office for Official Publications of the European Communities. Brussels, Belgium.

- CERALDI, C.; MORMONE, V.; ERMOLLI, E.; 2001 – “Resistographic inspection of ancient timber structures for the evaluation of mechanical characteristics”. *Materials and Structures*, RILEM, Vol. 34: pp. 59-64.
- CNS ELECTRONICS; 1995 – PUNDIT manual for use with the portable ultrasonic non-destructive digital indicating tester. London: CNS Electronics.
- CÓIAS e SILVA, V.; LOURENÇO, P.; RAMOS, L.; MESQUITA, C.; 2001 – “Accounting for the “block effect” in structural interventions in Lisbon’s old “Pombaline” downtown buildings”. *Historical Constructions*, P. B. Lourenço, P. Roca (Eds.), Guimarães: pp. 943-952.
- COOK, R.; MALKUS, D.; PLESHA, M.; 1989 – *Concepts and Applications of Finite Element Analysis*, 3rd edition, John Wiley and Sons, New York: 501 pp.
- COURTNEY, T.; 2000 – *Mechanical behaviour of materials*. McGraw-Hill International Editions.
- CRUZ, H.; MACHADO, J. S.; NUNES, L.; 1994 – “Problemas de conservação de madeira em edifícios”. 2º Encontro sobre Conservação e Reabilitação de Edifícios, ENCORE. Lisboa: LNEC: pp. 301-312.
- DAMKILDE, L.; HOFFMEYER, P.; PEDERSEN, T.; 1998 – “Compression strength perpendicular to grain of structural timber and glulam”. CIB-W18A/31-6-4.
- DANIEL, I.; ISHAI, O.; 1994 – *Engineering mechanics of composite materials*. Oxford University Press, New York.
- De GROOT, R.; ROSS, R.; NELSON, W.; 1998 – “Non destructive assessment of wood decay and termite attack in southern pine sapwood”. *Wood Protection*, Vol. 3(2): pp. 25-34.
- DE WITTE, F.; WOLTERS, A.; 2002 – *DIANA: Finite Element Analysis. User’s Manual*. TNO Building and Construction Research. Department of Computational Mechanics, Delft, The Netherlands.
- DE BORST, R.; FEENSTRA, P. H.; 1990 – “Studies in anisotropic plasticity with reference to the Hill criterion”. *International Journal of Numerical Methods in Engineering*, Vol. 29, pp. 315-336.
- DEPPE, H.; SCHMIDT, K.; 1998 – “Zur Witterungsbeständigkeit von unbehandeltem Massivholz”. *Holz-Zentralblatt*, Vol. 34: pp. 530-531
- DIANA (Release 8.2); 2002 – TNO Building and Construction Research. Department of Computational Mechanics, Delft, The Netherlands.
- DICKENS, J.; BENDER, D.; BRAY, D.; 1996 – “A critical-angle ultrasonic technique for the inspection of wood parallel-to-grain”. *Wood and Fiber Science*. Vol. 28(3), pp. 380-388.
- DIN 52192; 1979 – “Testing of wood; compression test perpendicular to grain”. Normenausschuss Holz im DIN, Germany.
- DINWOODIE, J.; 1989 – *Wood: Nature’s cellular polymeric fibre-composite*. The Institute of Materials. London, U.K.
- DIVÓS, F.; 2000 – “Defect detection in timber by stress wave time and amplitude”. *NDT.net* – March 2001, Vol. 6, No. 03.
- DRDÁČKÝ, M.; JIROVSKÝ, I.; SLÍŽKOVÁ, Z.; 2005 – “On Structural Health and Technological Survey of Historical Timber Structures”. *Proceedings of the International Conference The Conservation of Historic Wooden Structures*, Florence, Vol. I: pp. 278-284.

- EMERSON, R.; POLLOCK, D.; KAINZ, J.; FRIDLEY, K.; McLEAN, D.; ROSS, R.; 1998 – “Non-destructive evaluation techniques for timber bridges”. Proceedings of the 5th World Conference on Timber Engineering, Montreux, Vol. I: pp. 670-677.
- ERMAN, E.; 1999 – “A survey on structural timber joint classification and a proposal taxonomy”. Architectural Science Review, Vol. 42(3): pp. 169-180.
- ETHINGTON, R.L.; ESKELSEN, V.; GUPTA, R.; 1996 – “Relationship between compression strength perpendicular to grain and ring orientation”. Forest Products Journal, 46 (1): pp. 84-86.
- EUROCÓDIGO 5; 1998 – “EC5 – Projecto de Estruturas de Madeira. Parte 1.1: Regras gerais e regras para edificios (NP ENV 1995-1-1:1998)”.
- FEINBERG, J.; 2005 – “Frontier Architecture Found in the Wild Wild West – Conservation of U.S. Western Heritage Wooden Structures, 3 Studies”. Proceedings of the International Conference *The Conservation of Historic Wooden Structures*, Florence, Vol. I: pp. 383-390.
- FIORAVANTI, M.; GALOTTA, G.; 1998 – “Valutazione degli effetti del trattamento selvicolturale sulla qualità del legno di castagno (*Castanea sativa* Mill.) proveniente da bosco ceduo”. Convegno nazionale sul castagno, Cison di Valmarino (Treviso): pp. 367-376.
- FRANSSON, T.; NILSSON, P.; 2001 – “Non-destructive determination of interior properties of wood using waves”. Reports from MSI. Växjö University, School of Mathematics and Systems Engineering: 24 pp.
- FRATTARI, A.; PIGNATELLI, O.; 2005 – “Dendrochronology and non-destructive testing : synergies for dating ancient wooden structures of historic and cultural interest”. 8th International Conference on *Non Destructive Investigations and Micronalysis for the Diagnostics and Conservation of the Cultural and Environmental Heritage*. Lecce , Italy: 16 pp.
- GABRIELLI, A.; 1994 – “La civiltà del castagno”. Monti e boschi, Vol. 65: pp. 3.
- GEHRI, E.; 1991 – “Swiss comments to EN 384”. Zurich.
- GEHRI, E.; 1997a – “Timber as a natural composite: explanation of some peculiarities in the mechanical behaviour – Case: Assessment of the modulus of elasticity of timber parallel to grain”. CIB-W18A/30-6-3.
- GEHRI, E.; 1997b – “Timber in compression perpendicular to the grain”. Proceedings of the 1997 International Conference of IUFRO S 5.02 Timber Engineering. Copenhagen, Denmark.
- GEHRI, E.; 1998 – “Load introduction and load transfer perpendicular to grain”. Proceedings of the 5th World Conference on Timber Engineering. Montreux, Switzerland. Vol.I: 213-223 pp.
- GINDL, W.; 2002 – “Comparing mechanical properties of normal and compression wood in Norway spruce: The role of lignin in compression parallel to the grain”. *Holzforschung – International Journal of the Biology, Chemistry, Physics and technology of Wood*, 56: pp. 395-401.
- GIORDANO, G.; 1999 – Timber structures engineering. 5 th Edn. Hoepli, Milano.
- GIURIANI, E.; GUBANA, A.; 1993 – “penetration test to evaluate wood decay and its application to the Loggia monument”. RILEM Materials and Structures, Vol. 26: pp.8-14.

- GONG, M.; SMITH, I.; 2000 – “Failure of softwood under static compression parallel to grain”. *Journal of the Institute of Wood Science*, 15 (4): pp. 204-210.
- GONG, M.; SMITH, I.; 2004 – “Effect of load on failure mechanisms of spruce in compression parallel to grain”. *Wood Science and Technology*, 37: pp. 435-445.
- GÖRLACHER, R.; 1987 – “Non destructive testing of wood: an *in-situ* method for determination of density”. *Holz as Roh- und Werkstoff*. Vol. 45: pp. 273-278.
- GÖRLACHER, R.; HÄTTICH, R.; 1990 – “Untersuchung von altem Konstruktionsholz: Die Bohrenwiderstandsmessung”. *Sondernausdruck aus Bauen mit Holz*, Vol. 6(90): 6 pp.
- GOTOH, M.; 1978 – “A theory of plastic anisotropy based on a yield function of fourth order (plane stress state)”. *Int. J. Mech. Sci.*, Vol. 19: pp. 505-520.
- GRAVES, B.; BORRALHO, N.; RAYMOND, C.; FARRINGTON, A.; 1996 – “Use of Pilodyn for indirect selection of basic density in *Eucalyptus nitens*”. *Canadian Journal of Forest Research*, Vol. 26: pp. 1643-1650.
- GREEN, R.; 1991 – “Ultrasonic wave in anisotropic materials: past, present and future”. *ASNT Fall Conference and Quality Testing Show*, Boston, MA, pp. 42-46.
- HELMS, D.; NIEMZ, P.; 1994 – “New applications of the drill resistance method for quality evaluation of wood and wood products”. *Proceedings of the Ninth International Symposium on Nondestructive Testing of Wood*. Madison, WI; Washington State University: pp. 95-102.
- HILL, R.; 1950 – *The mathematical theory of plasticity*. Oxford University Press, London, UK.
- HOFFMAN, O.; 1967 – “The brittle strength of orthotropic materials”. *Journal of Composite Materials*, Vol. 1(2): pp. 200-206.
- HOFFMEYER, P.; 1978 – “The Pilodyn instrument as a non-destructive tester of the shock resistance of wood”. *Proceedings, 4th Non-destructive Testing of Wood Symposium*; Vancouver, WA. Pullman, WA: Washington State University: pp. 47-66.
- ISIK, F.; LI, B.; 2004 – “Rapid assessment of wood density of live trees using IML Resi for selection in tree improvement programs”. *Canadian Journal of Forest Research*, Vol. 33: pp. 1-10.
- ISO 8970; 1989 – “Timber structures – Testing of joints made with mechanical fasteners Requirements for wood density”.
- JAYNE, B.; 1959 – “Vibrational properties of wood”. *Forest Products Journal*, Vol. 9: pp. 413-416.
- JONES, R. M.; 1975 – *Mechanics of Composite Materials*, New York.
- KACHANOV, M.; 1993 – “On the effective moduli of solids with cavities and cracks”. *International Journal Fracture*, Vol. 59: pp. R17-R21.
- KASAL, B.; 2003 – “Semi-destructive method for *in-situ* evaluation of compressive strength of wood structural members”. *Forest Products Journal*, Vol. 53(11/12): pp. 55-58.
- KASAL, B.; DRDÁČKÝ, M.; JIROVSKÝ, I.; 2003 – “Semi-destructive methods for evaluation of timber structures”. *Proceedings STREMAH VIII, Series: Advances in Architecture*, Vol. 15: pp. 835-842.

- KASAL, B.; 2005 – “Estimate of the Design Values of the *In-Situ* Wood Structural Members Based on Semi-Destructive Experiments”. Proceedings of the International Conference *The Conservation of Historic Wooden Structures*, Florence, Vol. I: pp. 304-306.
- KENNEDY, R.W.; 1968 – “Wood in transverse compression – Influence of some anatomical variables and density on behavior”. *Forest Products Journal*, 18 (3): pp. 36-40.
- KOLLMANN, F.; 1959 – “The problem of transverse compressive strength of timber”. Translated by D.S.I.R. (Great Britain) from *Holzforschung und Holzverwertung*, 11 (5): pp. 109-121.
- KOLLMANN, F.P.; COTÉ, W.A.; 1968 – *Principles of Wood Science and Technology. I Solid Wood*. Springer – Verlag New York Inc.
- KORIN, U.; 1990 – “Timber in compression perpendicular to the grain”. CIB-W18A/23-6-1.
- KUIPERS, J.; 1986 – “Effect of age and/or load on timber strength”. Proceedings of 19th CIB-W18/19-6-1, Florence, Italy.
- KUNESH, R.H.; 1968 – “Strength and elastic properties of wood in transverse compression”. *Forest Products Journal*, 18 (1): pp. 65-72.
- LABOSSIERE, P.; NEALE, K.; 1987 – “On the determination of the strength parameters in the tensor polynomial failure criterion”. *Journal of Strain Analysis*, Vol. 22(7): pp. 155-161.
- LANG, J.; MIDDLETON, A.; 1997 – *Radiography of Cultural Material*. Butterworth-Heinemann, Oxford.
- LARSEN, H.J.; 1987 – “Determination of shear strength and strength perpendicular to grain”. CIB-W18A/20-6-3.
- LEE, I.; 1965 – “Ultrasonic pulse velocity testing considered as a safety measure for timber structures”. Proceedings, 2Nd Non-destructive testing of wood symposium, Washington State University: pp. 185-203.
- LEMASTER, R.; BEALL, F.; LEWIS, V.; 1997 – “Detection of termites with acoustic emission”. *Forest Products Journal*, Vol. 47(2): pp. 75-79.
- LEXA, J.; TOKOSOVA, M.; 1983 – “Evaluation of allowable stresses based on small specimens”. State Forest Products Research Laboratory, Bratislava, Slovakia. Research Report 9/SHL.
- LINDGREN, O.; DAVIS, J.; WELLS, P.; SHABOLD, P.; 1992 – “Non-destructive wood density distribution measurements using computed tomography: a comparison between two scanners”. *Holz as Roh- und Werkstoff*, Vol. 50(7/8): pp. 295-299.
- LORD, W.; LUDVING, R.; YOU, Z.; 1988 – “Finite element modelling of ultrasonic wave propagation in materials”. New directions in the non-destructive evaluation of advanced materials, Winter Annual Meeting of Mechanical Engineers, Chicago: pp. 1-7.
- LOURENÇO, P. B.; 1996 – *Computational strategies for masonry structures*. PhD thesis, Delft University of Technology.
- LOURENÇO, P. B.; DE BORST, R.; ROTS, J. G.; 1997 – “A plane stress softening plasticity model for orthotropic materials”. *International Journal of Numerical Methods in Engineering*, Vol. 40: pp. 4033-4057.

- MACHADO, J. S.; CRUZ, H.; NUNES, L.; 1992 – “Inspeções de elementos estruturais de madeira. Selecção das técnicas não destrutivas a aplicar *in situ*”. Encontro sobre Conservação e Reabilitação de Edifícios, ENCORE. Lisboa: LNEC: pp. 265-274.
- MACHADO, J. S.; CRUZ H.; 1997 – “Avaliação do estado de conservação de estruturas de madeira. Determinação do perfil densidade por métodos não destrutivos”. Revista Portuguesa de Engenharia de Estruturas. No 42: pp. 15-18.
- MACHADO, J. S.; 2000 – Avaliação da variação das propriedades mecânicas de pinho bravo (*Pinus Pinaster* Ait.) por meio de ultra-sons. Tese de Doutoramento em Engenharia Florestal, Universidade Técnica de Lisboa – Instituto Superior de Agronomia, Lisboa, Portugal. 265 pp.
- MADSEN, B.; HOOLEY, R.F.; HALL, C.P.; 1982 – “A design method for bearing in wood”. Canadian Journal of Civil Engineering, 9: pp. 338-349.
- MADSEN, B.; 1989 – “Proposal for including an updated design method for bearing stresses in CIB W18-Structural Timber Design Code”. CIB-W18A/22-100-1.
- MADSEN, B.; 1994 – “Radiological density scanning portable gamma camera based on backscatter tomography”. Proceedings of the 9th Non-destructive Testing of Wood Symposium. Washington State University: pp. 131-139.
- MALHOTRA, V.; 1984 – In Situ Nondestructive Testing of Concrete. ACI – American Concrete Institute, Detroit, USA, Publ. SP-82.
- MANNUCCI, M.; 2005 – “La Copertura della “Dogana Venet” in Lazise (Verona – Italia). Indagine Diagnostica Sullo Stato di Conservazione”. Proceedings of the International Conference *The Conservation of Historic Wooden Structures*, Florence, Vol. I: pp. 237-246.
- MEADE, E.; ANTHONY, A.; 2005 – “Assessment and Repair of Historic Timber Structures in the U.S.”. Proceedings of the International Conference *The Conservation of Historic Wooden Structures*, Florence, Vol. I: pp. 375-382.
- MIGLIORE, M.; RAMUNDO, F.; 2005 – “Identification of the mechanical properties of timber structures by combined non-destructive tests”. Structural Analysis of Historical Structures, Modena – Italy, Vol. I, pp. 361-368.
- MÜLLER, U.; GINDL, W.; TEISCHINGER, A.; 2003 – “Effects of cell anatomy on the plastic and elastic behaviour of different wood species loaded perpendicular to grain”. IAWA Journal, 24 (2): pp. 117-128.
- NEAL, D.; 1985 – “Establishment of elastic properties for in-place timber structures”. Proceedings of the 5th Non-destructive testing of wood symposium. Washington State University: pp. 353–359.
- NORMA BRASILEIRA; 1997 – “Nbr7190_1997 – Projeto de Estruturas de Madeira”. Brasil, in Portuguese.
- PARISI, M.; PIAZZA, M.; 1999 – “Mechanics of plain and retrofitted traditional timber connections”. Journal of Structural Engineering, Vol. 126(12): pp. 1395-1403.
- PATTON-MALLORY, M.; CRAMER, S.; 1987 – “Fracture mechanics: a tool for predicting wood component strength”. Forest Products Journal, Vol. 37: pp. 39-47.
- PATTON-MALLORY, M.; DEGROOT, R.; 1989 – “Detecting brown-rot decay in southern yellow pine by acousto-ultrasonics”. Proceedings of the 7th Symposium of Non-destructive Testing of Wood, Pullman, WA: pp. 29-43.

- PEREIRA, J.; XAVIER, J.; MORAIS, J., 2003 – “Estudo por elementos finitos dum novo método para a determinação das propriedades mecânicas da madeira de Pinus Pinaster AIT. nas direcções perpendiculares ao grão”. Livro de actas do VII Congresso Nacional de Mecânica Aplicada e Computacional, Vol. II. Universidade de Évora.
- POLLOCK, D.; BENDER, D.; SOLTIS, L.; 1996 – “Fasteners as damage indicators in timber structures”. Proceedings International Wood Engineering Conference. V.K. Gopu, ed. Louisiana State Univ., Baton Rouge, La: pp. 4-39 to 4-45.
- RENAUD, M.; RUEFF, M.; ROCABOY, A.; 1996 – “Mechanical behaviour of saturated wood under compression. Part 2: Behaviour of wood at low rates of strain: some effects of compression on wood structure”. Wood Science and Technology, 30: pp. 237-243.
- RINN, F.; 1994 – “Catalogue of relative density profiles of trees, poles and timber derived from Resistograph micro-drillings”. 9th International Symposium on Non-destructive Testing. Madison, USA: pp. 61-67.
- RINN, F.; SCHWEINGRUBER, F.; SCHÄR, E.; 1996 – “Resistograph and x-ray density charts of wood comparative evaluation of drill resistance profiles and x-ray density charts of different wood species”. Holzforschung – International Journal of the Biology, Chemistry, Physics and technology of Wood, Vol. 50(4): pp. 303-311.
- ROMAGNOLI, M.; CESETTI, S.; BIZZARRI, E.; ANZELMO, F.; SARLATTO, M.; 2004 – “Dendrochronological perspectives of wood ceiling of Palatina Chapel in Palermo (Sicily, Italy)”. Dendrochronologia, Vol. 21(3): pp. 117-130.
- ROMAGNOLI, M.; NOCETTI, M.; SARLATTO, M.; 2005 – “Datazione Dendrocronologica di Strutture Lignee nei Tetti in Italia Centro-Meridionale. Limiti e Prospettive” Proceedings of the International Conference *The Conservation of Historic Wooden Structures*, Florence, Vol. I: pp. 19-23.
- RONCA, P.; GUBANA, A.; 1998 – “Mechanical characterization of wooden structures by means of penetration test”. Construction and Building Materials, Vol. 12: pp. 233-243.
- ROSS, R.; PELLERIN, R.; 1994 – Non-destructive testing for assessing wood members in structures: A review. Gen. Tech. Rep. FPL-GTR-70 (Rev.). Madison, WI: U.S. Department of Agriculture, Forest Service, Forest Products Laboratory: 40 pp.
- ROSS, R.; McDONALD, K.; SOLTIS, L.; OTTON, P.; 1996 – “NDE of historic structures – USS Constitution”. SPIE. Vol. 2944: pp. 266-274.
- ROSS, R.; DeGROOT, R.; NELSON, W.; LEBOW, P.; 1997 – “The relationship between stress wave transmission characteristics and the compressive strength of biologically degraded wood”. Forest Products Journal, Vol. 47(5), pp. 89-93.
- ROSS, R.; BRASHAW, B.; PELLERIN, R.; 1998 – “Non-destructive evaluation of wood”. Forest Products Journal. Vol. 48 (1): pp. 101-105.
- ROSS, R.; PELLERIN, R.; VOLNY, N.; SALSIG, W.; FALK, R.; 1999 – Inspection of timber bridges using stress wave timing non-destructive evaluation tools – A guide for use and interpretation. Gen. Tech. Rep. FPL-GTR-114. Madison, WI: U.S. Department of Agriculture, Forest Service, Forest Products Laboratory: 15 pp.

- ROSS, R.; HUNT, M.; 2000 – “Stress wave timing non-destructive evaluation tools for inspecting historic structures – a guide for use and interpretation”. General Technical Report FPL-GTR – 119. Department of Agriculture Forest Service, 16 pp.
- ROTS, J. G.; 1988 – Computational Modeling of Concrete Fracture. PhD thesis, Delft University of Technology.
- SANDOZ, J.; 1989 – “Grading of construction timber by ultrasound”. *Wood Science Technology*, 23: pp. 95-108.
- SELBO, M.; 1962 – “A new method for testing glue joints of laminated timbers in service”. *Forest Products Journal*, Vol. 12(2): pp. 65-67.
- SHAJI, T.; SOMAYAJI, S.; MATHEWS, M.; 2000 – “Ultrasonic pulse velocity technique for inspection and evaluation of timber”. *Journal of Materials in Civil Engineering*: pp. 180-185.
- SHIH, C.; LEE, D.; 1978 – “Further developments in anisotropic plasticity”. *J. Eng. Math. Technol.*, Vol. 100: pp. 294-302.
- SLIKER, A., 1988 – “A method for predicting non-shear compliances in the RT plane of wood”. *Wood and Fiber Science*, 20 (1), pp: 44-55.
- SLIKER, A.; YU, Y.; 1993 – “Elastic constants for hardwoods measured from plate and tension tests”. *Wood and Fiber Science*, 25 (1): pp. 8-22.
- SOLTI, L.; HUNT, M.; ROSS, R.; WANG, X.; CAI, Z.; 2000 – “Non-destructive structural evaluation of wood floor systems in historic buildings”. *Proceedings 12th International Symposium on Non-destructive Testing of Wood*: pp. 279-288.
- SPRAGE, J.; TALBERT, J.; JETT, J.; BRYANT, R.; 1983 – “Utility of the Pilodyn in selection for mature wood specific gravity in loblolly pine”. *For. Sci.*, Vol. 29: pp. 696-701.
- SZYMANI, R; McDONALD, K.; 1981 – “Defect detection in lumber: state of the art”. *Forest Product Journal*, Vol. 31(11): pp. 34-44.
- TABARSA, T.; CHUI, Y.H.; 2000 – “Stress-strain response of wood under radial compression. Part I. Test method and influences of cellular properties”. *Wood and Fiber Science*, 32 (2): pp. 144-152.
- TABARSA, T.; CHUI, Y.H.; 2001 – “Characterizing microscopic behaviour of wood under transverse compression. Part II. Effect of species and loading direction”. *Wood and Fiber Science*, 33 (2): pp. 223-232.
- TAMPONE, G.; 1996a – *Il restauro delle strutture di legno*. Collana BTH. Hoepli, Milano.
- TAMPONE, G.; 1996b – *Timber structure rehabilitation*. 1st Edn. Hoepli, Milano.
- TAMPONE, G., MANNUCCI, S.; MACCHIONI, N.; 2002 – *Strutture di Legno*. De Lettera editore, Milano.
- TANAKA, T.; 2000 – “Wood inspection by thermography”. *NDT.net – March 2001*, Vol. 6, No. 03.
- THELANDERSSON, S.; MÅRTENSSON, A.; 1997 – “Design principles for timber in compression perpendicular to grain”. *CIB-W18A/30-20-1*.
- TIITA, M.; BEALL, F.; BIERNACKI, J.; 1998 – “Acousto-ultrasonic assessment of internal decay in glulam beams”. *Wood and Fiber Science*. 30(3): pp. 259-272.

- TOGNI, M.; 1995 – Elasticità e resistenza di travi lignee antiche di grande sezione: stima con metodologie non distruttive applicabili in opera. Tesi presentata per il conseguimento del titolo di dottore di ricerca in Scienze del Legno. Università degli Studi di Firenze, Firenze, Italia.
- TSAI, S. W.; WU, E. M.; 1971 – “A general Theory of Strength for Anisotropic Materials”. *Journal of Composite Materials*, Vol. 5(1): pp. 519-534.
- TURRINI, G.; PIAZZA, M.; 1983 – “Il recupero dei solai in legno. Esperienze e realizzazioni”. *Recuperare*, Vol. 7.
- U. S. FOREST PRODUCTS LABORATORY; 1999 – *Wood Handbook – Wood as an Engineering Material*. U. S. Department of Agriculture, Forest Service, Forest Products Laboratory. Madison, WI.
- UZIELLI, L.; 1992a – Restoring timber structures – Repair and Strengthening – STEP (Structural Timber Education Programme) lecture D4, STEP 2 (STEP/EUROFORTECH) Centrum Hout, The Netherlands, D4/1-D4/10.
- UZIELLI, L.; 1992b – “Valutazione della capacità portante degli elementi strutturali lignei”. *L’Edilizia*, Vol. 12: pp. 753-762.
- VARY, A.; 1991 – “Acousto-ultrasonics – retrospective exhortation with bibliography”. *Mat. Evaluation*, Vol. 49: 581-591.
- WANG, S.; CHIU, C.; LIU, C.; 2003 – “Application of the drilling resistance method for annual ring characteristics: evaluation of Taiwania (Taiwania cryptomerioides) trees grown with different thinning and pruning treatments”. *J. Wood Sci.*, Vol. 49: pp. 116-124.
- WATT, M.; GARNETT, B.; WALKER, J.; 1996 – “The use of the Pilodyn for assessing outerwood density in New Zealand radiate pine”. *Forest Products Journal*. Vol. 46(11/12): pp. 101-105.
- WEIGEL, T.; 1991 – Non-shear compliances and elastic constants measured for EIGHT hardwood trees. M.S. thesis, Michigan State University, E. Lansing, MI: 91 pp.
- WILLIAMS, J. M.; FRIDLEY, K. J.; COFER, W. F.; FALK, R. H.; 2000 – “Failure modelling of sawn lumber with a fastener hole”. *Finite elements in Analysis and Design*, Vol. 6: pp. 83-98.
- WITHRALL, P.; ROSS, R.; FARRIS, W.; 1992 – “Using today’s technology to help preserve USS Constitution”. *Naval Engineers Journal*. Vol. 104(3): pp. 124-134.
- WU, E. M.; 1972 – “Optimal experimental measurements of anisotropic failure tensors”. *Journal of Composite Materials*, Vol. 6: pp. 472-487.
- WYCKHUYSE, A.; MALDAGUE, X.: 2001a – “A Study of Wood Inspection by Infrared Thermography, Part I: Wood Pole Inspection by Infrared Thermography”. *Research Non-destructive Evaluation*: pp. 1-12.
- WYCKHUYSE, A.; MALDAGUE, X.: 2001b – “A Study of Wood Inspection by Infrared Thermography, Part II: Thermography for Wood Defects Detection”. *Research Non-destructive Evaluation*: pp. 13-21.
- YASUTOSHI, S.; 2000 – “Ultrasonic measurements of applied stresses in wood by acoustoelastic birefringent method”. *NDT.net – March 2001*, Vol. 6, No. 03.
- YOUNGS, R.L.; 1957 – “The perpendicular-to-grain mechanical properties of red oak as related to temperature, moisture content, and time”. *U.S. Forest Product Laboratory*, No. 2079: pp. 124-130.

- YU, Y.; 1900 – Non-shear compliances and elastic constants measured for nine hardwood trees. M.S. thesis, Michigan State University, E. Lansing, MI: 79 pp.
- ZIENKIEWICZ, O.; TAYLOR, R.; 2000a - The finite element method (5th ed.): Volume 1, The Basis. Butterworth-Heinemann, Oxford.
- ZIENKIEWICZ, O.; TAYLOR, R.; 2000b - The finite element method (5th ed.): Volume 2, Solid Mechanics. Butterworth-Heinemann, Oxford.
- ZINK, A.; HANNA, R.; STELMOKAS, J.; 1997 – “Measurements of poisson’s ratios for yellow-poplar”. Wood Engineering, March: pp. 78-80.
- ZOMBORI, B.; 2000 – “*In situ* non-destructive testing of built in wooden members”. NDT.net – March 2001, Vol. 6, No. 03.
- ZWARGER, K.; 2000 – Wood and wood joints: building traditions of Europe and Japan. Birkhäuser, Basel, Berlin, Boston: 280 pp.

Annex 1: Research conducted on the use of non-destructive techniques for *in situ* evaluation of wood members

Table A.1 summarizes some research conducted on the use of several non-destructive techniques for *in situ* evaluation of wood members.

Table A.1 – Research summary of non-destructive evaluation concepts for in-place evaluation of wood structures.

Reference	NDT Method	Type of Structure	Material	Analysis Performed Conclusions
Lee (1965)	Longitudinal stress wave	XVIII c. building roof	Solid-sawn timber	Developed empirical relationship between sound velocity transmission and residual strength
Browne & Kuchar (1985)	Longitudinal stress wave	Dielectric support stand for testing large aircraft in a simulated flight situation	Glulam, structural timbers	MOE determined, strength properties inferred
Neal (1985)	Longitudinal stress wave (parallel and perpendicular to the grain)	Large military test stand	Glulam	Structural framework was not degraded; exposed deck system was degraded
		Small military test stand	Glulam	Structural framework and decks were degraded
		Large military test stand	Glulam, solid-sawn timber	Accessible structural degradation had not occurred
Abbott & Elcock (1987)	Full-size static MOE test	Wood poles	Wood utility poles	Correlative relationship between MOE and residual strength of poles ($r^2 = 0.68$)
Witherall <i>et al.</i> (1992)	Longitudinal stress wave	Wooden ship	Ribs, hull, and cross members	Found decay degradation on several members. Replaced members containing decay
Ceccotti & Togni (1996)	Visual inspection; Ultrasonic tests; Superficial hardness; Longitudinal stress wave	XV c. building beam's	Structural timber	Found decay degradation on several members

Reference	NDT Method	Type of Structure	Material	Analysis Performed Conclusions
Lang & Middleton (1997)	X-rays	Frames of historic artwork	Wood framing	Radiography was used to show the presence of wood rot and insect damage
Ross <i>et al.</i> (1999)	Visual inspection; Longitudinal stress wave (perpendicular to the grain)	Wooden ship (USS Constitution)	Ribs, hull, and cross members	Evaluation techniques were used to successfully locate deteriorated wood
Soltis <i>et al.</i> (2000)	Longitudinal stress wave	Wood floor systems	Solid wood	Results indicate natural frequency decreases and damping ratio increases as joist ends were cut. Deterioration in the salvaged joist floor was detectable by a decrease in frequency and/or increase in damping ratio, when compared to a new floor
Wyckhuysse & Maldague (2001a)	Infrared thermography (IRT)	Wood poles	Wood utility poles	Due to defect depths, low wood thermal diffusivity, and the wood dependencies upon T°, moisture, species, and fiber orientation, IRT is not appropriate for the wood pole inspection unless defects are close to the surface
Wyckhuysse & Maldague (2001b)	Infrared thermography (IRT)	Wood poles	Wood utility poles	The authors concluded that IRT can be used for wood inspection but with some cautions due to many adverse variables such as unknown wood moisture content and very low thermal diffusivity
Cai <i>et al.</i> (2002)	Screw withdrawal; Longitudinal stress wave	Wood members from three different old buildings (1904 and 1909)	Solid wood	The results show a good correlation between screw withdrawal strength and density. The result indicates that a good relationship between the static MOE and the dynamic MOE

Reference	NDT Method	Type of Structure	Material	Analysis Performed Conclusions
Anthony (2003)	Digital radioscopy	Connections in trusses in large military warehouses built prior to 1950	Solid wood	X-ray was used to examine the connections and to determine the presence of split rings; their size, number and condition, and the condition of surrounding wood
Anthony & Kasal (2004)	Digital radioscopy	Rods that supported the wood balcony (Academical Village)	Solid wood	Post failure digital radioscopy was used to determine whether presence and corrosion of the iron rods in wood elements. These have been accurately detected
Blanchet (2005)	Resistograph	Canal Rideau miter gates	Solid wood	Evaluation of structural integrity
Mannucci (2005)	Resistograph	Second half XIV c. building (roof)	Solid wood	Preliminary diagnostic survey of the wooden structures, aimed at determining the actual state of conservation, possible static deficiencies, as well as other non structural aspects such as dendrochronology and assembling marks analysis
Augelli et al. (2005b)	Resistograph; Superficial hardness; Ultrasonic tests	Roof wooden structures of a Renaissance building	Solid wood	Structural diagnosis and inspection of wood elements
Migliore & Ramundo (2005)	Resistograph; Ultrasonic tests	XVII c. building (trusses)	Solid wood	The experimental campaign allowed to check the homogeneity of the wood specimens and to formulate an estimation of the modulus of elasticity. A more reliable evaluation of the experimental results was verified running laboratory tests

Reference	NDT Method	Type of Structure	Material	Analysis Performed Conclusions
Anthony (2003; 2005)	Digital radiosocopy	Mortise and tenon joints	Solid wood	Research conducted on a mortise and tenon joints showed that differences in the grain orientation of the mortise and tenon were visible
		Pernštejn Castle, village houses		Research used to assist in dating constructions showed promise for using image enhancement techniques to identify similarities in constructions
		Saint Anne's Church		
		Baroque-classical chateau		
Drdácký et al. (2005)	Core drilling; Non-standard/core compression and tension specimens; Digital radiosocopy; Resistograph	Maria's Tower of the Karlštejn Castle (end of XIX c.)	Solid wood	Correlations were proposed for elasticity modulus and compressive strength parallel to the grain, between standard and core specimens ($r^2 = 0.24-0.33$). Resistograph was applied for diagnostics of non-accessible joist heads walled into the masonry. X-ray was applied for investigation of the state and dimensions of metal connectors as well as for discovering and extent measurements of interior defects in timber members

V – Ultrasonic velocity.

E_{din} – Dynamic modulus of elasticity obtained from either transverse vibration or stress wave measurements.

MOE – Modulus of elasticity.

r^2 – Correlation coefficient.

DR – Drilling resistance.

Annex 2: Compression tests perpendicular to the grain

The results of all the tests (partial and global results), in terms of load-displacement diagrams and taking into account the orientation of the annual growth rings along the direction of the applied force, are represented in Figure A.2.1 to Figure A.2.4.

Figure A.2.1 shows the typical load-displacement envelopes for each considered group (NCW and OCW) and for all tests, concerning the Radial group.

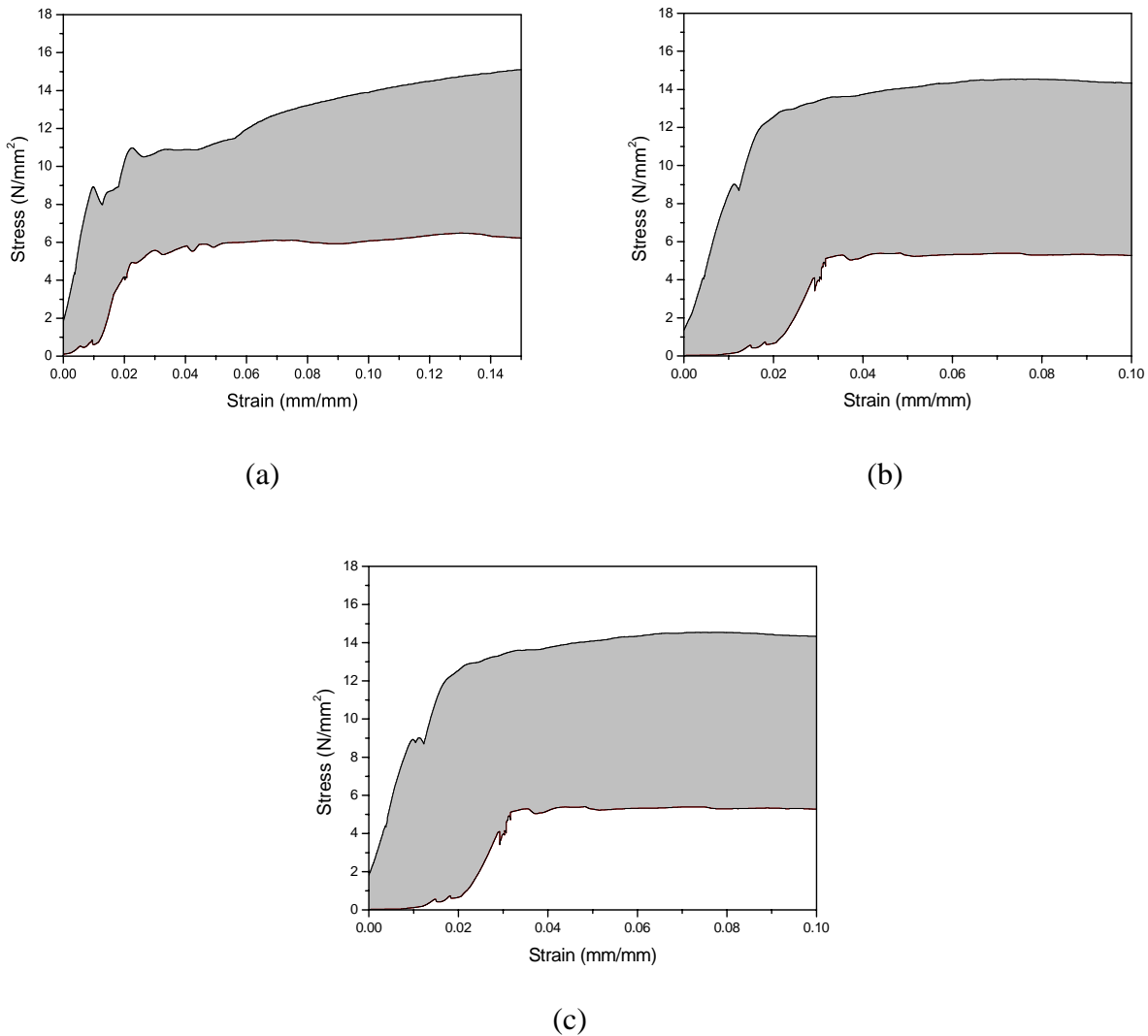
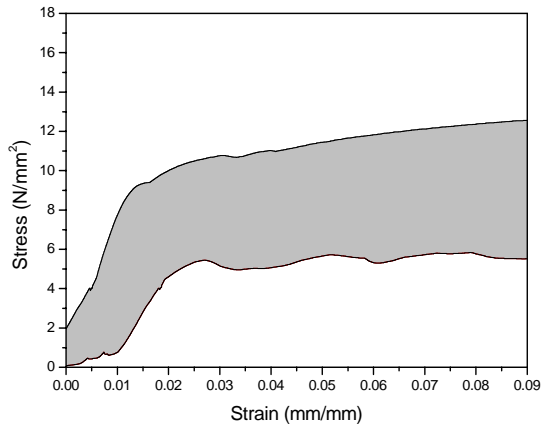
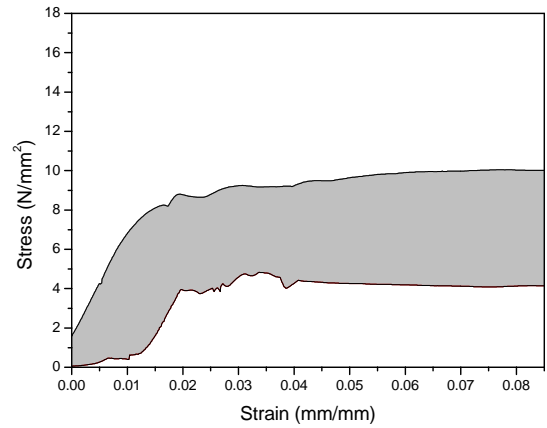


Figure A.2.1 – Envelope of load-displacement diagram for: (a) the NCW group, (b) the OCW group, and (c) all tests. Radial group is considered.

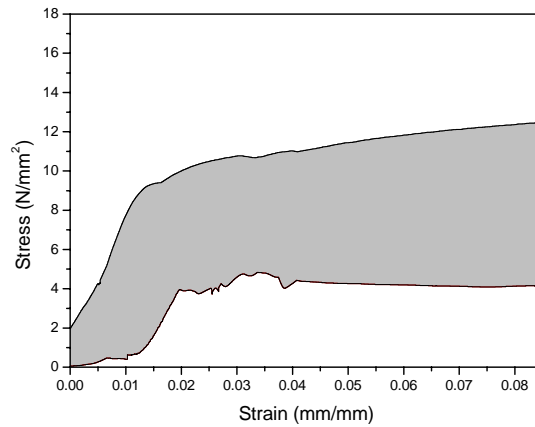
Figure A.2.2 shows the typical load-displacement envelopes for each considered group (NCW and OCW) and for all tests, concerning the Diagonal group.



(a)



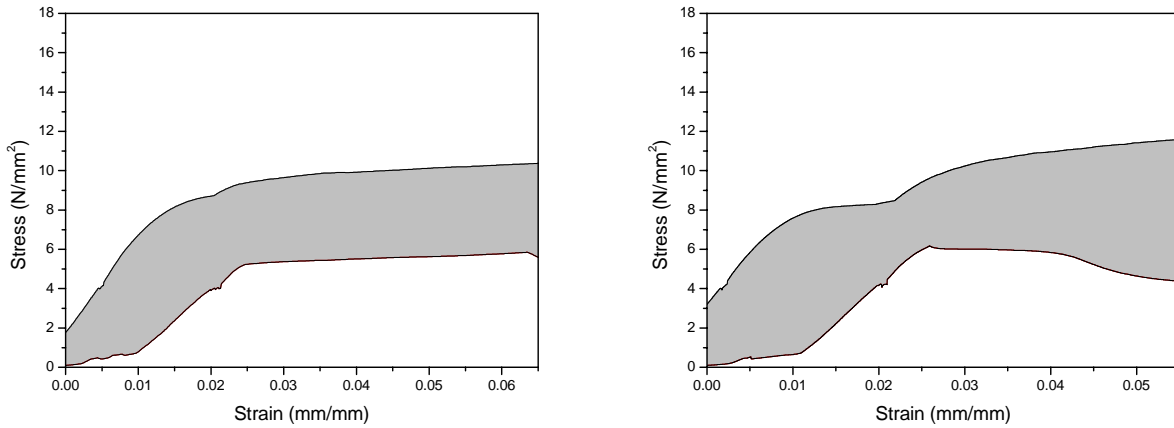
(b)



(c)

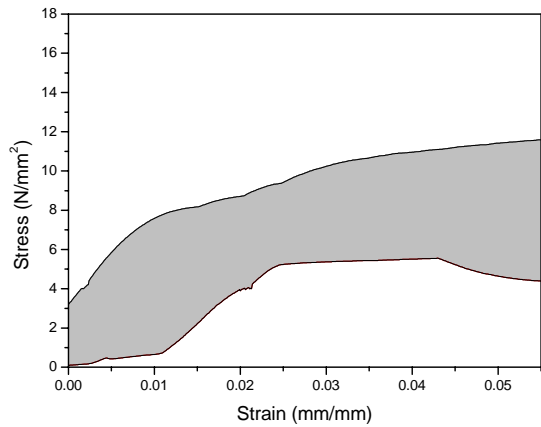
Figure A.2.2 – Envelope of load-displacement diagram for: (a) the NCW group, (b) the OCW group, and (c) all tests. Diagonal group is considered.

Figure A.2.3 shows the typical load-displacement envelopes for each considered group (NCW and OCW) and for all tests, concerning the Tangential group.



(a)

(b)



(c)

Figure A.2.3 – Envelope of load-displacement diagram for: (a) the NCW group, (b) the OCW group, and (c) all tests. Tangential group is considered.

Finally, Figure A.2.4 shows the typical load-displacement envelopes for each considered group (NCW and OCW) and for all tests, concerning the Diffuse group.

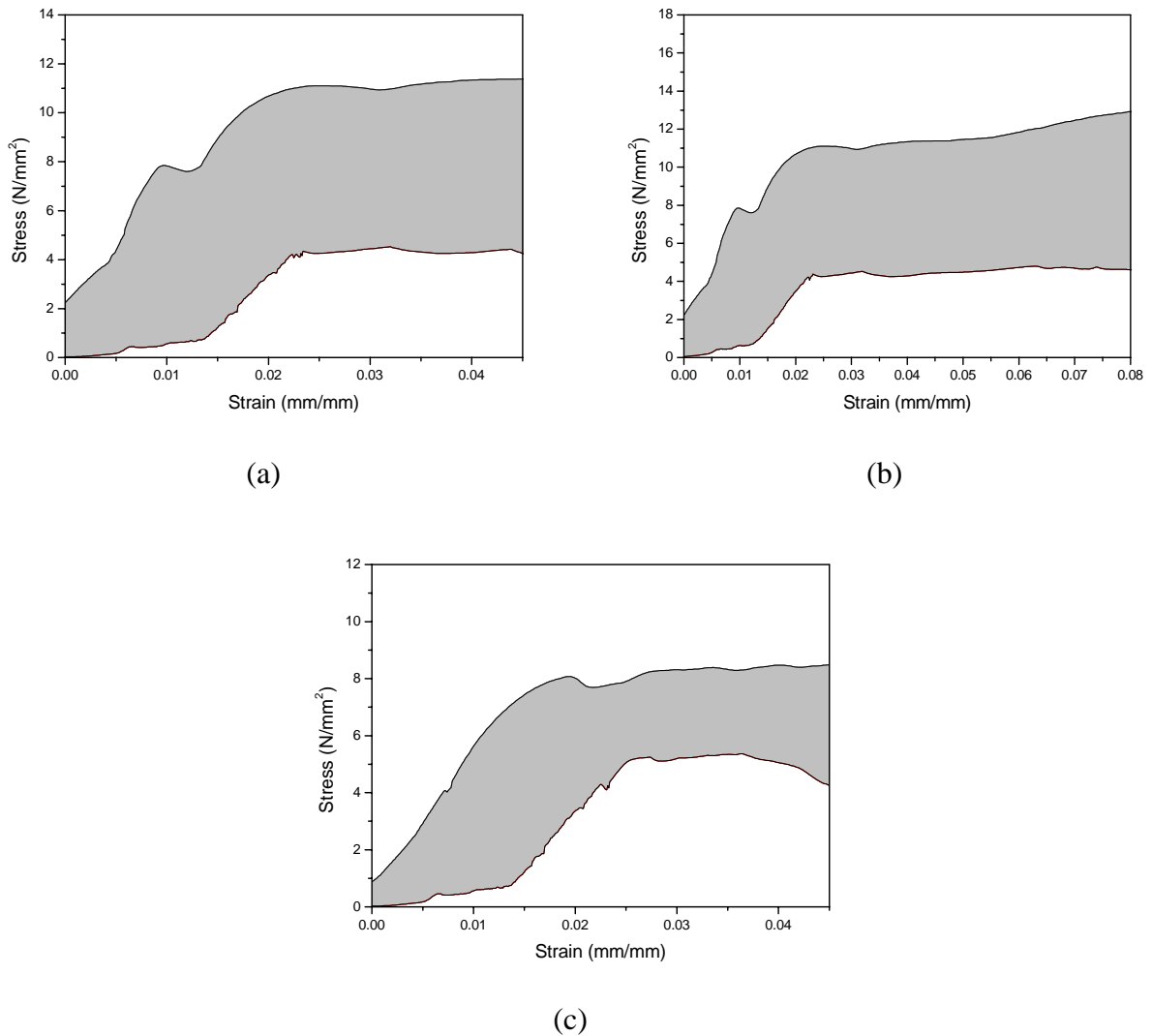
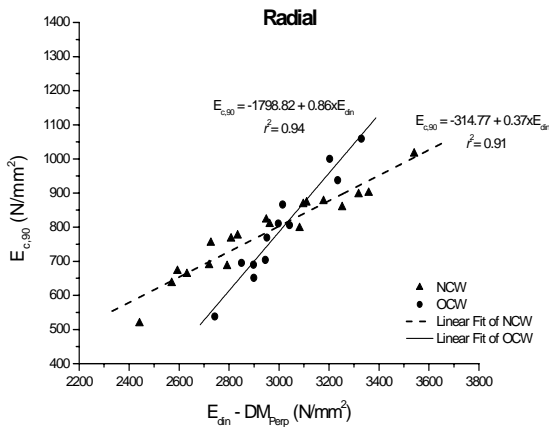


Figure A.2.4 – Envelope of load-displacement diagram for: (a) the NCW group, (b) the OCW group, and (c) all tests. Diffuse group is considered.

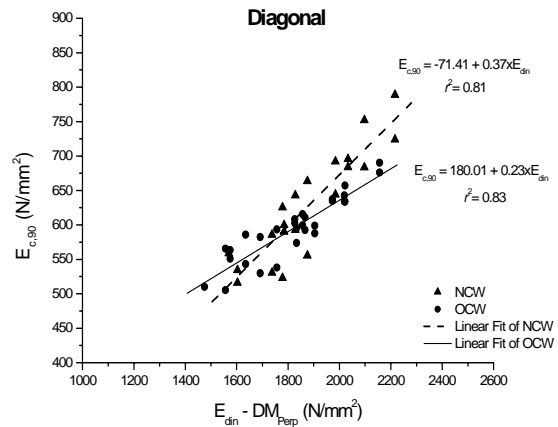
Figure A.2.5 shows the results between NCW and OCW using the Direct Method, perpendicular to the grain. Once again, very good linear correlations were found but it is necessary to use different correlations according to the load orientation and wood age. In the comparison of the same loading direction but different ages, it is striking that the slope of the linear correlations is equal in the case of the diagonal, tangential and diffuse specimens, and it is totally different in the case of the radial specimens. This is consistent with the orientation of the annual growth rings versus the orientation of the ultrasonic transmission.

Considering all tests together, a lower 95% confidence limit is given by the following expression:

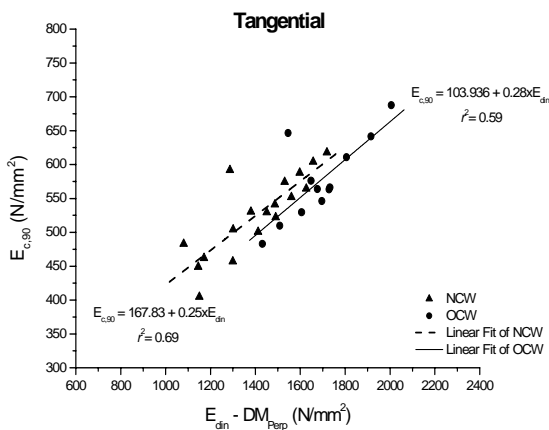
$$E_{c,90} = 209.63 + 0.177 \cdot E_{din} \tag{A.2.1}$$



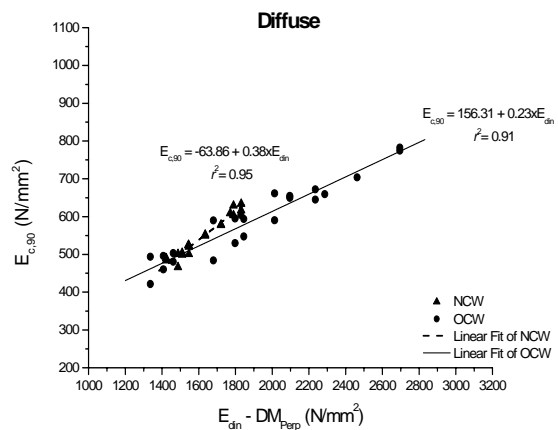
(a)



(b)



(c)



(d)

Figure A.2.5 – Relation between E_{din} and $E_{c,90}$, using the Direct Method, perpendicular to the grain, for the: (a) radial group, (b) diagonal group, (c) tangential group, and (d) diffuse group. Both NCW and OCW are considered.

Figure A.2.6 shows the correlations between NCW and OCW using the Direct Method, perpendicular to the grain. Good linear correlations were found but, again, it is necessary to use different correlations according to the load orientation and wood age. If the comparison is made for the same loading direction but different ages, it is even more striking that the slope of the linear correlations is equal in the case of the diffuse, diagonal and tangential specimens (analysed all

separately), and it is totally different in the case of the radial specimens. Considering all tests together, a lower 95% confidence limit is given by the following expression:

$$f_{c,90} = 3.75 + 9.6 \times 10^{-4} \cdot E_{din} \quad (\text{A.2.2})$$

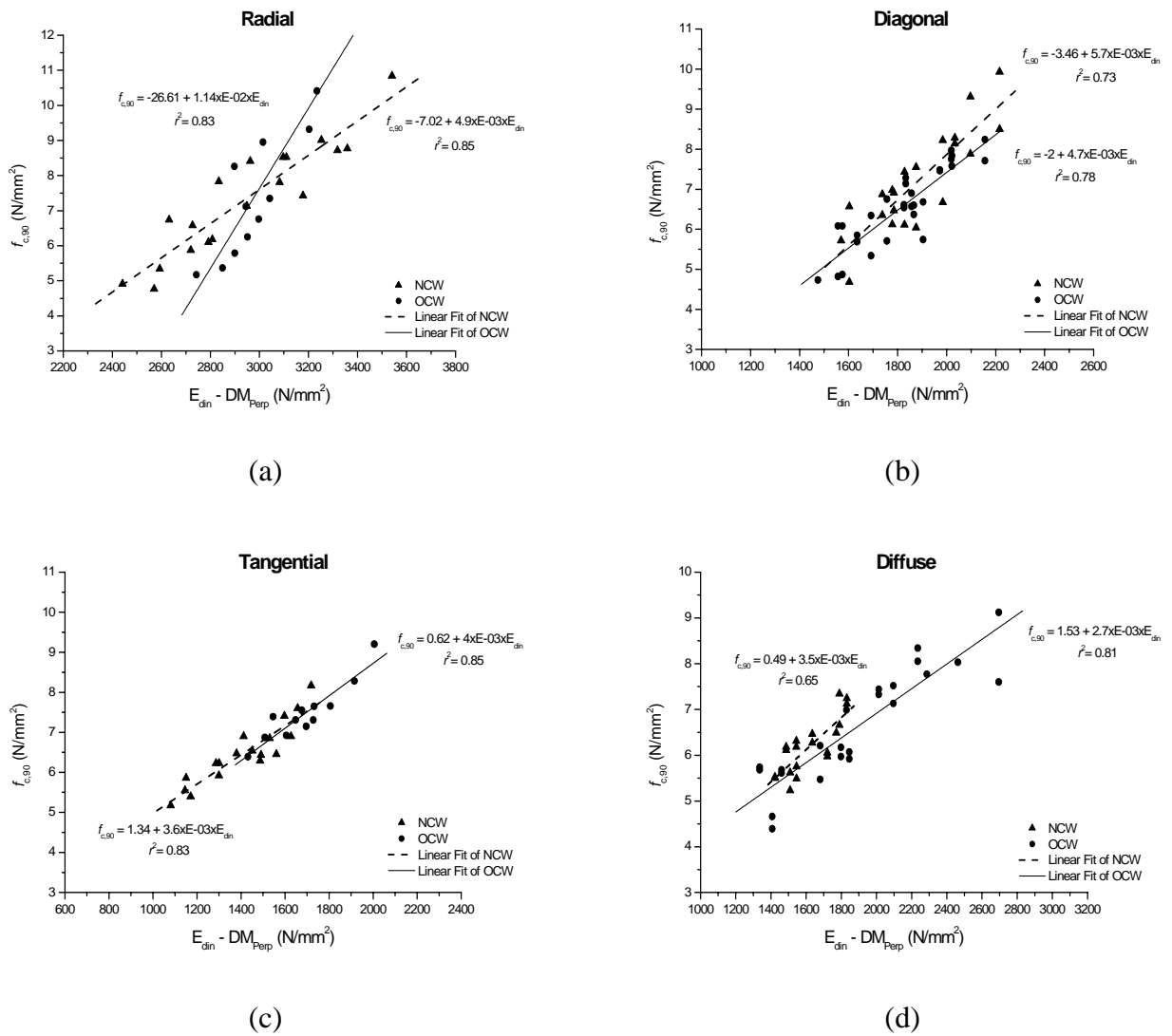
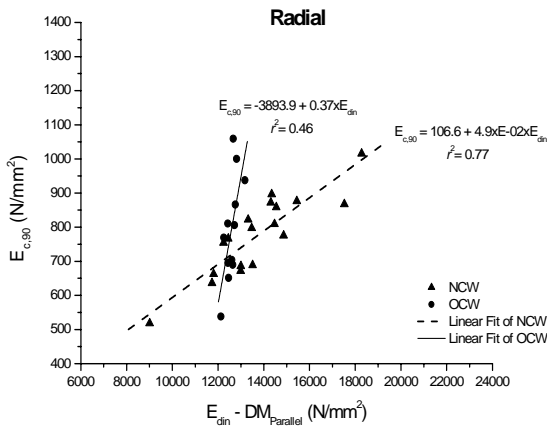


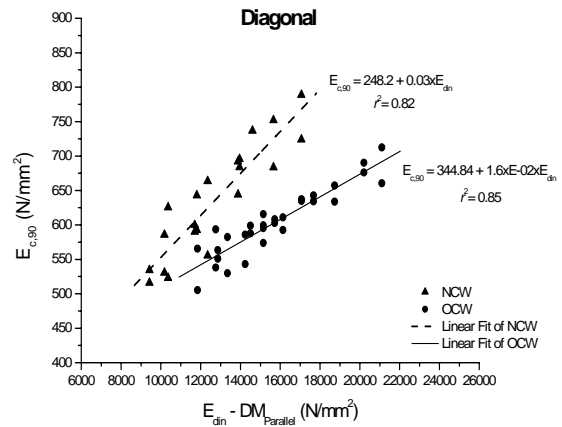
Figure A.2.6 – Relation between E_{din} and $f_{c,90}$, using the Direct Method, perpendicular to the grain, for the: (a) radial group, (b) diagonal group, (c) tangential group, and (d) diffuse group. Both NCW and OCW are considered.

Figure A.2.7 shows the results between $E_{c,90}$ and E_{din} using the Direct Method, parallel to the grain. Considering all tests together, a lower 95% confidence limit is given by the following expression:

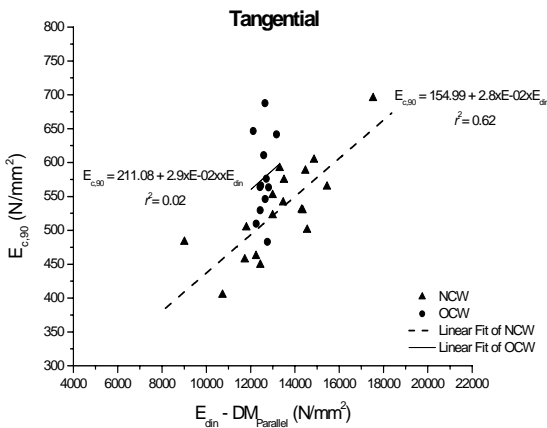
$$E_{c,90} = 286.37 + 9.5 \times E - 03 \cdot E_{din} \tag{A.2.3}$$



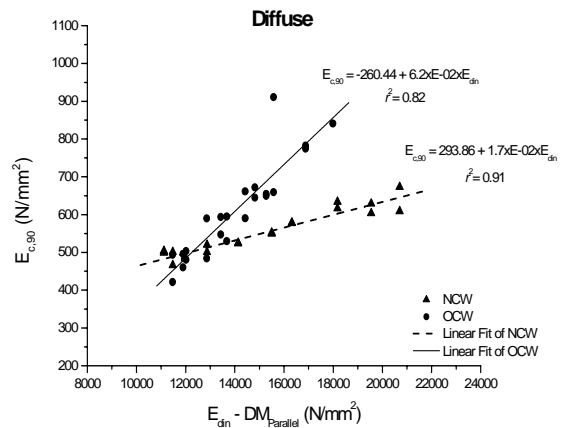
(a)



(b)



(c)



(d)

Figure A.2.7 – Relation between E_{din} and $E_{c,90}$, using the Direct Method, parallel to the grain, for the: (a) radial group, (b) diagonal group, (c) tangential group, and (d) diffuse group. Both NCW and OCW are considered.

Figure A.2.8 shows the correlations between E_{din} and $f_{c,90}$ using the Direct Method, perpendicular to the grain. Considering all tests together, a lower 95% confidence limit is given by the following expression:

$$f_{c,90} = 2.73 + 1.5 \times E - 04 \cdot E_{din} \quad (\text{A.2.4})$$

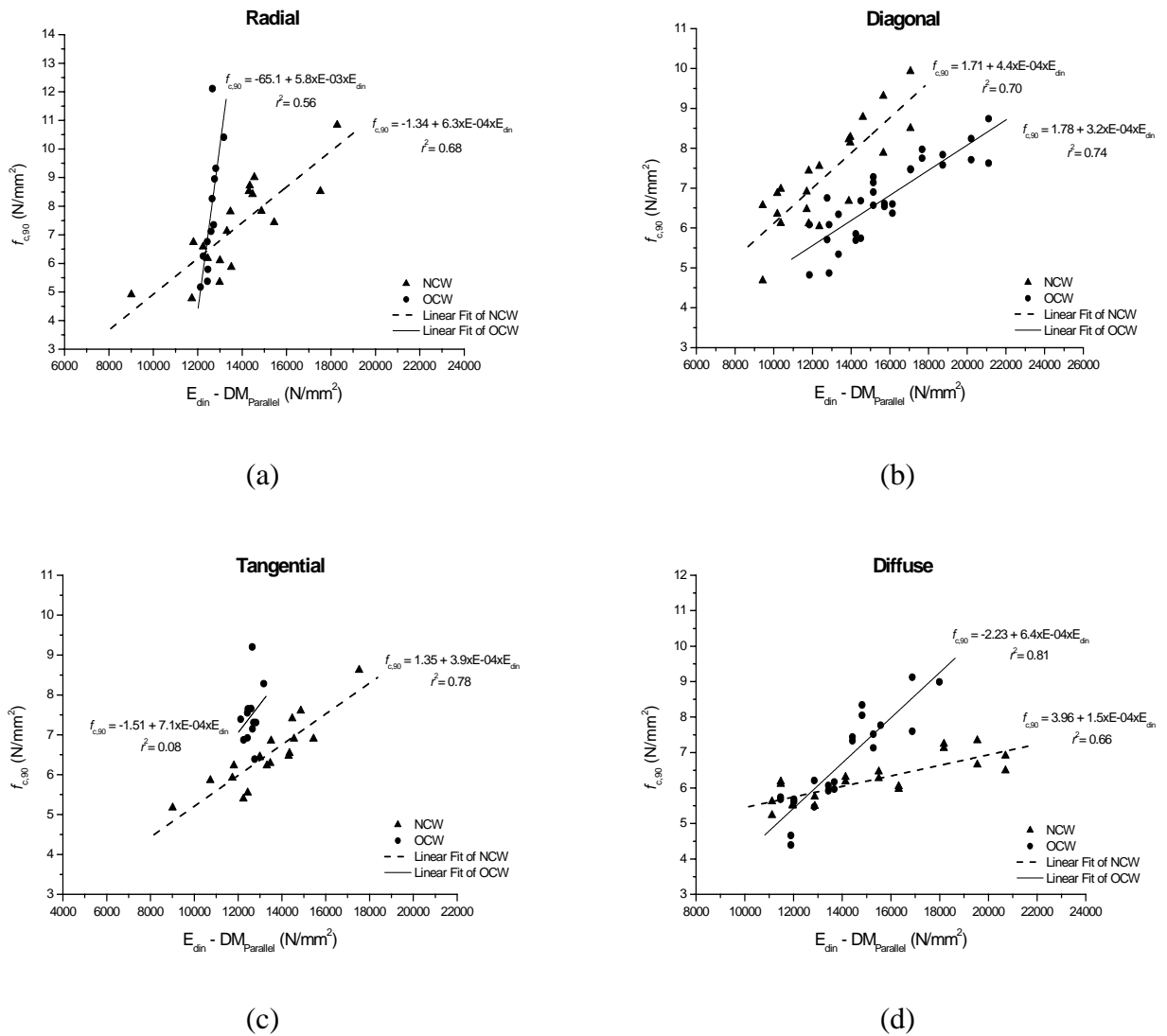


Figure A.2.8 – Relation between E_{din} and $f_{c,90}$, using the Direct Method, parallel to the grain, for the: (a) radial group, (b) diagonal group, (c) tangential group, and (d) diffuse group. Both NCW and OCW are considered.

Annex 3: Compression tests parallel to the grain

Figure A.3.1 illustrates the results between $E_{c,0}$ and E_{din} using the Direct Method, parallel to the grain. Only moderate linear correlations are found with a very large difference between NCW and OCW.

Also, these results are in agreement with Table 5.7. Considering all tests, a lower 95% confidence limit is given by:

$$E_{c,0} = 1962.66 + 2.89 \cdot E_{din} \tag{A.3.1}$$

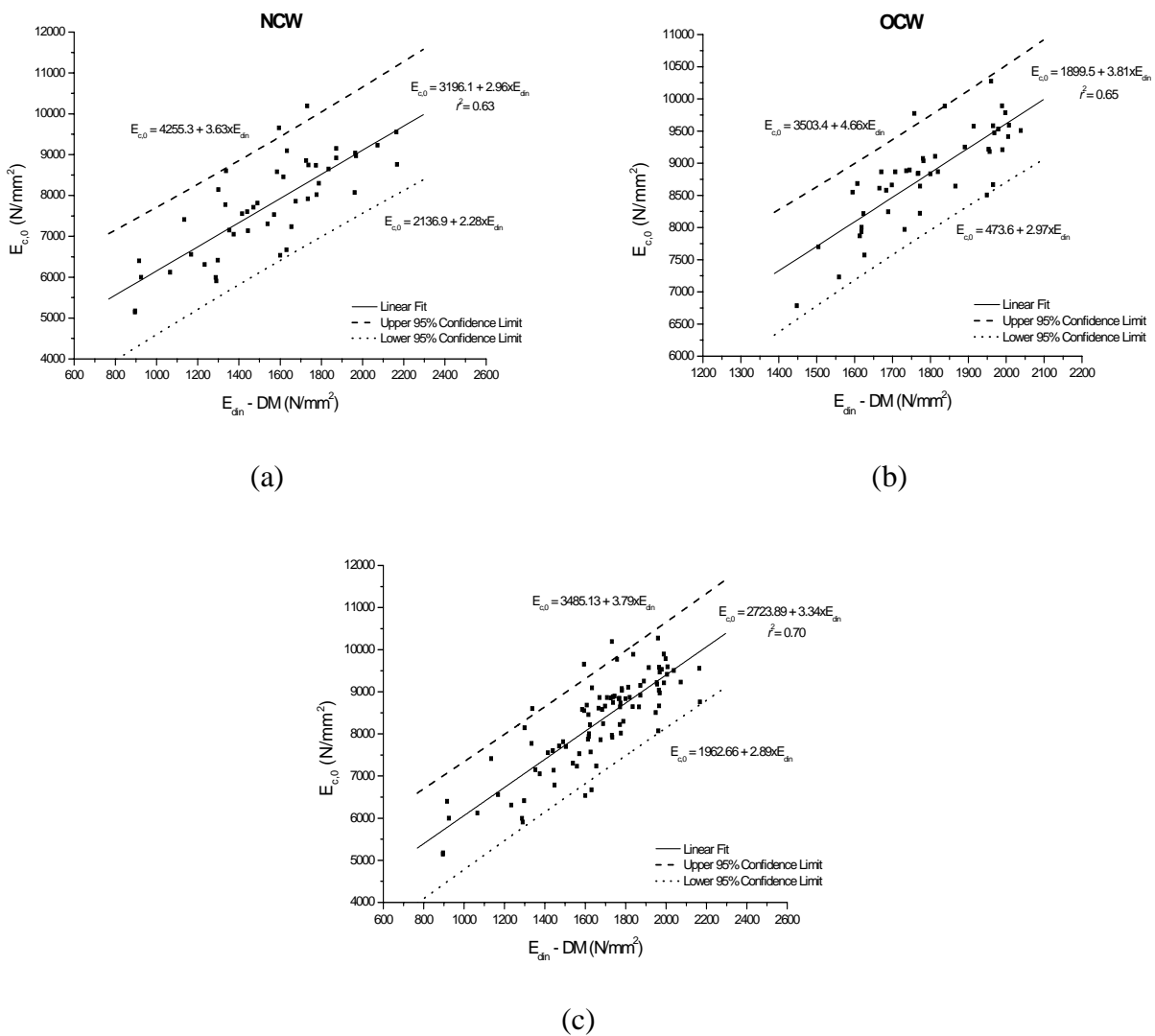
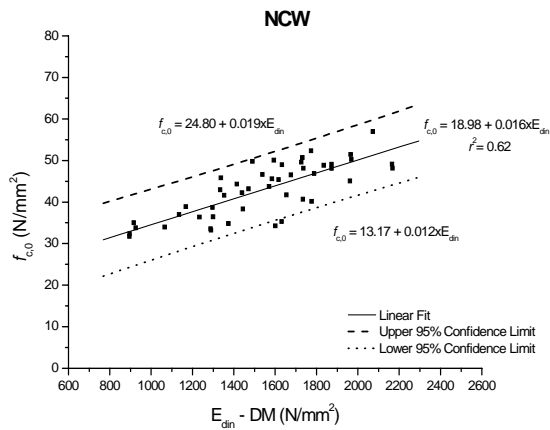


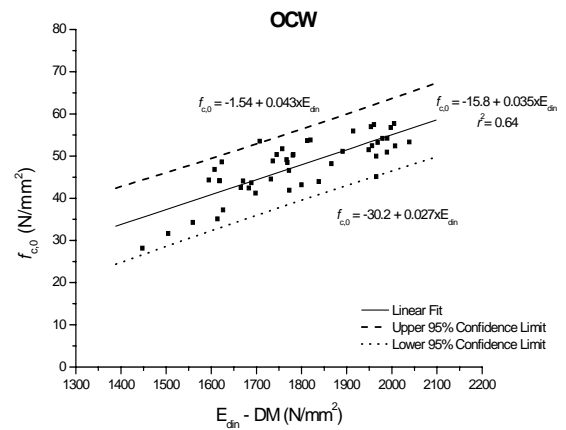
Figure A.3.1 – Relation between $E_{c,0}$ and E_{din} using the Direct Method, parallel to the grain: (a) NCW, (b) OCW, and (c) both groups.

Figure A.3.2 shows the results between $f_{c,0}$ and E_{din} using the Direct Method, parallel to the grain. Once, moderate linear correlations were found. Considering all tests together, a lower 95% confidence limit is given by the following expression:

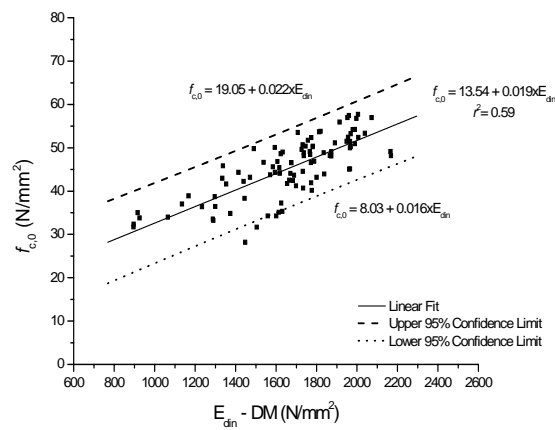
$$f_{c,0} = 8.03 + 0.016 \cdot E_{din} \quad (\text{A.3.2})$$



(a)



(b)



(c)

Figure A.3.2 – Relation between $f_{c,0}$ and E_{din} using the Direct Method, parallel to the grain:
(a) NCW, (b) OCW, and (c) both considered groups.

Annex 4: Tension tests parallel to the grain

A.4.1 FULL BRIDGE SYSTEM

The output full bridge tension related with the full bridge tension feed is given by:

$$\frac{\delta V}{V} = \frac{1 + G \cdot \varepsilon}{2 + (1 - \nu) \cdot G \cdot \varepsilon} - \frac{1 - \nu \cdot G \cdot \varepsilon}{2 + (1 - \nu) \cdot G \cdot \varepsilon} = \frac{(1 + \nu) \cdot G \cdot \varepsilon}{2 + (1 - \nu) \cdot G \cdot \varepsilon} \quad (\text{A.4.1})$$

where G is the gauge factor of the strain gauges, ν is the coefficient of Poisson and ε is the effective strain. This gauge factor could be defined by the unit electric resistance variation $\delta R/R$ correspondent to a unitary strain of the basis of the respective strain gauge ($\delta l/l$). The gauge factor could be defined by:

$$G = \frac{\delta R/R}{\delta l/l} \quad \text{with} \quad \delta l/l = \varepsilon \quad (\text{A.4.2})$$

Supposing a common lead wire with a length l and a section S , the Ohm formulation reads:

$$R = \rho \times \frac{l}{S} \quad (\text{A.4.3})$$

where ρ is the specific resistance of lead wires.

To measure strain in wood with an electrical resistance strain gauge, the gauge must be sufficiently large in width and length to cover a representative area of the specimens. Due to the strain gauges used, and taking into account the influence of the electrical grid and the joints, a gauge factor correction was made. This way:

$$G_0 = \frac{R}{R + \rho \cdot L} \cdot G \quad (\text{A.4.4})$$

where G_0 is the corrected gauge factor; G is the gauge factor indicated by the manufacturer, R is the resistance in ohms (Ω); r is the total resistance per meter of lead wires (Ω/m) and L is the length of lead wires in m. Because a 3-wire system was used, the influence of temperature variation of lead wires is null (3-wire system is independent of temperature).

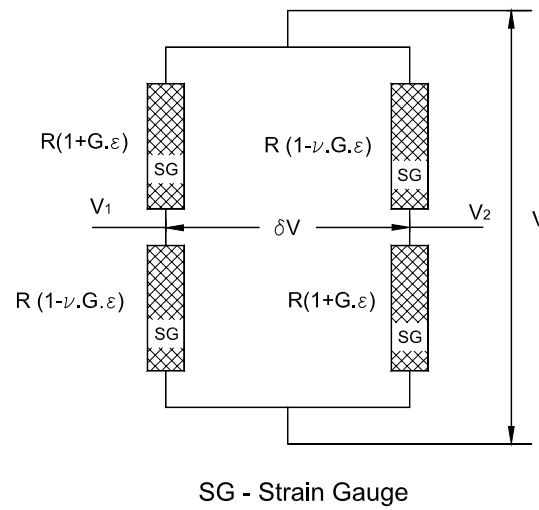


Figure A.4.1 – Full bridge (Wheatstone bridge).

In terms of full bridge it is possible to write:

$$G_0 = \frac{\frac{\delta R}{R}}{\frac{\delta L}{L}} \quad (\text{A.4.5})$$

$$V_1 = V \times \frac{R}{R \cdot (2 + G_0 \cdot \epsilon)} \quad \text{and} \quad V_2 = V \times \frac{R \cdot (1 + G_0 \cdot \epsilon)}{R \cdot (2 + G_0 \cdot \epsilon)} \quad (\text{A.4.6})$$

$$\frac{\delta V}{V} = \frac{1 - G_0 \cdot \epsilon}{2 + G_0 \cdot \epsilon} - \frac{1}{2 + G_0 \cdot \epsilon} = \frac{G_0 \cdot \epsilon}{2 + G_0 \cdot \epsilon} \approx \frac{G_0 \cdot \epsilon}{2} \quad (\text{A.4.7})$$

Taking an excitation tension equal to 5 V, the correspondent output tension of the full bridge is 6500 mV for the maximum strain of 1000×10^{-6} . This value of strain is equivalent to an output tension of 6500 mV.

The output signal amplification is mainly justified by the noise reduction effect and by the increasing accuracy in measuring micro-strains. The output amplification gain was chosen based on the hypothesis that a 1000×10^{-6} strain corresponds to the reading of 2500 mV in the acquisition unit. To a full bridge excitation value of 5 V the amplification value will be of:

$$A = \frac{2500}{6.5} = 384.6 \quad (\text{A.4.8})$$

A.4.2 RELATIONS BETWEEN THE ULTRASONIC PULSE VELOCITY METHODS

Figure A.4. and Figure A.4. illustrate the different relations (in terms of E_{din}) between the three used methods. In this figures one can observe that there are a good relation between the three methods, namely between the Direct Method and the Indirect Method ($d = 20$ cm).

It has to be emphasised that the tests were done with nearly clear wood specimens without visible cracks or splits, which often occur in structural size timber. In the case of structural timber coefficients of correlation are expected to be lower because of the strong effect of defects, especially knots and cracks.

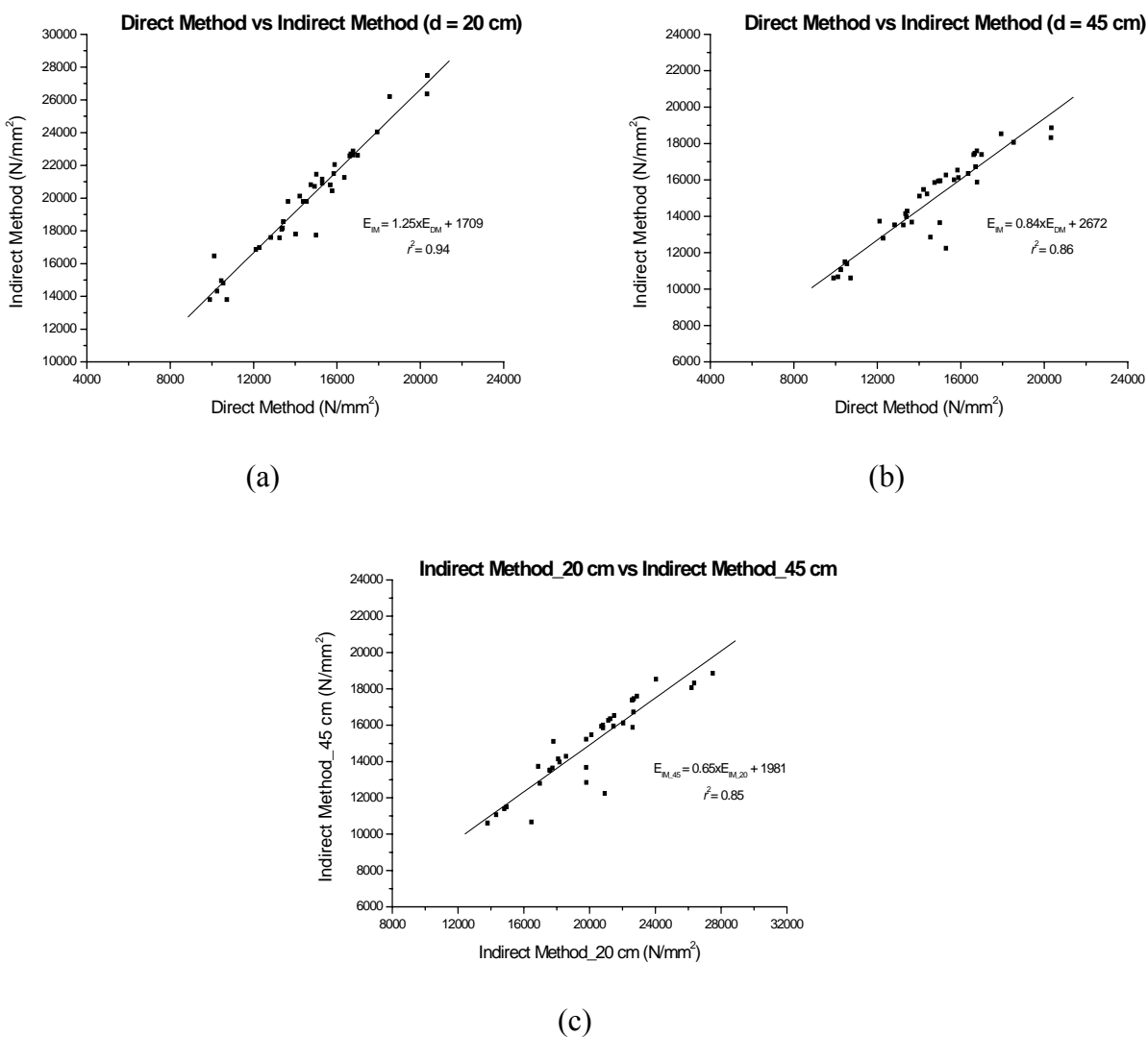


Figure A.4.2 – Comparison of the dynamic modulus of elasticity, for the NCW group: (a) Indirect Method vs Direct Method ($d = 20$ cm); (b) Indirect Method vs Direct Method ($d = 45$ cm); and (c) Direct Method ($d = 20$ cm) vs Direct Method ($d = 45$ cm).

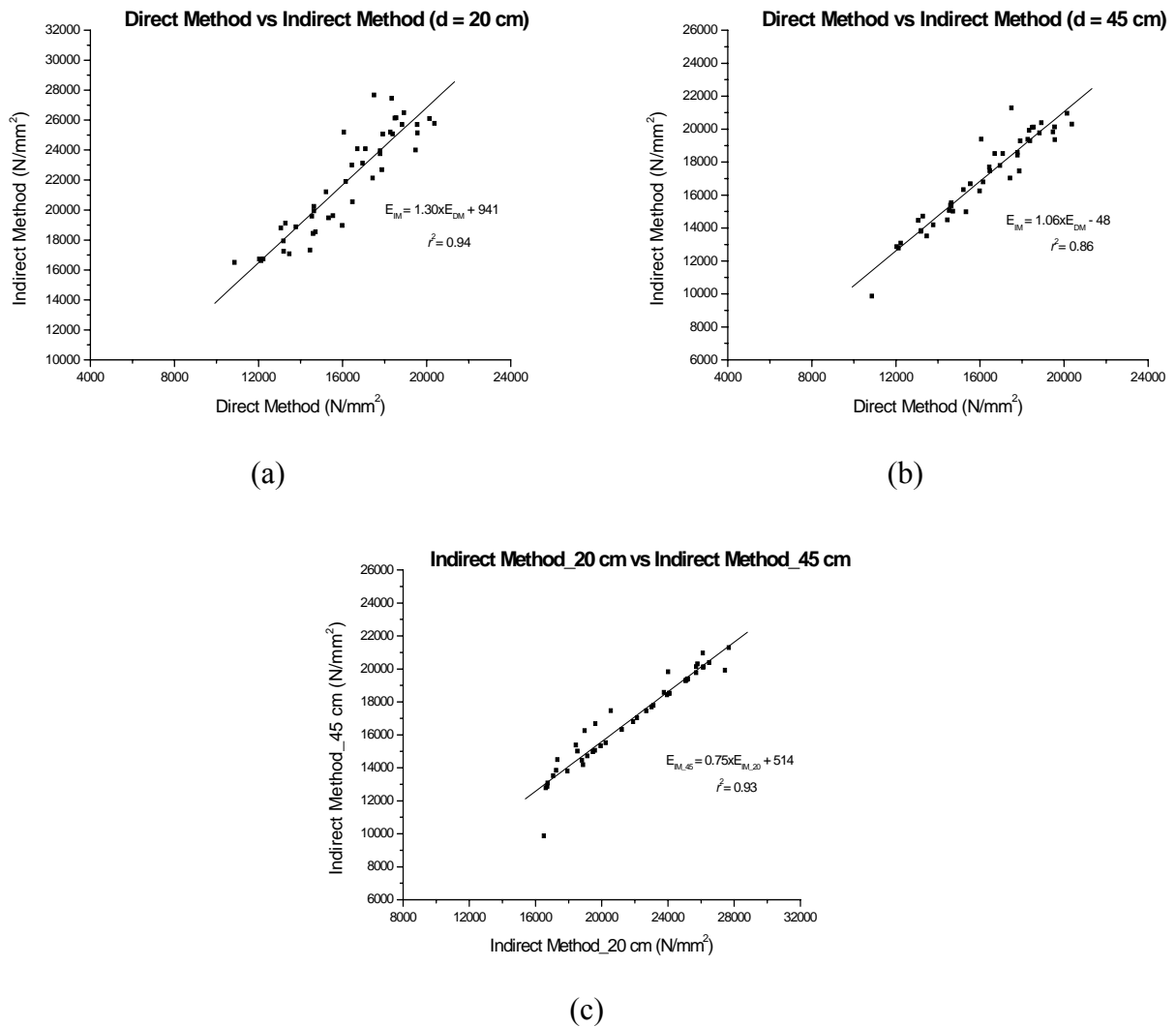


Figure A.4.3 – Comparison of the dynamic modulus of elasticity, for the OCW group: (a) Indirect Method vs Direct Method ($d = 20$ cm); (b) Indirect Method vs Direct Method ($d = 45$ cm); and (c) Direct Method ($d = 20$ cm) vs Direct Method ($d = 45$ cm).

A.4.2.1 Correlations with the elasticity modulus

Figure A.4. shows the correlations between the $E_{c,0}$ and E_{din} using the Indirect Method ($d = 45$ cm). Moderate linear correlations were found and the results are in agreement with Table 6.8 (see Chapter 6). Considering all tests, a lower 95% confidence limit is given by:

$$E_{t,0} = 3406.56 + 0.74 \cdot UPV \quad (A.4.9)$$

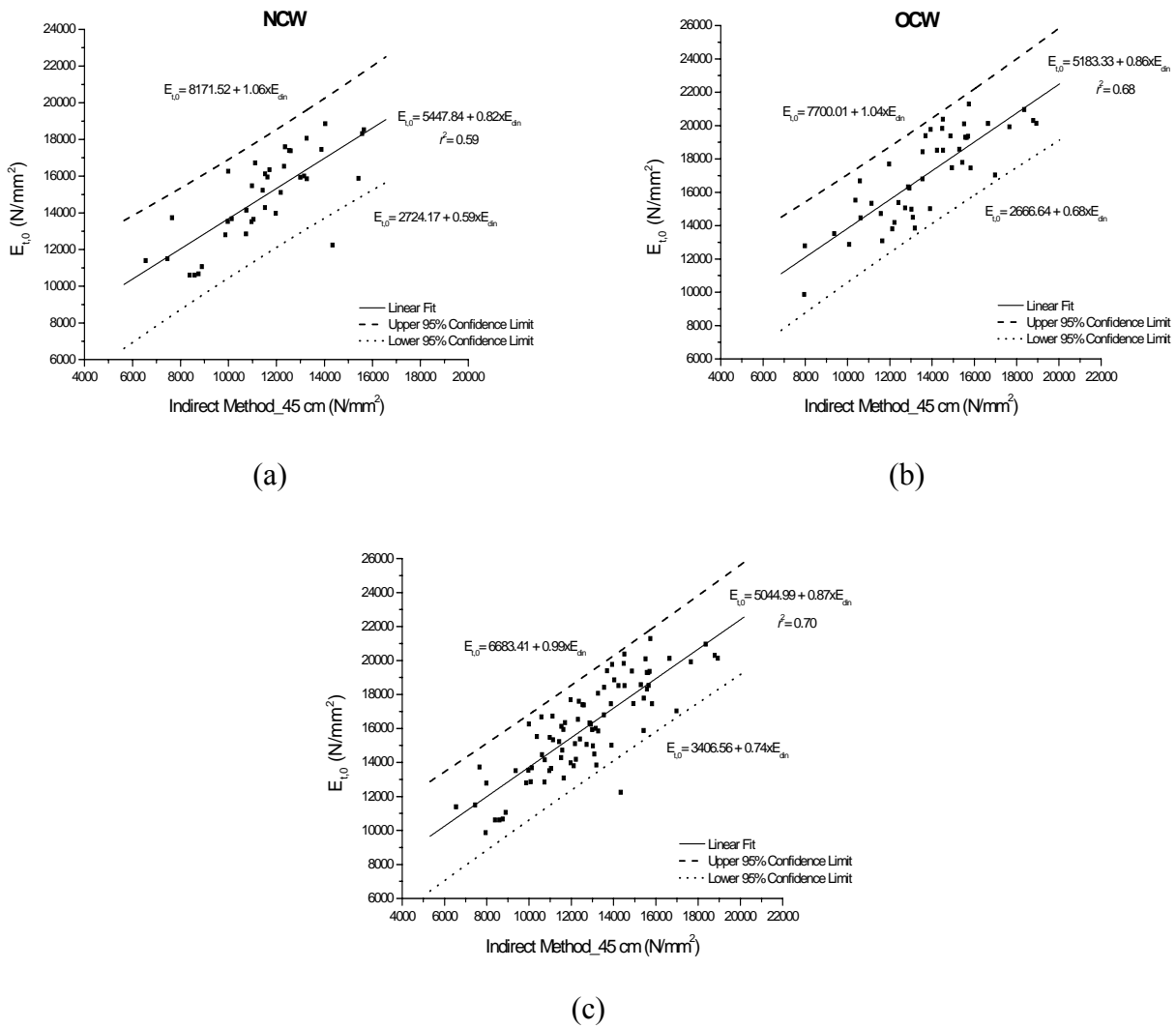


Figure A.4.4 – Relation between $E_{t,0}$ and E_{din} (Indirect Method – $d = 45$ cm): (a) for the NCW group, (b) for the OCW group, and (c) for both groups.

Figure A.4. shows the correlations between the $E_{c,0}$ and E_{din} using the Direct Method. Good linear correlations were found and the results are in agreement with Table 6.8 (see Chapter 6). These higher coefficients of correlation are justified by the direction of propagation of the ultrasonic waves, which follow the direction of the fibres, i.e., the direction of the load application. Considering all tests, a lower 95% confidence limit is given by:

$$E_{t,0} = -422.2 + 0.9 \cdot UPV \tag{A.4.10}$$

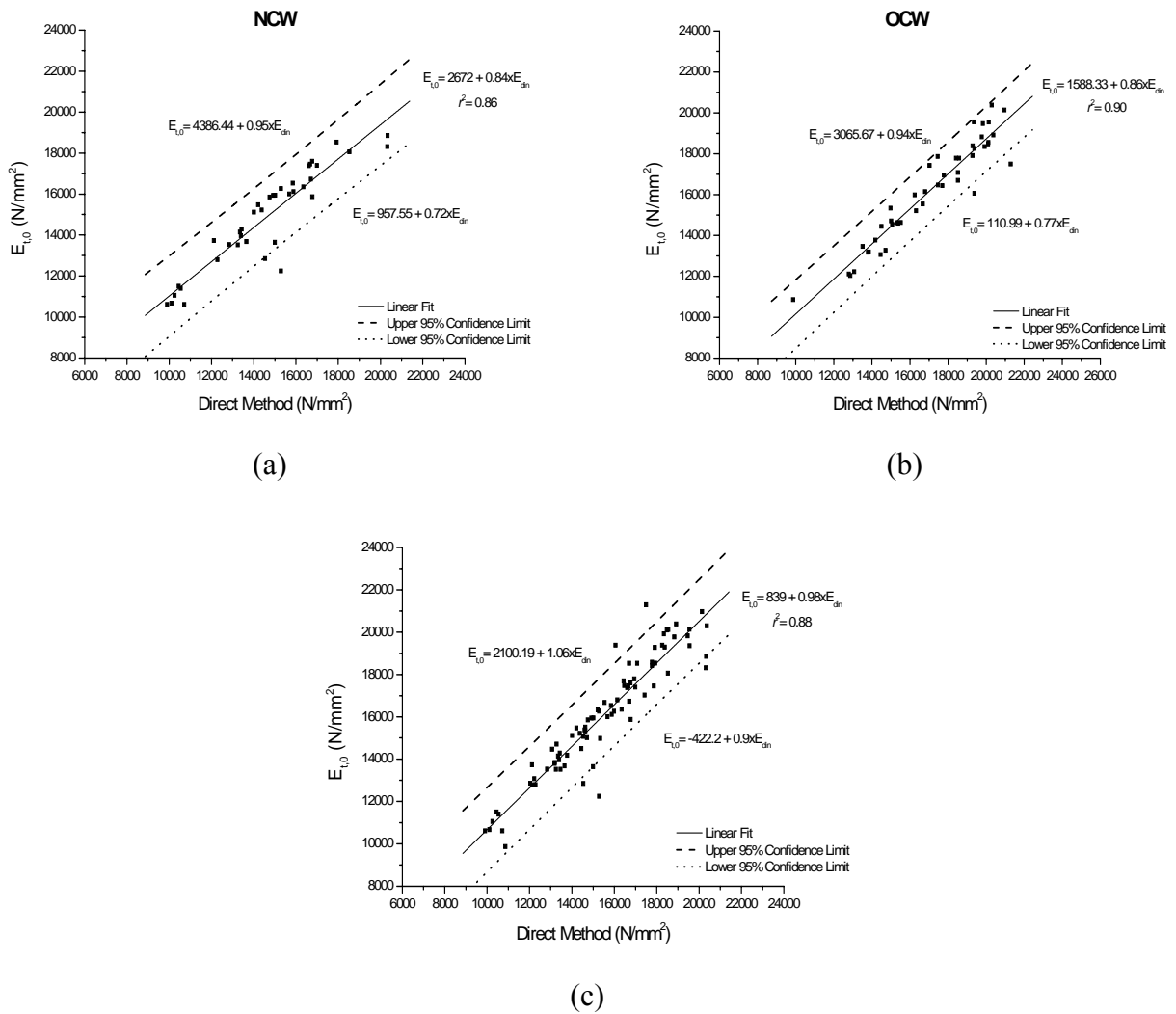


Figure A.4.5 – Relation between $E_{t,0}$ and E_{din} (Direct Method): (a) for the NCW group, (b) for the OCW group, and (c) for both groups.

A.4.2.2 Correlations with the strength

Figure A.4. shows the correlations between the $f_{c,0}$ and E_{din} using the Indirect Method ($d = 45$ cm). Moderate linear correlations were found and considering all tests, a lower 95% confidence limit is given by:

$$f_{t,0} = 14.5 + 1.86E - 03 \cdot UPV \quad (A.4.11)$$

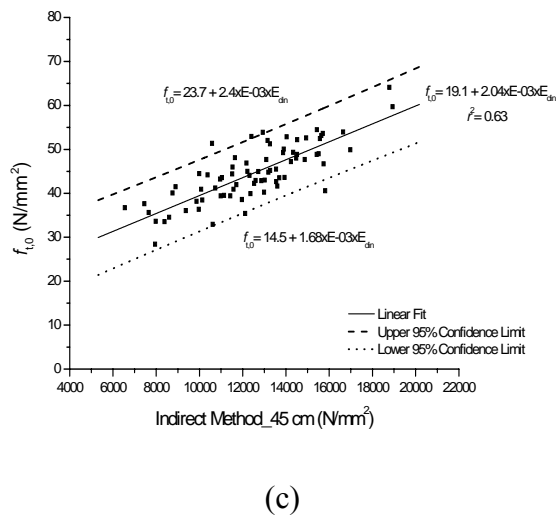
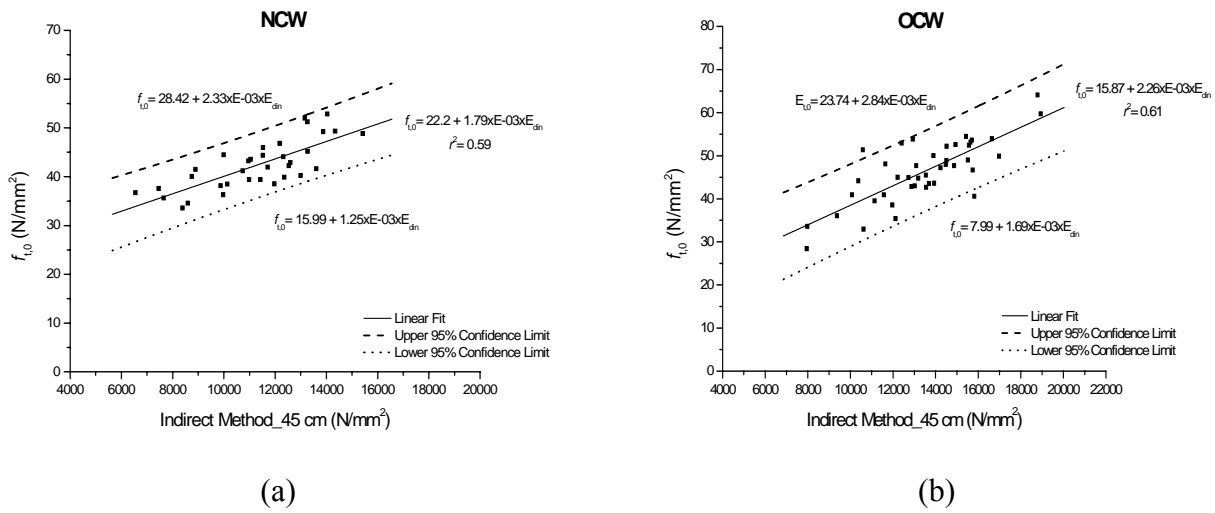
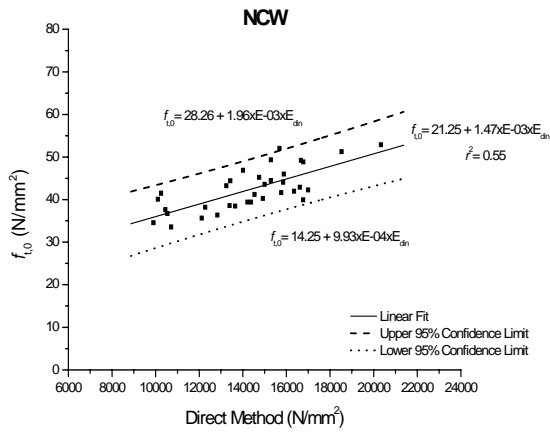


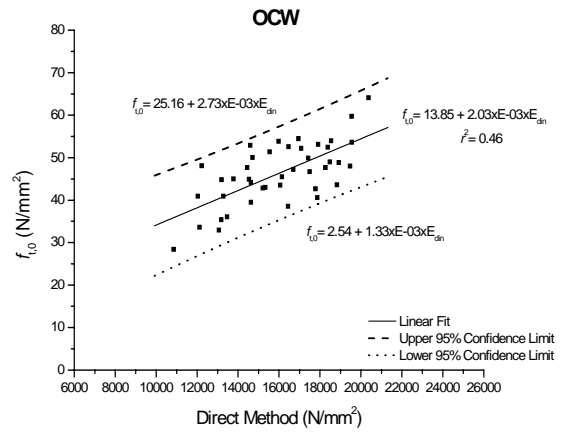
Figure A.4.6 – Relation between $f_{t,0}$ and E_{din} (Indirect Method – d = 45 cm): (a) for the NCW group, (b) for the OCW group, and (c) for both groups.

Figure A.4. shows the correlations between the $f_{c,0}$ and E_{din} using the Direct Method. Moderate linear correlations were found and considering all tests, a lower 95% confidence limit is given by:

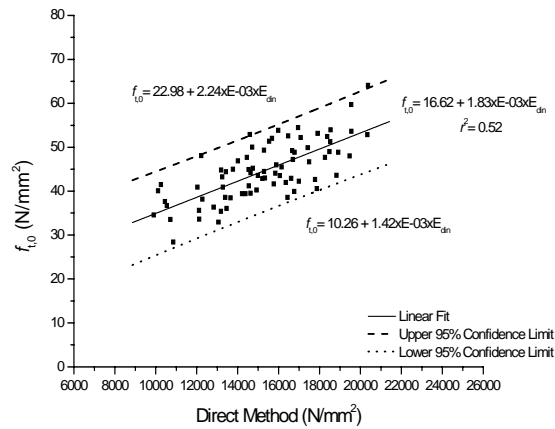
$$f_{t,0} = 10.26 + 1.42E - 03 \cdot UPV \tag{A.4.12}$$



(a)



(b)



(c)

Figure A.4.7 – Relation between $f_{t,0}$ and E_{dn} (Direct Method): (a) for the NCW group, (b) for the OCW group, and (c) for both considered groups.

Annex 5: Evaluation of load carrying capacity of a traditional timber joint

A.5.1 LOAD-DISPLACEMENT DIAGRAMS

Figure A.5.1 and Figure A.5.2 show the results of all tests in terms of load-displacement diagrams, given by the vertical force vs. vertical displacement.

The vertical load is measured by the load cell located between the vertical actuator and the brace and the vertical displacement is given by the average of the LVDT's located in the mid third of the brace.

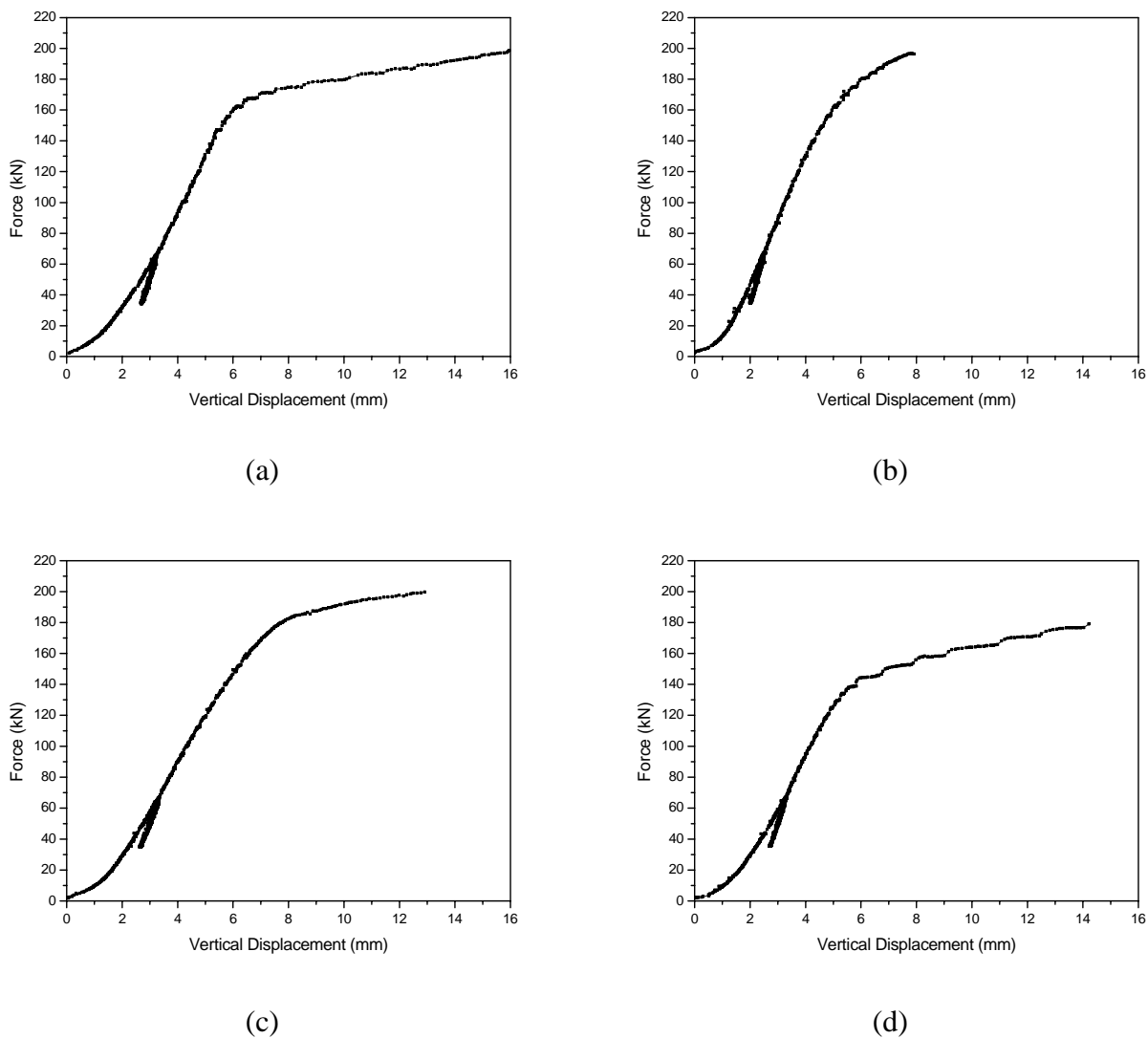
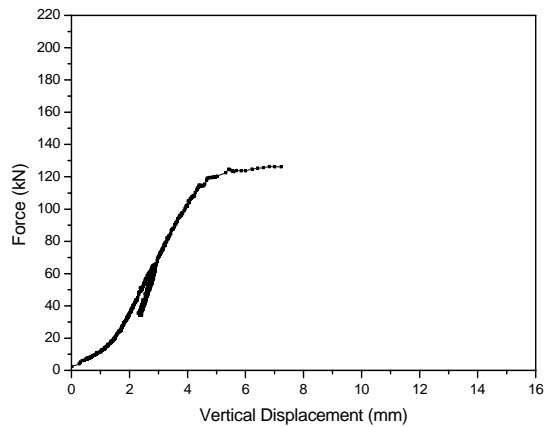
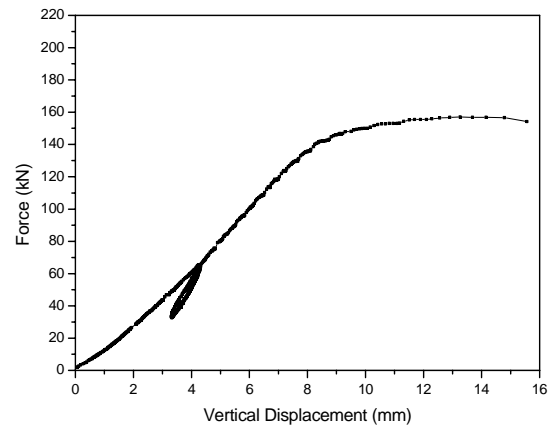


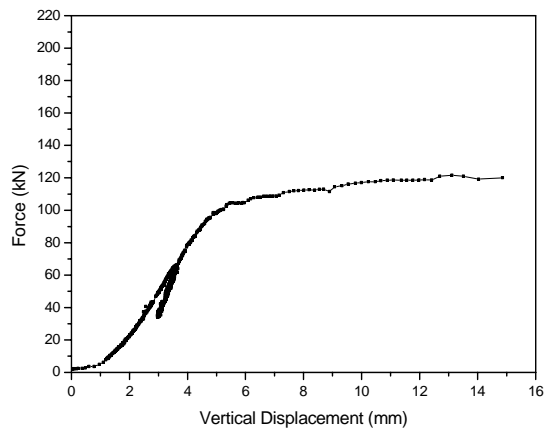
Figure A.5.1 – Load-displacement diagrams: (a) joint 1, (b) joint 2, (c) joint 3, and (d) joint 4.



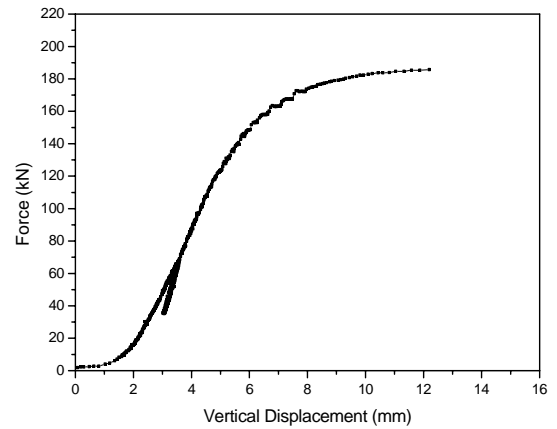
(a)



(b)



(c)



(d)

Figure A.5.2 – Load-displacement diagrams: (a) joint 5, (b) joint 6, (c) joint 7, and (d) joint 8.

Table A.5.1 present the final results, for each element and joint, of the ultrasonic tests for the NCW group and OCW group joints.

Table A.5.1 – Results of the Ultrasonic Tests (values in m/s).

NCW Joints

	Brace				Joint				Rafter	
	Side 1		Side 2		Side 1		Side 2		Side 1	Side 2
J_1	4342.1	4230.8	4125.0	4714.3	4230.8	4342.1	4024.4	3928.6	4459.5	4714.3
	4125.0	4125.0	4125.0	4459.5	4342.1	4024.4	3928.6	3928.6	4459.5	4714.3
	4125.0	4125.0	4125.0	4459.5	4125.0	3928.6	3928.6	4024.4	4459.5	4852.9

	Brace				Joint		Rafter			
	Side 1		Side 2		Side 1	Side 2	Side 1	Side 2		
J_3	4852.9	4125.0	4714.3	4852.9	4852.9	4852.9	4024.4	4024.4	5000.0	4583.3
	4714.3	4459.5	4583.3	4852.9	4583.3	4714.3	4024.4	4024.4	4852.9	4459.5
	4852.9	4714.3	4852.9	4852.9	4714.3	4852.9	4024.4	4024.4	4714.3	4714.3

	Brace				Joint		Rafter			
	Side 1		Side 2		Side 1	Side 2	Side 1	Side 2		
J_4	4459.5	3928.6	4583.3	4024.4	3837.2	4125.0	3666.7	3750.0	5500.0	4852.9
	4230.8	4125.0	4342.1	4125.0	3928.6	4125.0	3750.0	3750.0	4714.3	4714.3
	4125.0	4230.8	4459.5	4024.4	4024.4	4230.8	3750.0	3750.0	4714.3	4714.3

	Brace				Joint		Rafter			
	Side 1		Side 2		Side 1	Side 2	Side 1	Side 2		
J_7	5000.0	4583.3	5000.0	4583.3	5000.0	4024.4	4024.4	5000.0	4714.3	5000.0
	5000.0	4342.1	4583.3	4583.3	5000.0	4024.4	4125.0	5000.0	4714.3	5000.0
	5000.0	4583.3	5000.0	4583.3	5000.0	3928.6	4125.0	5000.0	5000.0	5000.0


OCW Joints

	Brace				Joint		Rafter			
	Side 1		Side 2		Side 1	Side 2	Side 1	Side 2		
J_2	3928.6	3928.6	3928.6	3928.6	3928.6	3928.6	3666.7	3666.7	3928.6	3837.2
	3928.6	3928.6	3928.6	3928.6	3928.6	3928.6	3666.7	3666.7	3928.6	3837.2
	3928.6	3928.6	3928.6	3928.6	3928.6	3928.6	3666.7	3666.7	3928.6	3837.2

	Brace				Joint		Rafter			
	Side 1		Side 2		Side 1	Side 2	Side 1	Side 2		
J_5	4583.3	4583.3	4583.3	4583.3	3750.0	4583.3	3587.0	3837.2	4852.9	4852.9
	4583.3	4852.9	4852.9	4583.3	4852.9	4583.3	3587.0	3837.2	4583.3	4583.3
	4583.3	4583.3	4583.3	4583.3	4852.9	4583.3	3587.0	3837.2	4852.9	4852.9

	Brace				Joint		Rafter			
	Side 1		Side 2		Side 1	Side 2	Side 1	Side 2		
J_6	4714.3	5000.0	4852.9	5156.3	4852.9	5000.0	4024.4	3928.6	5000.0	5000.0
	5000.0	4852.9	4852.9	5000.0	4852.9	4714.3	4024.4	4024.4	4852.9	4852.9
	4583.3	4714.3	4852.9	5000.0	4852.9	4714.3	4024.4	3928.6	5000.0	4852.9

	Brace				Joint		Rafter			
	Side 1		Side 2		Side 1	Side 2	Side 1	Side 2		
J_8	5000.0	4583.3	4714.3	5156.3	4024.4	5156.3	4125.0	3928.6	4583.3	5000.0
	4583.3	4583.3	4583.3	5000.0	4852.9	5000.0	3750.0	3837.2	4852.9	4852.9
	4852.9	4852.9	4852.9	5000.0	5000.0	5000.0	3837.2	4125.0	5000.0	5000.0

 Knot Presence

A.5.2 TEST SET-UP DETAILS

Figure A.5.3 shows some test set-up details. The system includes a support plate with stiffeners, and a toe so that the rafter does not suffer a displacement along its axis.

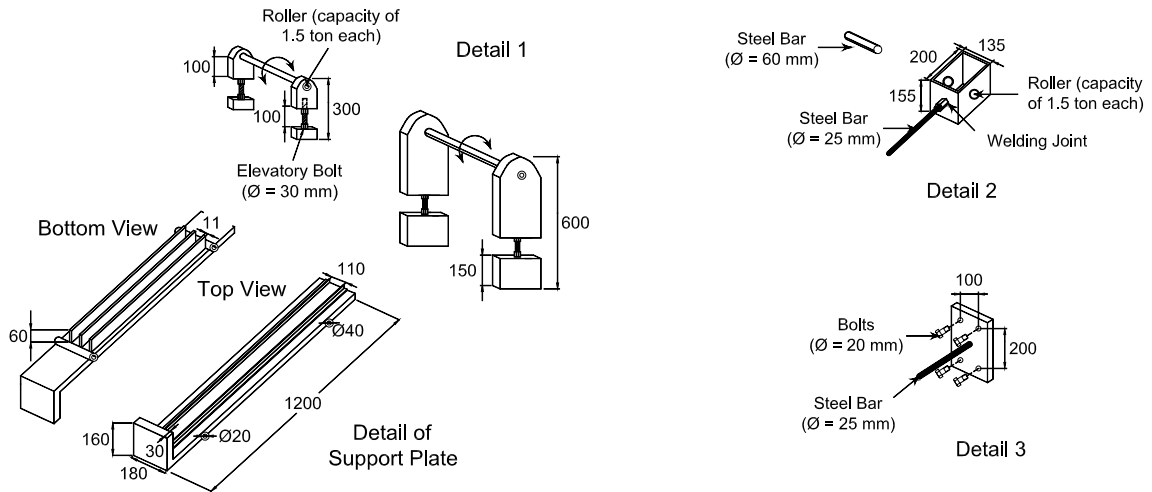


Figure A.5.3 – Test set-up details: details of plate and connections.

